

Adsorption of Macromolecules on Interfaces Studied by Isothermal Titration Calorimetry

Dissertation

zur Erlangung des Grades

”Doktor der Naturwissenschaften”

am Fachbereich Chemie, Pharmazie und Geowissenschaften

der Johannes Gutenberg-Universität Mainz

vorgelegt von

Khalid Chiad

geboren in Al-Kufa/Irak

Mainz 2011

Dekan:

1. Berichterstatter:

2. Berichterstatter:

Tag der mündlichen Prüfung: 03.02.2012

TABLE OF CONTENTS**CHAPTER 1 INTRODUCTION AND AIM OF WORK**

1.1	Introduction.....	2
1.2	Polymer-inorganic hybrid nanocomposites.....	3
1.2.1	Synthetic strategies for polymer-inorganic-nanocomposites	4
1.2.1.1	The grafting-to approach	5
1.2.1.2	The grafting-from approach.....	6
1.2.1.3	Emulsion polymersation approach	7
1.3	Host-guest systems.....	10
1.3.1	Host-guest chemistry involving dendrimers.....	12
1.3.1.1	Chemical synthesis of dendrimers.....	13
1.3.1.2	Polyphenylene dendrimers.....	15
1.4	Nature of supramolecular interactions (non-covalent Interactions).....	18
1.5	Microcalorimetric determination of the intermolecular interactions	22
1.6	Thermodynamics of binding	26
1.7	Thermodynamic signatures of non-covalent interactions	30
1.8	Aim of work.....	33
1.9	References.....	37

CHAPTER 2 THE ITC TITRATION EXPERIMENT

2.1	Introduction.....	43
2.2	Description of the ITC titration experiment.....	43
2.2.1	Sample preparation.....	44
2.2.2	Experimental parameters preparation.....	44
2.2.3	Measurement and reference cell loading.....	45
2.2.4	Filling and attachment of the injection syringe	45
2.2.5	Control experiments to determine heats of dilution	46
2.2.6	Data analysis.....	46
2.3	Troubleshooting	49
2.3	References.....	50

TABLE OF CONTENTS

**CHAPTER 3 ITC- A POWERFUL TECHNIQUE TO QUANTIFY
INTERACTIONS IN POLYMER-INORGANIC-HYBRID SYSTEMS**

3.1	Introduction.....	52
3.2	Experimental section.....	55
3.2.1	Materials.....	55
3.2.2	Sample preparation.....	56
3.2.3	ITC measurement.....	57
3.2.4	Dilution experiment	58
	Results and Discussions.....	59
3.3	Interaction of the low molecular weight model compounds	60
3.3.1	Interaction of EHMA with the SiO ₂ nanoparticles.....	60
3.3.2	Interaction of PEGMA, EGMP and 4VPSB with the SiO ₂ nanoparticles.....	62
3.3.3	Influence of the accessibility of functional groups on the adsorption.....	64
3.3.4	Investigation of monomers versus polymers.....	65
3.4	Interactions of the high molecular amphiphilic copolymers.....	68
3.4.1	Non-ionic amphiphilic copolymer /PEHMA-co-PPEGMA	68
3.4.1.1	The PEHMA-co-PPEGMA/SiO ₂ adsorption mechanisms	70
3.4.1.2	The influence of the copolymer composition on the adsorption	73
3.4.1.3	Adsorption of PEHMA-co-PPEGMA with Al ₂ O ₃ , CeO ₂	76
3.4.2	Zwitter -ionic amphiphilic copolymer/ PEHMA-co-P4VPSB	78
3.4.2.1	Effect of the sulfonate group on the adsorption process.....	81
3.4.3	Acidic amphiphilic copolymer	83
3.4.3.1	PEHMA-co- PEGMP	84
3.4.3.2	PEHMA-co- PMOEPA.....	87
3.4.3.3	The influence of the methylene spacers length.....	90
3.5	The temperature influence on the binding process.....	92
3.6	Screening and optimizing of the adsorption forces in polymer-hybrid systems	98
3.6.1	Thermodynamic optimization plot(TOP).....	99
3.6.2	Optimization regions in TOP	101
3.6.3	Optimization of the binding affinity in the copolymer/SiO ₂ interaction.....	105
3.7	Conclusion	107
3.8	References.....	114

TABLE OF CONTENTS

CHAPTER 4 THERMODYNAMIC OF THE HOST-GUEST CHEMISTRY OF POLYPHENYLENE DENDRIMERS USING ITC

4.1	Introduction.....	118
4.2	Experimental section.....	120
4.2.1	Materials.....	120
4.2.2	ITC measurement.....	120
4.2.3	Fluorescence spectroscopy.....	121
	Results and Discussions.....	122
4.3	VOCs sensor study.....	123
4.3.1	The interaction of the non-functionalized PPDs and VOCs.....	123
4.3.1.1	Stoichiometry of the host-guest interaction.....	127
4.3.1.2	Heat capacity change (ΔC_p) in Td-G2/VOCs interaction.....	129
4.3.1.3	Effect of solvent on the VOCs/Td-G2 complexation.....	133
4.3.2	VOCs/Td-G2 complexation a spectroscopic study.....	136
4.3.3	Study of the in scaffold functionalized polyphenylene dendrimers.....	144
4.3.3.1	Polyphenylene dendrimers bearing neutral functional groups.....	144
4.3.3.2	Polyphenylene dendrimers bearing acidic functional groups.....	148
4.3.3.3	Polyphenylene dendrimers bearing basic functional groups.....	151
4.3.4	The influence of the dendrimer generation on the VOCs/PPD.....	155
4.4	Triacetone triperoxide (TATP) sensor study.....	160
4.5	ITC of molecularly imprinted polymer nanospheres.....	167
4.6	Conclusion.....	170
4.7	References.....	174

CHAPTER 5 CONCLUSION AND OUTLOOK

	Conclusion and outlook.....	178
--	-----------------------------	-----

CHAPTER 6 APPENDIX

6.1	List of abbreviations.....	187
6.2	List of figures and schemas.....	189
6.3	List of tables.....	193
6.4	Publications.....	194
6.5	Curriculum Vitae.....	195
6.6	Acknowledgements.....	197

CHAPTER 1

INTRODUCTION AND AIM OF WORK

Abstract:

The essential theoretical background necessary to interpret and analyse the physicochemical reactions studied in this work is provided. The first section demonstrates the theoretical and the experimental approaches used for functionalization of inorganic particles, particularly in polymer-inorganic-hybrid systems. The next part shows the development in the host-guest chemistry over the last decades, predominantly, in systems where dendrimers act as host molecules. To understand the nature of the supramolecular interactions, the main types of the non-covalent bonds and their role as stabilizing forces in macromolecules are considered and discussed. The next section is presenting the Isothermal Titration Calorimetry (ITC) technique as a method used to analysis and quantifies the intermolecular interactions in the systems studded in this work. The last part of this chapter presents the aims of this work.

1.1 INTRODUCTION

Chemists generally are preoccupied with the molecular structure of their compounds, i.e. with the nature and reciprocal position or arrangement of the atoms and the nature of bonding forces which hold atoms in a molecule together. Only recently have chemists become intensively employed with intermolecular forces acting mainly in condensed phases, and with the structures of the systems which might result from such intermolecular interaction. The subject “intermolecular interaction” became particularly fashionable after J. M. Lehn¹, D. J. Cram², and C. J. Pedersen³ received the Nobel Prize for their work originating from the study of crown ethers and other species capable of trapping ions or molecules in their cavities.⁴ Since then the number of papers citing ‘supramolecular’ as a keyword has grown almost exponentially, the term has found its way into the titles of textbooks, specialist series and periodicals.⁵ As a whole, supramolecular chemistry can be considered an interdisciplinary field, which encompasses applications and problems from inorganic and organic chemistry, from biology to physics, as well as life and materials science (Figure 1.1).⁶⁻⁸

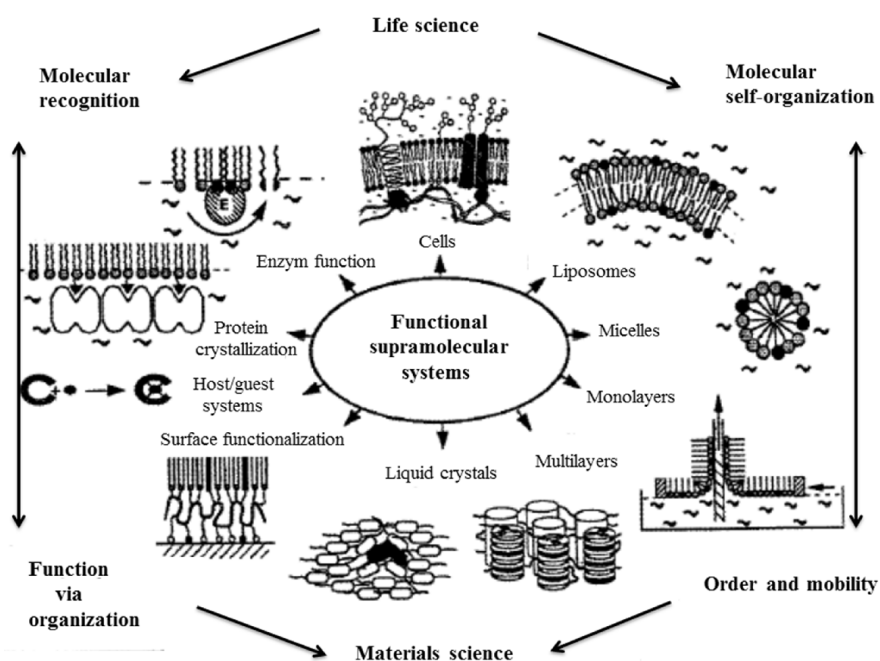


Figure 1.1: Functional supermolecular systems (Adapted from Ref. 9)

The function of supramolecular systems is achieved by the interplay between different functional units via non-covalent interactions. The term “non-covalent” covers a variety of forces, which are based on induced or permanent charge, aromatic π character, hydrogen bonding, or hydrophobic interactions (see *Chapter 1.4*). The use of these interactions for the directed self-assembly of a given structure requires knowledge of their strength and of their dependence on distances and directionality. Although a single interaction is generally much weaker than a covalent bond, the cooperative function of many of such interactions may lead to supramolecular species that are thermodynamically and kinetically stable under a variety of conditions.

In this work a special emphasis will be placed on the nature and role of the intermolecular interactions in two major materials science fields: firstly, the surface-functionalization of inorganic nanoparticles with various polymeric surfactants. Inorganic nanoparticles have gained much scientific interest in recent years.¹⁰⁻¹² Reasons for the fascination of this class of materials are their distinctively different electronic and surface properties compared to bulk materials and molecular compounds. These characteristics make them ideal building blocks for novel functional materials with unique properties. Secondly, host-guest system, in which, a molecule (host) binds non-covalently to another molecule (guest) and forms a host-guest complex or supramolecule.^{13, 14} Generally the hosts are defined as synthetic molecules containing convergent binding sites,¹⁵ and guests as molecules or ions containing divergent binding sites.¹⁶

1.2 POLYMER-INORGANIC HYBRID NANOCOMPOSITES

The mixing of nanoparticles with polymers to form composite materials has been applied for decades.¹⁷ They combine the advantages of polymers (e.g., elasticity, transparency, or dielectric properties) and inorganic nanoparticles (e.g., specific absorption of light, magneto resistance effects, chemical activity, and catalysis etc.). Nanocomposites exhibit several new characters that single-phase materials do not have.

For instance, research efforts by Charles and Nelson Goodyear, pioneers in the chemistry of rubber during the mid-19th century, showed that vulcanized rubber can be toughened significantly by the addition of zinc oxide and magnesium sulfate.¹⁸ In the early 1900s, Leo Baekeland introduced the use of silicate clay in phenolic resins “known as Bakelite™” as one of the first mass-produced synthetic polymer-nanoparticle composites.¹⁹ However, the scientific community was not aware of the advantages of nanocomposites until the 1993, when reports by Toyota researchers revealed that adding clay to nylon produced a five-fold increase in the yield and tensile strength of the material.^{18, 20}

Over the last two decades, polymer science has made much progress in developing novel methodologies of synthesis of a great variety of polymers with controlled macromolecular architecture and well defined morphology.^{21, 22} It appears possible to prepare block copolymers of various architectures from virtually all kinds of vinyl monomers by ionic and free-radical mechanisms by bulk, solution, suspension or emulsion processes. Amphiphilic block copolymers consisting of hydrophilic and hydrophobic blocks have been studied extensively for their ability to self-assemble in selective solvents.²³ They can form micelles and vesicles in diluted solutions. Their micelles have proven to be very efficient for the solubilisation²⁴ of substances in incompatible solvents, and have been used as transfer agents²⁵ and vehicles for drug delivery.²⁶ Amphiphilic block copolymers are also known as very efficient steric stabilizers, which provide dispersibility and long term stability for colloidal dispersions of particles.²⁷

1.2.1 Synthetic strategies for polymer-inorganic-nanocomposites

The greatest hindrance to the large-scale production and commercialization of polymer-inorganic-nanocomposites is the absence of cost-effective methods for controlling the dispersion of the nanoparticles in polymeric hosts. The nanoparticles typically aggregate,^{26, 28} which cancel out any benefits associated with the dimension. The particles must be integrated, in a way, leading to isolated and well-dispersed primary nanoparticles inside the matrix.

Therefore, synthetic strategies for polymer-inorganic-nanocomposites with high homogeneity are a severe challenge. Several surface modification/functionalization and stabilization methods have been developed in order to achieve this compatibility, e.g. the use of surfactants, grafting-to or -from methods (Figure 1.2),²⁹ or emulsion techniques (see Figure 1.5).³⁰

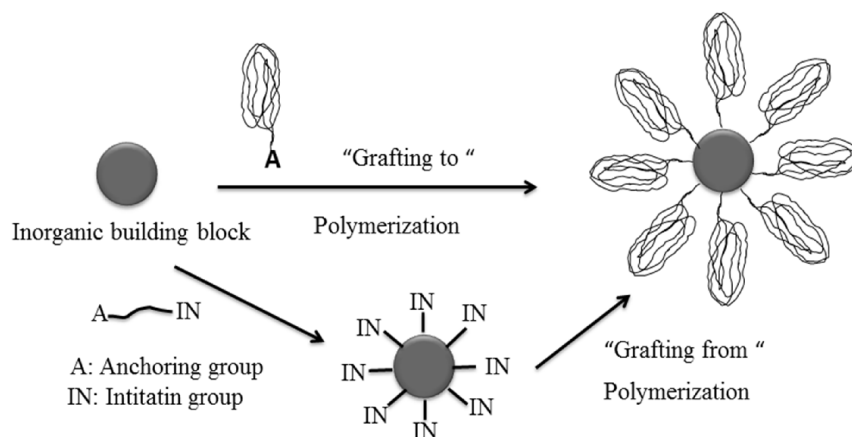


Figure 1.2: Schematic description of “grafting-to” and “grafting-from” approaches for the synthesis of polymer-inorganic-nanocomposites.

1.2.1.1 The grafting-to approach

The typical “grafting-to” approach is carried out by the coupling of end-functionalized polymers onto the surface of nanoparticles through ligand exchange chemistries (Figure 1.2).

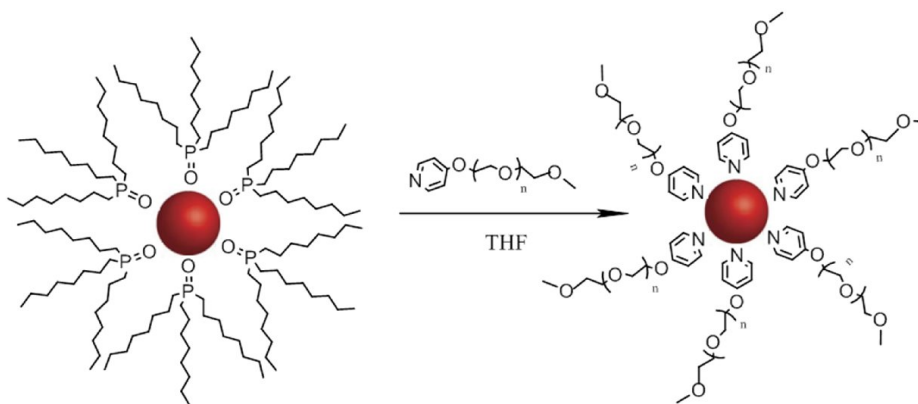


Figure 1.3: Ligand exchange of tri-*n*-octylphosphine oxide (TOPO)-covered CdSe with 4-hydroxypyridine-poly(ethylene glycol) ligands. (Adapted from Ref. 31).

Although this procedure is commonly used for the simplicity of the approach, less than optimum grafting density may result because of the steric shielding that arises on placement of each successive polymer chain onto the nanoparticle.

An example of this “*grafting-to*” method involves the ligand exchange of pyridine-functionalized poly (ethylene glycol) (PEG) on CdS nanoparticles,³¹ to afford water soluble, PEG functionalized quantum particle (see Figure 1.3) Nowadays, several researchers use this “*grafting-to*” method including thiol-functionalized polystyrene (PS) grafted to gold nanoparticles,³³ thiol-functionalized poly(caprolactone) grafted to CdS nanoparticles,³¹ and a variety of copolymers with end-thiol functionality, including water-soluble particles for stabilization of gold nanoparticles.³⁴

1.2.1.2 The grafting-from approach

The attachment of polymerization initiators to nanoparticle surfaces, followed by polymer growth outside of the surface, describes the “*grafting-from*” technique (Figure 1.2). This has proven to be an excellent approach in which polymerization initiators can be attached to nanoparticles, followed by polymerization to prepare a variety of nanoparticles-polymer hybrid materials. Critical to this “*grafting-from*” process is the compatibility of the nanoparticle with the polymerization conditions chosen, such that neither the attachment of functional ligands, nor the polymerization process significantly alters the fundamental features of the nanoparticles. A large variety of initiating mechanisms used in the “*grafting-from*”- method include free radical polymerization, which involves conventional radical polymerizations³⁵ and controlled radical polymerization (CRP),³⁶ living anionic polymerization,³⁷ living cationic polymerization,³⁸ ring opening polymerization (ROP),³⁹ ring opening metathesis polymerization (ROMP),⁴⁰ and others.⁴¹

Numerous examples for polymerization techniques utilized in the “*grafting-from*” method have been reported. For example: the surface functionalization of gold nanoparticles with norbornene derivatives that were used to prepare polynorbornene grafts by ROMP,⁴² the use of functionalized self-assembled monolayers of thiolates on gold nanoparticles to initiate living cationic ring-

opening polymerizations of 2-oxazoline monomers,⁴³ as well as via atom transfer radical polymerization (ATRP) from silica and core-shell nanoparticles have demonstrated the ability to grow well-defined poly(methyl methacrylate)(PMMA) layers from isobutryl-bromide modified inorganic surfaces (Figure 1.4).⁴⁴

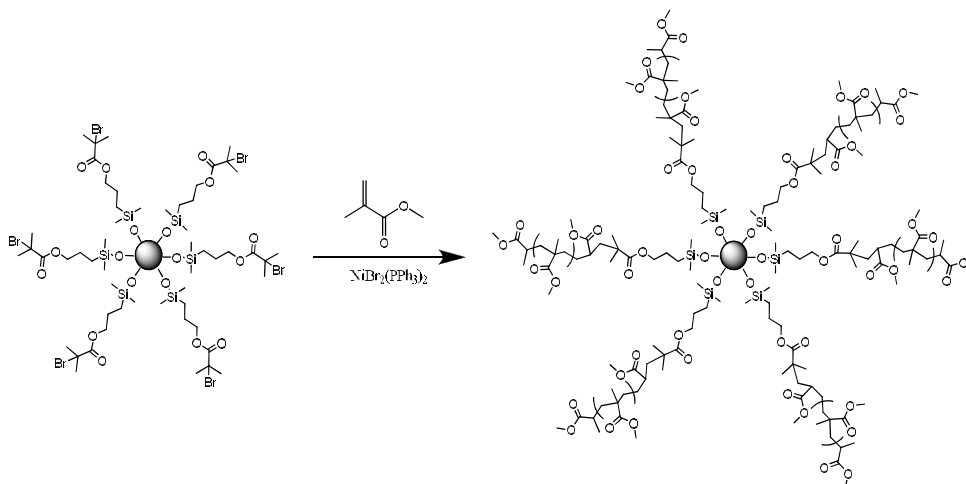


Figure 1.4: Atom transfer radical polymerization (ATRP) of methyl methacrylate from isobutryl-bromide functionalized silica nanoparticles as reported by Patten.⁴⁵

1.2.1.3 Emulsion polymerisation approach

Emulsion polymerization is the most frequently used method to synthesize polymer-inorganic nanocomposites in the last years.⁴⁶ In this process, the monomer is dispersed in an aqueous solution of surfactant with a concentration exceeding the critical micelle concentration and polymerization is carried out by means of an (most often water-soluble) initiator system (Figure 1.5).

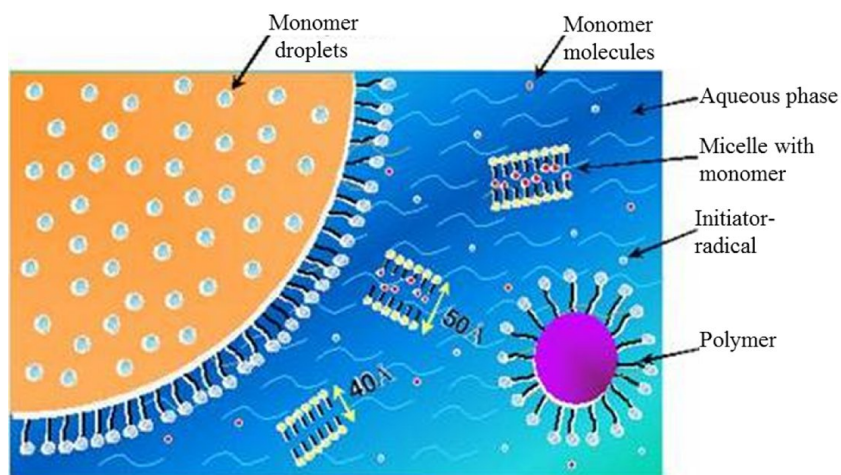


Figure 1.5: Simplified representation of an emulsion polymerization system.⁴⁷

However, during the traditional emulsion polymerization, the polymer particles can be formed either by entry of radicals into the micelles (heterogeneous nucleation), and/or precipitation of growing oligomers in the aqueous phase (homogeneous nucleation), and/or radical entry in monomer droplets.⁴⁸

Therefore, it is very tough to control the structure, morphology and size of nanocomposite spheres, especially to encapsulate inorganic nanoparticles inside polymer shells. To work out these problems, miniemulsion polymerization has been used to synthesize organic-inorganic nanocomposites.

Miniemulsion polymerization involves the use of an effective surfactant/costabilizer system to produce very small (0.01–0.5 μm) monomer droplets. The droplet surface area in these systems is very large, and most of the surfactant is adsorbed at the droplet surface. Particle nucleation occurs primarily via radical entry into monomer droplets, since little surfactant is present in the form of micelles, or as free surfactant available to stabilize particles formed in the continuous phase. Thus, in comparison with emulsion polymerization, the numbers and sizes of polymer particles in miniemulsion polymerization can be controlled, since the reaction proceeds by the polymerization of monomers in these small droplets and one monomer droplet leads to one polymer particle.⁴⁹

This monomer droplets nucleation of miniemulsion polymerization can provide more efficient encapsulation of inorganic nanoparticle. Generally, the formation of polymer-inorganic nanocomposite via miniemulsion polymerization has three steps, two dispersion steps and one polymerization step.

The system is obtained by high shear (for example: ultrasonication or high-pressure homogenizers). The high stability of the droplets is ensured by the combination of the amphiphilic component, the surfactant, and the co-stabilizer, which is soluble and homogeneously distributed in the droplet phase; the co-stabilizer has a lower solubility in the continuous phase than the rest of the droplet phase and therefore builds up an osmotic pressure in the droplets. Such small droplets can then act as nanocontainers in which reactions can take place, either inside the droplets or at the interface of the droplets, resulting in most cases in the formation of nanoparticles. The miniemulsion process is shown in Figure 1.6.

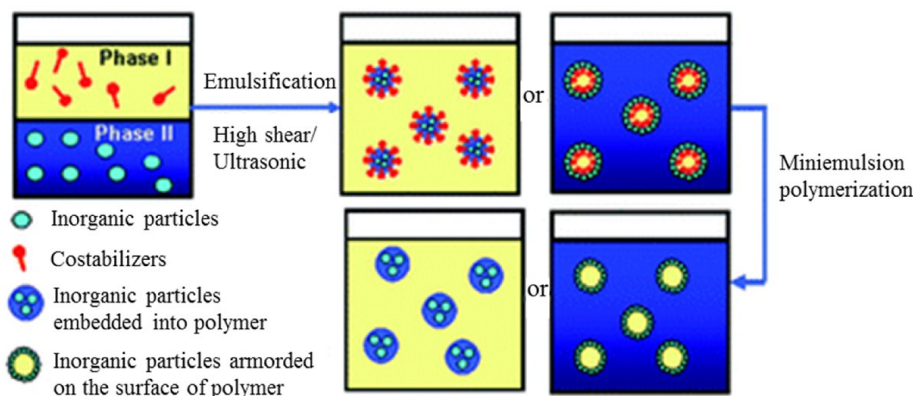


Figure 1.6.: The principle of miniemulsion polymerization.⁵⁰

The recent development of miniemulsion polymerization demonstrates that the inorganic nanoparticles, such as oxide magnets, clays, carbon, silica, titanium dioxide, etc., can be embedded inside the polymers or as armour on the surfaces of polymer particles via miniemulsion polymerization to form organic-inorganic nanocomposites with various morphologies. For example, development of high magnetization $\text{Fe}_3\text{O}_4/\text{Polystyrene}/\text{Silica}$ nanospheres by combined miniemulsion/emulsion polymerization,⁵¹ preparation of acrylate polymer/silica nanocomposites particles using the mixture of the 3-(trimethoxysilyl)propyl methacrylate (MPS) -modified silica and methyl methacrylate/butyl acrylate monomers⁵² as well to encapsulate of titanium dioxide (TiO_2) in styrene/n-butyl acrylate copolymer.⁵³

However, there are some limitations for the synthesis of organic-inorganic nanocomposites spheres using miniemulsion polymerization, such as: the inherent size range of monomer droplets (0.01–0.5 μm) in miniemulsion polymerization limits the encapsulation of large nanoparticles by the polymer shell; and the low solid content of nanocomposites via miniemulsion polymerization also influences the practical applications of nanocomposites. All these deserve to be watched out for in the future research on miniemulsion polymerization for organic-inorganic nanocomposite spheres, from both scientific and practical viewpoints. Anew approaches were established in our group, in which the synthesis and hydrophobisation of the inorganic particles is achieved in one step, this will be discussed intensively in *Chapter 3.1*.

1.3 HOST-GUEST SYSTEMS

Host-guest chemistry is the simplest form of supramolecular chemistry.⁵⁴ In this system; a molecule (host) binds non-covalently to another molecule (guest) and forms a host-guest complex or a supramolecule (Figure 1.7). Host-guest chemistry goes back for more than a century and its roots are based upon three historical concepts:⁵⁵ (i) The fact that selective binding must involve attraction or mutual affinity between host and guest. This is, a generalisation of Alfred Werner's 1893 theory of coordination chemistry, which metal ions are coordinated by a regular polyhedron of ligands binding by dative bonds. (ii) The recognition by Emil Fisher (1894) that binding must be selective,⁵⁶ as part of the study of receptor-substrate binding by enzymes. He described this by a 'lock and key' image of steric fit in which the guest has a geometric size or shape complementarity to the receptor or host. This concept laid the basis for molecular recognition, and (iii) the recognition by Paul Ehrlich in 1906 that molecules do not act if they do not bind; in this way Ehrlich introduced the concept of a biological receptor.

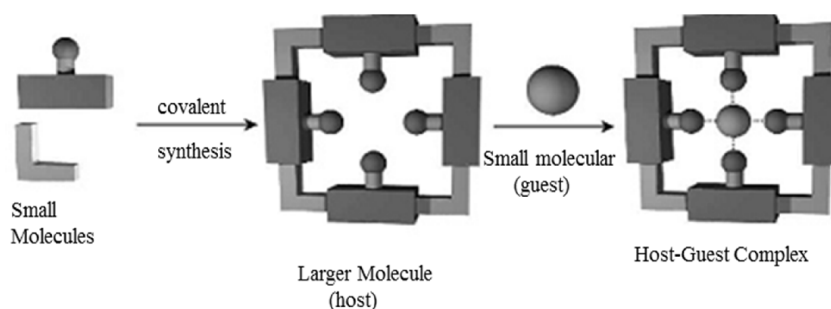


Figure 1.7: The host-guest complexation.⁵⁷

One of the most important factors in the design of a host is a clear definition and careful consideration of the target. This leads immediately to conclusions about the properties of the new host system. If a metal cation is to be the guest, then its size (ionic radius), charge density and chemical hardness are important. For anion complexation, these factors also affect spherical anions such as chloride, bromide etc., but for non-spherical anionic guests, other factors such as shape, charge and hydrogen bond donor characteristics come into play.

Organic cations and anions may require hosts with both hydrophilic and hydrophobic regions, while neutral molecule guests may lack specific handles such as polar groups that can strongly interact with the host.

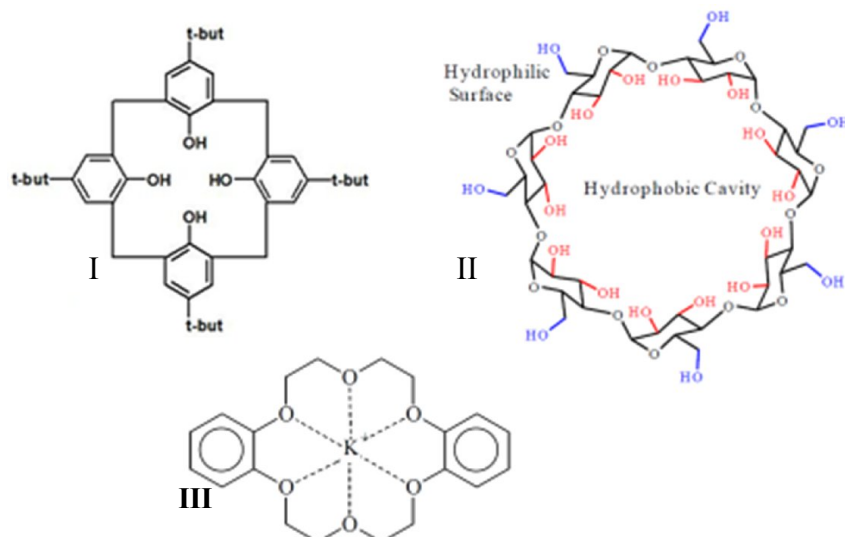


Figure 1.8: Common host molecules used in host-guest-chemistry: I) Calix[4]arenes, II) β -Cyclodextrin (β -CD) and III) inclusion of dibenzo-18-crown-6) and potassium ion.

Several examples for host compounds employed in the host-guest systems have been reported in the literature. For example: *Calixarenes* (Figure 1.8 I) are cyclic oligomers based on a hydroxyalkylation product of a phenol and an aldehyde.⁵⁸ Calixarenes are one of the most studied host molecules because of their cone- or calix-like conformation. The unique structure can be mentioned as a phenol unit linked by methylene bridges. These compounds exhibit the specific property to include various types of organic molecules and metal ions in the cavities. Calixarenes are used in commercial applications as sodium selective electrodes for the measurement of sodium levels in blood.⁵⁹

Cyclodextrins (CD) (Figure 1.8 II) are cyclic oligosaccharides which are prepared by enzymatic degradation of starch. The circularly linked glucose units result in a molecular shape of truncated cone with an internal cavity capable for hosting organic compound guests. Hydrophilic hydroxyl groups located at the outer rim make cyclodextrin dissolve in water. The inner rim of their cavities lined by hydrogen atoms and the glycosidic oxygen bridges result in a hydrophobic cavity.⁶⁰

A wide range of applications of cyclodextrins such as, solubilizers, diluents in pharmaceutical industries, catalysts, and separation media in chemical industries have been found. ⁶¹

Crown ethers, are macrocycles compounds that consist of a ring containing several ether groups (Figure 1.8 III). Crown compounds show the specific property to entrap not only alkali and alkaline earth metal ions, but also some transition metals through ion-dipole interaction held by unshared pairs of electrons of O, N, and S atoms. The complexation ability depends on the cavity size, donor atom, diameter, and cations. ⁶²

1.3.1 Host-guest chemistry involving dendrimers

Dendrimers are highly branched macromolecules with very well-defined chemical structures; they consist of three basic architectural components, (i) the core, (ii) the interior and (iii) the end-groups. The core is positioned at the center and branched wedges, called dendrons, are attached. The dendron size depends on the number of monomer layers and every added layer is represented by a generation (G). The interior consists of branching monomers that have AB_x functionality where $X \geq 2$ (see Figure 1.9).

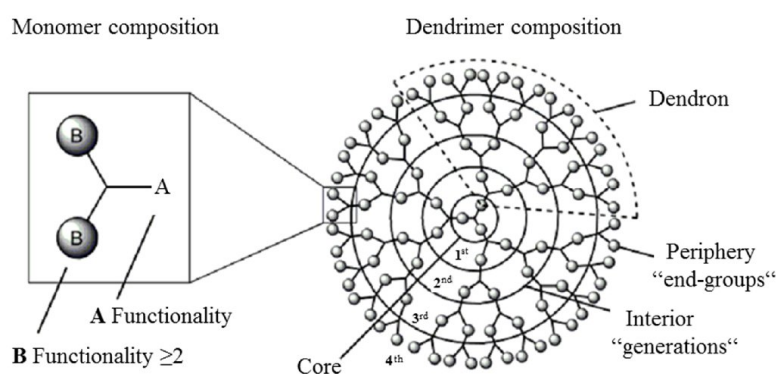


Figure 1.9: Schematic showing the basic architectural components of a dendrimer.

The amount and the chemical composition of B-functionality on the monomer will give the dendrimer some of its characteristic properties, e.g. many B-functionalities will provide a higher branching density and an aromatic branching unit will give a more thermally stable dendrimer. Furthermore, the B-functionality on the dendrimer surface is the most attractive part of the dendrimer

since it is accessible for further functionalization. The first dendritic structures that have been thoroughly investigated and that have received widespread attention are Tomalia's poly (amidoamine) PAMAM dendrimers⁶³ and Newkome's "arborol" systems.⁶⁴ The possibilities for encapsulating guest molecules in dendritic hosts were proposed by Maciejewski in 1982.⁶⁵ In 1990 Tomalia presented evidence for "unimolecular encapsulation" of guest molecules in dendrimers and pointed out that it was one of the possible future research areas in dendrimer chemistry.⁶⁶ Meijer and co-workers were the first to demonstrate physical encapsulation and release of guest molecules from a "dendritic box."⁶⁷ Three different encapsulation mechanisms have been explored: (i) the sequestration based on the respective solubilities of the dendrimer backbone (interior scaffold), dendrimer chain ends (periphery), guest molecules, and the medium employed;⁶⁸ (ii) localized interactions between the dendrimer backbone and guest through ion-pair formation or specific molecular recognition events;⁶⁹ and (iii) the physical or steric trapping of a guest in a dendritic cavity, where the chain ends are too bulky to allow release.⁷⁰

1.3.1.1 Chemical synthesis of dendrimers

Two methodologies have been developed to construct dendrimers, i.e. either the divergent 'from-core-to-periphery' route^{63, 71} or the convergent 'from-periphery-to-core' strategy.⁷²

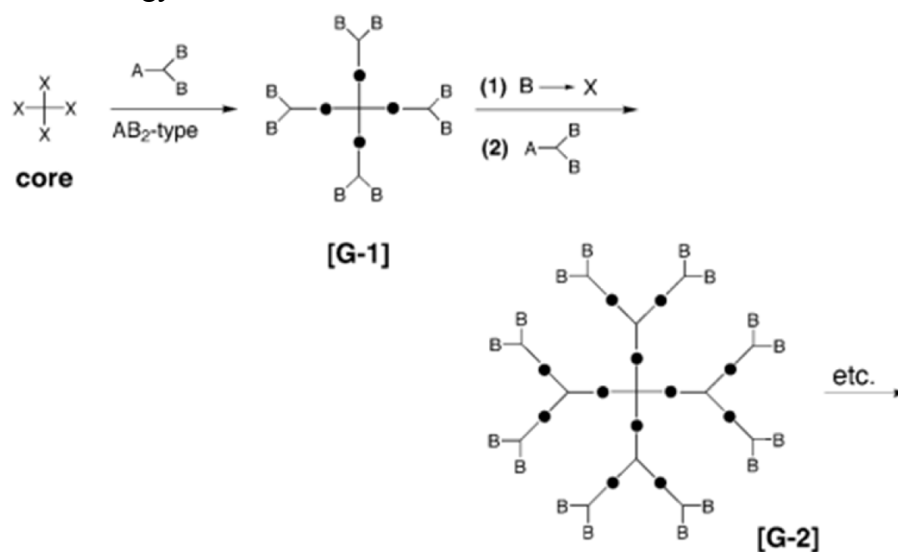


Figure 1.10: Dendritic growth via divergent approach.⁷²

Divergent growth approach (Figure 1.10). The synthesis of dendrimers using the divergent growth approach was first discussed by Vögtle in 1978 but it was the independent work reported by Tomalia⁶³ and Newkome⁶⁴ in 1985 that pioneered the strategy. In the divergent method, dendrimer grows outwards from a multifunctional core molecule. The core molecule reacts with monomer molecules containing one reactive and two or more dormant groups giving the first generation dendrimer.

Then the new periphery of the molecule is activated for reactions with further monomers. The divergent approach is successful for the production of large quantities of dendrimers. Problems occur from side reactions and incomplete reactions of the end groups that lead to structure defects. Well known dendrimers that are synthesized using the divergent growth approach are poly (amidoamine) PAMAM, poly (propylene imine) PPI and 2, 2-bis (methylol) propionic acid (bis-MPA) dendrimers.

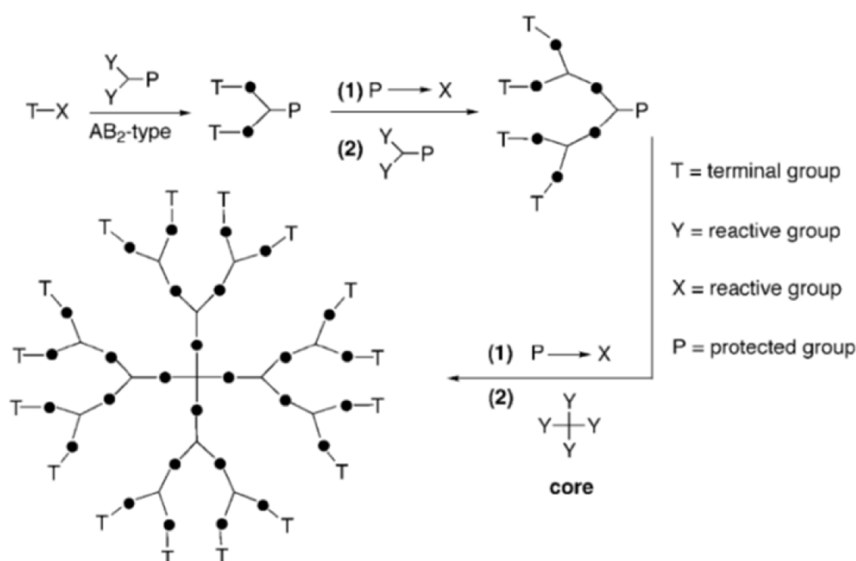


Figure 1.11: Dendritic growth via convergent approach.⁷²

Convergent growth approach (Figure 1.11). This approach was developed by Hawker and Fréchet^{72, 73} in 1990. The elegance in this strategy is the minimization of reaction sites, since there are never more coupling reactions that need to occur to form the next generation than the number of B-function of the branching monomer (see Figure 1.9). This since dendrons of the previous generation is coupled to one branching unit.

The final dendrimer is formed when dendrons are coupled to a multifunctional core that terminates further activation. A well-known dendrimer that is synthesized using the convergent growth approach is the aromatic poly (benzyl ether) dendrimer or Fréchet-type dendrimer⁷³ and Moore's phenylacetylene dendrimers.⁷⁴

Comparison of these methods shows that generally dendrimers prepared by the divergent approach are more polydisperse than those prepared by the convergent approach.⁷⁵ Furthermore, the convergent approach provides a fast access to second generation dendrimers but cannot be used to synthesise higher generation dendrimers. However, this method opens a pathway to import multi-type functionalized dendrons on an asymmetric core. In contrast, the divergent approach can be used up to the higher generations, but it only allows the order attachment of one type of functional group.⁷⁶

1.3.1.2 Polyphenylene dendrimers

Polyphenylene dendrimers (PPDs), molecules with multiple branched arms made of phenyl rings and emanating from a central core, are a new class of dendritic materials that have been synthesized in our group.⁷⁷

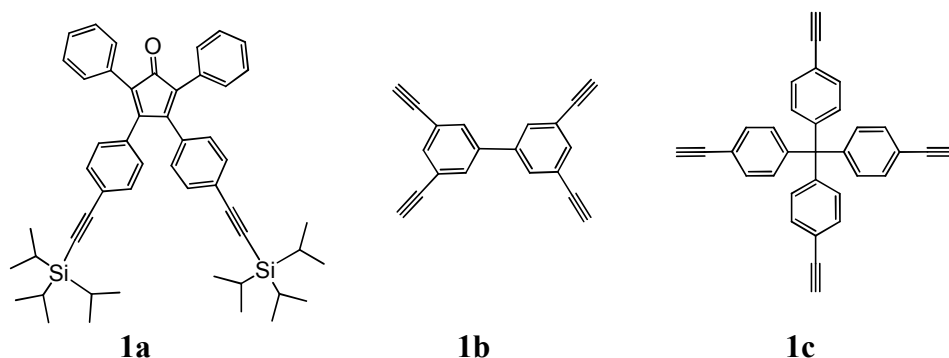


Figure 1.12: Building block (cyclopentadienone) and two tetra-functionalized cores leading to PPDs.

In particular, the 3,4-bis[4-(tri-iso-propylsilylethynyl)-phenyl]-2,5-diphenyl-cyclopentadienone (**1a**) was introduced as a building block for the synthesis of a new type of nanosized hydrocarbon dendrimers. The key-step of this dendrimer synthesis approach is the [2+4] Diels-Alder cycloaddition of **1a** to a wide variety

of hydrocarbon cores (Figure 1.12), such as 3, 3', 5, 5'-tetraethynylbiphenyl (**1b**) or tetrakis-(4-ethynylphenyl) methane (**1c**). After cleavage of the tri-isopropylsilyl groups, the obtained oligoethynyl is ready for further Diels-Alder reactions. Thus, by this repetitive cycloaddition-deprotection sequence, the construction of dendrimer generations G1, G2 and G3 can be accomplished. Furthermore, the surface of PPDs can be functionalized with different kind of functionalities, including halo, cyano, carboxy, amino and hydroxyl groups (Figure 1.13 A).⁷⁸ This functional groups on the surface donot change the shape and density of the PPDs, but they can influence the chemical and physical properties of the whole dendrimer.

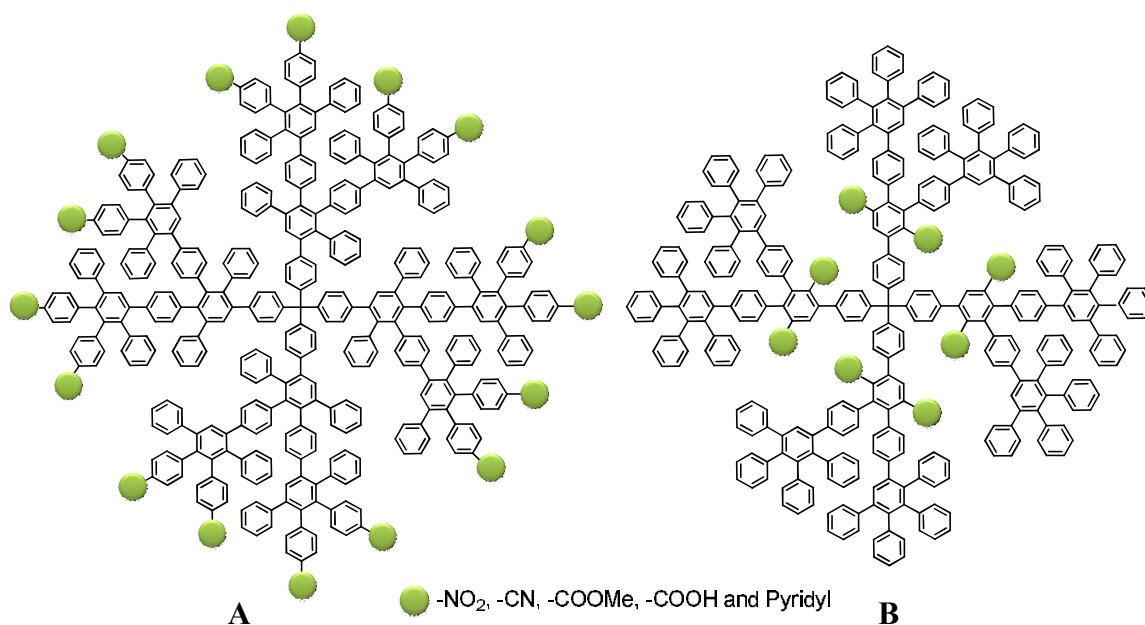


Figure 1.13: Chemical structure of the polyphenylene dendrimer functionalized at the, A) surface and B) in the scaffold.

The PPDs functionalized at the surface can modulate their polarity and open the way to water soluble systems, which are of interest as hosts for hydrophobic molecules. They can also serve as linkers for further modifications, e. g.; the attachment of catalysts and fluorescent dyes is possible.⁷⁹

Alternatively, functionalization of PPDs at the scaffold (Figure 1.13 B) can serve several purposes, e.g. fine tuning of charge or energy transfer properties through placing different chromophores at a well-defined distance from the core and

periphery, and the formation of substitute cavities. Generally, modification of PPDs scaffold can be achieved by using of suitable cyclopentadienones (**1a**).⁸⁰

The advantage of using functionalized cyclopentadienone is that it enables a diversity of functions to be introduced into dendrimers than by using a substituted core while avoiding any problem of isomer formation during the Diels-Alder reactions as can be seen for surface functionalization. Such substitution also provides a way of ensuring efficient energy or charge transfer between the core and the surface in larger dendrimers.

1.4 NATURE OF SUPRAMOLECULAR INTERACTIONS (NON-COVALENT INTERACTIONS)

Broadly, chemistry means covalent bonding. The covalent description is fully adequate when a molecule is considered in free space, i.e. isolated from any surroundings. Experimental conditions in molecular beams made from a supersonic jet expansion are close to these conditions.⁸¹ However, once the molecule is surrounded by other molecules, such as in solution or in the bulk, these surroundings affect the covalent bonding and the electronic system of the molecule is perturbed. This perturbation depends on the strength and extent of non-covalent interactions with the most pronounced changes occurring in ionic and H-bonded systems. These non-covalent forces are weak molecular interactions, with energies of formation that are at least one order of magnitude less than those of a covalent bond.⁸² The energy released in the formation of non-covalent bonds is only 1–5 kcal/mol, much less than the bond energies of single covalent bonds (Figure 1.14).

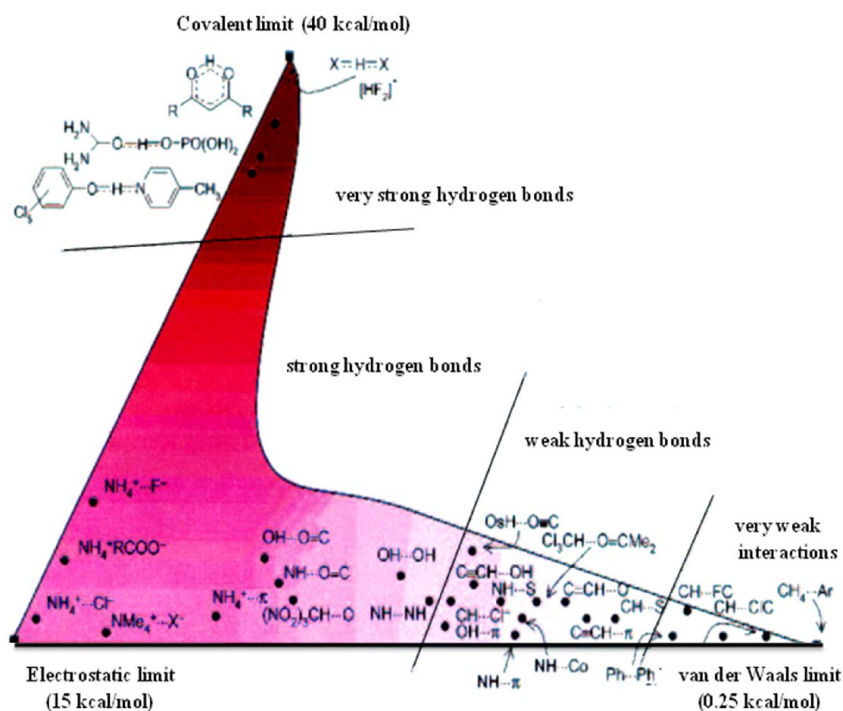


Figure 1.14: Energy of binding.⁸³

Because the average kinetic energy of molecules at room temperature (25 °C) is about 0.6 kcal/mol, many molecules will have enough energy to break non-covalent bonds.⁸³ Indeed; these weak bonds sometimes are referred to as interactions rather than bonds. Although non-covalent bonds are weak and have a transient existence at physiological temperatures (25 – 37°C), multiple non-covalent bonds often act together to produce highly stable and specific associations between different parts of a large molecule or between different macromolecules.⁸³ In this section the main types of the non-covalent bonds and their role as stabilizing forces in the polymer-inorganic-hybrid systems as well in the host-guest systems will be considered and discussed.

Electrostatic interactions occur between charged molecules. An attractive force is observed between oppositely charged molecules, and a repulsive force between molecules with the same type of charge (either negative or positive).⁸⁴ The magnitude of this interaction is relatively large compared to other non-covalent interactions, which means that the contributions from electrostatic interactions in supramolecular systems cannot usually be ignored. The strength of this interaction changes in inverse proportion to the dielectric constant of the surrounding medium. Therefore, in a more hydrophobic environment with a smaller dielectric constant, the electrostatic interaction becomes stronger.⁵⁷

A *hydrogen bond* is a particular kind of dipole-dipole interaction⁸⁵ in which a hydrogen atom, attached to an electronegative atom (or electron withdrawing group), is also attracted to a neighboring dipole on an adjacent molecule or functional group. The hydrogen bond is a complex interaction composed of several constituents that are different in their nature.⁸⁶ The total energy of a hydrogen bond is split into contributions from electrostatics, polarization, charge transfer, dispersion, and exchange repulsion.⁸⁷ The distance and angular characteristics of these constituents are very different. The hydrogen bond potential for any particular donor-acceptor combination is, therefore, dominated by electrostatics at long distances, even if charge transfer plays an important role at optimal geometry. Chemical variations of donor, acceptor, and the environment, can gradually change a hydrogen bond to another interaction type.⁸⁸

Aromatic–aromatic or π – π interactions are important non-covalent intermolecular forces similar to hydrogen bonding. They can contribute to self-assembly or molecular recognition processes when extended structures are formed from building blocks with aromatic moieties.⁸⁹ As such, π – π interactions range from large biological systems to relatively small molecules.⁹⁰ Non-covalent interactions between aromatic groups play a role in the binding and conformations from nucleic acids and proteins⁹¹ to benzene.⁹² Calculations give a bounding energy of about 2 kJ mol^{-1} for a typical aromatic– aromatic π -stacking interaction.⁹³

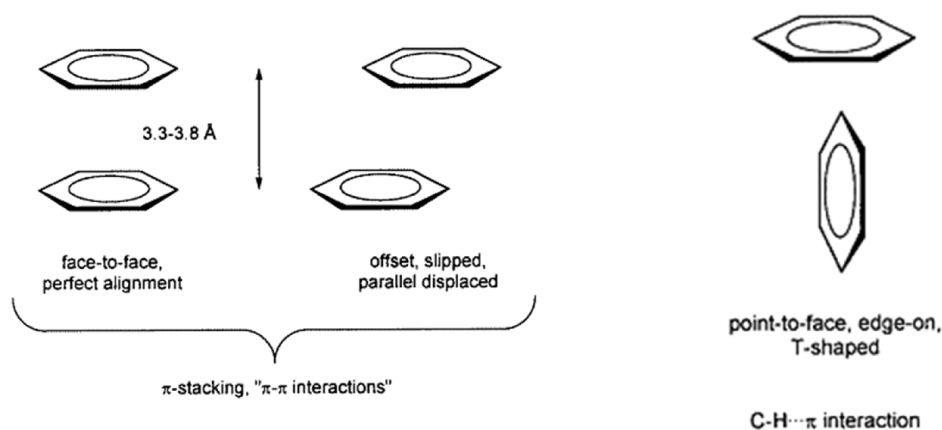


Figure 1.15: Principal orientations of aromatic–aromatic interactions.⁹⁴

In the arrangement of aromatic rings one can distinguish generally between a stacked arrangement and an edge- or point-to-face, T-shaped conformation (Figure 1.15).⁹⁴ The T-shaped conformation is a C–H···· π interaction.⁹⁵ Stacking does not necessarily have to be a perfect face-to-face alignment of the atoms, but can also be an offset or slipped packing. Both face-to-face and T-shaped conformations are limiting forms in aromatic interactions. Among these, the stacked (facial) arrangements are of particular interest as π – π interactions.

Van der Waals interaction is weaker and less specific than those described above, but it is undoubtedly important because this interaction generally applies to all kinds of molecules. It is driven by the interactions of dipoles created by instantaneous unbalanced electronic distributions in neutral substances. Although individual interactions are negligible, the combined cooperative contributions from numerous van der Waals interactions make a significant contribution to

molecular recognition. The energy of the van der Waals interaction is about 1 kcal/mol (see Figure 1.14), only slightly higher than the average thermal energy of molecules at 25 °C. Thus, the van der Waals interaction is even weaker than the hydrogen bond, which typically has energy of 1–5 kcal/mol in aqueous solutions. The attraction between two large molecules can be appreciable, however, if they have precisely complementary shapes, so that they make many van der Waals contacts when they come into proximity.

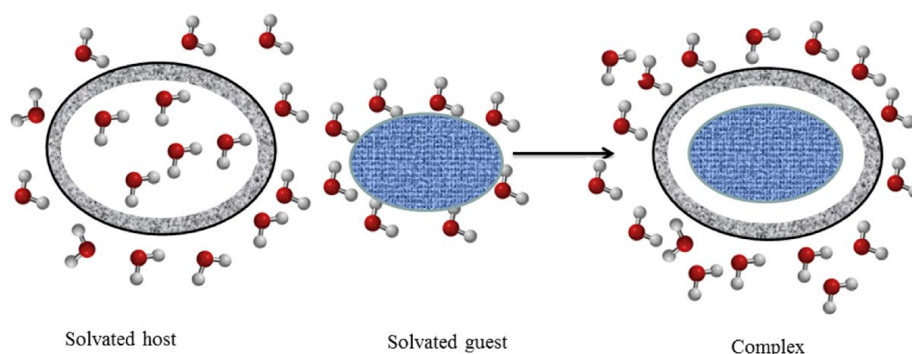


Figure 1.16: Schematic representation of the hydrophobic binding of organic guests in aqueous solution.⁹⁷

In an aqueous solution (Figure 1.16), nonpolar groups and molecules tend to stick together. The relative absence of interactions between nonpolar groups or molecules and water causes interactions among the nonpolar groups themselves to be more favorable than would be the case in other solvents, thus nonpolar molecules greatly prefer nonpolar environment. This preference of nonpolar groups or molecules for nonaqueous environments is known as the *hydrophobic interaction*.⁹⁶ The hydrophobic interaction can be taken as a transfer of nonpolar molecules or regions of molecules from water into a close association with one another. These hydrophobic regions are in an environment similar to an inert solvent. The number of water molecules immobilized around the hydrophobic region is decreased. As a consequence, water molecules are freed from the structural area around the hydrophobic regions resulting in an increase in the entropy (see Figure 1.16). These interactions to some extent compensate the inefficiency of polar interactions in water, which results from the high dielectric constant and strong proton-acceptor capacity of this solvent.⁹⁷

1.5 MICROCALORIMETRIC DETERMINATION OF THE INTERMOLECULAR INTERACTIONS

All chemical, physical and biological processes result in either heat production or heat consumption. Calorimetry is a versatile technique for studying these thermal activities in terms of heat, heat flow and heat capacity. Calorimetry can be completely non-destructive and non-invasive to the sample. It seldom requires any prior sample treatment, nor does it limit analysis to a physical state of the sample. Solids, liquids and gases can all be investigated.

Currently, two modernized high-accuracy automated types of equipment are available with accompanying convenient software. One is known as differential scanning calorimetry (DSC), and the other is known as Isothermal Titration Calorimetry (ITC). DSC measures the heat capacity (which at constant pressure is the temperature derivative of enthalpy) of interactions under investigation by incrementally varying the temperature of the system over a specified range. Ultrasensitive ITC ($1\mu\text{W}$)⁹⁸ is the only technique that can directly measure the heat change that is associated with reactions in solution at a constant temperature. ITC has the ability to precisely determine the Gibbs energy, enthalpy, entropy, and heat capacity changes associated with binding. ITC has gained much attention for the study of different kinds of binding events in biochemical processes on the basis of their thermodynamic parameters. Host-guest interaction of protein-protein,⁹⁹ small molecule/drug-protein,¹⁰⁰ DNA-drug interactions¹⁰¹ as well as enzyme kinetics or antibody activity have already been successfully examined by ITC.¹⁰²

To investigate the intermolecular interactions and their binding equilibrium in any supramolecular system, ITC competes with several established methods, for instance fluorescence, UV/Vis¹⁰³ and NMR spectroscopy,¹⁰⁴ surface plasmon resonance (SPR)¹⁰⁵ and analytical ultracentrifugation (AUC).¹⁰⁶ However, all these techniques have certain drawbacks, such as SPR technique, which requires multiple sequential injections of analyte at different concentrations (and at different temperatures). Since this is very time-consuming it is only practical to perform equilibrium analysis (binding affinity and enthalpy) on interactions that

attain equilibrium within about 30 min (blockages or air bubbles in the microfluidic system are also common in long experiments, especially when many samples are injected)¹⁰⁵ In the same way one major disadvantage with NMR is its insensitivity: for proton NMR relatively large amounts of analyte (1-5 g) are required to give good signals (see Table 1.1).¹⁰⁶

Table 1.1: Standard techniques for the determination of binding constants.

Method	Signal	Information	Advantage	Disadvantage
UV/Vis	change of absorption or emission of light	K_B (10^4 - 10^{11} M ⁻¹)	in solution	probe needed, intervention due to labeling ¹⁰³
NMR	shift of magnetic resonance frequency	K_B (10^3 - 10^6 M ⁻¹)	in solution, structural information	slow, large sample, expensive ¹⁰⁴
SPR	change of relative index due to mass	K_B (10^3 - 10^{13} M ⁻¹) k_{+1} , k_{-1}	small sample, automated	high mole.mass of the ligand expensive ¹⁰⁶
AUC	absorption at different radii for different times	K_B (10^3 - 10^8 M ⁻¹)	good for homomeric interactions	slow, particle density ^{110,111}
ITC	heat of binding	K_B (10^3 - 10^{11} M ⁻¹) ΔH , ΔS , ΔC_p , n	in solution, no labels	large sample size

In contrast, ITC offers a fast calorimetric response and thermal equilibration combined with a simple sample preparation.¹⁰⁷ The most important feature of ITC includes the determination of the entire thermodynamic profile (binding affinity (K_B), enthalpy change (ΔH), entropy change (ΔS), free energy (ΔG) and stoichiometric ratio) of an interaction in only one experiment. Since use of ITC is less common in polymer and material science,¹⁰⁸ a comparison of the strengths and weaknesses of other methods, is given in Table 1.1.

A very high-sensitivity computerized titration calorimeter can facilitate the characterization of molecular interactions, which exhibit binding constants between 10^2 M⁻¹ and 10^9 M⁻¹.¹¹²

The ITC instrument used in this work was a VP-ITC microcalorimeter (Microcal, Inc., Northampton, MA). As one can see in Figure 1.17,¹¹³ this type of calorimeter consists essentially of two cells: a) A sample cell (SC), usually containing a solution of one of the interacting molecules (called “macromolecule/host” M (such as: *monomer*, *polymer*, *dendrimer*, *etc...*) and b) the reference cell (RC), containing distilled water or buffer solution as a thermal reference.¹¹⁴

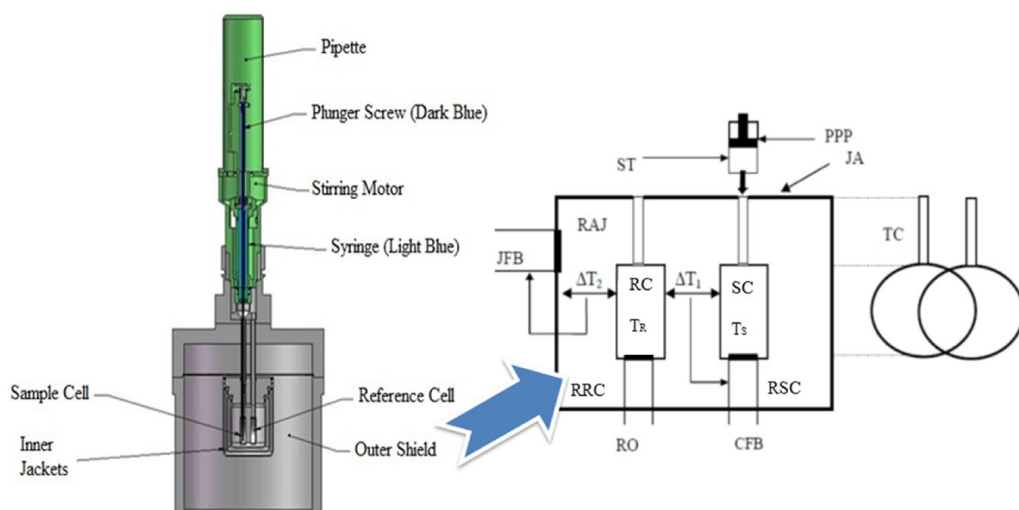


Figure 1.17: Simplified scheme of a VP-ITC calorimeter used in this work.¹¹³

A solution of the other molecule (called “small molecule/guest”, L , (for example: metal oxide, solvent, anion, cation, *etc...*)) is injected, in small quantities (5-15 μL), by the aid of a rotating syringe (ST) the plunge of which is driven by a stepping motor according to a pre-established programme. ITC can perform the power (heat flux) compensation only above the ambient temperature, without an additional refrigerating device. The heat flux ($\mu\text{cal/s}$) produced or absorbed, as a consequence of the interaction between M and L is measured for each injection, as a function of time.

A characteristic output of an ITC thermogram is depicted in (Figure 1.18) showing the titration of a 278 mM solution of poly(ethylene glycol) methacrylate (PEGMA^{n \approx 5}) in 1,4-dioxane/ethanol/ H_2O into a dispersion of SiO_2 (10 mg mL^{-1}) in the same solvent at 298 K (for more details see *Chapter 3*). The upper section of Figure 1.18 represents the raw data as supplied by the instrument and the

progression of the experiment in time. The peaks correspond to the individual aliquots of added macromolecule solution and the current applied for the compensation of the reaction heat is plotted in energy units against time. The lower part of Figure 1.18 shows the titration curve, resulting from the integration of the individual peaks and plotted as ΔH in kcal/mol against the molar ratio macromolecule/SiO₂.

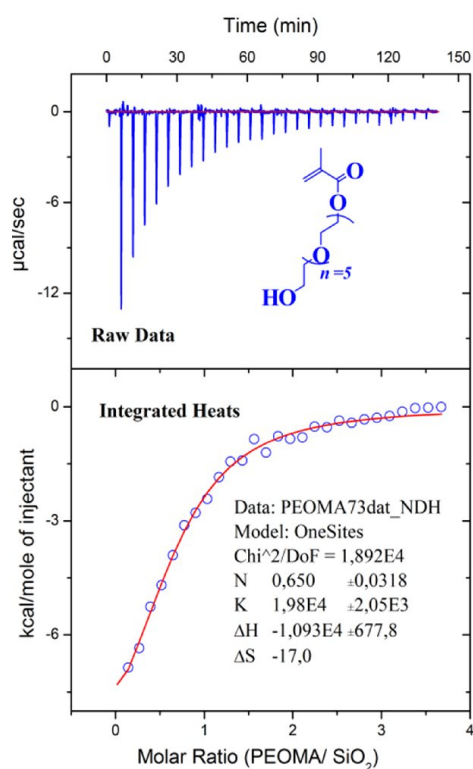
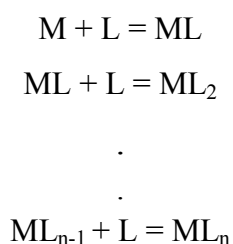


Figure 1.18: ITC experimental curve for the titration of a 278 mM solution of PEOMA^{n≈5} in 1,4-dioxane/ethanol/H₂O into a dispersion of SiO₂ (10 mg mL⁻¹) in the same solvent at 298 K, the upper panel shows the thermal power (dQ/dt) obtained during the injection. The lower panel illustrates the titration curve, which is obtained by the integration of the peaks from the upper panel, together with a line of best fit, to estimate ΔH , ΔG , K and the stoichiometry N.

1.6 THERMODYNAMICS OF BINDING

Generally, ITC allows the characterization of any type of physico-chemical interaction, which releases ($Q > 0$) or absorbs ($Q < 0$) heat. ITC is based on the state functions (internal energy, U , entropy, S , Gibbs free energy, G and enthalpy, H) and on the first and second thermodynamic principles. From the first principle, $\Delta U = Q - L$, one can deduce that at constant pressure and volume $\Delta U = Q = \Delta H$. From the second principle it results that $\Delta S > 0$, $\Delta G < 0$, and $\Delta H > 0$ or $\Delta H < 0$. The supramolecular Interactions may be *endergonic*, if $\Delta G > 0$ or *exergonic* if $\Delta G < 0$. Only the *exergonic* interactions are spontaneous, while the *endergonic* interactions must be driven by a coupled *exergonic* reaction. Therefore, *in vitro*, that is inside a sample cell of the calorimeter, only the case $\Delta G < 0$ is considered, a situation compatible both with $\Delta H < 0$ and $\Delta H > 0$. The most commonly used models for analysis of macromolecular-ligand binding data are the one-site and two-site models. For the one-site binding model the common feature of these methods is that they rearrange an original non-linear equation into a linear form.¹¹⁵

Analysis of the equilibrium in a particular reaction between guest **L** (for example: solvents, anions, etc.) binding to a single set of n identical sites on host molecule **M** (such as: nitrogen-containing macrocycles, dendrimers, etc.), i.e.



where the single-site binding constant is:^{99, 116}

$$K_B = \frac{[\text{ML}]}{[\text{M}][\text{L}]} \quad (1.1)$$

If the total concentrations of the free host molecule $[\text{M}]$ plus bound $[\text{ML}]$ is $[\text{M}_T]$, and the total concentrations of the free guest $[\text{L}]$ plus bound $[\text{ML}]$ is $[\text{L}_T]$, one can write the following equations:

$$[M_T] = [M] + [ML] \quad (1.2)$$

$$[L_T] = [L] + [ML] \quad (1.3)$$

$$[M] = [M_T] - [ML] \quad \text{and} \quad [L] = [L_T] - [ML] \quad (1.4)$$

From the last two equations (1.3 and 1.4) and equation (1) one can obtain:

$$K_B = \frac{[ML]}{[[L_T] - [ML]].([M_T] - [ML])} \quad (1.5)$$

and

$$\Delta G = RT \ln K_B = \Delta H - T\Delta S \quad (1.6)$$

where R is the gas universal constant, T is the absolute temperature and K_B is the equilibrium constant. ΔG , ΔH and ΔS represent the standard variation of G , H and S . At a molecular level, this equation reflects two fundamental processes: the trend to decrease the energy (the binding formation, $\Delta H < 0$) and the thermal movement (the breaking of different bindings, $\Delta S > 0$).

For the spontaneous reactions, $\Delta G < 0$ (*exergonic* reactions), and this condition is imposed both in exothermic and endothermic reactions:

$$\Delta G = \Delta H - T\Delta S < 0 \quad (1.7)$$

or

$$T\Delta S > \Delta H = Q \quad (1.8)$$

The standard free energy is described by two terms: a caloric one (the standard enthalpy variation, ΔH) and an entropic one (the standard entropy variation, ΔS), as one can see from the next fundamental equation:

$$\Delta G = \Delta H - T\Delta S \quad (1.9)$$

from this relation one can calculate the standard variation of the entropy:

$$\Delta S = \frac{\Delta H + RT \ln K_a}{T} \quad (1.10)$$

In the case of an *endothermic process*, for every process at constant pressure and volume, from the first thermodynamic principle it results that $L = 0$, that is:

$$\Delta H_{p,V=ct} = Q > 0, \quad T\Delta S > 0, \Delta S > 0 \quad (1.11)$$

In this case, the system entropy increases, the reaction being characterized as *entropically driven*. As the interaction progresses, the number of the degrees of freedom decreases, the consequence being an entropy decrease ($\Delta S_{assoc} < 0$), meaning that the order of the system increases, by the association of the two partners. So, the global increase of the entropy $\Delta S > 0$ is due to the compensatory molecules' disorganization of the environment (e.g. water) after the complex formation, $\Delta S_{water} > 0$. Therefore, the total entropy variation of the system is described by two terms:

$$\Delta S = \Delta S_{assoc} + \Delta S_{water} > 0, \text{ where } \Delta S_{assoc} > 0 \text{ and } \Delta S_{water} > 0 \quad (1.12)$$

from (1.12) it results that:

$$\Delta S_{water} > |\Delta S_{assoc}| \quad (1.13)$$

For an *exothermic process* $\Delta H_{p,V=ct} = Q < 0$ three cases are possible:

1. $T\Delta S < 0$, when ΔG has a minimum negative value, and the reaction is enthalpically driven. In this case, the environmental molecules are not much perturbed.
2. $T\Delta S = 0$, when $\Delta G = \Delta H > 0$, and the reaction is enthalpically driven.
3. $T\Delta S > 0$. In this case it results that ΔG has a maximum negative value, and the reaction is both enthalpically and entropically favorable.

The heat capacity (ΔC_p) of a reaction predicts the change of ΔH and ΔS with temperature. The heat capacity can be expressed as:

$$\Delta C_p = \frac{\Delta H_{T_2} - \Delta H_{T_1}}{T_2 - T_1} \quad (1.14)$$

$$\Delta C_p = \frac{\Delta S_{T_2} - \Delta S_{T_1}}{\ln\left(\frac{T_2}{T_1}\right)} \quad (1.15)$$

The subscript p in (1.14) and (1.15) denotes that the system is at constant pressure. In some cases, ΔH and ΔS will be constant over a particular temperature range and $\Delta C_p = 0$. In other cases, ΔH and ΔS may change as the temperature of the reaction changes and $\Delta C_p \neq 0$. It is known that if ΔC_p is negative, then hydrophobic bonds are formed.^{32, 33} If ΔC_p is positive, then hydrophobic bonds are broken.³⁴ The value ΔC_p is itself temperature-dependent in some cases, and this may complicate the interpretation of ΔC_p . Because there is no way to predict this temperature dependence, ΔC_p is usually determined to examine the change of ΔH and ΔS with temperature.

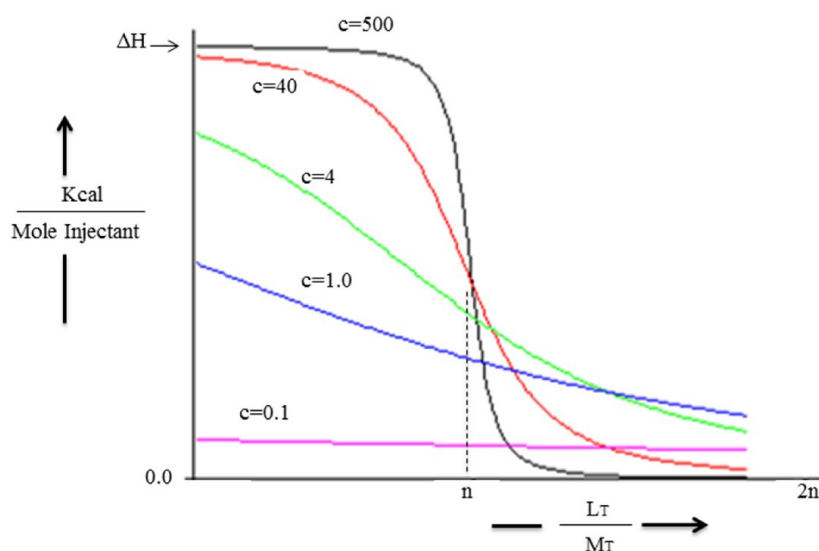


Figure 1.19: Binding isotherms for different values of c parameter.

The critical parameter which determines the shape of the binding isotherm is the dimensionless constant c , defined as,

$$c = K_B \cdot M_T \cdot n \quad (1.16)$$

where M_T is the total host concentration in the cell at the start of the experiment, and n is the stoichiometry parameter.

Very large c values lead to a very tight binding and the isotherm is rectangular in shape with the height corresponding exactly to ΔH with the sharp drop occurring precisely at the stoichiometric equivalence point n in the molar ratio L_T/M_T (see Figure 1.19). The shape of this curve is invariant to changes in K_B so long as the c value remains above 5000.

As c is reduced by decreasing M_T , the drop near the equivalence point becomes broadened and the intercept at the Y axis becomes lower than the true ΔH . In the limit of very low initial M_T concentration ($c = 0.1$), the isotherm becomes featureless and traces a nearly horizontal line indicative of very weak binding. The shape of these isotherms is sensitive to binding constant only for c values in the range $1 \leq c \leq 1000$. For ideal measurements the range is even more restricted $5 \leq c \leq 500$.

1.7 THERMODYNAMIC SIGNATURES OF NON-COVALENT INTERACTIONS

Observed enthalpies arise largely as a result of changes in intermolecular interactions,^{131, 132} The magnitude of the interacting enthalpy is dependent on bond lengths and bond angles. However, the sign of the enthalpy indicates whether there is a net favorable (negative) or unfavorable (positive) redistribution of the non-covalent forces (e.g. hydrogen bond) between the reacting species (including solvent). *Hydrophobic interactions* are related to the relative degrees of disorder in the free and bound systems and therefore these interactions are reflected in the entropy change.

The release of water/solvent molecules from a 'wet' surface to the bulk solvent is a common source of favorable entropy (Figure 1.16). This, coupled together with the inability of non-polar groups to hydrogen bond with surrounding water molecules, is the main reason for the strong energetic influence of hydrophobicity in biology. The thermodynamic signature of this force is typically characterized by a small enthalpy, either positive or negative, and favorable (positive) entropy.

A large negative ΔC_p is thought to arise from the accommodation of non-polar groups by water and is therefore another useful indicator of hydrophobic interactions. Conformational changes are entropically unfavorable.¹¹⁸ Large unfavorable entropies are often indicative of an "induced fit" during the interaction. Such modes of binding often play an important physiological role.

For example, large conformational changes may be required for allosteric processes common in signalling pathways or receptor binding.¹¹⁹

“Rigid body” interactions also incur an entropic penalty, but to a lesser extent. This is because there are always losses in the rotational and translational degrees of freedom, or flexibility when two molecules are brought together to form a complex.¹²⁰ All these processes result from a delicate balance of enthalpic and entropic forces. Using these energetic signatures it is often possible to determine the energetic source of the interaction.

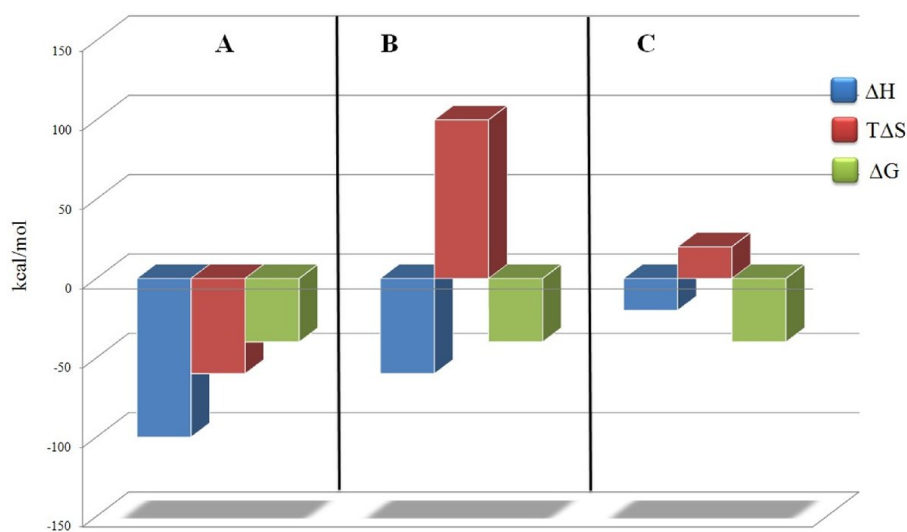


Figure 1.20: A schematic diagram to show the different thermodynamic profiles that might be observed for distinct types of molecular interaction often observed.

Figure 1.20 is a schematic representation of a range of thermodynamically distinct interactions. A molecular interpretation is given for each. In *scheme A* the dominant negative *enthalpy* suggests that there are a large number of favorable hydrogen bond contacts or van der Waals interactions between the macromolecule and ligand. The unfavorable entropy implies a conformational change in either or both of the molecules. An unopposed ΔH of -100 kJmol^{-1} would result in a K_d of 3 attomolar (if $T\Delta S=0$). In comparison, an unopposed energy of only 40 kJmol^{-1} less (equivalent to two hydrogen bonds)⁶⁸ would result in a 10 million-fold reduction in the affinity to 30 picomolar. Thus, these relatively small changes in entropy and enthalpy can potentially result in huge changes in the affinity of an interaction. The large positive *entropy* in *scheme B* signifies that this reaction is dominated by solvent rearrangement and hydrophobic forces. This type of profile is often observed in interactions that involve nucleic acids due to the displacement of site

specifically bound water molecules from the minor groove, hydrophobic transfer of ligand from bulk solvent to the macromolecule binding site and release of condensed counterions.¹²¹ In *scheme C* there is a small favorable redistribution of the hydrogen bonding network and a modest overall hydrophobic contribution.

1.8 AIM OF WORK

The aim of this work is to quantify and investigate the adsorption process and binding efficiencies in organic-inorganic-hybrid-systems, in particular, those based on inorganic fillers incorporated into a polymer matrix. As reviewed above, filling the polymeric matrix with an inorganic material requires its homogeneous distribution in order to achieve the highest possible synergetic effect.¹²² To fulfill this requirement, the incompatibility between the filler and the matrix, originating from their opposite polarity, has to be resolved. Therefore, adequate modification agents are adsorbed on the surface of the inorganic filler.¹²³ This adsorption is mostly accomplished by a non-covalent interaction between amphiphilic substances and the inorganic material.¹²⁴ A very important parameter here is the strength and irreversibility of the adsorption of the surface active compound on the inorganic material. While investigations of this adsorption process have already been performed by using common Batch or Flow Reaction Calorimeters, but yielding only ΔH by a complex data evaluation.¹²⁵ Isothermal titration calorimetry ITC (see *Chapter 1.5*) is capable of determining several other important thermodynamic parameters (ΔH , ΔS , ΔG , K_B as well as the stoichiometry n) by a single experiment.

These values provide quantification and detailed understanding of the adsorption process of surface active molecules onto inorganic particles. In this way, a direct correlation between the adsorption strength and structure of the surface active compounds can be achieved. Above all, knowledge of the adsorption mechanism in combination with the structure should facilitate a more rational design into the mainly empirically based production and optimization of nanocomposites.

In this regards, the interactions of amphiphilic copolymers on the surface of inorganic nanoparticles in a multicomponent solvent system¹²⁶ (see *Chapter 3.1*) will be investigated. In order to accomplish the aim of work:

- The influence of the hydrophobic as well the hydrophilic segment of the amphiphilic copolymer on the adsorption process (amphiphilic copolymer/nanoparticles) should be studied. For that purpose, 2-ethylhexyl methacrylate (EHMA) as a representative of the hydrophobic

part and poly-(ethylene glycol) methacrylate (PEGMA), 4-vinyl-1-(3-sulfopropyl) pyridinium inner salt (4VPSB) and (ethylene glycol) methacrylate phosphate (EGMP) was chosen as a representative of the hydrophilic part (Figure 1.21).

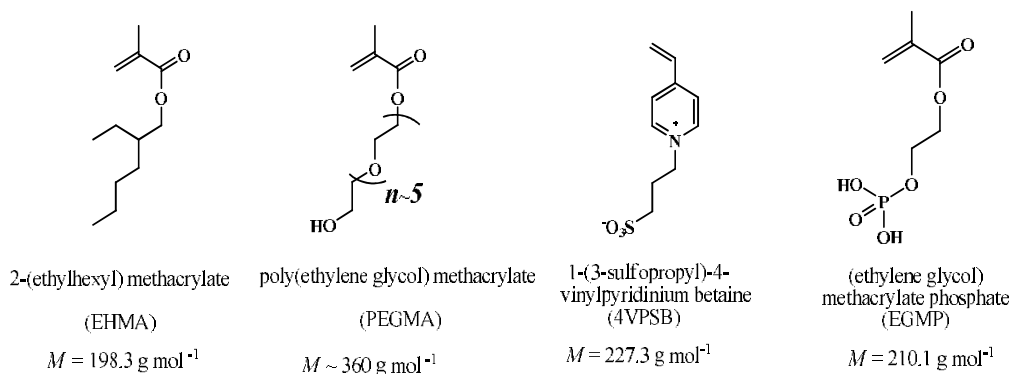


Figure 1.21: Chemical structure and molar mass of the monomers used in this study.

- The effect of the accessibility, quantity and the nature of the functional groups in the hydrophilic segment on the adsorption process are investigated using different kind of functional groups (such as: non-ionic, zwitterionic and acidic)(Figure 1.22).

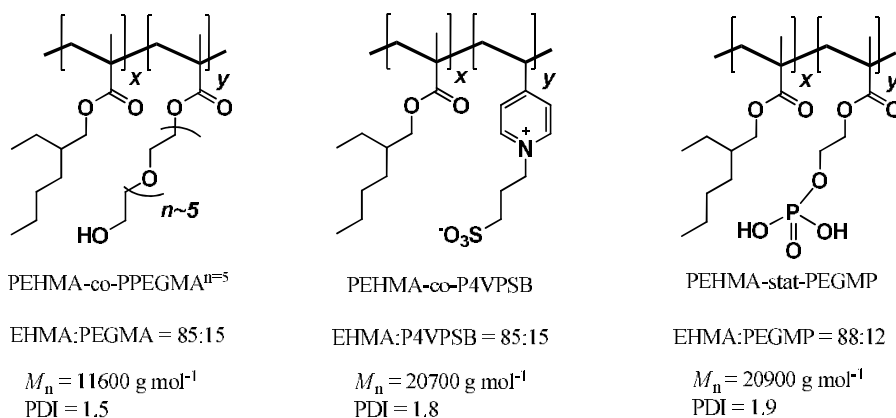


Figure 1.22: Chemical structure and molar mass of the amphiphilic copolymers used in this study.

- For analysing the influence of the nature of the inorganic nanoparticles on the adsorption process as well on the stabilization and functionalization of the nanoparticles, different kinds of inorganic nanoparticles (such as Al_2O_3 , CeO_2 , ZnO , ZrO_2 , TiO_2 and Fe_3O_4) will be considered.

- With an aim to investigate the influence of the copolymer composition on the adsorption process, as well as the lower amount of the hydrophilic segment in the copolymer, to achieve even a sufficient adsorption, different proportion of hydrophilic part should be examined.
- Additionally, with the purpose to study the effect of the temperature on the binding process of the amphiphilic copolymers onto the inorganic particles surfaces as well as on the adsorption mechanism, the binding process should be performed over a range of temperatures.

Another goal of this work is to quantify and analyse reaction mechanisms and binding efficiencies in a dendrimer-based host-guest system. Particularly, based for systems in which polyphenylene dendrimers (PPDs) act as a host. Various methods have been developed to quantify the strength of the interactions in the host-guest chemistry (such as: spectroscopic imaging techniques; NMR- and Raman spectroscopy), in which the strength of a host-guest interaction is commonly reported as the binding constant (K_B) or as the Gibbs' free energy of binding (ΔG),¹²⁷ but the contributions of the enthalpy change (ΔH) and the entropy change (ΔS) to the binding are not routinely measured.

In this work ITC technique opens a new approach to deepen the understanding of the adsorption behavior and reaction mechanisms in host-guest systems by the direct measurement of the thermodynamic parameters of the interactions between the host and guest molecules in the system.

Initially, this approach will be investigated experimentally for improving the sensitivity and selectivity of polyphenylene dendrimers (PPDs) (based on tetraphenylmethane core (Td)) as host (Figure 1.13) to uptake small molecules like volatile organic compounds (VOCs)¹²⁸ and explosive materials (such as: triacetone triperoxide (TATP))¹²⁹ as a guest. In order to accomplish the aim of work:

- The capability and the sensitivity of the ITC as a method to analyse and detect the PPDs interactions with small guest molecules should be first investigated by studying the behavior of non-functionalized polyphenylene dendrimer (Td-G2- (phenyl)) as a host with different kind of VOCs (polar

aromatic, non-polar aromatic, ketones, nitro compound, nitrile compound as well cyclic amide) as a guest at very low concentration (micromolar level).

- For analysing the influence of adding functional groups in the interior layers (scaffold) of the polyphenylene dendrimer (Td-G2) on the sensitivity and the selectivity to detect/uptake VOCs, different kinds of functionalized polyphenylene dendrimers bearing *methyl ester-*, *carboxyl-*, *cyano-*, *nitro-* and *pyridyl* groups are supposed to be studied (Figure 1.13B).
- With the intention to understand the interaction mechanisms of PPDs/ VOCs and the effect of the solvent as well as the temperature on the energetics of the system, the interaction mechanism should be studied in different solvents (non-polar and polar) and at different range of temperatures.
- With the aim to study the ability and sensitivity of PPDs for detecting the high explosive materials such as TATP, different types of polyphenylene dendrimers will be investigated at very low concentrations (ppm level).
- Further application of ITC technique to understand any other host-guest systems should be exploited for molecular imprinted polymer particles to study the imprinting effect and the rebinding efficiency. In this respect, a standard monomer mixture of methacrylic acid and ethylene dimethacrylate, containing (\pm)-propranolol as a template will be used.

1.9 REFERENCES

- [1] J. M. Lehn, *Angew. Chem.*, **1988**, 100, 91, *Angew. Chem. Int. Ed. Engl.*, **1988**, 27, 89.
- [2] D. J. Cram, *Angew. Chem.*, **1988**, 100, 1041, *Angew. Chem. Int. Ed. Engl.*, **1988**, 27, 1009.
- [3] C. J. Pedersen, *Angew. Chem.*, **1988**, 100, 1053, *Angew. Chem. Int. Ed. Engl.*, **1988**, 27, 1053.
- [4] J. M. Lehn, *Struct. Bonding*, **1973**, 6, 1.
- [5] J. M. Lehn, *Pure Appl. Chem.*, **1978**, 50, 871.
- [6] Steed, J. W., Atwood, J. L., *Supramolecular Chemistry*, Wiley & Sons Ltd.: Chichester, England, **2000**.
- [7] Schneider, H.-J., Yatsimirsky, A., *Principles and Methods in Supramolecular Chemistry*, Wiley & Sons: Chichester, England, **2000**.
- [8] Lehn, J.-M., *Supramolecular Chemistry: Concepts and Perspectives*, VCH, Weinheim, Germany, **1995**.
- [9] Atwood, J. L., Davies, J. E. D., MacNicol, D. M., Vögtle, F., Lehn, J. M., *comprehensive Superamolecular Chemistry*, Vol. 9, Pergamon, Oxford, **1996**.
- [10] Giesenberg, T., Hein, S., Binnewies, M., Kickelbick, G., *Angew.* **2004**, 116, 5816; *Angew. Chem. Int. Ed.* **2004**, 43, 5697.
- [11] Holzinger, D., Kickelbick, G., *J. Mater. Chem.*, **2004**, 14, 2017.
- [12] Kickelbick, G., Feth, M. P., Bertagnolli, H., Puchberger, M., Holzinger, D., Gross, S., *J. Chem. Soc., Dalton Trans.* **2002**, 3892.
- [13] Cram, D. J., *Science*, **1988**, 240, 760.
- [14] Chapman, R. G., Sherman, J. C., *Tetrahedron*, **1997**, 53, 15911.
- [15] Hawker C.J., Fréchet, J.M.J., *J. Am. Chem. Soc.*, **1990**, 112, 7638.
- [16] Wörner C., Mülhaupt R., *Angew. Chem. Int. Ed. Engl.*, **1993**, 32, 1306.
- [17] Balazs A. C., Emrick, T. Thomas P. Russell, *Science*, **2006**, 314, 1107.
- [18] Goodyear, C., *Dinglers Polytechnisches Journal*, **1856**, 139, 376
- [19] Baekeland, I. H., *Scientific American Supplement*, **1909**, 68, 322
- [20] Kojima, Y., Usuki, A., Kawasumi, M., Okada, A., Fukushima, Y., Kurauchi, T. Kamigaito, O., *J. Mater. Res.*, **1993**, 8, 1185.
- [21] Shvarcz, M., Levy, M., Milkovich, R., *J. Am. Chem. Soc.*, **1956**, 78, 2656.
- [22] Berger, G., Levy, M., Vofsi, D., *Polym Lett.*, **1966**, 4, 183.
- [23] a) Förster, M. A. S., *Adv. Mater.*, **1998**, 10, 195; b) Chen, S., Yang, B., Guo, C., Ma, Yang, J.-H., L.-R., Liang, X., Hua, C., Liu, H.-Z., *J. Phys. Chem. B*, **2008**, 112, 15659.
- [24] a) Gabelle, F., Koros, W. J., Schechter, R. S., *Macromolecules*, **1995**, 28, 4883; b) Paterson, I. F., Chowdhry, B. Z., Leharne, S. A., *Langmuir*, **1999**, 15, 6187.
- [25] Tani, H., Matsuda, A., Kamidate, T. H., Watanabe, *Anal. Sci.*, **1997**, 13, 925.
- [26] Chowdhary, R. K., Chansarkar, N., Sharif, I., Hioka, N., Dolphin, D., *Photochem. Photobiol.*, **2003**, 77, 299.
- [27] Harris, L. A., Goff, J. D., Carmichael, A. Y., Riffle, J. S. J., Harburn, J., Pierre, T. G. St., Saunders, *M. Chem. Mater.*, **2003**, 15, 1367.
- [28] Balazs, A.C., Emrick, T., Russell, T.P., *Science*, **2006**, 314, 110710.

- [29] Von Werne, T., Patten, T. E., *J. Am. Chem. Soc.*, **2001**, 123, 7497.
- [30] a) Luna-Xavier, J.-L., Guyot, A., Bourgeat-Lami, E., *J. Colloid Interface Sci.*, **2002**, 250, 82.; b) Landfester, K., *Macromol. Rapid Commun.*, **2001**, 22, 896.
- [31] Carrot, G., Scholz, S. M., Plummer, C. J. G., Hilborn, J., Hedrick, J., *Chem. Mater.*, **1999**, 11, 3571.
- [32] Skaff, H., Emrick T., *Chem. Commun.*, **2003**, 52.
- [33] Jia, H., Grillo, I. Titmuss, S., *Langmuir*, **2010**, 7482.
- [34] Corbierre, M. K., Cameron, N. S., Sutton, M., Mocherie, S. G.J., Lurio, L. B., Ruhm, A., Lennox, R. B., *J. Am. Chem. Soc.*, **2001**, 123, 10411.
- [35] (a) Shirai, Y., Tsubokawa, N., *React. Funct. Polym.*, **1997**, 32, 153; (b) Hayashi, S., Takeuchi, Eguchi, Y., M., Iida, T., Tsubokawa, N., *J. Appl. Polym. Sci.*, **1999**, 71, 1491.
- [36] (a) von Werne, T., Patten, T. E. *J. Am. Chem. Soc.* **1999**, 121, 7409; (b) von Werne, T., Patten, T. E., *J. Am. Chem. Soc.*, **2001**, 123, 7497; (c) Perruchot, C., Khan, M. A., Kamitsi, A., Armes, S. P., von Werne, T., Patten, T. E. *Langmuir*, **2001**, 17, 4479.
- [37] Zhou, Q. Y., Wang, S. X., Fan, X. W., Advincula, R., Mays, J., *Langmuir*, **2002**, 18, 3324.
- [38] (a) Spange, S., *Prog. Polym. Sci.*, **2000**, 25, 781; (b) Eismann, U., Spange, S., *Macromolecules*, **1997**, 30, 3439.
- [39] a) Carrot, G., Rutot-Houze', D., Pottier, A., Dege'e, P., Hilborn, J., Dubois, P., *Macromolecules*, **2002**, 35, 8400; b) Yoon, K. R., Lee, Y. W., Lee, J. K., Choi, I. S. *Macromol. Rapid Commun.*, **2004**, 25, 1510.
- [40] a) Mingotaud, A. F., Reculosa, S., Mingotaud, C., Keller, P., Sykes, C., Duguet, E., Ravaine, S., *J. Mater. Chem.*, **2003**, 13, 1920.; b) Jordi, M. A., Seery, T. A. P., *J. Am. Chem. Soc.*, **2005**, 127, 4416.
- [41] (a) Wang, Y. P., Pei, X. W., Yuan, K., *Mater. Lett.*, **2005**, 59, 520, (b) Wang, Y. P., Pei, X. W., He, X. Y., Yuan, K., *Eur. Polym. J.*, **2005**, 41, 1326.
- [42] Watson, K. J., Zhu, J., Ngyen, S. T., Mirkin, C. A., *J. Am. Chem. Soc.*, **1999**, 121, 462-463.
- [43] Jordan, R., West, N., Ulman, A., Chou, Y. M., Nuyken, O., *Macromolecules*, **2001**, 34, 1606.
- [44] a) Steven C. Farmer and Timothy E. Patten, *Chem. Mater.*, **2001**, 13, 3920; [45] Dissertation of Kevin N. Sill, University of Massachusetts Amherst, **2006**.
- [46] a) Schmid, A., Armes, S. P., Leite C. A. P., Galembeck, F., *Langmuir*, **2009**, 25, 2486; b) Voorn, D. J., Ming W., van Herk, A. M., *Macromolecules*, **2006**, 39, 2137; c) Schmid, A., Fujii, S., Armes, S. P., *Langmuir*, **2006**, 22, 4923; d) Wu, D., Ge, X., Zhang, Z., Wang M., Zhang, S., *Langmuir*, **2004**, 20, 5192.
- [47] Mlynar, M, Rohm & Haas Co, "Chemical Binders", INTC **2003**, Sept 15.
- [48] a) Asua, J. M., *Prog. Polym. Sci.*, **2002**, 27, 1283; b) Guyot, Landfester, K., Schork, F. J., Wang, C. P., *Prog. Polym. Sci.*, **2007**, 32, 1439.
- [49] a) Landfester K., Weiss, C. K., *Adv. Polym. Sci.*, **2010**, 229, 1; b) Landfester, K., *Angew. Chem., Int. Ed.*, **2009**, 48, 4488.
- [50] Hu, J., Chen, M., Wu, L., *Polym. Chem.*, **2011**, 2, 760.
- [51] Xu, H., Cui, L., Tong, N. H., Gu, H., *J. Am. Chem. Soc.*, **2006**, 128, 15582.

- [52] Qi, D., Bao Y., Weng Z., Huang Z., *Polymer*, **2006**, 47, 4622.
- [53] Ghurmallah, H. A., Sudol E. D., Dimonie V. L., El-Aasser, M. S. , *J. Appl. Polym. Sci.*, **2006**, 101, 3479.
- [54] a) Cram, D. J., *Science*, **1988**, 240, 760; b) Chapman, R. G., Sherman, J. C., *Tetrahedron*, **1997**, 53, 15911.
- [55] Lehn, J.M., *Supramolecular Chemistry Concepts and Perspectives*, **1995**.
- [56] Fischer, E., *Chem. Ber.*, **1894**, 27, 2985.
- [57] Steed, J. W., Atwood J. L., *Supramolecular Chemistry*, Wiley & Sons Ltd.: Chichester, England, **2009**.
- [58] Gutsche, C. David, **1989**, *Calixarenes*. Cambridge: Royal Society of Chemistry. ISBN 0-85186-385-X.
- [59] Carden E., Diamond, D., Miller, J., *J. Exp. Bot.*, **2001**, 5 , 1353.
- [60] Chankvetadze, B., Endresz, G., Blaschke, G. *Chem. Soc. Rev.*, **1996**, 141.
- [61] a) Artiss, J.D., Brogan, K., Brucal, M., Moghaddam, M., Jen, K.L.C. *Metabolism*, **2006**, 55 195.
- [62] Izatt, R. M., Bradshaw, J. S. S., Nielsen, A., Lamb, J. D., Christensen, J. J., Sen. D., *Chemical Reviews*, **1985**, 85: 271.
- [63] a) Tomalia, D. A., Baker, H., Dewald, J., Hall, M., Kallos, G., Martin, S., Roeck, J., Ryder, J., Smith, P., *Polymer J. (Tokyo, Japan)*, **1985**, 17, 117, b) Tomalia, D. A., Baker, H., Dewald, J., Hall, M., Kallos, G., Martin, S., Roeck, J., Ryder, J., Smith, P., *Macromolecules*, **1986**, 19, 2466.
- [64] Newkome, G. R., Yao, Z., Baker, G. R., Gupta, V. K., *J. Org. Chem.*, **1985**, 50, 2003.
- [65] Maciejewski. M.J., *J. Macromol. Sci.-Chem.*, **1990**, A17, 689.
- [66] Tomalia, D.A., Naylor, A.M., Goddard W.A., *Angew. Chem., Int. Ed. Engl.*, **1990**, 29, 138.
- [67] Johan F. G. A., Jansen, Ellen M., Brabander-van den Berg, M., de Meijer, E. W., *Science*, **1994**, 266, 1226.
- [68] a) Newkome, G. R., Moorefield, C. N., Baker, G. R., Saunders, M. J., Grossman, S. H., *Angew. Chem., Int. Ed. Engl.*, **1991**, 30, 1178; b) Kohn, F. J., Hofkens, U. M., Wiesler, M., Cotlet, M., van der Auweraer, Müllen K., Schryver, F. C., *De Chem. Eur. J.*, **2001**, 7, 4126.
- [69] Huang, F. H., Jones, J. W., Slebodnick, C., Gibson, H. W., *J. Am. Chem. Soc.*, **2003**, 125, 14458.
- [70] Jansen, J. F. G. A., de Brabander-van den Berg E. M. M., Meijer, E. W., *Science*, **1994**, 266, 1226.
- [71] de Brabander-van den Berg, EMM., Meijer, EW., *Angew Chem Int Ed Engl*, **1993**, 32,1308.
- [72] a) Hawker, C.J., Fréchet, J. M. J., *J. Am. Chem. Soc.*, **1990**, 112, 7638; b) Zeng, F.W., Zimmerman, S.C., *J. Am. Chem. Soc.*, **1996**, 118, 5326.
- [73] Hawker, C. J., Fréchet, J. M. J., *Chem. Comm.*, **1990**, 1010.
- [74] Moore, J. S., Xu, Z., *Macromolecules*, **1991**, 24, 5893.
- [75] Mansfield, M.L., *Macromolecules*, **1993** 26, 3811.
- [76] Fréchet, J. MJ, Hawker, C.J. Wooley, K.L., *J. Macromol. Sci. Pure. Appl. Chem.*, **1994**, A31:1627.

- [77] a) Morgenroth, F., Müllen, K., *Tetrahedron*, **1997**, 53, 15349; b) Berresheim, A.J., Müller, M., Müllen, K., *Chem Rev.*, **1999**, 99 1747.
- [78] Wiesler, U. M., Weil, T., Müllen, K., in *Dendrimers III: Design, Dimension, Function*, Vögtle, F., Ed. Topics in Current Chemistry. Springer-Verlag: Berlin, Vol., **2001**, 2121.
- [79] Knapen, J.W.J., Vandermade, A.W., Dewilde. J.C, Vankoten, G., *Nature*, **1994**, 372, 61.
- [80] Bauer R. E., Clark C. G., Müllen K., *New J. Chem.*, **2007**, 31, 1275.
- [81] March, J. “*Advanced Organic Chemistry*” 4th Ed. J. Wiley and Sons, **1991**: New York. ISBN 0-471-60180-2.
- [82] Stan T., C., *Biomacromolecules: introduction to structure, function, and Informatics*. **2007** John Wiley & Sons, Inc. ISBN-13: 978-0-471-71397-5.
- [83] Williams D. H., Stephens E., Brien O., and Zhou M., *Angew. Chem. Int. Ed.*, **2004**, 43, 6596.
- [84] Bianchi A, James B.- & Espana G. E., *supramolecular chemistry of anions*, **1997**, Wiley-VCH, New York.
- [85] T. Steiner, *Angew. Chem.*, **2002**, 114, 50.
- [86] B.T. Holland, L. Abrams, A. Stein, *J. Am. Chem. Soc.*, **1999**, 121, 4308.
- [87] M. Schwartz, G. Miehe, A. Zerr, E. Krohe, B.T. Poe, H. Fuess, R. Riedel, *Adv.Mater.*, **2000**, 12, 883.
- [88] Schneider H-J., Yatsimirsky A. *Principles and methods in supramolecular chemistry*, **2000**, John Wiley & Sons Ltd, chichester, England.
- [89] a) Amabilino D. B. , Stoddart J. F., *Chem. Rev.*, **1995**, 95, 2725; b) Claessens C. G., Stoddart J. F., *J. Phys. Org. Chem.*, **1997**, 10, 254.
- [90] a) Lightfoot M. P., Mair F. S., Pritchard R. G., Warren J. W., *Chem. Commun.*, **1999**, 1945; b) Ning G. L., Wu L. P., Sugimoto K., Munakata M., Kuroda- Sowa T. , Maekawa M., *J. Chem. Soc., Dalton Trans.*, **1999**, 2529.
- [91] Burley S. K., Petsko G. A., *J. Am. Chem. Soc.*, **1986**, 108, 7995.
- [92] Müller-Dethlefs K., Hobza P., *Chem. Rev.*, **2000**, 100, 143.
- [93] Jorgensen W. L. , Severance D. L., *J. Am. Chem. Soc.*, **1990**, 112, 4768.
- [94] Nishio M., Hirota M., Umezawa Y., *The CH/π Interaction (Evidence, Nature and Consequences)*, Wiley-VCH, New York, **1998**.
- [95] a) Janiak C., Temizdemir S., Dechert S., *Inorg. Chem. Commun.*, **2000**, 3, 271.
- [96] Privalov, P.L., Gill, S.J., *Pure Applied Chemistry*, **1988**, 61, 1097.
- [97] a) Müller, N., *Account Chemistry Research*, **1990**, 23, 23; b) Pimentel, G.C., Mc Lellan, A.L. *Annual Review of Physical Chemistry*, **1971**, 22, 347.
- [98] Wadso, I., *Thermochimica Acta*, **1995**, 267, 45.
- [99] Wu, J. G., Li, J. Y., Li, G. Y., Long, D. G., Weis, R. M. *Biochemistry*, **1996**, 35, 4984.
- [100] Garciafuentes, L., Reche, P., Lopezmayorga, O., Santi, D. V., Gonzalez pacanowska, D., Baron, C., *Eur. J. Biochem.*, **1995**, 232, 641.
- [101] Qu, X. G., Ren, J. S., Riccelli, P. V., Benight, A. S., Chaires, J. B. *Biochemistry*, **2003**, 41, 11960-11967.
- [102] Livingstone, J. R., *Nature*, **1996**, 384, 491.

- [103] Engman, K. C., Sandin, P., Osborne, S., Brown, T., Billeter, M., Lincoln, P., Norden, B., Albinsson, B., Wilhelmsson, L. M. *Nucleic Acids Res.*, **2004**, 32, 17, 5087.
- [104] Ramstad, T., Hadden, C. E., Martin, G. E., Speaker, S. M., Teagarden, D. L., Thamann, T. J., *Int. J. Phar.*, **2005**, 296, 55.
- [105] Muh, E., Stieger, M., Klee, J. E., Frey, H., Mulhaupt, R. *J. Polym. Sci., Part A: Polym. Chem.*, **2001**, 39, 4274.
- [106] Myszka, D. G., *Curr. Opin. Biotechnol.*, **1997**, 8, 50.
- [107] Victoria M., Elipe S., *Analytica Chimica Acta*, **2003**, 497, 1.
- [108] Pauck, T., Colfen, H. *Anal. Chem.*, **1998**, 70, 3886.
- [109] Wiseman, T., Williston, S., Brandts, J. F., Lin, L. N. *Anal. Biochem.*, **1989**, 179, 131.
- [110] Phillips, R. L., Kim, I. B., Tolbert, L. M., Bunz, U. H. F., *J. Am. Chem. Soc.*, **2008**, 130, 6952.
- [111] Green, D. B., Lane, J., Wing, R. M., *Appl. Spectrosc.*, **1987**, 41, 847.
- [112] Grewer T., *Thermal Hazards of Chemical Reactions*, Elsevier, Amsterdam, **1994**.
- [113] a) Chilom, C. G., Craescu C. T., Popescu A. I., *Rom. Journ. Phys.*, **2006**, 51, 443; b) www.microcal.com.
- [114] Tuma L. D., *Thermochim. Acta.*, **1991**, 192, 121.
- [115] Wang, Z-X., Jiang, R-F., *FEBS Letters*, **1996**, 392, 245.
- [116] Indyk, L., Fisher H.F., *Meth., In Enzymol.*, **1998**, 295, 350.
- [117] a) Campoy, V., Kiso, A., Freire, E., *Arch. Biochem. Biophys.*, **2001**, 390, 169; b) Holdgate, GA., *Biotechniques*, **2001**, 31, 164-184.
- [118] a) Ward, WH., Holdgate, GA., *Prog. Med. Chem.*, **2001**, 38, 309; b) Kwong, P., Doyle, ML., Casper, DJ., Leavitt SA., Majeed, S., *Nature*, **2002**, 420, 678.
- [119] a) Borea PA., Varni K., Gessi S., Gill P., Gilli G., *Biochem. Pharmacol.*, **1998**, 55, 1189; b) Ayala YM., Vindigni A., Nayal M., Spolar RS., Record MT., DiCera E., *J. Mol. Biol.*, **1995**, 253, 787.
- [120] Spolar, RS., Record MT Jr., *Science*, **1994**, 263, 777.
- [121] Haq I, Arch., *Biochem. Biophys.* **2002**, 403, 11.
- [122] Gomez-Romero P., *Adv. Mater.*, **2001**, 13, 163.
- [123] a) Schubert U., *Chem. Mater.*, **2001**, 13, 3487; b) Descalzo A. B., Martínez-Máñez R., Sancenón F., Hoffmann K., Rurack K., *Angew. Chem. Int. Ed.*, **2006**, 45, 5924.
- [124] Bourgeat-Lami E., *J. Nanosci. Nanotechnol.*, **2002**, 2, 1.
- [125] a) Corkill, J. M., Goodman, J. F., Tate, J. R., *Trans. Faraday Soc.*, **1966**, 62, 979; b) Killmann, E., Winter, K., *Angew. Makromol. Chem.*, **1975**, 43, 53.
- [127] Houk K. N., Leach A. G., Kim S. P., Zhang X., *Angew. Chem. Int. Ed.*, **2003**, 42, 4872.
- [128] Atkinson R., Arey J., *Chem. Rev.*, **2003**, 103, 4605.
- [129] <http://www.globalsecurity.org/military/systems/munitions/explosives.htm>.

CHAPTER 2

THE ITC TITRATION EXPERIMENT

Abstract:

In order to accomplish an ITC experiment for analysis and quantify the adsorption behavior in the systems studied in this work, different steps should be take on like: sample preparation, sample and reference cell loading, injection syringe loading, experimental parameters, control experiments, and data analysis. A typical ITC experiment requires only about 1-2 hours, with only a few minutes of “hand-on time”. ITC experiments are non-destructive and non-invasive and can be applied over a broad range of solution conditions, including turbid solution.

2.1 INTRODUCTION

The isothermal titration calorimetry (ITC) is a particular calorimetric method specially designed to measure small amounts of heat, generally associated to any process, be it exothermic or endothermic one, as it is the case of the physico-chemical interaction between two reactants, usually in a liquid solution. Measuring heats involved in successive series of interactions between the same partners one can determine their affinity and the associated thermodynamics parameters.^{1,2} If the ITC experiments are performed at different temperatures one can obtain the heat capacity variation, (ΔC_p). ITC is the only technique that is universally applicable to all reactions regardless of chemical nature or size of the interacting components, which does not require sample reloading between each concentration used to define the binding isotherm curve, and has a short equilibration and analysis time.³

2.2 DESCRIPTION OF THE ITC TITRATION EXPERIMENT

The following section describe an ITC experiment, which can be divided into the following steps: sample preparation, sample and reference cell loading, injection syringe loading, experimental parameters, control experiments, and data analysis; Figure 2.1 illustrated the ITC experimental preparation.

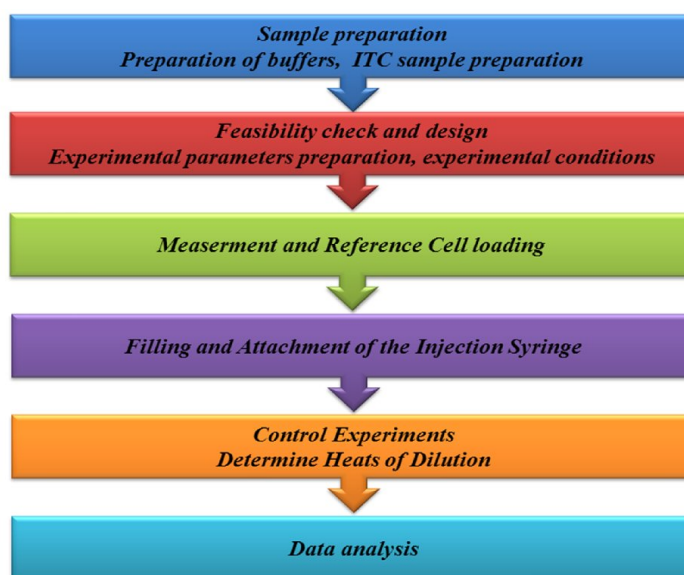


Figure 2.1: Overview of an ITC experiment.

2.2.1 Sample preparation

Sample preparation is a key step in achieving quality results with ITC. Two significant criteria should be paid attention in this part of ITC-experiment. Firstly, the solubility of the interacting components; both of the interacting molecules (*host* and *guest*) have to be in identical solutions (pH, buffer composition, ionic strength, reducing agent, detergent, etc.). ITC is very sensitive, and even small buffer mismatches can generate large heats of dilution with each injection, which can mask heat changes from ligand binding. Secondly, concentration of the interacting molecules; accurate determination of binding parameters is only possible if concentrations are known precisely. The correctness of stoichiometry, binding constant and enthalpy determination is directly proportional to the accuracy with which the syringe reactant concentration is determined. This is in contrast to the precision of the cell reactant concentration which only affects stoichiometry.⁴ Immediately prior to loading the sample cell and injection syringe, the guest (L) and host (M) solution are degassed to remove residual air bubbles. Even the smallest air bubbles remaining in the cell or injection syringe can interfere with the feedback circuit. Air bubbles can additionally lead to poor baselines.

2.2.2 Experimental parameters preparation

The parameters of the titration are input into the software program controlling data acquisition. The number, volume, and length of time of injections are critical and are discussed below. To determine accurately the enthalpy of binding, it is critical that the first several shots define a baseline region where all added guest is bound to the host. The equivalence region should also be well defined by the concentration range spanned by the injections, to determine an accurate value of the association constant. It is necessary that concentrations be chosen so that measurable amounts of free and bound guest are in equilibrium within the titration zone defined by the titrant injections. Several injections should be performed after complete saturation of the macromolecule by the guest.

The heat evolved or absorbed following saturation represents the heat of dilution of the titrant. The length of time of injection should be such that proper mixing is achieved. Typically 7- to 10- seconds injections of guest.⁵ To ensure proper mixing the injection syringe is fitted with a Teflon paddle and attached to a stirring motor by a rubber belt. Stirring at approximately 400 rpm should ensure good mixing.

2.2.3 Measurement and reference cell loading

The reference cell (Figure 1.17) usually contains water or buffer and need not be changed after every experiment. The cell reactant (usually but not necessarily the larger component of the interaction) is added to the (measurement) sample cell of the calorimeter using a long needle glass syringe. Typically, 1.5 to 2 ml of the solution is prepared to fill a cell with a volume of 1.3–1.5 ml. Once the cell is completely filled, several rapid additions of solution will dislodge any residual air bubbles that cling to the side of the cell. Any excess solution remaining in the reservoir is removed.

2.2.4 Filling and Attachment of the Injection Syringe

The syringe should be lowered gently and vertically to the bottom of the sample cell and the solution injected until a meniscus is observed at the top of the filling tube. The concentration of guest solution should be such that the molar ratio of guest molecule to host macromolecule, following the last injection, is approximately 2. Typically, a complete titration will involve approximately fifteen to fifty injections of guest (5- to 10- μ L).

Handling of the injection syringe is extremely critical, because of any bending of the injection syringe needle can result in some of the titrant solution being expelled into the macromolecule solution, causing the first injection to be useless. Any minor bending in the syringe can also result in poor baselines when the injection apparatus is stirring.

2.2.5 Control Experiments to Determine Heats of Dilution

The observed binding isotherm is usually normalized as kilocalories per mole of guest injected and plotted versus the molar ratio of guest to host. The observed heats of binding include contributions from the dilution of the titrant (such as: inorganic nanoparticles, solvents, anions, etc.) and dilution of the macromolecule (such as: polymers, dendrimers, etc.). A small contribution arising from stirring is also included in the observed binding enthalpy. Several control experiments must be performed to correct for the heats of dilution. The heat of dilution of the guest is usually the most significant. This is generally true since the initial concentration and the dilution factor for the guest molecules are typically 10–20 times greater than those of the macromolecule. The heat of dilution of the guest can be determined by performing an identical titration experiment in which guest is injected into a sample cell containing buffer only (no macromolecule). The heat of dilution of the macromolecule (which is typically less significant than the heat of dilution of the guest) is determined by titrating buffer solution into the sample cell containing the macromolecule. The two heats of dilution are used to correct the concentration-normalized binding isotherm. Since injection of guest following saturation of the molecule is essentially a measurement of the heat of dilution of the guest, the measured enthalpies of the last several injections can be averaged and subtracted to correct for heats of dilution.

2.2.6 Data analysis

The data analysis was performed using the ORIGIN[®] 7.0 based software. The thermodynamic parameters (K_B , ΔH) were estimated as adjustable parameters in the fitting procedure: one set of sites and two set of sites, to the experimental data using a nonlinear least-squares approach (Levenberg-Marquardt algorithm).^{6, 7} The heat content is just the product of the excess enthalpy per mole of macromolecule, $\langle \Delta H \rangle$, the total concentration of macromolecule (both bound and free), $[M]_{tot}$, and the volume. Thus, the heat for injection number i is given as:

$$Q_i = (\Delta H)_i [M]_{tot,i} \cdot V_{cell} - (\Delta H)_{i-1} [M]_{tit,i-1} (V_{cell} - V_{inj}) \quad (2.1)$$

In the case of one-to-one binding, the excess enthalpy is given as:

$$(\Delta H) = \Delta H \frac{K[L]}{1 + K[L]} \quad (2.2)$$

Experimentally, the total concentration of guest (i.e., the sum of both bound and free) is known, but the concentration of unbound guest is not and must be calculated from known quantities. In setting up the experiment, the concentration of macromolecule (host) initially in the cell of the calorimeter and the concentration of titrant (guest) initially in the syringe are both known quantities (typically with uncertainties on the order of 5 to 10%). Because an equal volume of the solution in the calorimeter cell is ejected from the cell with each injection of titrant, the concentration of macromolecule decreases at injection number i as:

$$[M]_{tot,i} = [M]_{tot,0} D^i \quad (2.3)$$

where $[M]_{tot,i}$ is the total concentration of macromolecule in the cell after injection step i , $[M]_{tot,0}$ is the total concentration of macromolecule in the cell before any injections are made, and D is a dilution factor defined as:

$$D = 1 - \frac{V_{inj}}{V_{cell}} \quad (2.4)$$

Here, V_{inj} is the injection volume and V_{cell} is the volume of the calorimetric cell. The total concentration of the titrant increases with each injection step as:

$$[L]_{tot,i} = [L]_{tot,0} (1 - D^i) \quad (2.5)$$

where $[L]_{tot,i}$ is the total concentration of titrant solution after injection step I and $[L]_{tot,0}$ is the total concentration of titrant (guest) in the injection syringe. Using of Eqs. (2.3-2.5), the total concentration of macromolecule and guest at any step can be determined (the subscript i is omitted for clarity):

$$[M]_{tot} = [M] + [ML] = [M] \cdot (1 + K[L]) \quad (2.6)$$

Likewise, the total concentration of guest is given as:

$$[L]_{tot} = [L] + [ML] = [L] \cdot (1 + K[M]) \quad (2.7)$$

Eq. 2.6 can be rearranged to give the concentration of free [M] as:

$$[M] = \frac{[M]_{tot}}{1 + K[L]} \quad (2.8)$$

which can be substituted into Eq. 2.7 and rearranged to give the following quadratic expression:

$$K[L]^2 + (1 + K([M]_{tot} - [L]_{tot})) [L] - [L]_{tot} = 0 \quad (2.9)$$

Consequently, the concentration of free guest, [L], can be determined after any injection step from the known total concentrations of M and L using the quadratic equation:

$$[L] = \frac{-[1 + K([M]_{tot} - [L]_{tot})] + \sqrt{[1 + K([M]_{tot} - [L]_{tot})]^2 + 4K[L]_{tot}}}{2K} \quad (2.10)$$

The free concentration of guest from Eq. 2.10 can be substituted into Eq. 2.2 at each injection step. This result can then be substituted into Eq. 2.1 in order to give the expected heat for each injection. The fitting programs provided by instrument manufacturers use the above equations to find the values of K and ΔH that give a result in the best agreement between the calculated and experimental values of q at each injection. In addition to determining K and ΔH , ITC data are also fit for the best value of the stoichiometry, n , which does not appear in the above equations. Even for a system that is known to have a single guest binding site, the value of n can differ from unity.

2.3 TROUBLESHOOTING

Routine problems are expected during ITC experiments, most of which are easily corrected through practice. One common problem frequently observed is that the enthalpy of binding measured for the initial injection is less than that of subsequent injections. This is due to ligand solution slowly leaking from the injection syringe or due to the syringe plunger not being exactly flush with the driving piston. To avoid slow leakage of ligand from the injection syringe simply reduces the length of time that the injection syringe is in contact with the macromolecule prior to the first injection. Some equilibration following attachment of the injection apparatus is required. It is recommended that a baseline be initiated following the insertion of the injection syringe into the sample cell. The signal will level off on thermal equilibration of sample, reference cell, and jacket. The experiment should be started after the baseline has leveled and remained steady for several minutes. Low binding enthalpies measured after the initial injection can be observed if the injection syringe and drive piston are not exactly aligned. Aligning the drive piston exactly flat with the injection syringe can be a difficult task. The use of a magnifying glass will greatly aid in the proper alignment of the injection syringe and drive piston.

These problems can also be corrected by injecting a small volume of the ligand for the first addition and discarding the observed data. If a reinjection is used, the concentration of added ligand must be taken into consideration during analysis. Baseline stability is also a common problem occurring during ITC experiments and can arise for several reasons. As mentioned previously, a bent injection syringe can lead to poor baselines. Air bubbles can also result in reduced quality of baselines and can be corrected by degassing solutions longer (5–10 min should be sufficient) as well as by taking additional care in loading the sample cell. Condensation around the adiabatic jacket may also lead to poor baselines.

2.3 REFERENCES

- [1] Brandts J.; Lin L.-N.; Wiseman T.; Williston S.; Yang C.P., *AM LAB*, **1990**, 22,30-&.
- [2] Bundle D.R.; Sigurskjold W., *Method. Enzymol* , **1994**, **247**, 288–305.
- [3] Ward, WH.; Holdgate, GA., *Prog. Med. Chem.*, **2001**, 38, 309-376.
- [4] Labury J.E., *Thermochimica Acta*, **2001**, 380, 209–215.
- [5] Wiesman T; Willston S.; Brandts J.F. ; Lin L.N., *Anal. Biochem.*, **1989**, 179, 131-137.
- [6] Jelesarov, I.; Bosshard, H. R. *J. Mol. Recognit.* **1999**, 12, (1), 3-18.
- [7] Indyk L.; Fisher, H. F. *Methods Enzymol.* **1998**, 295, 350-364.

CHAPTER 3

ITC - A POWERFUL TECHNIQUE TO QUANTIFY INTERACTIONS IN POLYMER-INORGANIC HYBRID SYSTEMS

Abstract:

In this chapter, a detailed study of the adsorption process of surface active amphiphilic copolymers with various inorganic nanoparticles in a multicomponent solvent system has been demonstrated. Therefore, the influences of the accessibility, quantity and nature of the functional groups (non-ionic, zwitterionic and acidic) in the amphiphilic copolymers on the adsorption process were investigated. Moreover, the effect of the copolymer composition and the temperature on the binding affinity as well as adsorption mechanisms were studied and discussed. These studies show effectively the ability to quantify and analyse the adsorption behaviour in the polymer-inorganic hybrid systems by evaluation of the thermodynamic parameters (ΔH , ΔS , ΔG and K_B). Finally, the knowledge of the complete thermodynamic profile of the polymer/inorganic particle interaction leads to screening and improving of the binding strength and the binding affinity in the polymer-inorganic hybrid systems.

3.1 INTRODUCTION

In contrast to the drawbacks of the current synthetic methods (such as: the particles used are too costly, the dispersion in the matrix is not complete, or the hydrophobization is not stable during the extrusion) (*Chapter 1.2*), which are applied to modify the surface of inorganic particles with low molecular surfactants, two synthetic approaches have been established in our group to prepare surface functionalized inorganic particles to overcome these drawbacks.^{1,2} The first approach describes the formation and hydrophobization of particles by a single step using an inverse emulsion technique (Figure 3.1).³⁻⁵

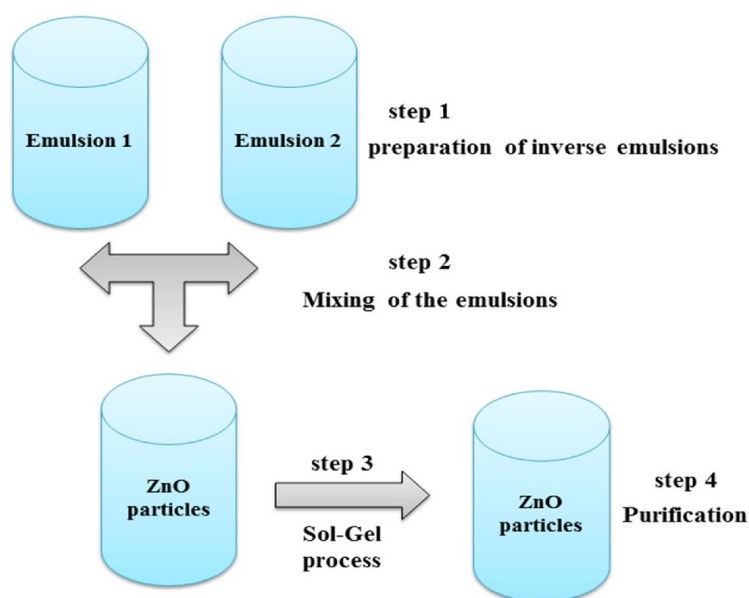


Figure 3.1: Preparation of ZnO particles, using an inverse emulsion technique.

These emulsions were stabilized by statistical amphiphilic copolymers obtained by free radical polymerization. In the first step two inverse emulsions were prepared from an aqueous solution of an inorganic salt and a precipitation agent, e.g. Zn(OAc) as the inorganic salt and NaOH as the precipitating agent to form ZnO particles, by ultrasonification of the aqueous salt solutions with a solution of the amphiphilic copolymer in toluene (Emulsion 1 and Emulsion 2). The amphiphilic copolymer serves as surfactant to stabilize both emulsions. In step 2, the two emulsions were combined and treated by ultrasound to guarantee a perfect mixing. In step 3, the ZnO particles were formed inside the micelles by a sol-gel

process and after removal of the solvent, isolated and purified by washing with water (step 4). Various inorganic particles were synthesized by this method (such as: Cu, CdS and Ni),⁴ which indicated the broad versatility of this process.

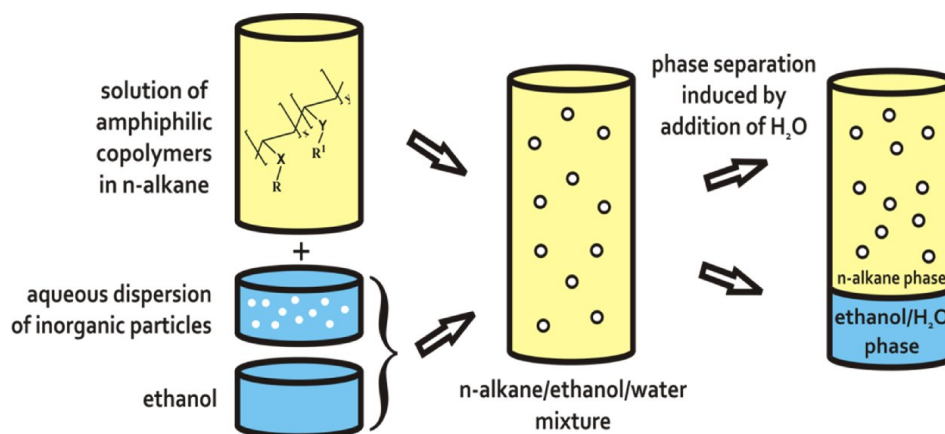


Figure 3.2: Illustration of the functionalization of the inorganic nanoparticles in the multicomponent solvent system.

The second approach (Figure 3.2) depicts the quantitative transfer of readily available inorganic particles from their aqueous dispersions into non-polar environment by using a latent miscible multicomponent solvent system in combination with surface active amphiphilic copolymers.^{2, 6} Particularly, the functionalization of inorganic nanoparticles in a multicomponent solvent system is a two-step procedure. The quantitative transfer of the hydrophilic inorganic nanoparticles into the non-polar phase is achieved after the phase separation. The aqueous dispersion of inorganic nanoparticles was first diluted with ethanol before mixing with the copolymer solution. The role of ethanol is to suppress the miscibility gap between the non-polar phase and the aqueous dispersion of the particles. Further addition of water compensates this effect and leads to a phase separation.

An example of this method is the surface functionalization of the SiO₂ particles with amphiphilic copolymers. The used amphiphilic copolymer was prepared by free radical polymerization of (EHMA), poly (ethylene glycol) methacrylate (PEGMA) and 2-(dimethylaminoethyl) methacrylate (DMAEMA) in various compositions. After dissolving the amphiphilic copolymers in the non-polar

phase, this solution was combined with the aqueous dispersion of the SiO₂ particles, which had been preliminarily diluted with the alcohol. As a result, a clear monophasic solution was formed. After inducing the phase separation by increasing the amount of water, the functionalized SiO₂ particles were exclusively present in the non-polar phase. The functionalized SiO₂ particles were isolated by removing the polar phase, and were fully re-dispersible in common organic solvents without any further aggregation. Recently, different inorganic particles (like: Al₂O₃, CeO₂ and TiO₂) can also be functionalized by this method.⁷ However, a fine tuning of the amphiphilic copolymers, in regard to the surface characteristics of the inorganic particles, was necessary. Therefore, understanding the adsorption and intermolecular interactions of these polymeric surfactants on the inorganic nanoparticles surfaces is the key to knowing how these molecules act as stabilizers against particle aggregation.

Consequently, the ITC technique was presented in this work as a method for analyzing and quantifying the mechanisms of adsorption and intermolecular interactions in polymer-inorganic-hybrid systems. Hereby, the thermodynamic parameters of the non-covalent interactions between the polymeric surfactants and the inorganic particles will be determined. For this, the interaction of SiO₂, Al₂O₃, CeO₂, TiO₂, ZnO, ZrO₂ and Fe₃O₄ nanoparticles with surface active amphiphilic copolymers consisting of 2-ethylhexyl methacrylate (EHMA) as the hydrophobic part and poly-(ethylene glycol) methacrylate (PEGMA), 4-vinyl-1-(3-sulfonopropyl) pyridinium inner salt (4VPSB) and (ethylene glycol) methacrylate phosphate (EGMP) as the hydrophilic part in a multicomponent solvent system have been studied (Figure 3.2).

3.2 EXPERIMENTAL SECTION

3.2.1 Materials

2-Ethylhexyl methacrylate (EHMA), poly(ethylene glycol) methacrylate (PEGMA^{n≈5}), 4-vinylpyridine (4VP), (ethylene glycol) methacrylate phosphate (EGMP), 1,3-propanesultone, 2-ethyl-1-hexanol, isobutyryl chloride and hexaethylene glycol were purchased from Aldrich and used as received. Methacryloyl chloride was obtained from Fluka. SiO₂ nanoparticles, with an average diameter of approximately 10 nm, were donated as a 30 wt.-% aqueous dispersion from Merck KGaA. Al₂O₃, CeO₂ and TiO₂ particles were applied in the form of their aqueous dispersion with an average diameter of approx. 25 nm for Al₂O₃, 10 nm for CeO₂ and 100 nm for TiO₂ (solids content: 25 wt.-% for Al₂O₃; 20 wt.-% for CeO₂; 10 wt.-% for TiO₂). 2-Ethylhexyl isobutyrate (EHIB) and poly(ethylene oxide) isobutyrate (PEOIB) were prepared from methacryloyl chloride and 2-ethyl-1-hexanol and hexaethylene glycol, respectively. Therefore, 2-ethyl-1-hexanol/hexaethylene glycol (25 mmol) was dissolved in 80 mL dichloromethane and triethylamine (25 mmol) was added. The mixture was cooled to 0 °C and isobutyryl chloride (26 mmol), dissolved in 20 mL dichloromethane, was slowly added over a period of 30 minutes. After stirring for 24 hours, the formed colorless precipitate was filtered off. The resulting solution was washed twice with 25 mL of brine and twice with 10 wt.-% aqueous solution of sodium hydrogen carbonate. After drying the extract with anhydrous sodium sulfate, colorless oil remained (75 % yield). 1-(3-Sulfopropyl)-4-vinylpyridinium betaine (4VPSB) was prepared according to the described procedure in the literature.⁷ The amphiphilic copolymers PEHMA-co-PPEGMA^{n≈5}, PEHMA-co-P2EM, PEHMA-co-PEGMP and PEHMA-co-P4VPSB were prepared by free radical polymerization of EHMA and PEGMA^{n≈5}, EGMP respectively 4VPSB, as described in the literature (molar ratio of EHMA:PEGMA^{n≈5} = 85:15, PEHMA:PMOEPa = 85:15, EHMA:PEGMP = 85:15 and EHMA: P4VPSB = 85:15) (see Figure 3.3).⁸

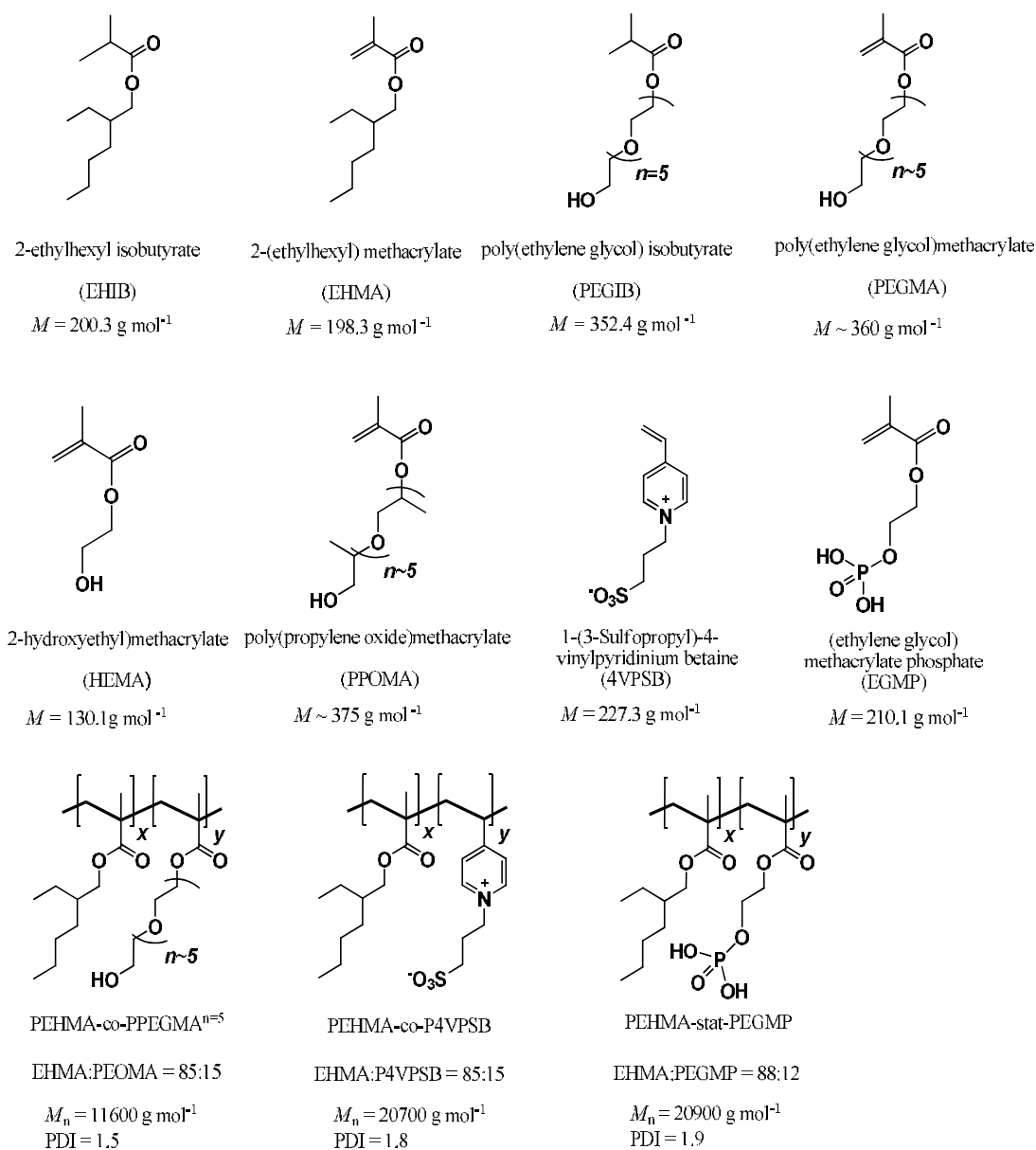


Figure 3.3: Chemical structure and molar mass of the monomers and amphiphilic copolymers used in this study.

3.2.2 Sample preparation

To carry out a binding experiment, the inorganic nanoparticle solution (55.6 μL of an aqueous SiO_2 dispersion (30 wt.-% in H_2O) in 1.5 mL 1,4-dioxane, 0.5 mL ethanol) was placed in the sample cell and the reference cell filled with the solvent mixture (1.5 mL 1,4-dioxane, 0.5 mL ethanol and 46.8 μL H_2O). Both cells were mounted in an adiabatic chamber, whose temperature was kept constant during the

measurement. A long-needle syringe (nominal volume 250 μL), with a twisted paddle fastened to its end, was filled with the solution of the organic compound (EHIB, PEOIB, EHMA, PEGMA^{n \approx 5}, HEMA, PPOMA^{n \approx 5}, 4VPSB, EGMP and the copolymers PEHMA-co-PPEGMA^{n \approx 5}, PEHMA-co-P4VPSB and PEHMA-co-PEGMP) in 7.5 mL 1,4-dioxane, 2.5 mL ethanol and 233.8 μL H₂O. The syringe was placed inside the sample cell and the entire syringe assembly was rotated continuously to provide proper mixing of the content of the sample cell within a few seconds after an injection (see *Chapter 2*).⁹

3.2.3 ITC measurement

All the measurements were studied at constant temperature of 298 K. After reaching thermal equilibrium, the injection of the ligand (polymer and/or copolymer) was automatically conducted stepwise until the metal oxide surface was saturated with the ligand. The first injection was set to very small volume of 1.5 μL (due to the possible dilution during the equilibration time preceding the measurement and then the first injection was ignored in the analysis of data),¹⁰ and was followed by 27/50 injections of 5/10 μL each. The chosen time interval between two consecutive injections was 300 sec in order to ensure that the thermodynamic equilibrium was reached prior to the next injection. The calorimetric data were analyzed by using the software Origin v7.0 Microcal Inc.

The following experimental parameters were set:

Number of injections:	28 and 51
Run temperature:	25°C
Reference power:	10 $\mu\text{cal/s}$
Initial delay:	200 s
Syringe concentration:	55 mM (<i>Monomers and/or Copolymers</i>)
Cell concentration:	16 mM (<i>inorganic particles</i>)
Stirring speed:	307 rpm
Injection volume:	250 μL
Duration:	3 and 21 s
Spacing:	300 s

3.2.4 Dilution experiment

In order to subtract the influence of the dissolving enthalpy of the ligand, a dilution experiment was conducted. In this experiment the ligand was injected into the sample cell, containing only the solvent mixture. The released/absorbed heat caused by the solvent enthalpy was subtracted from the data obtained from the titration of the metal oxide nanoparticles with the monomers or copolymers (Figure 3.4). After this subtraction, the normalized heat was plotted against the molar ratio of the polymer *versus* the inorganic particle.

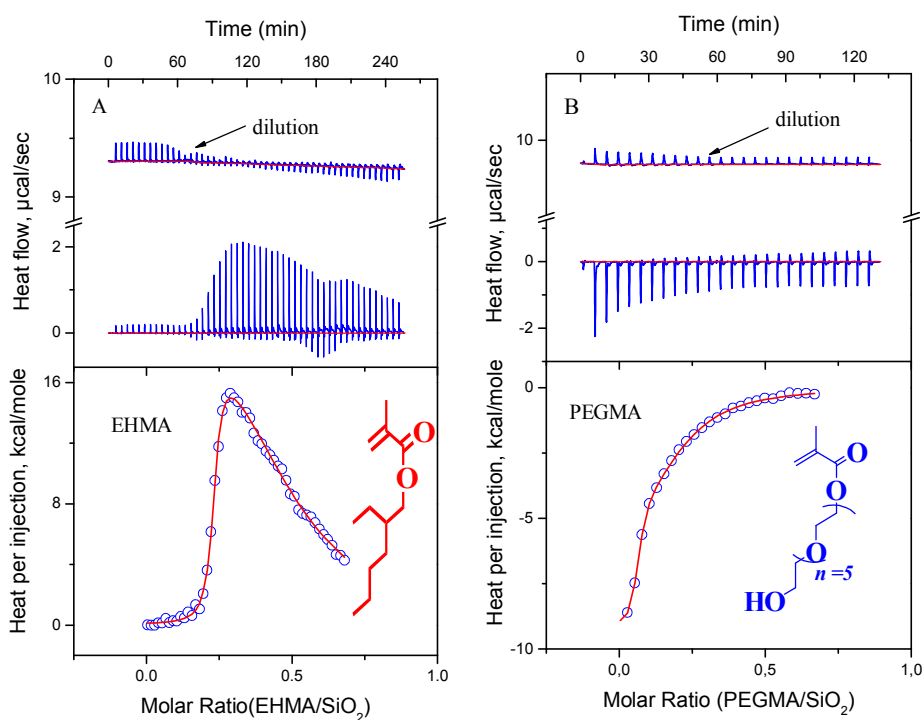


Figure 3.4: Binding isotherms and dilution measurement of 55 mM solution of. A) EHMA B) PEGMP in 1, 4-dioxane/ethanol/H₂O into a dispersion of SiO₂ (10 mg mL⁻¹) in the same solvent at 298 K.

RESULTS AND DISCUSSIONS

The interactions of metal oxide nanoparticles in a multicomponent solvent system with the hydrophobic monomer EHMA, the hydrophilic monomers PEGMA^{n≈5} (with 5 ethylene oxide units and OH terminal group), 2-hydroxyethyl methacrylate (HEMA), 4-vinyl-1-(3-sulfopropyl) pyridinium (4VPSB), P2EM and (ethylene glycol) methacrylate phosphate (EGMP) as well as the copolymers PEHMA-co-PPEGMA^{n≈5}, PEHMA-co-P4VPSB, PEHMA-co-PMOEPSA and PEHMA-co-PEGMP were investigated (see Figure 3.3).

In the first step, the adsorption of the SiO₂ inorganic particles with the low molecular weight EHMA, HEMA, PEGMA^{n≈5}, PPOMA^{n≈5}, EGMP and 4VPSB were analyzed, in order to obtain a better understanding of their role and influence during the interaction as well as to understand the mechanisms of the adsorption on the inorganic particle surfaces. SiO₂ was selected as the inorganic material to study the interactions with the low molecular weight model compounds due to its enormous relevance in the area of nanocomposites as impact modifiers and also as additive to improve scratch resistance.¹¹

In the second step, the adsorption of amphiphilic copolymer PEHMA-co-PPEGMA^{n≈5} on the surface of the SiO₂, Al₂O₃, CeO₂, TiO₂, ZnO, ZrO₂ and Fe₃O₄ particles were explored. Moreover, the copolymers PEHMA-co-P4VPSB, PEHMA-co-PMOEPSA and PEHMA-co-PEGMP were applied in an analogous manner to detect the impact of different classes of anchor groups (non-ionic versus zwitterionic or acidic) on their adsorption behavior.

To ensure reproducibility and to increase the accuracy of the results, each experiment was repeated at least three times under the same conditions. To illustrate the potential of the ITC as a novel tool to examine organic-inorganic hybrid materials, the measurements of the ITC experiments for EHMA, PEGMA^{n≈5} and PEHMA-co-PPEGMA^{n≈5} will be discussed in detail. All the other experiments were performed in a similar way only the decisive values will be given.

3.3 INTERACTION OF THE LOW MOLECULAR WEIGHT MODEL COMPOUNDS

3.3.1 Interaction of EHMA with the SiO₂ nanoparticles

In a first series of experiments, EHMA was applied as a model compound to monitor the influence of the hydrophobic part of the copolymers on the adsorption process. The ITC curve in Figure 3.5 shows the binding isotherm for the titration of a 55 mM solution of EHMA in 1,4-dioxane/ethanol/H₂O into a dispersion of SiO₂ (10 mg mL⁻¹) in the same solvent at 298 K. The observed thermogram indicated a complex adsorption behavior, since the first injections lead to weak endothermic process, which becomes larger after increasing of the EHMA concentration in the cell (dispersion of SiO₂) improved steadily to strong endothermic process, which reflect an increase in the endothermic interaction in the system. This endothermic process was coupled with weak exothermic process which can be related to the dilution interaction (see dilution measurement in Figure 3.5

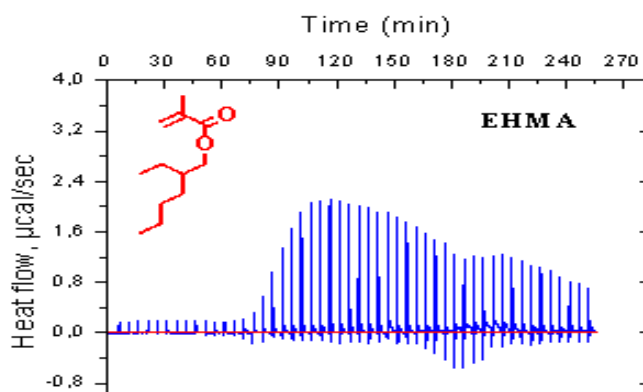
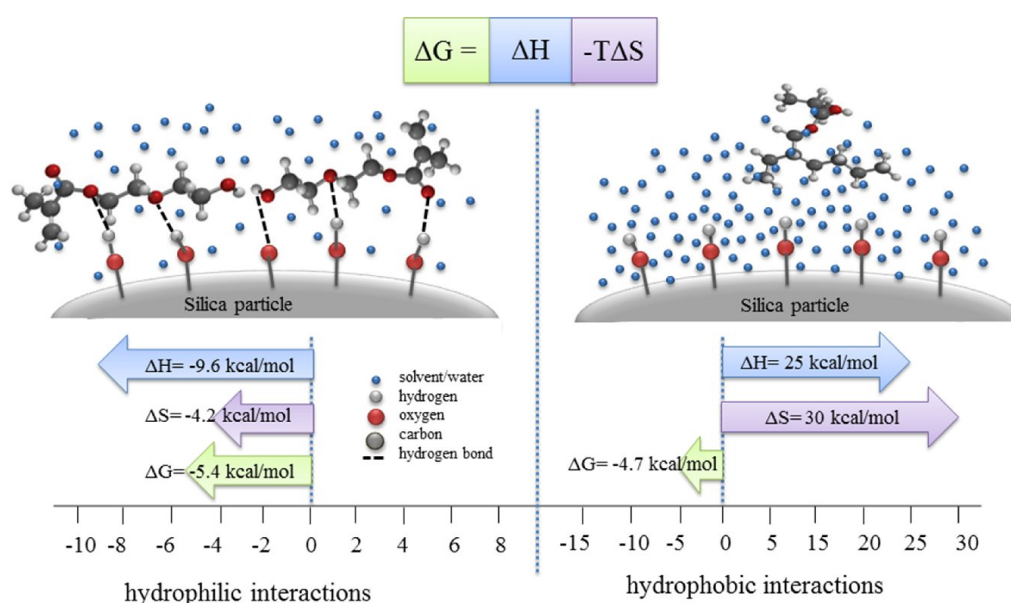


Figure 3.5: Binding isotherms for the titration of 55 mM solution of EHMA in 1, 4-dioxane/ethanol/H₂O into a dispersion of SiO₂ (10 mg mL⁻¹) in the same solvent at 298 K.

The determination of the thermodynamic parameters *via* a fitting procedure (see *Chapter 1.6* and *2.2.6*) indicating that a hydrophobic process was dominating in this system (Table 3.1). Evaluation of this data by integration followed a non-linear least-square approach (*Levenberg-Marquardt algorithm*),^{12, 13} which leads to an entropically driven adsorption process with both positive entropy (30.11 kcal/mol) and enthalpy (25.50 kcal/mol) contributions (Table 3.1). Such a thermodynamic profile is usually characteristic for hydrophobic interactions.¹⁴⁻¹⁶

In general, ΔH primarily reflects the strength of the non-covalent interactions between the monomers/copolymer and the surface of the SiO_2 nanoparticles (e.g. van der Waals, hydrogen bonds, etc.)¹⁷ relative to those existing within the solvent.¹⁸ As a result of the obtained values of ΔH for the titration of SiO_2 with EHMA, no interaction of EHMA with the particle surface occurred. The entropy change (ΔS) reflects a change in the order of the system due to two contributions: a favorable (positive) and unfavorable (negative) entropy change (Scheme 3.1).



Scheme 3.1: Schematic representation of the changes in enthalpy (ΔH), entropy (ΔS), and Gibbs free energy (ΔG) in the interactions of monomers on the surface of SiO_2 nanoparticles (for more detail see *Chapter 3. 3. 2 and 3.4.1.1*).

The positive value of ΔS could be attributed to a collapse of the so-called “iceberg structure”,¹⁹ which was caused by water and/or solvent molecules surrounding the hydrophobic chain of EHMA forming rigid, ice-like assemblies and also resembling icebergs. At the same time solvent molecules were transferred from the solvation shell of EHMA to the bulk, which also represented an entropy increasing process.^{20, 21} In conclusion, this thermodynamic investigation of the EHMA/ SiO_2 interaction, confirmed as expected the role of EHMA to impart hydrophobicity to the SiO_2 particles in stabilization process for inorganic particles.²

3.3.2 Interaction of PEGMA, EGMP and 4VPSB with the SiO₂ nanoparticles

The monomers PEGMA, EGMP and 4VPSB were investigated in a similar manner to EHMA, as a model compound to monitor the influence of the hydrophilic segment of the copolymers on the adsorption process. In detail, the binding isotherm of the interaction of a 55 mM solution of PEGMA^{n≈5} in 1, 4-dioxane/ethanol/H₂O into a dispersion of SiO₂ (10 mg mL⁻¹) in the same solvent at 298 K was presented in Figure 3.6 A. An exothermic effect for each titration step was observed. The first eight injections lead to strong exothermic effects, which become smaller the more PEGMA^{n≈5} is added to the cell.

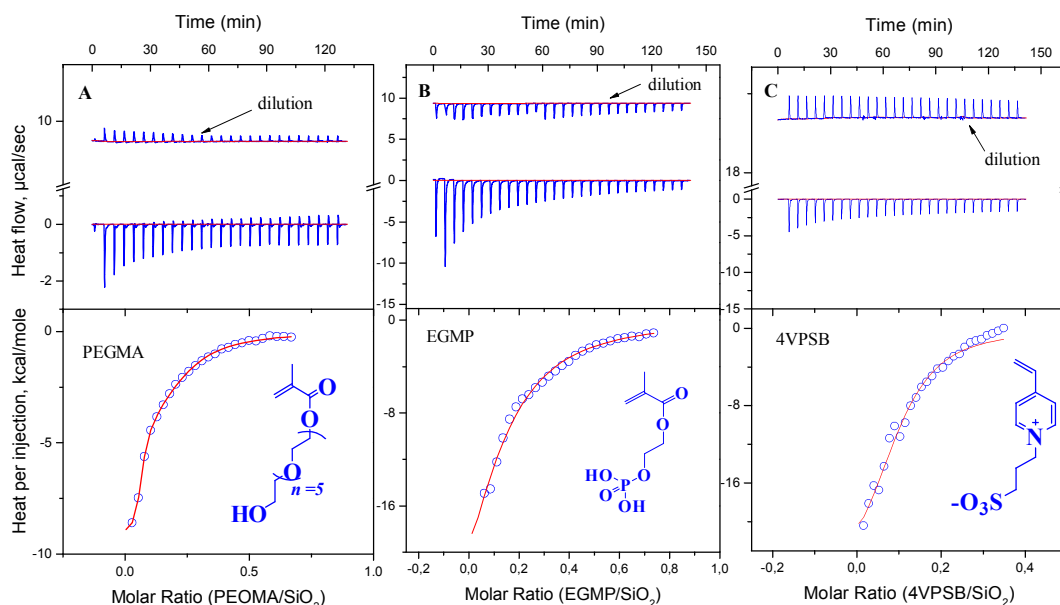


Figure 3.6: Binding isotherms for the titration of 55 mM solution of A) PEGMA, B) EGMP and C) 4VPSB in 1,4-dioxane/ethanol/H₂O into a dispersion of SiO₂) in the same solvent at 298 K.

This behavior was attributed to a direct interaction between the PEO chains and the hydroxyl groups on the SiO₂ surface^{22, 23} (a detailed study to analyse the role of PEO chain and the terminal hydroxyl on the PEGMA/ SiO₂ adsorption process was described in *Chapter 3.4.1.1*). In this case, the binding enthalpy ΔH was found to be negative (-9.60 kcal/mol) and compensated by a negative ΔS value (-4.20 kcal/mol) as illustrated in Figure 3.9 and Table 3.1. The obtained binding constant K_B ($6.1 \times 10^4 \text{ M}^{-1}$) corresponded to a moderate interaction affinity of this

monomer with the surface of the SiO₂ nanoparticles. The dominant negative enthalpy suggested that the presence of a large number of van der Waals interactions and/or hydrogen bonds between the monomer PEGMA and the SiO₂ particles.^{22,24} The entropy change (ΔS) mainly reflected the solvation entropy and changes in conformational entropy. The change in the solvation entropy occurred during the adsorption process, when the oxygen atom of the EO groups released the associated solvent molecules before interacting with the nanoparticle surface. This process yielded a positive change in entropy. At the same time, the adsorption of PEGMA with the SiO₂ nanoparticles resulted in the loss of the translational and conformational freedom, which caused a negative change in conformational entropy (see scheme 3.1).^{25,26} Since the overall entropy detected by ITC was negative, the highest impact on this term was represented by the change in the conformational freedom.

These results identify the use of the PEGMA monomers as a surfactant in a multicomponent system for stabilization of the inorganic particles by providing interactions with their surfaces.² Furthermore, to the best of our knowledge, no report has been published using the complete thermodynamic parameters (ΔH , ΔS , ΔG and K_B) to quantify and analyse the adsorption process of PEGMA monomers/copolymers on solid surfaces.²⁷⁻³⁰

Similarly, the adsorption of the EGMP and 4VPSB monomers on the SiO₂ nanoparticles surfaces were carried out. As illustrated in Figure 3.6 **B** the interaction of the 55mM solution of EGMP with the SiO₂ nanoparticles shows a strong exothermic effect in the first five injections, and it becomes smaller and similar to the reference peaks when the more EGMP was added to the cell. The shape of the titration curve for the EGMP-SiO₂ nanoparticles system was an indicative for a strong binding reaction. The calculated thermodynamic parameters for this interaction leads to an enthalpically driven adsorption process with a highly negative enthalpy of ($\Delta H = -29.85$ kcal/mol) and also negative entropy contribution ($T\Delta S = -23.39$ kcal/mol) (Table 3.1).

As expected, the observed thermodynamic profile confirmed a hydrophilic interaction between EGMP/SiO₂ surface driven by very strong hydrogen bonding and/or a covalent binding (see *Chapter 1*). This strong interaction (dependent on

the observed highly negative enthalpy contribution) can be related to the presence of the phosphate group, which can anchor strongly on the inorganic particle surface by replacing the surface hydroxyl groups (a detailed study to analyse the role of the phosphate group in the EGMP/inorganic particles adsorption process was described in *Chapter 3.4.3*).³¹⁻³⁵

Similar thermogram was obtained for the system 4VPSB-SiO₂ nanoparticles, but weaker than the EGMP with SiO₂ nanoparticles (Figure 3.6 C). A negative enthalpy ($\Delta H = -10.57$ kcal/mol) and negative entropy ($T\Delta S = -3.42$ kcal/mol) contributions were recorded. This thermodynamic profile was usually characteristic for hydrophilic interactions driven by electrostatic forces and/or hydrogen bonds formation. Additionally on the basis of binding constant K_B , which reflects the affinity of EGMP and/or 4VPSB with the surface of the SiO₂ particles, a stronger interaction affinity K_B ($4.34 \times 10^5 \text{ M}^{-1}$) was detected between EGMP molecules and the surface of SiO₂ particles, opposing an average interaction affinity of 4VPSB monomer on the SiO₂ particles was detected ($1.74 \times 10^4 \text{ M}^{-1}$).

3.3.3 Influence of the accessibility of functional groups on the adsorption process

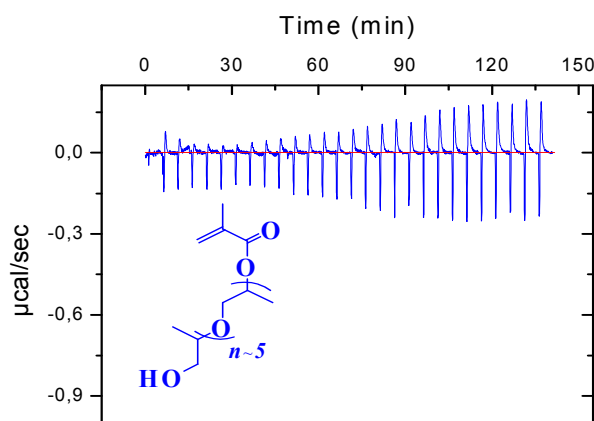


Figure 3.7: Binding isotherms for the titration of 55 mM solution of PPGMA^{n≈5} in 1,4-dioxane/ethanol/H₂O into a dispersion of SiO₂ (10 mg mL⁻¹) in the same solvent at 298 K.

In addition, the effect of the accessibility of the ethylene oxide units (EO) on the interaction with the inorganic particles surfaces was studied. If the EO units were sterically shielded as in PPGMA^{n≈5} by a CH₃-group, the interaction enthalpy ΔH

decreased dramatically from -9.60 to -0.22 kcal/mol as well as the binding affinity K_B from 6.10×10^4 to $1.58 \times 10^3 \text{ M}^{-1}$ (Figure 3.7 and Table 3.1).

This observation demonstrated clearly that the easy access of the interacting groups was of great importance for the interaction with the particle surface. For that reason, monomers having less accessible functional groups should not be considered as surfactant to stabilized inorganic particles.

3.3.4 Investigation of monomers versus polymers

Due to the fact that all measurements were conducted with monomers, yet the corresponding polymers consisted of their saturated analogs and the influence of the double bond had to be determined. Hence, the corresponding saturated compounds EHIB (2-Ethylhexyl isobutyrate) (as the analog of EHMA) and PEGIB (poly (ethylene glycol) isobutyrate) (as the analog of PEGMA) were applied in the ITC measurements.

These results displayed an almost identical behavior compared to EHMA and PEGMA and so, no significant influence of the double bond on the adsorption behavior was monitored (see Figure 3.8 and Table 3.1). These results show that, the hydrophilic monomers can be directly applied in ITC measurements without the need to synthesize either model compounds or the amphiphilic copolymers.

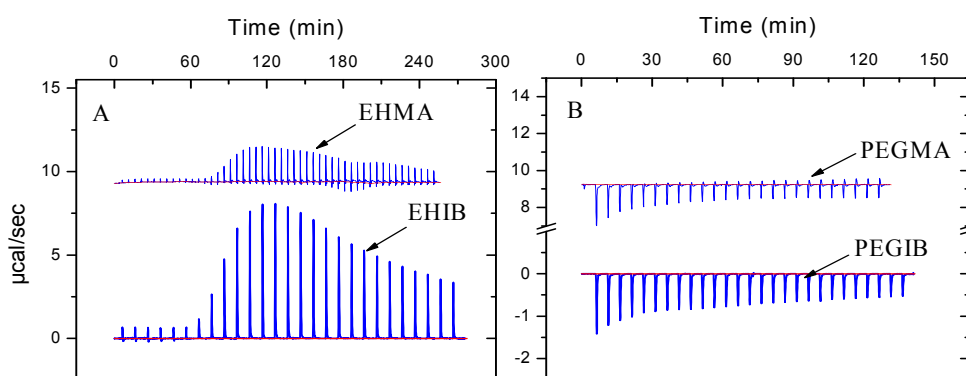
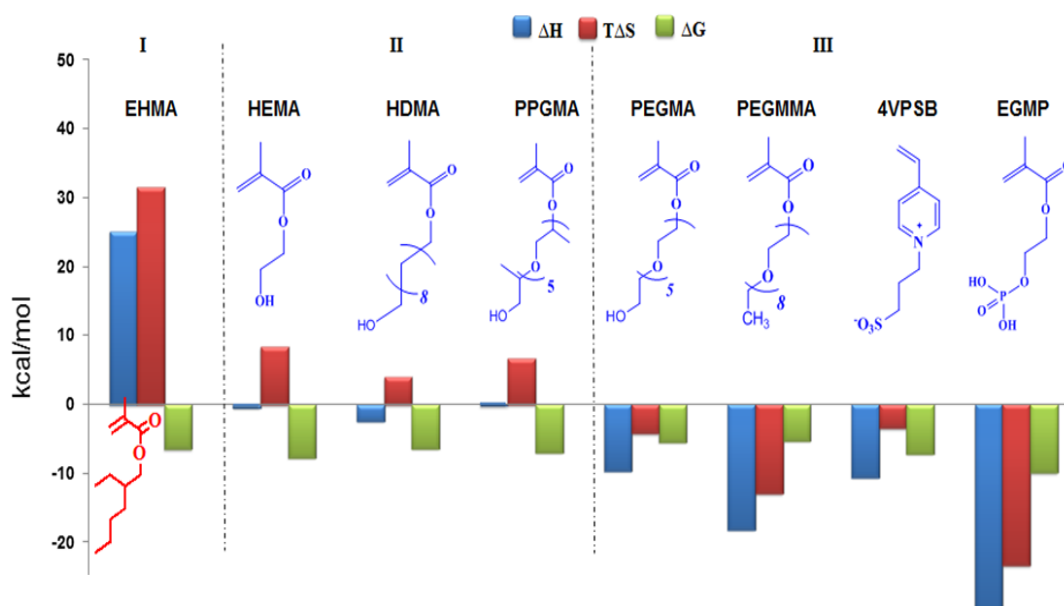


Figure 3.8: Binding isotherms for the titration of 55 mM solution of A) EHIB, B) PEGIB, in 1,4-dioxane/ethanol/H₂O into a dispersion of SiO₂ (10 mg mL⁻¹) in the same solvent at 298 K.

Table 3.1: Thermodynamic parameters obtained by the ITC measurements of the studied surface active compounds with SiO₂ nanoparticles at 298K.

Surface active Compound	K _B M ⁻¹	ΔH kcal/mol	TΔS kcal/mol	ΔG kcal/mol
EHIB	$(1.00 \pm 0.15) \times 10^5$	63.46 ± 2.70	70.36	-6.88
PEGIB	$(3.87 \pm 1.33) \times 10^4$	-13.60 ± 1.99	-7.33	-6.25
EHMA	$(1.70 \pm 0.62) \times 10^4$	25.50 ± 1.43	30.11	-4.61
PEGMA ^{n≈5}	$(6.10 \pm 0.65) \times 10^4$	-9.60 ± 1.23	-4.20	-5.40
HEMA	$(2.80 \pm 0.22) \times 10^6$	-0.50 ± 0.04	8.30	-7.70
HDMA	$(5.19 \pm 0.10) \times 10^4$	-2.40 ± 0.51	4.00	-6.40
PEGMMA ^{n≈8}	$(6.80 \pm 0.35) \times 10^3$	-18.10 ± 1.20	-12.90	-5.20
PPGMA ^{n≈5}	$(1.58 \pm 0.16) \times 10^3$	-0.22 ± 0.12	6.21	-6.43
4VPSB	$(1.74 \pm 0.30) \times 10^4$	-10.57 ± 1.24	-3.42	-7.15
EGMP	$(4.33 \pm 0.23) \times 10^4$	-29.85 ± 0.80	-23.39	-6.46

**Figure 3.9:** Schematic diagram presenting the thermodynamic profiles observed for the applied low molecular weight monomers on the SiO₂ nanoparticles.

In summary, the Figure 3.9 and Table 3.1 show that the thermodynamic profiles observed for the applied low molecular weight monomers bearing different classes of anchor groups (*non-ionic*, *zwitter-ionic* and *acidic*) as well as different

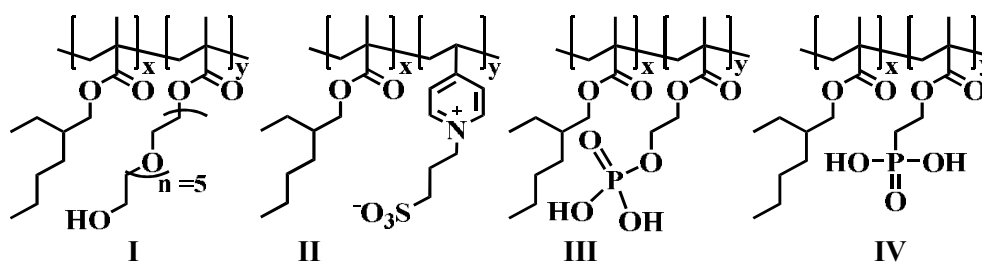
quantity of EO-groups on the surface of SiO₂ nanoparticles. The enthalpic and entropic contributions of binding differ noticeably for the monomers used. Several general characteristics binding processes can be observed: (I) Bindings take place with great unfavorable (positive) enthalpic changes (ΔH) and high favorable (positive) entropic changes (ΔS), such as the adsorption of the EHMA with the SiO₂ surface. This thermodynamic profile is specific for an interaction dominated by hydrophobic forces. (II) Interactions with small favorable (negative) enthalpic changes (ΔH) and low favorable (positive) entropic changes ΔS , like in the interaction of the monomers (HEMA, HDMA and PPOMA) with the SiO₂ surface. This thermodynamic signature indicates an adsorption process dominated by hydrophobic forces, but accompanied with weak electrostatic forces (van der Waals, H-bonding, etc.) (see *Chapter 3.4.4.1*). (III) Bindings occurred with high favorable (negative) enthalpic changes (ΔH) and lower unfavorable (negative) entropic changes ΔS , such as the interaction of (PEGMA, PEOMMA, 4VPSB and EGMP) with the SiO₂ surface. This thermodynamic signature indicates a predominantly enthalpic binding, driven by electrostatic forces.

These results reflect the importance of low molecular weight monomers and also the nature of their anchor groups to stabilize the inorganic particles. Therefore, selecting monomers bearing a high number of anchor groups and/or functional groups able to build strong interactions with the surface of the inorganic particles is an important requirement to synthesize a suitable surfactant. Generally, these studies offer for the first time, a complete and comprehensive thermodynamic study of monomer/inorganic particles adsorption process in solution. An illustration of the usefulness of the microcalorimetry method is illustrated by the study of the effect of different classes of anchor groups on the binding affinity, enthalpy and the entropy of the adsorption without need to complex data evaluation and/or employing another supporting technique.³⁶⁻³⁸

3.4 INTERACTIONS OF THE HIGH MOLECULAR AMPHIPHILIC COPOLYMERS

In contrast to the low molecular weight surfactants, polymeric surfactants have a great number of anchor groups which can bind to the surface of the particles. Similar to the *chelation effect* in complex chemistry,^{39, 40} this should lead to increase interactions between the high molecular weight amphiphilic compounds and the particles. This may be the key to the stabilization of inorganic particles under uniform conditions and related functionalization.

In the present section, the adsorption behaviors of four different amphiphilic copolymers (Scheme 3.2) with various common inorganic particles (SiO_2 , Al_2O_3 , CeO_2 , ZnO , ZrO_2 , TiO_2 and Fe_3O_4) were studied. All this amphiphilic copolymers (*synthesis by Stelzig et. al*)^{41, 42} were studied in a similar way as it was described for the low molecular weight compounds.



Scheme 3.2: Chemical structures of amphiphilic copolymers bearing different anchor groups: **I**) PEHMA-co-PPEGMA, **II**) PEHMA-co-P4VPSB, **III**) PEHMA-co-PEGMP and **IV**) PEHMA-co-PMOEPA applied in this study.

3.4.1 Non-ionic amphiphilic copolymer /PEHMA-co-PPEGMA

Copolymers bearing a non-ionic anchor groups i.e. polyethylene glycol (PEG) were used in many biochemical and industrial applications.⁴³ Due to its nontoxic character and it can be found in cosmetics, food, and pharmaceutical products.⁴⁴ The mild action of PEG on the biological activity of cell components explains the success of this polymer in biotechnological applications. PEG is commonly used for liquid–liquid partitioning and precipitation of biomacromolecules.^{45, 46} All these applications make PEG by far the most widely used polymer in aqueous solutions of biological molecules.⁴⁷

Here in this chapter the interaction of the copolymer (PEHMA-co-PPEGMA^{n≈5}) and the inorganic particles was studied. Experimentally, in the beginning the titration of SiO₂ particles with the copolymer PEHMA-co-PPEGMA^{n≈5} was carried out (Figure 3.10). The raw data obtained from this experiment resembled with the one of PEGMA^{n≈5} (*Chapter 3.3.2*). The thermodynamic data exhibited a favorable negative enthalpy ($\Delta H = -2.18$ kcal/mol) and favorable positive entropy values ($T\Delta S = 1.84$ kcal/mol).

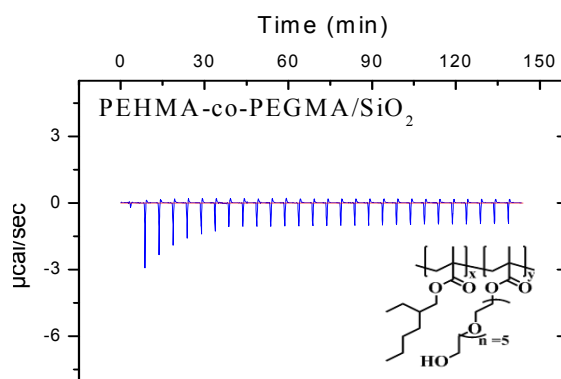


Figure 3.10: Binding isotherm for the titration of 55 mM solution of PEHMA-co-PPEGMA into a dispersion of SiO₂ at 298 K.

The measured thermodynamic parameters suggest a hydrophilic dominated interaction (i.e. hydrogen bond formation) accompanied by solvent rearrangement and hydrophobic forces (Table 3.3). Relating to the observed enthalpy contribution of the PEHMA-co-PPEGMA^{n≈5}/SiO₂ adsorption process, the interaction of the copolymer was unexpectedly weaker than that found for the PEGMA/SiO₂ interaction (*Chapter 3.3.2*). This can be related to: firstly, the difficulty of access of the function groups (EO and/or the terminal hydroxyl group) in the PEGMA monomer to reach the surface of SiO₂ particle (a detailed study to clarify the PEGMA/SiO₂ adsorption mechanism was described in *Chapter 3.4.1.1*). Secondly, the presence of the EHMA monomer in the system, which increases the entropy of the system and as result, leads to decrease the enthalpy of the interaction (see *Chapter 1.6* and *3.3.1*).

3.4.1.1 The PEHMA-co-PPEGMA/SiO₂ particle adsorption mechanisms

A comparison of all binding experiments performed herein pointed to the existence of different mechanisms for the adsorption processes of the applied compounds. For example, the adsorption of the copolymer PEHMA-co-PPEGMA^{n≈5} and the hydrophilic segment PEGMA revealed an exothermic interaction (i.e. enthalpy driven process), whilst an endothermic process was found (entropy driven process) in case of EHMA. This outcome suggested that the different interaction patterns of the monomers as well as the copolymer with the surface of the SiO₂ particle. Based on the obtained results for PEHMA-co-PPEGMA^{n≈5}, the copolymer showed a similar adsorption behavior as the hydrophilic PEGMA^{n≈5} monomer (Figure 3.6A). That means that the hydrophobic monomer (EHMA) does not react on the particles surface at all, therefore this monomer can as expected only act as a compatibilizer of the hybrid particles in the polymer matrix.²

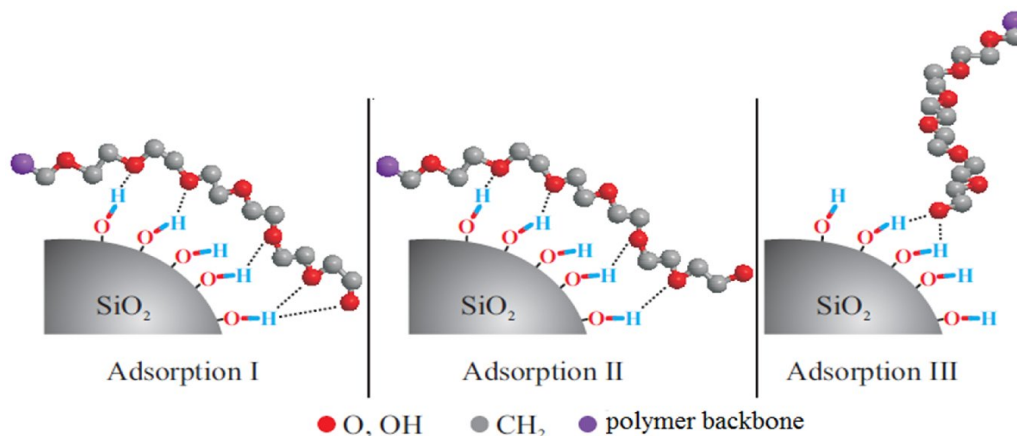


Figure 3.11: Possibilities of interactions of the PEO side chain with the surface of the SiO₂ particles Adsorption (I): interaction of the terminal hydroxyl group and Ether function groups; (II) adsorption interaction only through the Ether function groups; (III) adsorption interaction only via the terminal hydroxyl function.⁴²

In detail, the hydrophilic part of the amphiphilic copolymer (PEHMA-co-PPEGMA^{n≈5}) that holding two potential groups (ether oxygen and the terminal hydroxyl group) are responsible for the interactions with the OH groups on the SiO₂ particle surface.

The question at this point, which of the two groups was dominant or whether both groups in about equal measure contributed to the adsorption process. There were basically three ways of interaction imaginable. *First*, the interaction could take place on both the ether oxygen of PEG chain and the terminal hydroxyl function. *Second*, the interaction was almost entirely achieved through the ether oxygen, or *third*, for the interaction was only the terminal hydroxyl group responsible (Figure 3.11).

In order to inspect the mechanisms of the adsorption process on the inorganic particles in detail, the interaction of different monomers with the SiO₂ particle surfaces was studied. For this purpose, monomers with either terminal hydroxyl group (OH) or ethylene oxide groups (EO) bearing were used (see Figure 3.3 and Figure 3.9). Practically the monomers HEMA (2-Hydroxyethylmethacryl) and HDMA (10-Hydroxydecylmethacryl) were used to study the OH group's effect together with the effect of the methylene chain length (Figure 3.12 A and B). The monomer PEGMMA (Poly (ethylene glycol) methyl methacrylate) without a terminal OH group was used to study the role of the EO groups in the adsorption process with the inorganic particle surfaces (Figure 3.12 C).

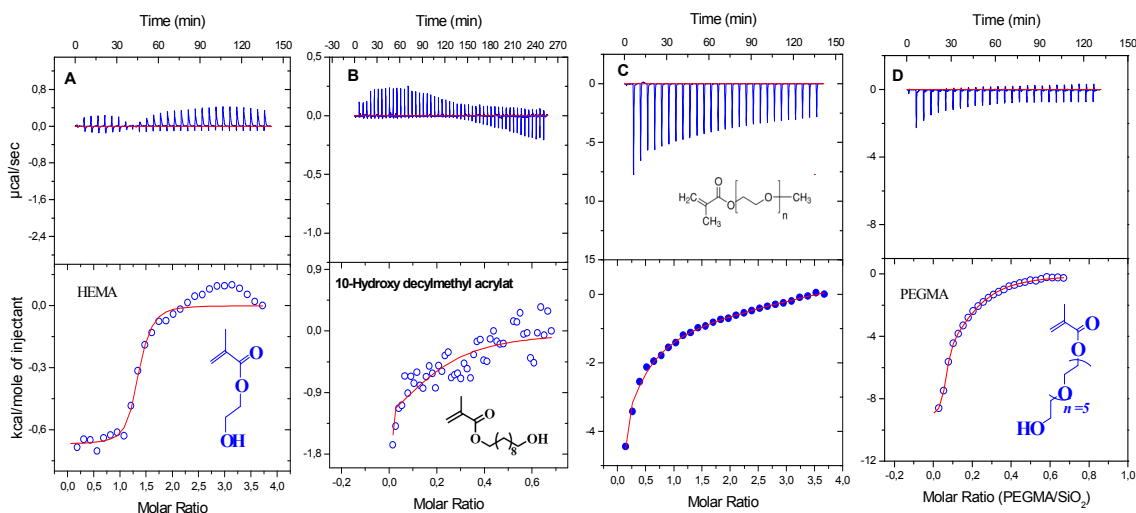


Figure 3.12: Binding isotherms for the titration of a 55 mM solution of A) HEMA, B) HDMA, C) PEGMMA and D) PEGMA ⁿ⁼⁵ in 1,4-dioxane/ethanol/H₂O into a dispersion of SiO₂ (10 mg mL⁻¹) in the same solvent at 298 K.

In detail, the binding isotherm of the adsorption of the 55 mM solution of HEMA into the dispersion of SiO₂ at 298 K shows at the beginning a small exothermic

effect followed by an endothermic process (Figure 3.12 A), the evaluation of the thermodynamics data leads to an entropically driven interaction with positive entropy ($T\Delta S = 8.30$ kcal/mol) and small negative enthalpy of ($\Delta H = -0.50$ kcal/mol) (see Table 3.1). Such a thermodynamic profile is usually characteristic for hydrophobic interactions comparable with very weak hydrogen bonding interactions (see *Chapter 1.4*). On the other hand the interaction of the HDMA monomer with the SiO_2 nanoparticles showed a weak endothermic process followed by an exothermic process but weaker than the interactions of the EGMP and/or PEGMA monomers (Figure 3.6). Higher negative enthalpy contribution of ($\Delta H = -2.40$ kcal/mol) and lesser positive entropy contribution ($T\Delta S = 4.0$ kcal/mol) compared to HEMA were recorded. This thermodynamic profile reflects a hydrophobic interaction compared with a higher contribution of hydrogen bond formation than in the case of the HEMA monomer, however with lower binding affinity (Figure 3.12 B and Table 3.1).

On the other hand the functionalization of SiO_2 particle with PEGMMA monomer (with 8 EO-units) (Figure 3. 12 C) leads to highly dominant negative enthalpy contributions ($\Delta H = 18.10$ kcal/mol), which can be related to a large number of formed hydrogen bonds between the PEGMMA and the surface of the SiO_2 particle. This result confirmed our expectation that increase of the anchor groups in the monomer/polymer backbone enhanced the possibility of the monomer / polymer to interact with the surface of the inorganic particle.

The thermodynamic parameters observation for the monomers HEMA and HDMA also showed, however, that there is an interaction of its OH groups with the OH groups of the SiO_2 particle, but this was weak as compared to that of the total EO units. Likewise in the case of the ΔH value of PEGMMA monomer which was about 36 times greater than that of HEMA. As it can be recognized from the observed thermodynamic profiles (Table 3.1), the main interactions take place on the ethylene oxide units.

These indicate, unexpectedly, that the terminal hydroxyl group in the monomer was not necessary to get strong binding on the particle surfaces. Additionally the strength of the interaction increases again from PEGMA to PEGMMA.

The difference between the two monomers was the length of the side chain, although this is the case for PEGMMA with 3 EO-units longer.

In summary, these results demonstrate the dominant role of the EO function group to link the amphiphilic copolymers *via* hydrogen bonding to the inorganic particles surfaces. This specificity of hydrogen bonding between the surface hydroxyls and the ether oxygen of PEG may be utilized to synthesize polymers that predominantly adsorb *via* hydrogen bonding. This could be of major significance, for example, in processing of low-grade mineral ores and purification of ceramic powders.^{48, 49}

3.4.1.2 The influence of the copolymer composition on the adsorption process

From the above findings, specifically the adsorption of copolymer/SiO₂ particles takes place solely by the hydrophilic segment of the copolymer (*Chapter 3.4.1.1*). This leads to the question of the influence of the composition of the copolymer (hydrophilic vs. hydrophobic), as well as the lower limit of the PEGMA amount in the copolymer, to achieve even a sufficient adsorption.

To have a sufficiently stable interaction of the copolymer with the surface of the particle, high number of PEG side chains may be required. Furthermore, an upper limit on the proportion of PEGMA should exist, since the increasing hydrophilic character of the copolymer would lead to its insolubility in the non-polar solvents. In order to get an indication of the upper and lower limit of the mol-% of PEGMA, whose share in the copolymers at levels of 4, 10, 15 and 18 was varied (Table 3.2).⁴² For better comparability with the previous experiments of PEHMA-co-PPEGMA/SiO₂ in the multicomponent system (1, 4-dioxane/ethanol/H₂O) (*Chapter 3.4.1*), for the copolymers **I**, **III** and **IV**, the same reaction conditions were applied. Experimentally, as illustrated in Figure 3.13, all the interactions of the copolymers **I-IV** with the surface of SiO₂ nanoparticles show an exothermic effect, which decreased slightly during the addition of the copolymers **I-IV** into the sample cell (SiO₂ nanoparticles).

The calculated thermodynamic parameters for these interactions lead to an entropically driven process change to an enthalpically driven process with the increase of the hydrophilic PEGMA mol-% (Table 3.2).

Table 3.2: Thermodynamic parameters for the titration of PEHMA-co-PPEGMA with different hydrophilic PEGMA –mol-% I) 96:04, II) 90:10, III) 86:15 and IV) 82:18 at 298 K.

PEHMA-co-PEGMA	K_B M^{-1}	ΔH kcal/mol	$T\Delta S$ kcal/mol	ΔG kcal/mol
Copolymer I 96:04	$(1.63 \pm 0.11) \times 10^3$	-0.15 ± 0.04	4.32	-4.47
Copolymer II 90:10	$(3.69 \pm 0.19) \times 10^3$	-1.96 ± 0.50	2.90	-4.86
Copolymer III 85:15	$(7.17 \pm 2.24) \times 10^3$	-3.18 ± 0.15	1.24	-4.42
Copolymer IV 82:18	$(2.28 \pm 0.44) \times 10^4$	-5.31 ± 0.25	0.79	-6.10

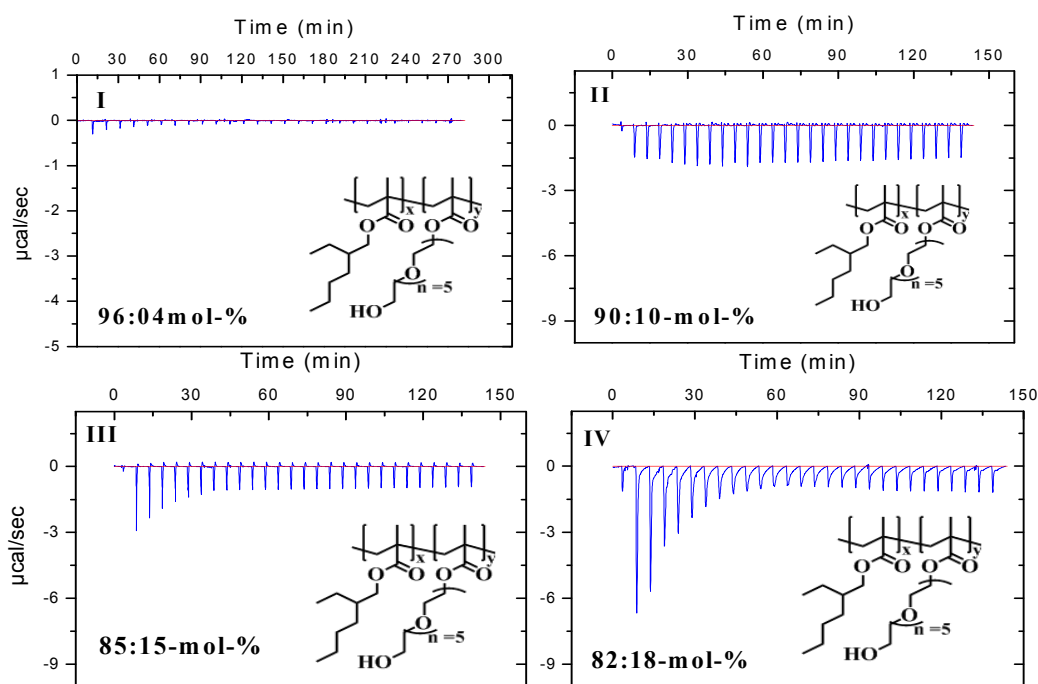


Figure 3.13: Binding isotherms for the titration of PEHMA-co-PPEGMA with different hydrophilic PEGMA –mol-% I) 96:04, II) 90:10, III) 86:15 and IV) 82:18.

In detail, the adsorption behavior of **copolymer I/SiO₂** with 96:4 mol-% results in an entropically driven process with high positive entropy value ($T\Delta S = 4.32$ kcal/mol) (Table 3.2), as compared to a small negative ΔH contribution of -0.15 kcal/mol.

This reflects that an insignificant interaction resulted from very weak hydrogen bond and/or van der Waals forces. The high entropy contribution suggests that an aggregation process that takes over in the system (as proved by SEM).⁴² On the other hand, increasing the amount of PEGMA to 10 mol-% as in the **copolymer II** leads to gain in the binding enthalpy to -1.96 kcal/mol with decreasing in the entropy contribution of 2.9 kcal.mol⁻¹.

This thermodynamic profile suggests an interaction taking place between the **copolymer II** and the SiO₂ particles through a weak hydrogen bond formation as compared to hydrophobic interaction process. Likewise, further increasing the amount of PEGMA to 18 mol-% as in the **copolymer IV** shows a noticeable gain in the enthalpy (ΔH) to -5.31 kcal/mol, which reflects a clear enthalpically dominant process (i.e. hydrogen bond formation) in the **copolymer IV/SiO₂**. The entropy contribution on the other hand shows no aggregation and/or solvation effect in this system.

Summing up the results for the adsorption of the **copolymers I-IV** with SiO₂ particle, the proportion of the hydrophilic PEGMA in the copolymers is of crucial importance for the successful functionalization: It requires a minimum PEGMA amount in the copolymer of about 10 mol% to reach a sufficiently stable adsorption (i.e. favorable ΔH contribution) with the inorganic particle surfaces. Attempts to functionalize SiO₂ particles with **copolymer I** showed that a molar proportion of PEGMA of 4 mol% was therefore not enough for a successful adsorption of the copolymer on the SiO₂ particle surface (i.e. favorable ΔH contribution) (see Table 3.2). However an increase in the hydrophilic PEGMA – mol-% leads to increased adsorption probability of the copolymer with SiO₂ particles surfaces. This outcome guides to choose the suitable amount of PEGMA units, which achieves a stable, irreversible adsorption of the copolymers on the surface of the SiO₂ particles. This was achieved with a total of about PEGMA 10-15 mol %.

3.4.1.3 Adsorption of PEHMA-co-PPEGMA with Al₂O₃, CeO₂, TiO₂, ZnO, ZrO₂ and Fe₃O₄ nanoparticles

After the successful characterization of the adsorption processes of the PEHMA-co-PPEGMA copolymer with SiO₂ particles using the ITC technique, the study was expanded towards the numerous inorganic particles such as Al₂O₃, CeO₂, TiO₂, ZnO, ZrO₂ and Fe₃O₄. The interactions with the inorganic particles were investigated in a similar manner as compared to SiO₂ particles (*Chapter 3.4.1*).

Table 3.3: Thermodynamic parameters obtained by the ITC measurements of the studied surface active compounds (PEHMA-co-PPEGMA) with Al₂O₃, CeO₂, SiO₂, TiO₂, ZnO, ZrO₂ and Fe₃O₄ particle.

surface-active compound	K _B M ⁻¹	ΔH kcal/mol	TΔS kcal/mol	ΔG kcal/mol
Al ₂ O ₃	(2.73 ± 0.61) x10 ⁴	0.04 ± 0.01	6.08	-6.04
CeO ₂	(2.71 ± 0.30) x10 ³	-0.20 ± 0.03	4.47	-4.67
Fe ₃ O ₄	(2.59 ± 0.60) x10 ³	-0.93 ± 0.04	3.42	-4.13
SiO ₂	(7.17 ± 0.24) x10 ³	-2.18 ± 0.15	1.84	-4.02
TiO ₂	(6.47 ± 1.07) x10 ⁴	-0.64 ± 0.12	5.90	-6.54
ZnO	(6.15 ± 0.41) x10 ³	0.36 ± 0.04	5.55	-5.18
ZrO ₂	(1.05 ± 0.05) x10 ⁴	-0.38 ± 0.08	5.81	-6.19

As calculated (Table 3.3) from the titration curves of the interactions (Figure 3.14), the enthalpic and entropic contributions to the free energy of binding differ noticeably for the inorganic particles used. Some of the general characteristics can be observed:

(i) Bindings with both favorable enthalpy ΔH (negative) and favorable entropy ΔS (positive) were detected, which shows that those bindings are dominated by hydrophobic forces, but characterized by weak electrostatic forces, suggesting that the inorganic particles were also established a number of bonds with the amphiphilic copolymers, like the interaction with CeO₂, TiO₂, ZrO₂ and Fe₃O₄ particles. (ii) Bindings occurred with unfavorable (positive) enthalpy ΔH and high favorable (positive) entropic changes ΔS, as the interaction with Al₂O₃ and ZrO₂

particles. This thermodynamic profile is specific for an adsorption process dominated by hydrophobic interactions only.

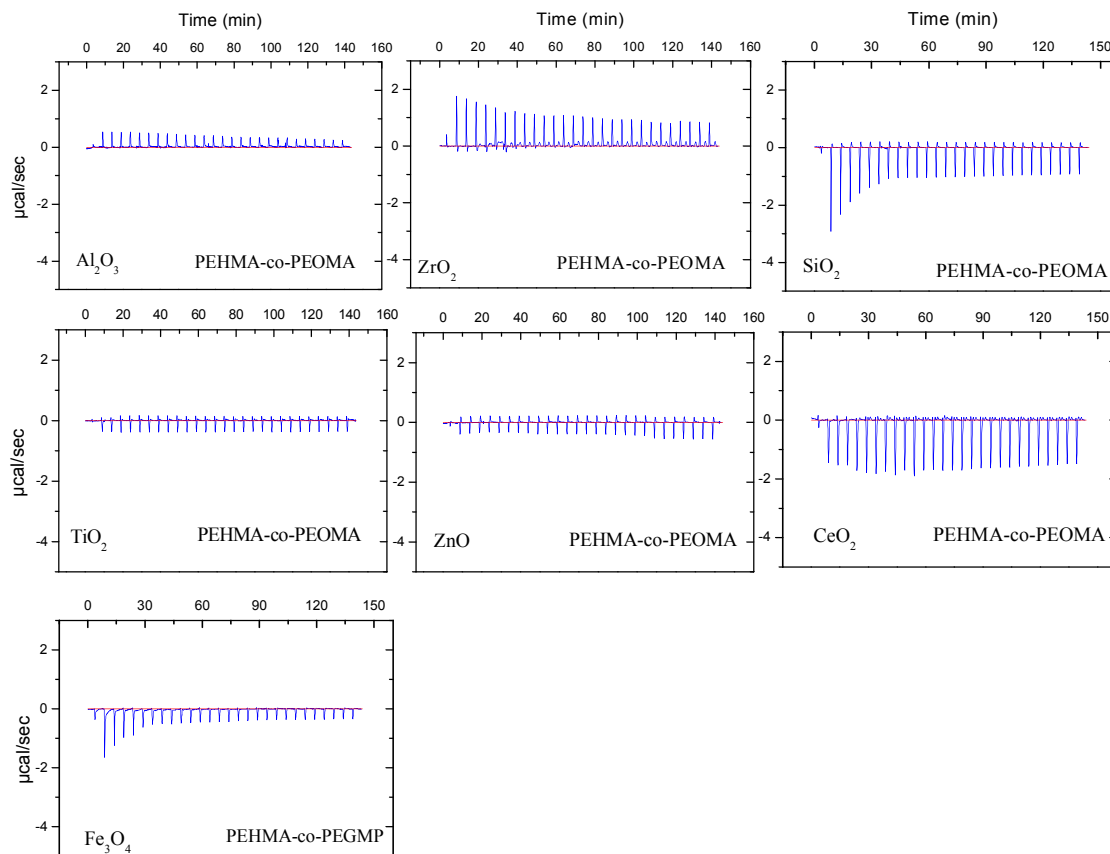


Figure 3.14: Binding isotherms for the interactions of amphiphilic copolymer (PEHMA-co-PPEGMA) with Al_2O_3 , CeO_2 , TiO_2 , SiO_2 , ZnO , ZrO_2 and Fe_3O_4 particles.

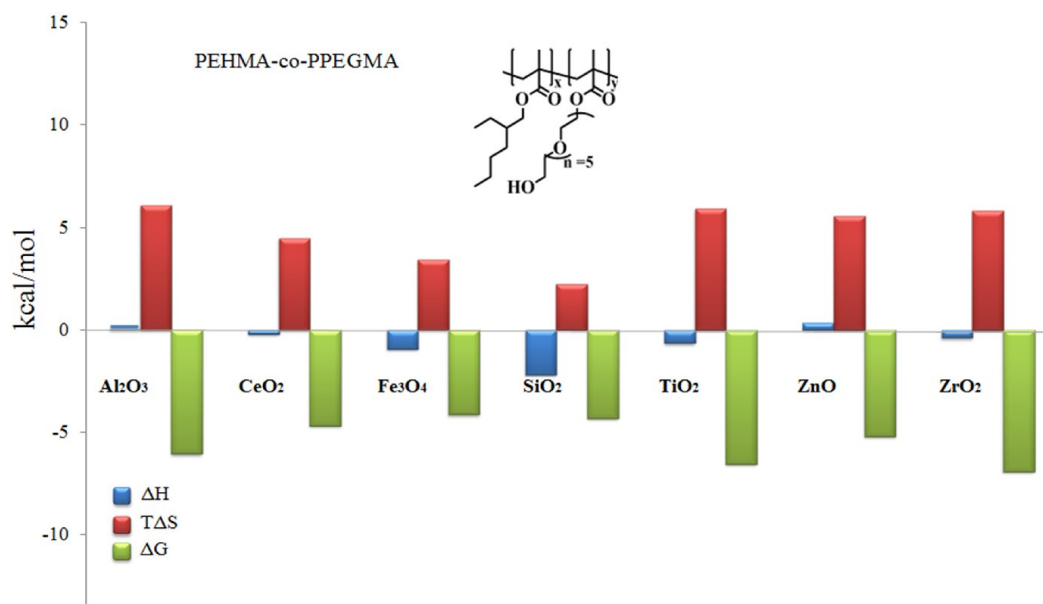
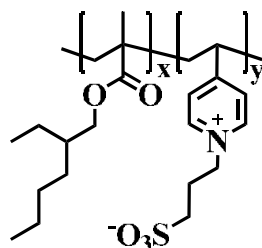


Figure 3.15: Schematic diagram presenting the thermodynamic profiles observed for Adsorption of PEHMA-co-PPEGMA/ Al_2O_3 , CeO_2 , SiO_2 , TiO_2 , ZnO , ZrO_2 and Fe_3O_4 .

This observation proved that the interaction between the PEHMA-co-PPEGMA and the Al_2O_3 , CeO_2 , TiO_2 , ZnO , ZrO_2 and Fe_3O_4 particles ($\Delta H = 0.04$ to -0.93 kcal/mol) was weaker than the interaction of PEHMA-co-PPEGMA with the SiO_2 particles surface ($\Delta H = -2.18$ kcal/mol) (see Figure 3.15 and Table 3.3). Possibly, these inorganic particles formed less strong hydrogen bonding with the PEO side chains as SiO_2 (Chapter 3.4.1.1).⁵⁰ This signifies that the interaction between PEHMA-co-PPEGMA/ Al_2O_3 , CeO_2 , TiO_2 , ZnO , ZrO_2 and Fe_3O_4 particles was not enough to provide a stable adsorption process.

3.4.2 Zwitter -ionic amphiphilic copolymer/ PEHMA-co-P4VPSB



Scheme 3.3: PEHMA-co-P4VPSB amphiphilic copolymer bearing zwitterionic anchor group.

Zwitterionic surfactants have both a positive and negative group and they are also able to act as an acid or a base, they have many excellent properties, such as detergency, foaming, emulsification and solubility in water.⁵¹ Moreover, zwitterionic surfactants have low toxicity and irritation to eye and skin,⁵² which makes them widely used in the cosmetic industry and textile production.⁵³ Recently, in our group these sulfonate and sulfobetain structures were used in an inverse emulsion system by Khrenov and Schwager, acting as emulsifiers and compatibilizers at the same time.⁴⁻⁶

In order to realize whether the zwitterionic surfactants are sufficient to modify the inorganic particles in the multicomponent solvent system, the adsorption of the zwitterionic surfactant PEHMA-co- P4VPSB (Scheme 3.3) with SiO_2 , Al_2O_3 , CeO_2 , TiO_2 , ZnO , ZrO_2 and Fe_3O_4 inorganic particles was studied.

The titration thermograms from the interaction of the PEHMA-co-P4VPSB with the inorganic particles show an endothermic titration effect with TiO_2

nanoparticles, which decreased slightly with increasing the PEHMA-co-P4VPSB concentration in the cell. On the contrary the interaction with Al_2O_3 , CeO_2 , SiO_2 , ZnO and ZrO_2 nanoparticles showed clearly exothermic effect, but different in the intensity of the heat released with each nanoparticles (see Figure 3.16).

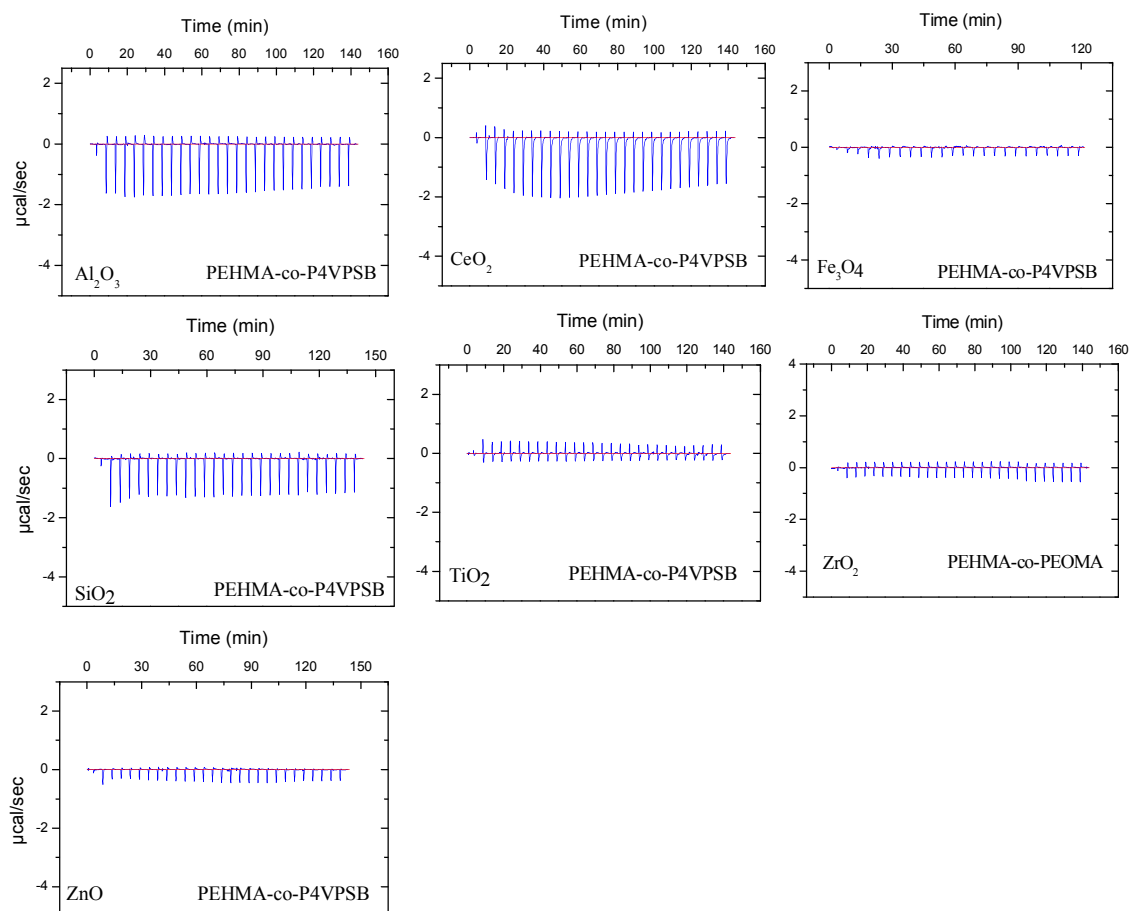


Figure 3.16: Binding isotherms for the interactions of amphiphilic copolymer (PEHMA-co-P4VPSB) / Al_2O_3 , CeO_2 , TiO_2 , SiO_2 , ZnO , ZrO_2 and Fe_3O_4 particles.

A favorable (negative) ΔH is achieved in the interaction with Al_2O_3 , CeO_2 , SiO_2 , ZnO and ZrO_2 , with a favorable (positive) entropy ΔS were detected (see Table 3.4 and Figure 3.17), which suggests a hydrophobically dominated interaction accompanied by an electrostatic binding forces. On the other hand, the interactions with the TiO_2 and Fe_2O_3 particles show an unfavorable (positive) enthalpy ΔH compared with the highly favorable (positive) entropy, which present only a dominated hydrophobic forces. A favorable (negative) ΔH is achieved in the interaction with Al_2O_3 , CeO_2 , SiO_2 , ZnO and ZrO_2 , with a favorable (positive) entropy ΔS were detected, which suggests a hydrophobically dominated

interaction accompanied by an electrostatic binding forces. On the other hand, the interactions with the TiO_2 and Fe_2O_3 particles show an unfavorable (positive) enthalpy ΔH compared with the highly favorable (positive) entropy, which present only a dominated hydrophobic forces (Table 3.4 and Figure 3.17).

Table 3.4: Thermodynamic parameters obtained by the ITC measurements of the studied surface active compounds (PEHMA-co-P4VPSB) with Al_2O_3 , CeO_2 , SiO_2 , TiO_2 , ZnO , ZrO_2 and Fe_3O_4 particle.

surface-active compound	K_B M^{-1}	ΔH kcal/mol	$T\Delta S$ kcal/mol	ΔG kcal/mol
Al_2O_3	$(1.34 \pm 0.02) \times 10^4$	-1.09 ± 0.001	4.97	-6.06
CeO_2	$(1.19 \pm 0.11) \times 10^4$	-0.95 ± 0.005	4.51	-5.46
Fe_3O_4	$(1.64 \pm 0.24) \times 10^3$	0.17 ± 0.008	6.52	-6.35
SiO_2	$(1.06 \pm 0.22) \times 10^3$	-0.52 ± 0.017	5.30	-5.82
TiO_2	$(5.44 \pm 0.90) \times 10^3$	0.04 ± 0.004	5.19	-5.15
ZnO	$(6.74 \pm 1.08) \times 10^3$	-0.12 ± 0.001	5.10	-5.22
ZrO_2	$(1.51 \pm 0.04) \times 10^3$	-0.44 ± 0.077	3.91	-4.35

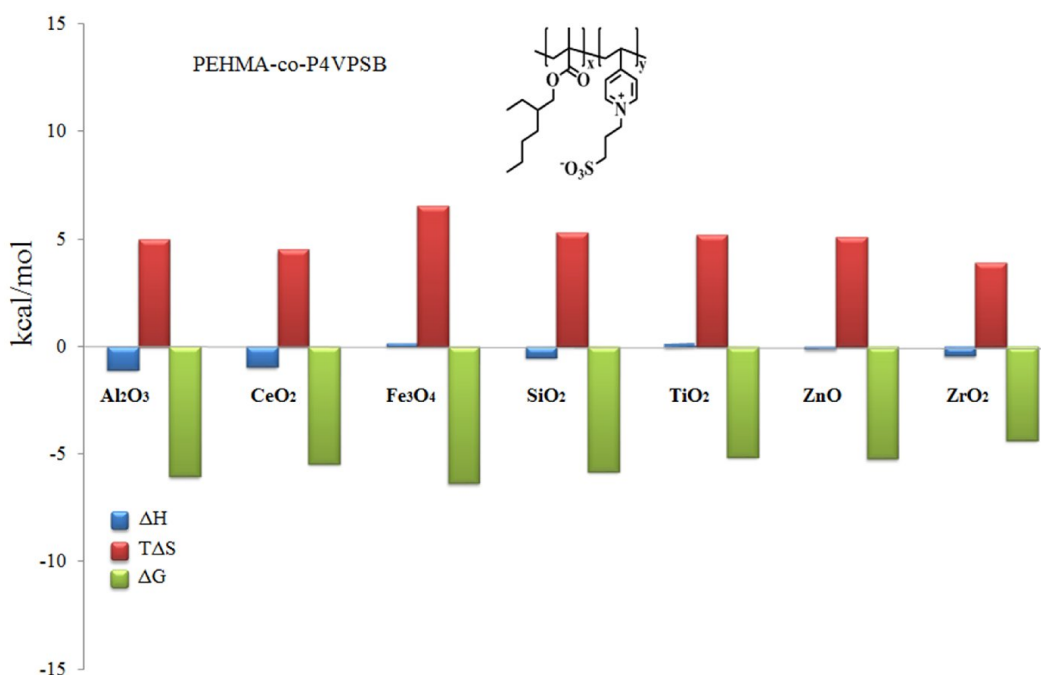


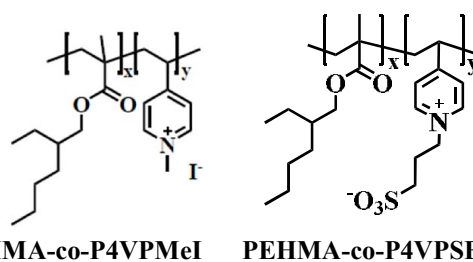
Figure 3.17: Schematic diagram presenting the thermodynamic profiles observed for adsorption of PEHMA-co-P4VPSB/ Al_2O_3 , CeO_2 , SiO_2 , TiO_2 , ZnO , ZrO_2 and Fe_3O_4 .

These results, in contrast to PEHMA-co-PPEGMA (*chapter 3.4.1.3*), show that the interactions of the sulfonate anchor group with the surfaces of Al_2O_3 and CeO_2 particles were relatively stronger than for PEO anchor groups. The reason was probably the presence of the sulfobetaine $[-\text{N}^+(\text{CH}_2)_3\text{SO}_3^-]$ group in the monomer backbone and its ability to form additional ionic interactions with the inorganic particles surfaces,⁵⁴ while in the case of the PEG chains only hydrogen bonds were formed (see Figure 1.14 and *Chapter 3.4.1.1*) (effect of the sulfonate anchor groups (SO_3^-) in the adsorption process was discussed in *Chapter 3.4.2.1*). Additionally, on the basis of binding constant K_B , which reflects the interaction affinity of PEHMA-co-P4VPSB to the surface of the inorganic particles, a highest binding affinity K_B (1.19 to $1.34 \times 10^4 \text{M}^{-1}$) was found between PEHMA-co-P4VPSB molecules and the surface of Al_2O_3 and CeO_2 particles. In comparison to the binding affinity on the other studied particles surfaces was found about one order of magnitude weaker (1.06 to $6.74 \times 10^3 \text{M}^{-1}$).

These observations demonstrate the capability of the PEHMA-co-P4VPSB copolymer to interact strongly with the Al_2O_3 and CeO_2 particles *via* ionic interactions and /or hydrogen bond formation; therefore sulfonates anchor groups were suitable to functionalized commercially available aqueous dispersions of Al_2O_3 and CeO_2 particles.

3.4.2.1 Effect of the sulfonate group on the adsorption process

Additionally, in order to determine the effect of the sulfonate group (SO_3^-) on the adsorption process with the inorganic particles, the copolymer PEHMA-co-P4VPMeI (schema 3.4) was used as a substitute for PEHMA-co-P4VPSB and also titrated to Al_2O_3 particles.



Scheme 3.4: Amphiphilic copolymers bearing zwitterionic anchor group.

As illustrated in Figure 3.18, the binding isotherm of the used zwitterionic copolymers (PEHMA-co-P4VPMeI and PEHMA-co-P4VPSB) with Al_2O_3 particle showed that in both of them an exothermic process was occurred, but different in the intensity of the heat released by each injection. In the interaction of PEHMA-co-P4VPMeI/ Al_2O_3 particles, a small favorable (negative) ΔH (- 0.15 kcal/mol) was achieved with a high favorable (positive) entropy ΔS (5.30 kcal/mol).

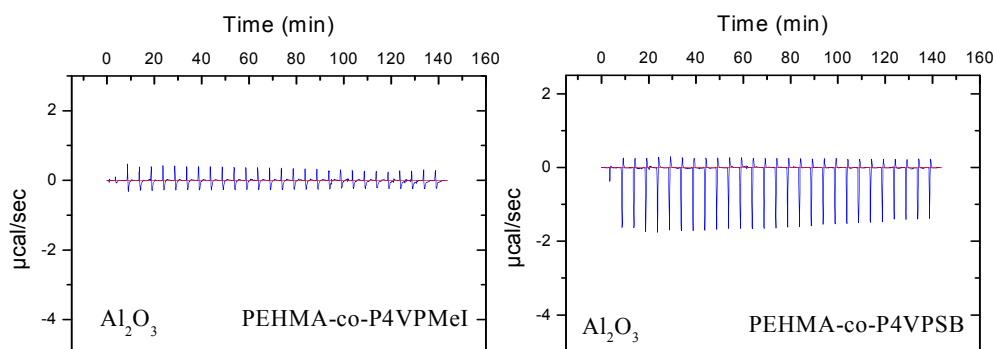
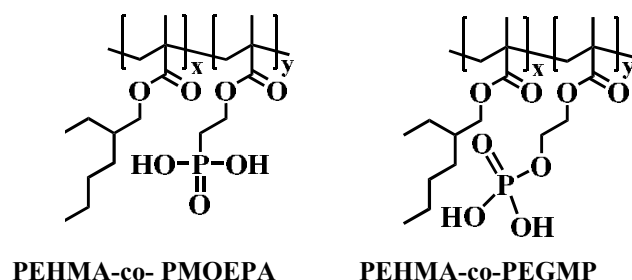


Figure 3.18: Binding isotherms for the interactions of amphiphilic copolymer PEHMA-co-P4VPMeI and PEHMA-co-P4VPSB with Al_2O_3 particles.

On the other hand the interaction of the PEHMA-co-P4VPSB monomer (bearing SO_3^- group) with the Al_2O_3 particles shows stronger interaction, which was reflected in the highly negative enthalpy ($\Delta H = -1.09$ kcal/mol) and lower entropy ΔS contributions (4.97 kcal/mol) (see Table 3.4). This observation confirmed our expectation that sulfonate anchor groups played a noticeable responsibility to form strong interactions with the inorganic particles surfaces. These result, can be related possibly to the nature of the SO_3^- group and its ability to interact in different ways (i.e. acidic and/or hydrophilic) with the inorganic particles. Moreover, the short linked hydrophobic group $(\text{CH}_2)_3$ increased the flexibility and/or possibility of the SO_3^- group to contacts the surface of the particles easily than the quaternary ammonium ion. This propose the possibility to use various kinds of sulfobetaine, carboxybetaine, and phosphobetaine derivatives (which have been found to be dermatologically inert and blood-compatible)⁵⁵ as a surfactant to functionalized inorganic particles.

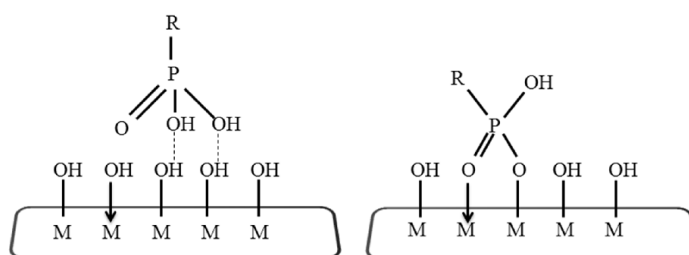
3.4.3 Acidic amphiphilic copolymer



Scheme 3.5: Chemical structures of the amphiphilic copolymers bearing acidic anchor groups applied in this study.

After the investigation of the suitability of sulfobetain and PEG as anchor groups they can be used to functionalized/stabilized of inorganic particles. The suitability of polymers with phosphonic/ phosphoric acid moiety (Scheme 3.5) to functionalize inorganic particles has been considered. Polymers with phosphonic/ phosphoric acid moiety $-P(O)_n(OH)_2$ has been studied for many applications such as chelation of metal ions,⁵⁶ templates for inorganic crystal growth⁵⁷ and fuel cell membranes.⁵⁸

The adsorption process of organic phosphates on metal oxide surfaces can be made by hydrogen bonding and/or covalent bonding (Scheme 3.6) depending on the reaction conditions and the chemical, electronic, and steric properties of the reaction compounds.^{59, 60}

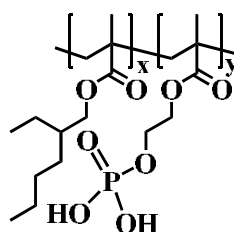


Scheme 3.6: Schematic representation of the formation of hydrogen bond (left) and bidentate phosphonate monolayer on the metal oxide surfaces.

Despite the fact, that organic-phosphonated compounds are known to adsorb strongly on transition and heavy metal ions, all adsorption studies so far have been conducted in aqueous phase⁶³ and/or solid-state using potentiometric titrations, atomic force microscope (AFM), FTIR and NMR techniques.⁵⁹⁻⁶³

In this study, we apply ITC as a new technique to analyse and quantify the adsorption of copolymers bearing phosphonic and phosphoric acids functional groups with various inorganic particles surfaces (Al_2O_3 , CeO_2 , SiO_2 , TiO_2 , ZnO , ZrO_2 and Fe_3O_4) in a multicomponent solvent system (H_2O , 1,4-dioxane and ethanol).

3.4.3.1 PEHMA-co- PEGMP



Based on the results from *Section 3.3.2* in which (ethylene glycol) methacrylate phosphate (EGMP) demonstrated that the aptitude to interact strongly with SiO_2 particles. This allowed a rapid assessment based on phosphates/phosphonates methacrylate as an anchor group for the adsorption of amphiphilic copolymers.

In order to recognize the fact that the acidic surfactants are capable of modify the inorganic particles in the multicomponent solvent system, the adsorption of the phosphoric as well as phosphonic acid based copolymers (Scheme 3.5) with SiO_2 , Al_2O_3 , CeO_2 , TiO_2 , ZnO , ZrO_2 and Fe_3O_4 inorganic particles were studied.

Primarily, the interaction of the phosphoric acid based copolymer poly (2-ethylhexyl-co-2-(phosphonoethoxy)- ethyl methacrylate) PEHMA-co- PEGMP with the inorganic particles surface was investigated.

As shown in Figure 3.19, the titration of 55 mM solution of PEHMA-co- PEGMP in (1,4-dioxane/ethanol/ H_2O) into 16 mM dispersion of SiO_2 , Al_2O_3 , CeO_2 , TiO_2 , ZnO , ZrO_2 and Fe_3O_4 in the same solvent, provides a significant exothermic heat signal for all particles, which becomes weaker with increasing the PEHMA-co-PEGMP concentration in the cell.

The binding isotherms show in all cases that the exothermic effect increased radically after (4 to 7 injections) of PEHMA-co- PEGMP solution. This rapid increasing in the exothermic effect (i.e. PEHMA-co-PEGMP/ CeO_2 interaction as illustrated in Figure 3.19) can be related to the strong interaction with the surfaces

of the particles in the beginning. Accordingly, an early saturation of the surfaces of the particles can be detected (this phenomena was not detected by the other investigated copolymers PEHMA-co-PPEGMA and PEHMA-co-P4VPSB (see *chapter 3.4.1* and *3.4.2*).

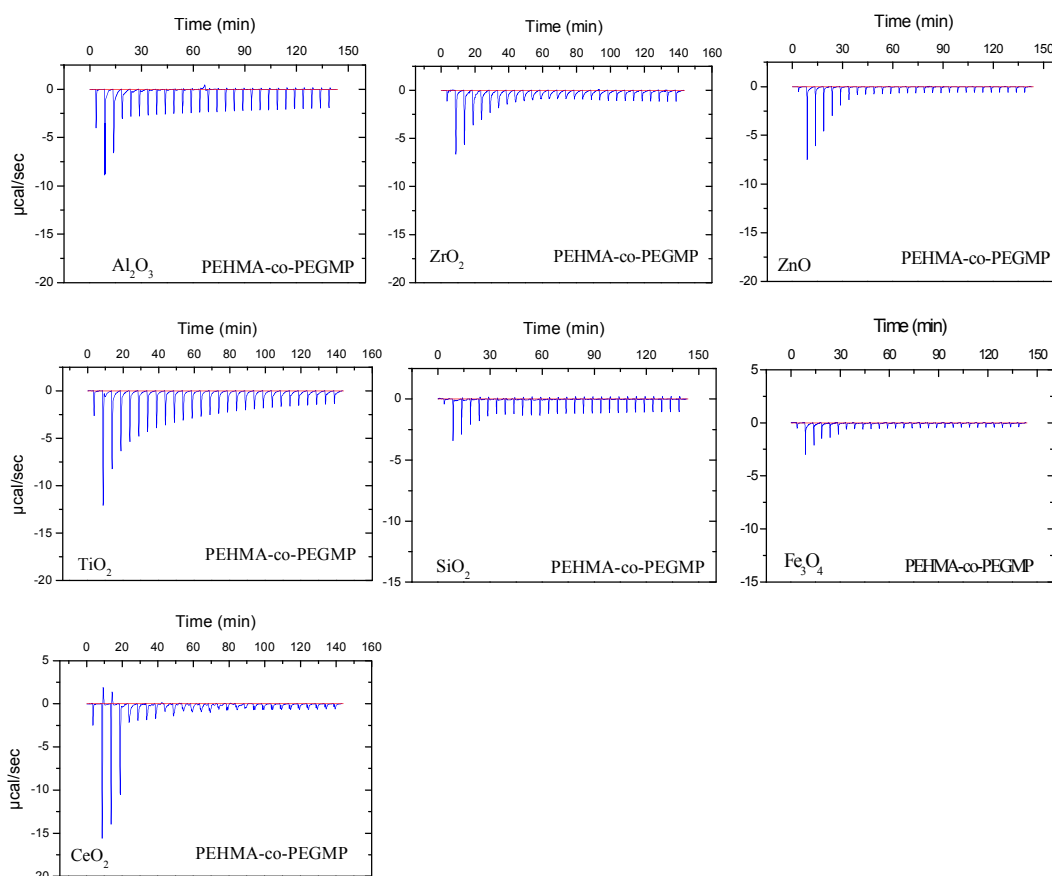


Figure 3.19: Binding isotherms for the interactions of amphiphilic copolymer (PEHMA-co-PEGMP) with Al_2O_3 , CeO_2 , TiO_2 , SiO_2 , ZnO , ZrO_2 and Fe_3O_4 particles.

A determination of the thermodynamic parameters by the method of least squares (Marquardt algorithm), using the "One site of sites" model shows a favorable (negative) ΔH and favorable (positive) $T\Delta S$ contribution with the SiO_2 , Al_2O_3 , CeO_2 , ZnO , ZrO_2 and Fe_3O_4 particles, but favorable (negative) ΔH and unfavorable (negative) $T\Delta S$ contribution with the TiO_2 particles (see Figure 3.20 and Table 3.5). These reflect an enthalpically driven interaction process for the CeO_2 , ZnO and TiO_2 particles.

Table 3.5: Thermodynamic parameters obtained by the ITC measurements of the studied surface active compounds (PEHMA-co-PEGMP) with Al_2O_3 , CeO_2 , SiO_2 , TiO_2 , ZnO , ZrO_2 and Fe_3O_4 particle.

surface-active compound	K_B M^{-1}	ΔH kcal/mol	$T\Delta S$ kcal/mol	ΔG kcal/mol
Al_2O_3	$(8.36 \pm 1.39) \times 10^4$	-2.18 ± 0.13	4.56	-6.74
CeO_2	$(2.28 \pm 0.09) \times 10^4$	-5.19 ± 0.14	2.98	-8.17
Fe_3O_4	$(1.91 \pm 0.16) \times 10^4$	-2.38 ± 0.04	3.65	-6.03
SiO_2	$(8.53 \pm 0.09) \times 10^4$	-1.85 ± 0.03	4.31	-6.16
TiO_2	$(2.68 \pm 0.37) \times 10^4$	-7.88 ± 0.20	-1.83	-6.05
ZnO	$(1.51 \pm 0.20) \times 10^3$	-2.93 ± 0.32	1.40	-4.33
ZrO_2	$(5.03 \pm 0.83) \times 10^3$	-1.69 ± 0.15	2.06	-3.75

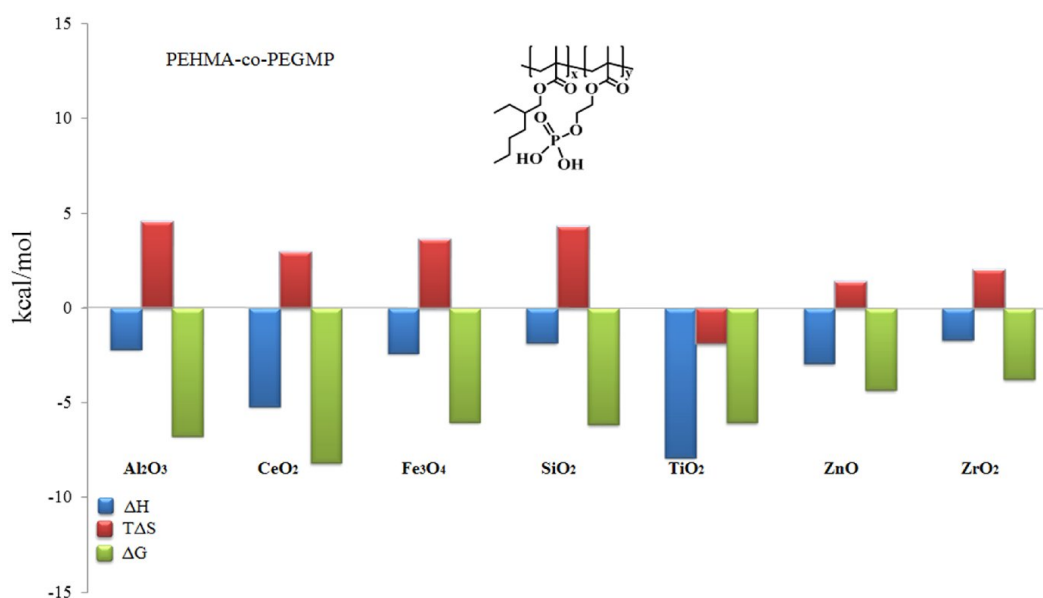


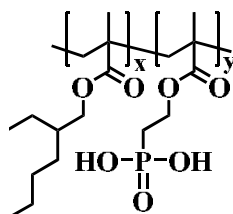
Figure 3.20: Schematic diagram presenting the thermodynamic profiles observed for adsorption of PEHMA-co-PEGMP/ Al_2O_3 , CeO_2 , SiO_2 , TiO_2 , ZnO , ZrO_2 and Fe_3O_4 .

Formation of the P-O-M bonds and/or multiple hydrogen bonds is considered as the possible main source of the negative ΔH values. Depending on the observed ΔH contributions from those interactions (see Table 3.5), the strength of the adsorption of the PEHMA-co-PEGMP with the inorganic particles detected that the non-covalent interactions (such as: hydrogen bonding and/or van der Waals) were the dominant forces in the system. That was on the contrary to what was

expected like covalent binding. This can be related to the bulky nature of the PEHMA-co-PEGMP copolymer and/or the presence of solvents (H_2O , 1,4-dioxane and ethanol), which expected to limit the possibility of the direct interaction with the metal ion, and therefore reduce the ability to form covalent bonds. Furthermore, the favorable (positive) entropy contributions reflects the changes in solvation entropy occurred during the adsorption process, when the oxygen atom of the phosphoric acid anchor groups released the associated solvent molecules before interacting with the inorganic particles surface.

These results demonstrated the capability of PEHMA-co-PEGMP copolymer in a multicomponent system (see *Chapter 3.1*) to form strong interactions with most inorganic particles used in this study (i.e. CeO_2 , ZnO and TiO_2). Consequently, this confirmed the suitability of these polymers to functionalize readily available aqueous dispersions of inorganic particles in a simple and highly efficient way.

3.4.3.2 PEHMA-co- PMOEPA



Here the copolymer poly (2-ethylhexyl methacrylate-co-2-(methacryloyloxy)-ethyl phosphonic acid) PEHMA-co-PMOEPA with phosphonic acid anchor groups was applied to functionalized the inorganic particles. The advantage of the phosphonic acid is due to their higher hydrolysis resistance as compared to the phosphoric acid groups.⁶⁴

The results of the PEHMA-co-PMOEPA/inorganic particles interactions were presented in Figure 3.21. In all investigated samples an exothermic titration curve was generated, but the intensity of the heat released was different between the inorganic particles. Therefore, the observed thermodynamic contributions (ΔH , $T\Delta S$ and K_B) differ for the inorganic particles used. All the interactions with the inorganic particles outcome in a favorable (negative) enthalpy changes ΔH and favorable (positive) $T\Delta S$ contribution (Table 3.6 and Figure 3.22), which proved

that these bindings are dominated by hydrophobic interactions, but also accompanied with favorable redistribution of the hydrogen bonding network and/or other electrostatic forces, suggesting that the inorganic particles are also established a number of bonds with the amphiphilic copolymers.

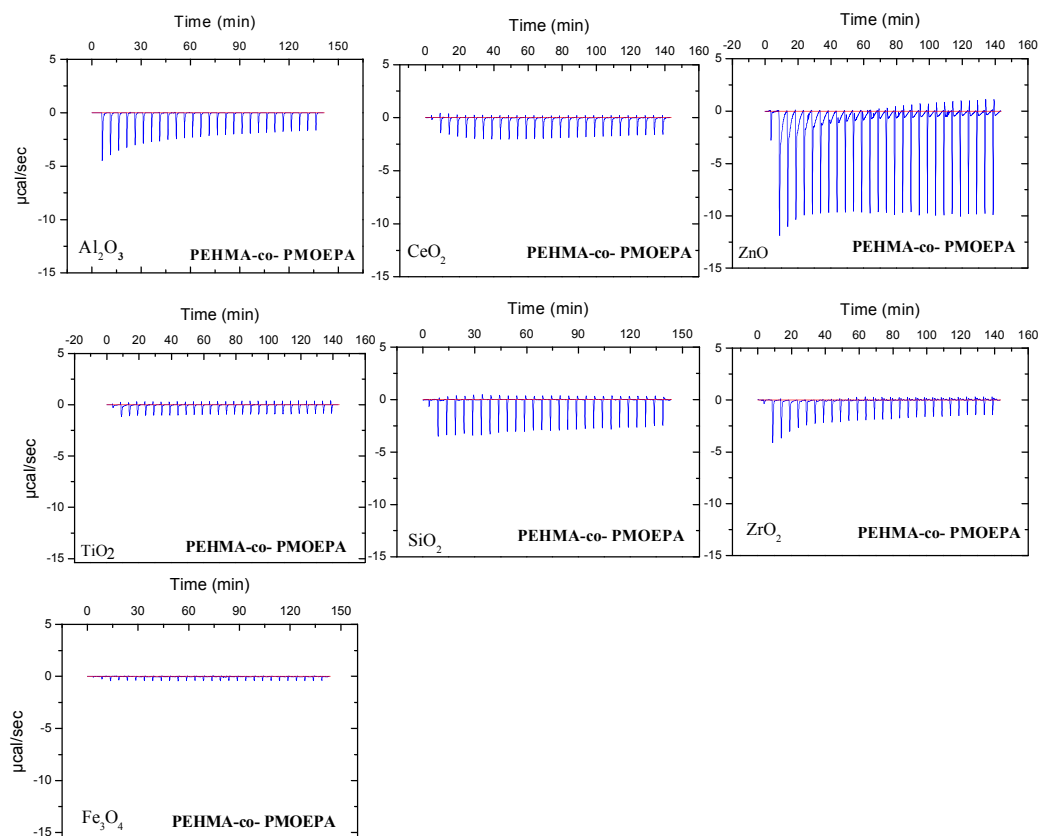


Figure 3.21: Binding isotherms for the interactions of amphiphilic copolymer PEHMA-co-PMOEPA with Al_2O_3 , CeO_2 , TiO_2 , SiO_2 , ZnO , ZrO_2 and Fe_3O_4 particles.

Depending on the observed ΔH contributions, PEHMA-co-PMOEPA shows weaker interaction with all the inorganic particles as compared to (PEHMA-co-PEGMP), however stronger than the copolymers bearing PEO or sulfobetain anchor groups (*Chapter 3.4.1* and *3.4.2*). This was possibly due to a high number of rotational degrees of freedom of phosphoric acid groups as compared to the phosphonic acid group. The reason for this was the linking of the hydrophilic anchor groups in the monomer with a C-O-P bond instead of a C-P linkage. This additional O-P bond of the phosphoric acid group apparently give a higher mobility and thus resulted in a stronger interaction with the surface of inorganic particles.⁸ Furthermore the binding affinity for the interactions shows that this

copolymer interacts with high binding affinity on the inorganic particles surface (i.e. the interactions with Al_2O_3 and CeO_2) particles with K_B (1.31×10^5 and 1.12×10^5) respectively.

Table 3.6: Thermodynamic parameters obtained by the ITC measurements of the studied surface active compounds (PEHMA-co-PMOEPS) with Al_2O_3 , CeO_2 , SiO_2 , TiO_2 , ZnO , ZrO_2 and Fe_3O_4 particle.

surface-active compound	K_B M^{-1}	ΔH kcal/mol	$T\Delta S$ kcal/mol	ΔG kcal/mol
Al_2O_3	$(1.31 \pm 0.39) \times 10^5$	-1.26 ± 0.02	5.72	-6.98
CeO_2	$(1.12 \pm 0.17) \times 10^5$	-1.13 ± 0.03	6.08	-7.21
Fe_3O_4	$(1.93 \pm 0.23) \times 10^4$	-1.03 ± 0.11	5.63	-6.66
SiO_2	$(1.16 \pm 0.17) \times 10^4$	-1.38 ± 0.25	5.42	-6.80
TiO_2	$(2.84 \pm 0.27) \times 10^4$	-1.18 ± 0.02	4.88	-6.06
ZnO	$(4.86 \pm 0.36) \times 10^3$	-2.07 ± 0.19	2.95	-5.02
ZrO_2	$(2.18 \pm 0.22) \times 10^3$	-1.42 ± 0.22	3.13	-4.55

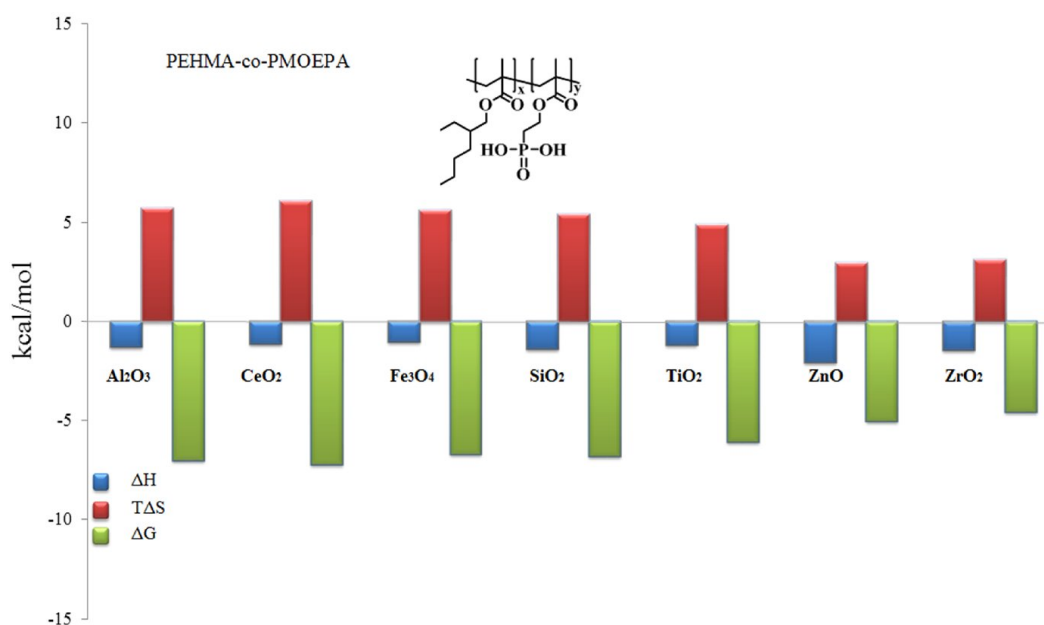
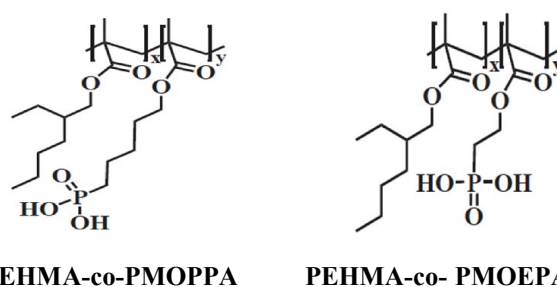


Figure 3.22: Schematic diagram presenting the thermodynamic profiles observed for adsorption of PEHMA-co-PMOEPS/ Al_2O_3 , CeO_2 , SiO_2 , TiO_2 , ZnO , ZrO_2 and Fe_3O_4 .

3.4.3.3 The influence of the methylene spacer length on the interaction of PEHMA-co- PMOEPA with inorganic nanoparticles

In order to study the effect of the methylene spacer between the polymer backbone and the hydrophilic anchor group on the functionalization process of the inorganic particles, the interaction of the copolymer poly (2-ethylhexyl methacrylate-co-5-(methacryloyloxy)- pentyl phosphonic acid) PEHMA-co-PMOPPA bearing 5 methylene groups were studied (Scheme 3.7).



Scheme 3.7: Amphiphilic copolymers bearing acidic anchor group.

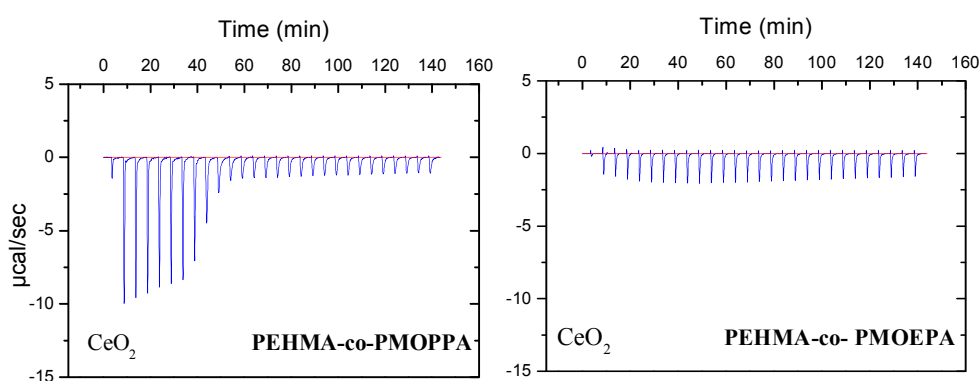


Figure 3.23: Binding isotherms for the interactions of amphiphilic copolymer PEHMA-co-PMOPPA and PEHMA-co-PMOEPA with CeO_2 particles.

Figure 3.23 showed the titration thermogram of the used acidic copolymers PEHMA-co-PMOPPA (bearing - $(\text{CH}_2)_5$ - group's distance of the phosphonic acid anchor groups on the polymer backbone) and the copolymer PEHMA-co-PMOEPA (with - $(\text{CH}_2)_2$ - groups) with the CeO_2 particle surface. In both of them an exothermic process take place, however the intensity of the heat released was different between the two copolymers. The interaction of PEHMA-co-PMOPPA with CeO_2 particles lead to strong exothermic effect, which become increasingly smaller than the more PEHMA-co-PMOPPA was added to the cell.

The calculated thermodynamic parameters for this interaction (PEHMA-co-PMOPPA/ CeO₂) show an enthalpically driven interaction with clearly gain the negative enthalpy of ($\Delta H = -5.51$ kcal/mol) compared with low (positive) entropy ΔS (1.04 kcal/ mol). In comparison to PEHMA-co-PMOEPA with only two methylene groups distance as spacer (see *Chapter 3.4.3.2*), which show weaker interaction with ΔH (-1.13 kcal/mol) (see Table 3.6). This observation proved that the presence of longer alkyl spacer leads to an increasing of the flexibility of the –P(O)(OH)₂ anchor group to interact on the surfaces of the inorganic particles and thus its better suitability for the functionalization of these particles.

3.5 THE TEMPERATURE INFLUENCE ON THE BINDING PROCESS

Additionally in order to investigate the influence of the temperature on the binding process of the amphiphilic copolymers with the inorganic particles as well as on the mechanisms of the interactions independently, the calorimetric titrations of the amphiphilic copolymers (Scheme 3.2) with the ZnO particle surface were performed over a range of temperature of 15-35 °C in 5 °C steps. Despite the limited temperature range over which the titration were carried out, the heat capacity changes ΔC_p upon complex formation were calculated.

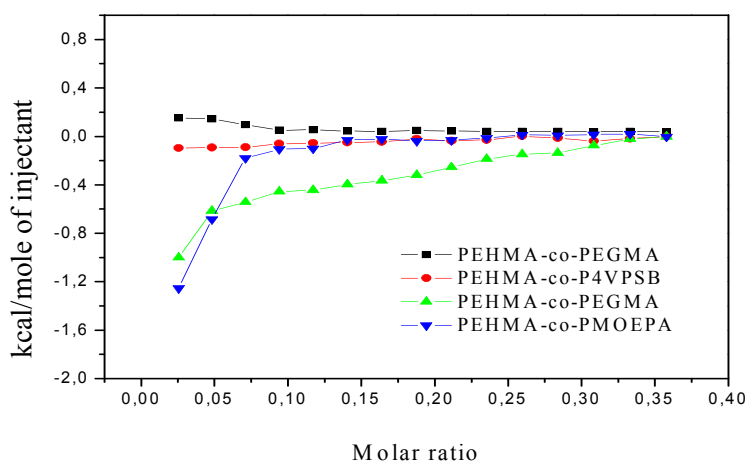


Figure 3.24: Calorimetric binding isotherms of the amphiphilic copolymers (non-ionic, zwitter-ionic and acidic) to ZnO inorganic particles at 25 °C.

Figure 3.24 shows that the binding isotherms of the four different copolymers on the ZnO particle surfaces (see *Chapter 3.4*) at 25 °C. PEHMA-co-PEGMP, the phosphoric acid groups containing copolymer had the highest negative binding enthalpy followed by the PEHMA-co- PMOEPA, PEHMA-co-P4VPSB and PEHMA-co-PEGMA. Upon increasing the titration temperatures (Table 3.7), the interactions of the PEHMA co-PEGMP with ZnO particle were dominated by an enthalpically driven process (will be assumed as a result of the formation of the P-O-M bonds or multiple hydrogen bonding with the particle surfaces).⁶⁵ On the other hand, the entropically driven interactions with the contribution of hydrogen bonds were observed for the PEHMA-co- PMOEPA and PEHMA-co-P4VPSB.

The independency of each amphiphilic copolymer on the temperature during the interaction with the ZnO particles is demonstrated in Figure 3.25. One can clearly see that the heat of injecting amplified upon increasing the experimental temperature. For the quantitative determination of the binding enthalpy and the binding affinity K_B the titration curves were fitted using a model of identical and independent binding sites as mentioned in *Chapter 2* and *Chapter 3.4*. The values of the binding affinity at different temperature as well as the other thermodynamic parameters are summarized in Table 3.7.

Table 3. 7: Thermodynamic parameters of binding of amphiphilic copolymers with ZnO surfaces at different temperatures.

surface-active compound	T °C	K_B M ⁻¹	ΔH kcal/mol	T ΔS kcal/mol	ΔG kcal/mol
PEHMA-co-PEGMA	15	$(1.27 \pm 0.34) \times 10^4$	0.04 ± 0.02	6.35	-6.31
	20	$(1.01 \pm 0.67) \times 10^4$	0.06 ± 0.05	5.48	-5.44
	25	$(6.15 \pm 0.41) \times 10^3$	0.36 ± 0.04	5.55	-5.18
	30	$(4.10 \pm 0.58) \times 10^3$	0.71 ± 0.10	6.20	-5.19
PEHMA-co-P4VPSB	15	$(3.10 \pm 0.27) \times 10^4$	0.06 ± 0.05	6.26	-6.20
	20	$(1.46 \pm 0.15) \times 10^4$	-0.09 ± 0.07	5.66	-5.75
	25	$(6.74 \pm 1.08) \times 10^3$	-0.12 ± 0.01	5.10	-5.22
	30	$(4.25 \pm 1.12) \times 10^3$	-0.16 ± 0.03	4.80	-4.96
PEHMA-co-PEGMP	15	$(1.87 \pm 0.14) \times 10^5$	-1.13 ± 0.10	3.87	-5.00
	20	$(3.94 \pm 0.18) \times 10^4$	-1.26 ± 0.17	3.60	-4.86
	25	$(4.51 \pm 0.26) \times 10^3$	-2.93 ± 1.32	1.40	-4.33
	30	$(1.10 \pm 0.01) \times 10^3$	-3.05 ± 0.04	1.93	-4.98
PEHMA-co-PMOEPA	15	$(5.60 \pm 0.94) \times 10^4$	-1.49 ± 0.14	5.30	-6.79
	20	$(1.17 \pm 0.25) \times 10^4$	-1.85 ± 0.13	3.66	-5.51
	25	$(4.86 \pm 0.76) \times 10^3$	-2.07 ± 0.19	2.95	-5.02
	30	$(1.56 \pm 0.03) \times 10^3$	-5.25 ± 1.01	-0.06	-5.19

In details, the titration curves in the Figure 3.25 as indicated that all the binding reactions of PEHMA-co-PEGMP, PEHMA-co- PMOEPA, and PEHMA-co-P4VPSB with ZnO particle were exothermic, but the binding reactions of PEHMA-co-PEGMA were endothermic at all temperatures. Practically, the interactions of the PEHMA-co-PEGMA with ZnO inorganic particles presented in

all temperatures were entropically driven, i.e. with unfavorable (positive) enthalpy and favorable (positive) entropy contributions. The binding of PEHMA-co-P4VPSB containing zwitter-ionic anchor groups at 15 °C were entropically driven with both positive enthalpy and entropy contributions, upon rising the titration temperature 20 to 30°C the interaction turn out to be less entropically driven by increasing the favorable (negative) enthalpy contributions.

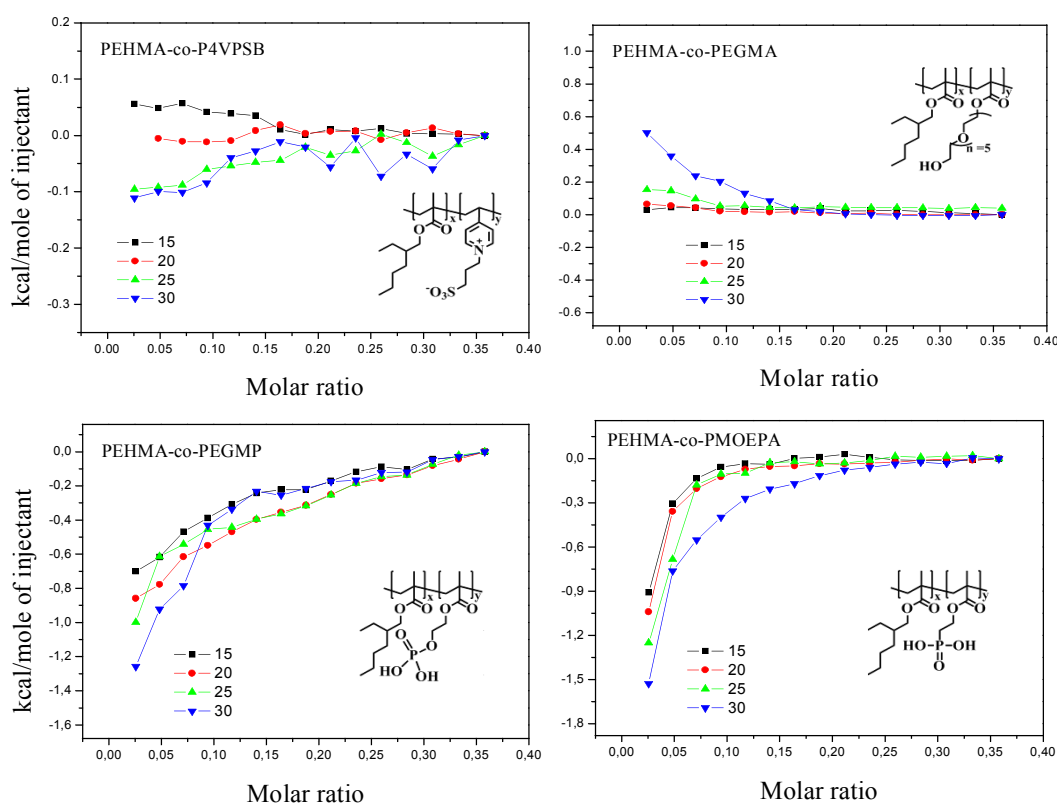


Figure 3.25: The binding isotherms for the binding of amphiphilic copolymers (non-ionic, zwitter-ionic and acidic) with ZnO inorganic particles at different temperatures.

On the other hand, the interactions of the PEHMA-co-PEGMP and PEHMA-co-PMOEPA containing acidic anchor groups indicated an enthalpically as well as entropically driven binding interactions, i.e. with low favorable (negative) enthalpy and high favorable (positive) entropy, suggesting that the adsorption process mainly controlled by the hydrophobic forces compared with a weak hydrogen bonding formation with the surface of the ZnO particles (see Table 3.7). Alternatively, upon increasing the temperature of the system from 25 to 30 °C the interaction were improved, in practical the interactions were driven by high

favorable enthalpy and low favorable (positive) entropy contributions, which suggests that the interactions take place through the formation of the P-O-M bonds or by multiple hydrogen bonds with the particle surfaces (*Chapter 3.4.1*).

Furthermore, the binding affinity K_B showed that the PEHMA-co-PEGMP had the highest binding affinity ($K_B = 1.87 \times 10^5 \text{ M}^{-1}$ at 15°C). This value was about one order of magnitude higher than that found for the PEHMA-co-P4VPSB and PEHMA-co-PEGMA at the same temperature. The PEHMA-co-PMOEPA copolymer showed the next stronger binding ($K_B = 5.60 \times 10^4 \text{ M}^{-1}$ at 15°C) which was only slightly higher than (1.8x) that of the PEHMA-co-P4VPSB (Figure 3.26 and Table 3.7).

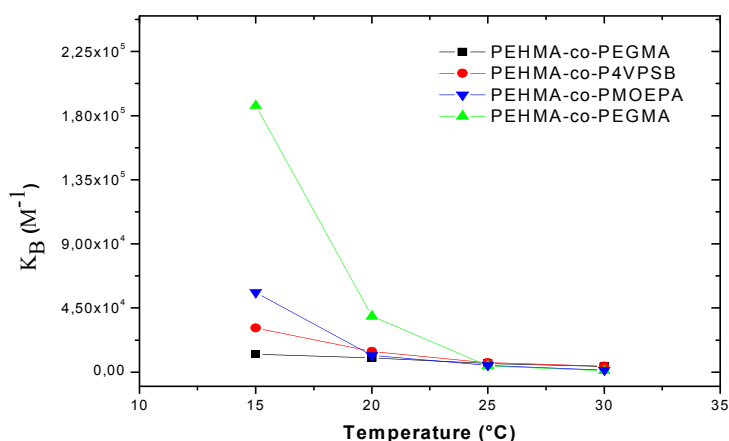


Figure 3.26: Temperature dependence of K_B for the binding of the amphiphilic copolymers (non-ionic, zwitter-ionic and acidic) with ZnO inorganic particles.

In order to confirm the above hypothesis and to probe the mechanism of the interactions, the change in heat capacity (ΔC_p) of the interaction were measured. The change in specific heat capacity (ΔC_p) of the binding process was calculated from the slope of ΔH versus temperature curves (as illustrated in Figure 3.27) assuming a temperature independent ΔC_p .²⁶ ΔC_p values as well as the correlation coefficients of fitting the data points are listed in Table 3.8.

As it is found that the ΔC_p for the PEHMA-co-PEGMA and PEHMA-co-P4VPSB were positive as compared to the PEHMA-co-PEGMP and PEHMA-co-PMOEPA which were negative, i.e. the complex had lower heat capacities than the components.⁶⁷

The similarity of the ΔC_p values for the PEHMA-co-PEGMA, PEHMA-co-P4VPSB from one side and the PEHMA-co-PEGMP, PEHMA-co-PMOEPA from the other side indicated a basic similarity in the binding process and thermodynamic prosperities.

Table 3.8: Calculated ΔC_p values and correlation coefficients assuming a linear relation between ΔH and temperature.

surface-active compound	ΔC_p k cal.mol ⁻¹ .K ⁻¹	Correlation coefficient (R ²)
PEHMA-co-PEGMA	0.046	0.8993
PEHMA-co-P4VPSB	0.160	0.6400
PEHMA-co-PEGMP	-0.148	0.8549
PEHMA-co-PMOEPA	-0.214	0.7330

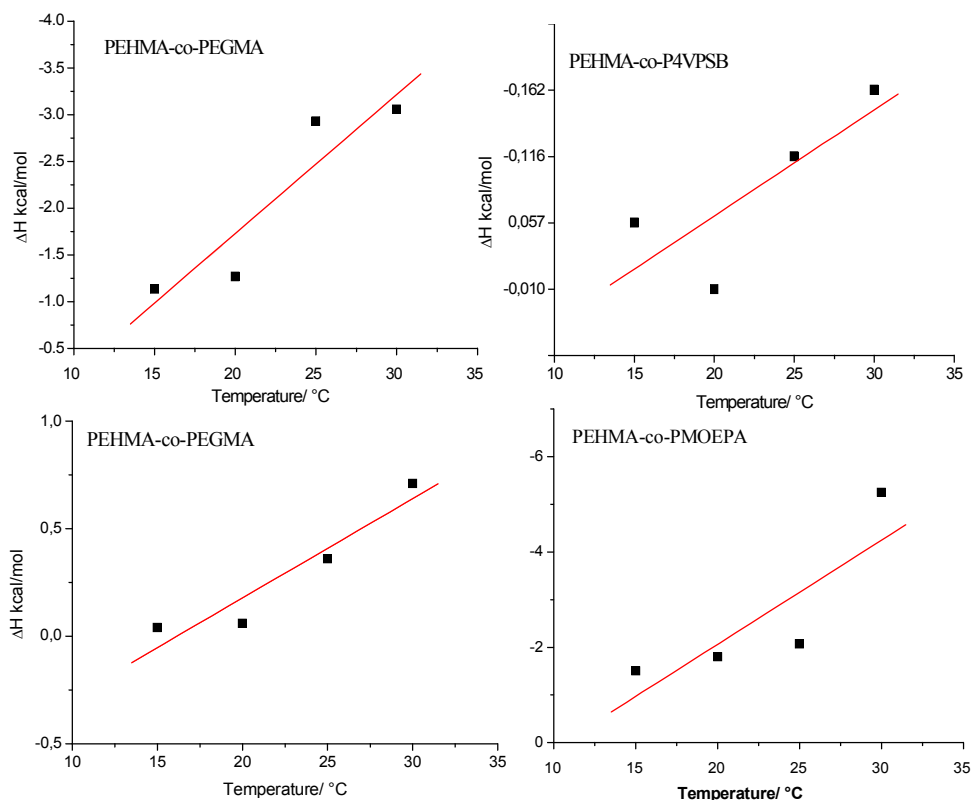


Figure 3.27: Plot of ΔH versus temperature for calculation of ΔC_p for the amphiphilic copolymers (non-ionic, zwitter-ionic and acidic) with ZnO inorganic particles.

The observed ΔC_p for the interaction PEHMA-co-PEGMA and PEHMA-co-P4VPSB/ZnO particles were found to be positive (0.047 and 0.16 kcal.mol⁻¹.K⁻¹), which suggests, that these binding are attributed mainly to the extensive additional solvation, and partially to the burial of the polar groups of the interacting molecules.⁶⁸ This means, that these interactions are dominated by hydrophobic forces. Conversely, the ΔC_p values for the interactions of the copolymers bearing acidic anchor groups PMOEPA and PEGMP on the ZnO surface, were negative (-0.15 and -0.21 kcal.mol⁻¹. K⁻¹). This small contribution of ΔC_p suggests that electrostatic forces play a significant role in the heat capacity change, resulting from solvation upon binding.⁶⁹ Furthermore, if small negative changes in the heat capacity are associated with a favorable (positive) entropic change (Table 3.7); hydrophobic interactions are supposed to be involved in the binding reactions accompanied with a favorable electrostatic forces.⁷⁰

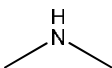
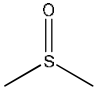
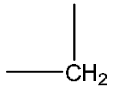
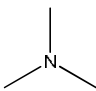
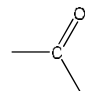
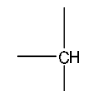
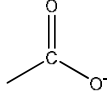
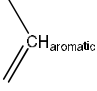
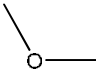
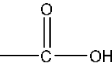
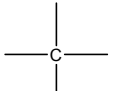
3.6 SCREENING AND OPTIMIZING OF THE ADSORPTION FORCES IN POLYMER-INORGANIC HYBRID SYSTEMS

After the thermodynamic profile observation (binding affinity, binding enthalpy and binding entropy) from the calorimetric titration of the amphiphilic copolymers with the inorganic particles (*Chapter 3.3, 3.4 and 3.5*), the ITC technique was presented here as a method to screen and optimize of binding strength and the binding affinity in the polymer-inorganic hybrid systems.

One of the most important goals in the development of the organic-inorganic hybrid systems is the improving of the binding affinity of the organic part towards the inorganic surface part, as binding affinity is directly related to the strength of the interactions.⁷¹ The binding affinity of a compound can be improved by generating: (i) a favorable (negative) binding enthalpy, (ii) favorable (positive) solvation entropy, or by (iii) minimizing the unfavorable (negative) conformational entropy.^{72,73}

Obviously, extremely high affinity is achieved when the three factors are optimized simultaneously.⁷⁴ The degree of difficulty associated with improving the enthalpy is not the same as the one associated with improving the entropy. Historically, it has proven much easier to optimize the entropy.⁷⁵

Table 3.9: Desolvation enthalpy of different chemical functionalities at 25 °C.⁷⁷

Group	ΔH kcal/mol	Group	ΔH kcal/mol	Group	ΔH kcal/mol
—NH ₂	7.9	—OH	8.7	H ₃ C—	0.57
	9.4		12.7		0.77
	9.3		5.5		0.73
O ₂ N—	4.7		5.4		0.7
	5.2		8.4		1.1

As the major favorable contributor is the hydrophobic effect, which is proportional to the number of non-polar groups that are buried from the solvent, the tendency throughout the years have been toward an increase in the hydrophobicity of compounds candidates.⁷⁶ Compounds that exhibit extremely high affinity have been shown to display both favorable entropic and enthalpic interactions.^{78, 79} Even though enthalpic interactions are required for extremely high affinity and improved selectivity, the optimization of the binding enthalpy has been notoriously more difficult than the optimization of the binding entropy, the reason being that the enthalpy of desolvation of polar groups is very large and unfavorable, as shown in Table 3.9.

Polar groups take a desolvation penalty about one order of magnitude larger than non-polar groups. A polar group needs to establish a very good interaction with the target in order to compensate for the desolvation penalty and make a favorable contribution. For this reason, they are often engineered as solubilizers of otherwise extremely hydrophobic compounds rather than major contributors to affinity. As the major contributors to the binding enthalpy are polar groups, a common misconception is that enthalpically driven compounds must be highly polar and that consequently their availability will be compromised.

3.6.1 Thermodynamic optimization plot

As soon the calorimetric titration of the amphiphilic copolymers with the inorganic particles surface carried out, a thermodynamic optimization plot (TOP) can be constructed. This plot (see Figure 3.28) is defined by setting as ordinate the binding enthalpy (ΔH) and as abscissa the entropy contribution to affinity ($-T\Delta S$). A straight line (optimization line) is drawn between the experimental ($-T\Delta S$, ΔH) point and the point (0, ΔG).^{80, 81} The point (0, ΔG) is obtained by considering that when $-T\Delta S = 0$, $\Delta H = \Delta G$.

The resulting thermodynamic optimization plot has a slope of -1; it is built with a single experimental point corresponding to the binding thermodynamics of a selected complex (i.e. the interaction of the PEHMA-co-P4VPSB with SiO₂ inorganic particles was chosen as example for the binding optimization) and

should not be confused with so-called 'enthalpy / entropy compensation' plots. Enthalpy / entropy compensation plots are built by plotting enthalpy and entropy values for many compounds and then performing a linear least squares fit of the data.^{82, 83}

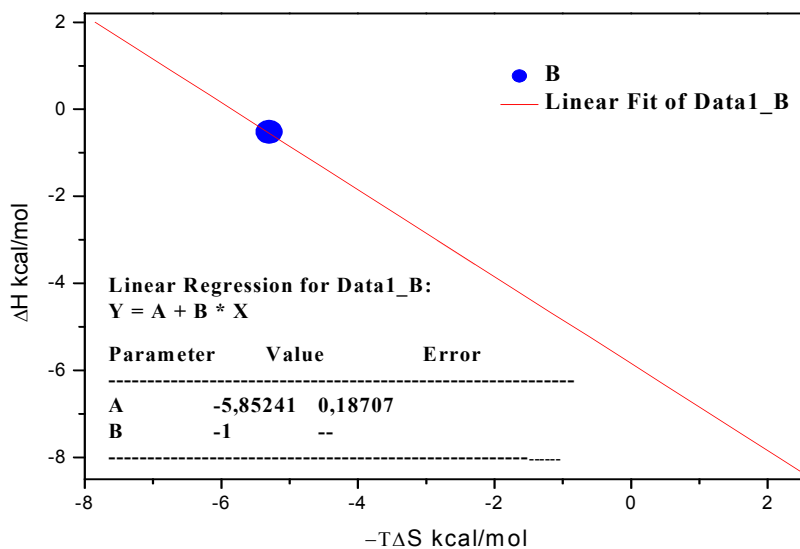


Figure 3.28: The TOP for the interaction of PEHMA-co-P4VPSB into the SiO₂ inorganic particles. The coordinates of the selected compound for optimization are plotted (blue point) and a straight line is traced between that point and (0, ΔG).

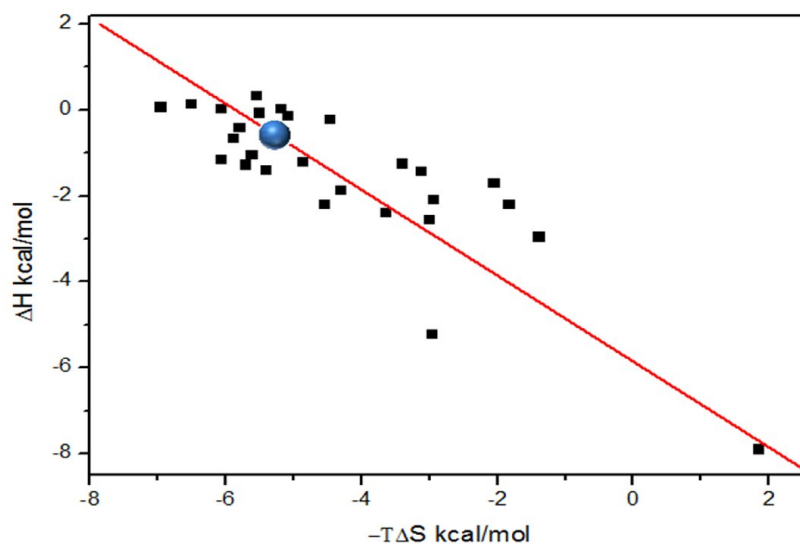


Figure 3.29: The $-T\Delta S$, ΔH points (■) for all complexes used in this study.

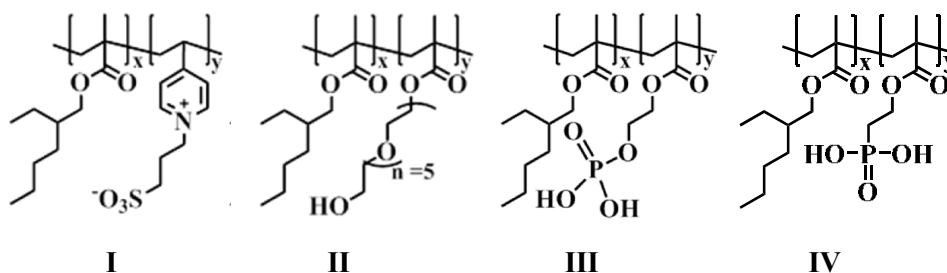
Once the first complex has been plotted, the binding thermodynamics of the other complexes are measured by ITC (see *Chapter 3.4*). Their measured ΔH and $-T\Delta S$ values (see Table 3.10) were added to the thermodynamic optimization plot as

shown in Figure 3.29. In this plot, all points that fall above the optimization line defined in Figure 3.28 have a lower binding affinity (K_B) than the selected complex (less than $1.06 \times 10^4 \text{ M}^{-1}$), and all points that fall below the optimization line have a higher binding affinity (K_B) (higher than $1.06 \times 10^4 \text{ M}^{-1}$). As the slope of the optimization line is -1, it follows that, for any given complex in the graph, the actual change in ΔG relative to the selected complex (PEHMA-co-P4VPSB / SiO_2) is given by either the vertical or horizontal distance from the coordinates of the complex to the optimization line.

3.6.2 Optimization Regions in TOP

By tracing a vertical and horizontal line through the experimental ($-T\Delta S$, ΔH) values for the optimization point (PEHMA-co-P4VPSB / SiO_2), six different regions can be defined. These regions are characterized not only by a higher or lower binding affinity but, most importantly, by different enthalpic and entropic contributions (see Figure 3.30).

As each point present the experimental ($-T\Delta S$, ΔH) values for every copolymer/nanoparticles complex (see Scheme 3.8), it is possible to identify the location and the type of chemical functionalities that will maximize a favorable enthalpy and entropy of binding.



Scheme 3.8: Chemical structures of the amphiphilic copolymers bearing different anchor groups: **I**) PEHMA-co-P4VPSB, **II**) PEHMA-co-PPEGMA, **III**) PEHMA-co-PEGMP and **IV**) PEHMA-co-PMOEPSA applied in this study.

The optimization plot is divided in the following regions: *Regions I* and *II* define the regions in which the binding entropy is more favorable but the binding enthalpy is less favorable related to other regions.

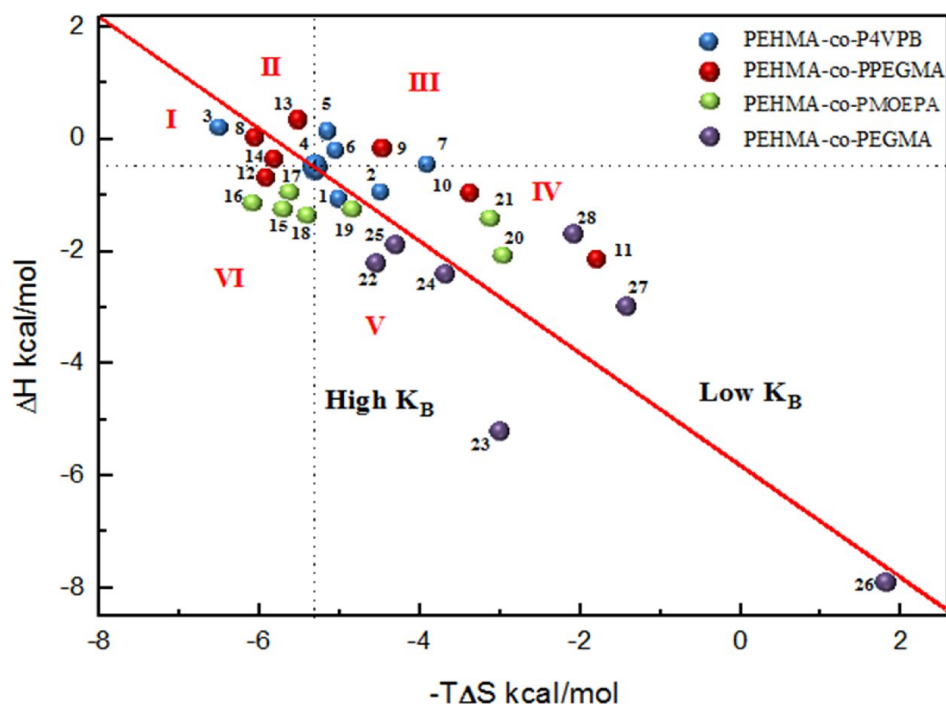


Figure 3.30: The thermodynamic optimization plot for all copolymer/nanoparticles complexes (numbered color balls) used in this study (see Table 3.10), six different regions can be defined.

The difference between region I and II is that in region I, the entropy gain upon binding is stronger than the enthalpy loss, resulting in an increase of the binding affinity. *Region III* is the region where the interactions result in both entropy and enthalpy loss. In *region IV*, the binding enthalpy is more favorable compared to the regions I, II as well as III, but not sufficient to overcome the associated entropy loss. In *regions V* and *VI*, the interaction of the amphiphilic compounds with the oxides surface results in a stronger binding affinity. In *region V*, the enthalpy gains are able to overcome the entropy loss while in *region VI* both the enthalpy and entropy changes are favorable.

Resulting from this classification, the adsorption and binding affinity for the selected complexes can be optimized. The complexes in regions *I*, *V* and *VI*, that result in better binding affinities than in the other regions, can be additionally explored with additional functionalities to expand the enthalpy gains. In *region III*, the interactions can be improved by replacing their functionalities into new functionality classes, which able to overcome the enthalpy and entropy losses as

well as increasing the binding affinity of the interaction (i.e. the adsorption and binding affinity optimization of the interactions with TiO₂, ZnO and CeO₂ particles) see Table 3.10.

In region *II*, the binding entropy is improved but the binding affinity diminishes because of a larger enthalpy loss. Conversely, in region *IV* the binding enthalpy is improved but the binding affinity diminishes because of a larger entropy loss. In the both cases, the entropy or enthalpy gain should be maintained while minimizing the enthalpy or entropy losses.⁸⁴ Under those conditions, strategies proposed to minimize the entropic compensation involve: (a) targeting several hydrogen bonds anchor groups to the hydrophilic part of the copolymer and/or on the surface of the nanocomposites (*Chapter 3.4.1.1*), (b) replacing the hydrophilic part of the copolymer (*Chapter 3.3.2*), (c) varying the concentration of the hydrophilic segment in the polymer chain (*Chapter 3.4.1.2*), and (d) selecting a stereochemistry that lowers the solvent exposure of hydrophobic groups and minimizes desolvation entropy losses (*Chapter 3.3.3*). These strategies can be able to defeat enthalpy/entropy compensation, rescue a complex from region *IV*, bring it to region *V* and consequently improve its binding affinity.

Table 3.10: The thermodynamic data of the interaction of the amphiphilic copolymers with SiO₂, Al₂O₃, CeO₂, ZnO, ZrO₂, TiO₂, Fe₃O₄ nanoparticles.

surface-active compound	K mol.L ⁻¹	ΔH kcal/mol	TΔS kcal/mol	ΔG kcal/mol
1 PEHMA-co-P4VPB Al ₂ O ₃	(1.34 ± 0.02) x10 ⁴	-1.09±0.001	4.97	-6.06
2 CeO ₂	(1.19 ± 0.12) x10 ³	-0.95±0.005	4.51	-5.46
3 Fe ₃ O ₄	(1.64 ± 0.24) x10 ⁴	0.17±0.008	6.52	-6.35
4 SiO ₂	(1.06 ± 0.22) x10⁴	-0.52±0.017	5.30	-5.82
5 TiO ₂	(5.44 ± 0.90) x10 ³	0.04±0.004	5.19	-5.15
6 ZnO	(6.74 ± 1.08) x10 ³	-0.12±0.001	5.10	-5.22
7 ZrO ₂	(1.51 ± 0.04) x10 ²	-0.44±0.07	3.91	-4.35
8 PEHMA-co-PPEGMA Al ₂ O ₃	(2.73 ± 0.61) x10 ⁴	0.04±0.01	6.08	-6.04
9 CeO ₂	(2.71 ± 0.30) x10 ³	-0.20±0.03	4.47	-4.67
10 Fe ₃ O ₄	(2.59 ± 0.60) x10 ³	-0.93±0.04	3.42	-4.13
11 SiO ₂	(7.17 ± 0.24) x10³	-2.18±0.15	1.84	-4.02
12 TiO ₂	(6.47 ± 1.07) x10 ⁴	-0.64±0.12	5.90	-6.54
13 ZnO	(6.15 ± 0.41) x10 ³	0.36 ±0.04	5.55	-5.18
14 ZrO ₂	(1.05 ± 0.05) x10 ⁴	-0.38±0.08	5.81	-6.19
15 PEHMA-co-PMOEP Al ₂ O ₃	(1.31 ± 0.39) x10 ⁵	-1.26±0.02	5.72	-6.98
16 CeO ₂	(1.12 ± 0.17) x10 ⁵	-1.13±0.03	6.08	-7.21
17 Fe ₃ O ₄	(1.93 ± 0.23) x10 ⁴	-1.03±0.11	5.63	-6.66
18 SiO ₂	(1.16 ± 0.17) x10⁴	-1.38±0.25	5.42	-6.80
19 TiO ₂	(2.84 ± 0.27) x10 ⁴	-1.18±0.02	4.88	-6.06
20 ZnO	(4.86 ± 0.36) x10 ³	-2.07±0.19	2.95	-5.02
21 ZrO ₂	(2.18 ± 0.22) x10 ³	-1.42±0.22	3.13	-4.55
22 PEHMA-co-PEGMP Al ₂ O ₃	(8.36 ±1.39) x10 ⁴	-2.18±0.13	4.56	-6.74
23 CeO ₂	(2.28 ± 0.09) x10 ⁴	-5.19±0.14	2.98	-8.17
24 Fe ₃ O ₄	(1.91 ± 0.16) x10 ⁴	-2.38±0.04	3.65	-6.03
25 SiO ₂	(8.53 ± 0.09) x10⁴	-1.85±0.03	4.31	-6.16
26 TiO ₂	(2.68 ± 0.37) x10 ⁴	-7.88±0.20	-1.83	-6.05
27 ZnO	(1.51 ± 0.20) x10 ³	-2.93±0.32	1.40	-4.33
28 ZrO ₂	(5.03 ± 0.83) x10 ³	-1.69±0.15	2.06	-3.75

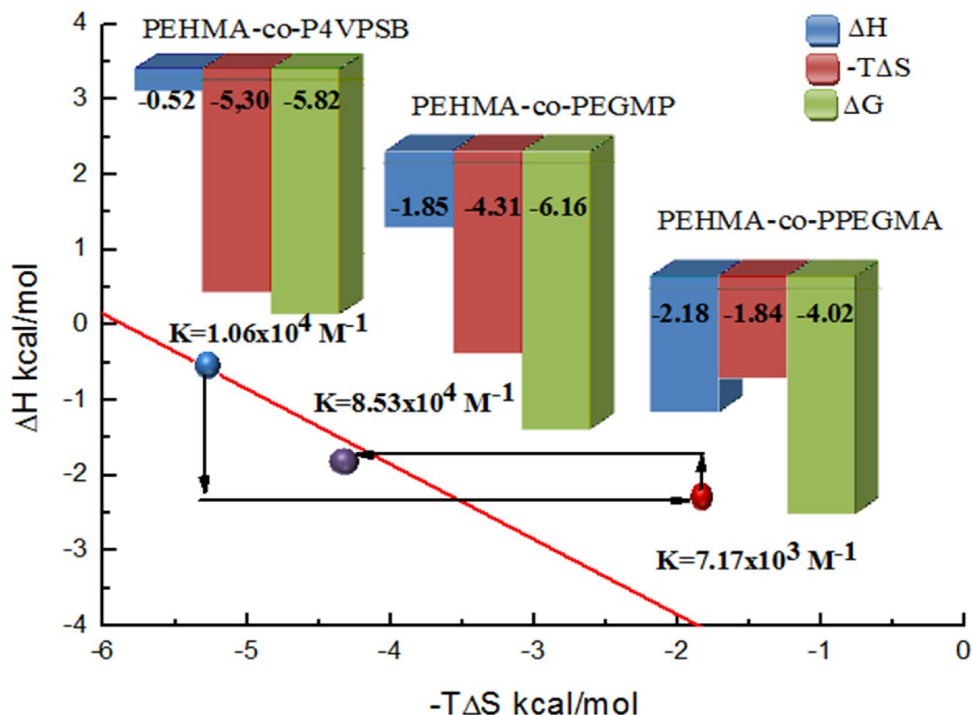
3.6.3 Optimization of the binding affinity in the copolymer/SiO₂ interaction

Figure 3.31: A situation encountered during affinity optimization of the amphiphilic copolymers (non-ionic, twitter-ionic and acidic) into the SiO₂ nanoparticles surfaces.

Figure 3.31 demonstrated a situation encountered during the affinity optimization of the bindings of the amphiphilic copolymers (non-ionic, twitter-ionic and acidic) on the SiO₂ nanoparticles surface (Table 3.10). At this point, the non-ionic anchor group PEG present in the amphiphilic compound, in contrast to the twitter-ionic group 4VPSB, results in a loss in the binding affinity. This loss in the binding affinity originates from a large entropy loss that over compensates the associated enthalpy gain of (-1.66) kcal/mol. The enthalpy gain is consistent with the formation of hydrogen bond by the ether and/or hydroxyl group (*Chapter 3.4.1.1*).⁸⁵ Replacing the functional group by adding an acidic anchor group like PO-(OH)₂ yield a copolymer, that maintains the enthalpy gain without the drawback of a significant entropy loss. As a result, the binding affinity of such a copolymer is improved from 7.73×10^3 to 8.53×10^4 M⁻¹.

This example clearly demonstrates the importance of balancing enthalpic and entropic contributions in order to maximize binding affinity as well as to generate

a higher binding affinity. It shows, that not the number of polar groups that matters but the quality of their interactions with the surfaces. It is better to have few groups that establish strong interactions than a large number of groups' mostly paying the desolvation penalty.

In this part, the ITC technique has been demonstrated as a method to screening and improving the bindings of the amphiphilic copolymers with inorganic nanoparticles surface by illustrating a thermodynamic optimization plot (TOP) resulting from the calorimetric measurements. The TOP provide a platform that allows the classification of the measured compounds into six different regions characterized by different enthalpy/entropy profiles. Compounds that fall into any of these regions can be further ranked in terms of their enthalpic and entropic gains, thus clearly demonstrates the importance of balancing enthalpic and entropic contributions in order to maximize binding affinity and illustrates important steps in the synthesis process. This study provides a practical guideline aimed at screening and improving the binding affinity in the organic–inorganic hybrid systems as well as other systems.

3.7 CONCLUSION

In this chapter, the interactions of the amphiphilic copolymers (PEHMA-co-PPEGMA^{n≈5}, PEHMA-co-P4VPSB, PEHMA-co-PMOEPA and PEHMA-co-PEGMP) with the inorganic nanoparticles (SiO₂, Al₂O₃, CeO₂, TiO₂, ZnO, ZrO₂ and Fe₃O₄) in a multicomponent solvent system have been investigated using the ITC technique.

In the first series of experiments, the adsorption of the low molecular weight model compounds with inorganic nanoparticles were studied, i.e., EHMA as a model compound to monitor the influence of the hydrophobic part of the copolymers on the adsorption process with inorganic particles, and the monomers PEGMA, EGMP and 4VPSB in a similar manner to EHMA, as a model compound to monitor the influence of the hydrophilic segment of copolymers on the adsorption process. It was found that the interaction of the hydrophobic monomer EHMA with the inorganic particle leads to an entropically driven process, which is usually characteristic of hydrophobic forces. This observation, confirmed the role of EHMA to impart hydrophobicity to the inorganic particles in the stabilization process.

On the other hand the titration of the hydrophilic monomers PEGMA, EGMP and 4VPSB showed a clear enthalpically driven process with a higher (negative) binding enthalpy ΔH compensated by a negative ΔS value. The dominant negative enthalpy suggested the presence of a large number of van der Waals interactions or hydrogen bonds between the monomers PEGMA, EGMP and 4VPSB and the inorganic particles surfaces (*Chapter 3.3*). These results identify the used of the hydrophilic monomers (bearing PEG, sulfonates or phosphonates anchor groups) as a surfactant in a multicomponent system for stabilization of the inorganic particles by providing interactions with their surfaces.

In the second series of experiments, the interactions of the amphiphilic copolymers PEHMA-co-PPEGMA^{n≈5}, PEHMA-co-P4VPSB, PEHMA-co-PMOEPA and PEHMA-co-PEGMP with SiO₂ particles were studied.

The obtained results, showed an adsorption behavior similar to the corresponding hydrophilic monomer. This behavior demonstrated that the hydrophilic side chains

of the copolymer were adsorbed on the surface of the particles, whereas the hydrophobic side chains, bearing no interaction with the particle surface, protruded into the solution, e.g. in the case of PEHMA-co-PPEGMA^{n≈5}/SiO₂, in which the interaction with the particle surface occurred mainly through the ethylene oxide (EO) functional group of the PEG segment whereas the terminal hydroxyl group shows only a minor role in the interaction of the PEHMA-co-PPEGMA^{n≈5}/SiO₂, however, was involved in the adsorption (see Figure 3.32 and Chapter 3.4.1.1).

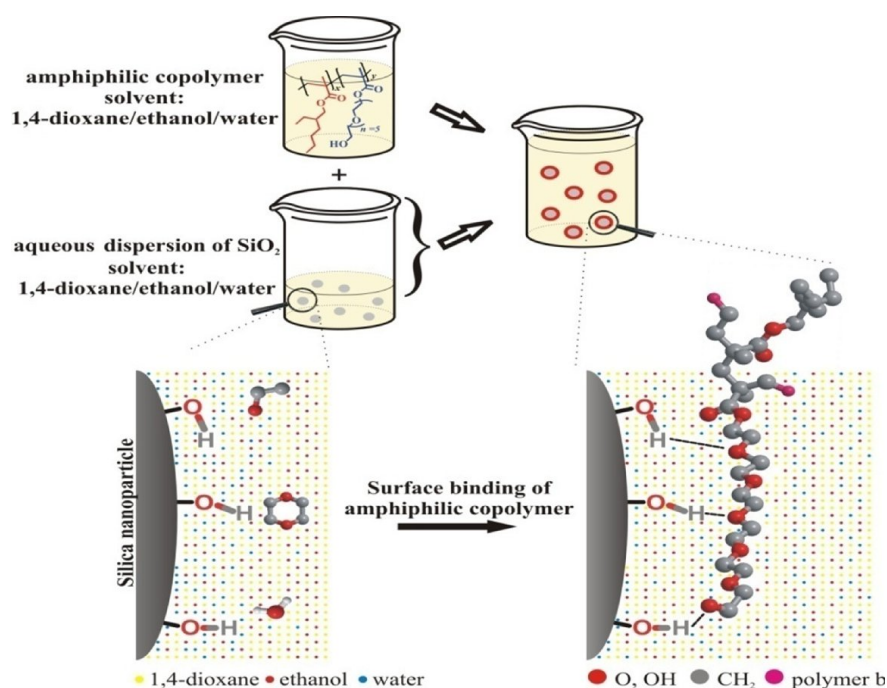


Figure 3.32: Schematic representation of the role of the monomers in the copolymer PEHMA-co-PPEGMA^{n≈5}, EHMA imparted hydrophobicity to the SiO₂ particles; PEGMA, as the hydrophilic part, provided the interaction of the polymer with the SiO₂ surface.

Furthermore, the accessibility of the anchor groups of the polymer for the interaction with the particle surface was of great importance, as demonstrated for the PPOMA vs. PEGMA (Figure 3.7 and Table 3.1). The anchor groups in both cases were identical (oxygen of the EO-groups and terminal OH-group), but for PPOMA the EO-groups were sterically shielded by a CH₃-group, which decrease the ability to form hydrogen bonds with the surface of the inorganic particles.

This moderate steric hindrance already leads to a dramatic decrease in the enthalpy and the binding affinity K_B of the interaction (see *Chapter 3.3.3*).

In order to compare the adsorption behavior between the different classes of anchor groups, *non-ionic vs. zwitter-ionic vs. acidic* with the inorganic particles, the interaction PEHMA-co-PPEGMA^{n≈5}, PEHMA-co-P4VPSB, PEHMA-co-PMOEPA and PEHMA-co-PEGMP with Al₂O₃, CeO₂, TiO₂, ZnO, ZrO₂ and Fe₃O₄ nanoparticles were investigated (see *Chapter 3.4*).

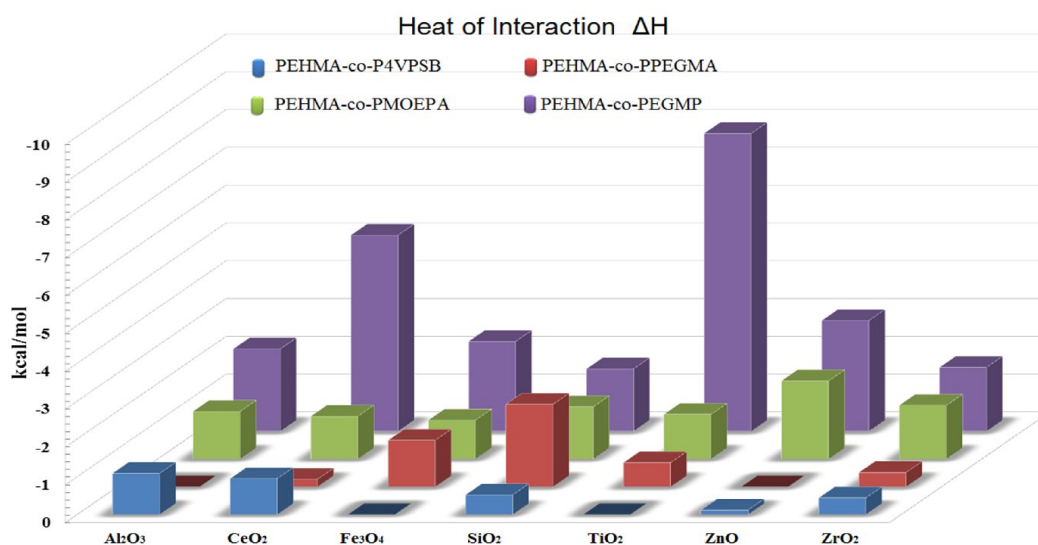


Figure 3.33: The enthalpy change ΔH signatures for the interactions of amphiphilic copolymers (non-ionic, zwitter-ionic and acidic) with various inorganic particles.

The enthalpic and entropic contributions to the free energy of binding differ noticeably for the amphiphilic copolymers and also for the inorganic particles used in this study. Several general characteristics can be observed (Figure 3.33):

- (i) Bindings with high favorable (negative) enthalpy ΔH and low unfavorable (negative) entropic changes ΔS , like in the interaction of the amphiphilic copolymer bearing the acidic $-P(O)(OH)_2$ group on the TiO₂ surface. This thermodynamic signature indicates a predominant enthalpic binding; driven by electrostatic forces
- (ii) Bindings occurred with low unfavorable (positive) enthalpy ΔH and high favorable (positive) entropic changes ΔS , such as the interaction of the amphiphilic copolymers bearing non-ionic with

the Fe_3O_4 particle or zwitter-ionic anchor groups with the Al_2O_3 particle. This thermodynamic profile is specific example for an interaction dominated by hydrophobic forces;

- (iii) Both favorable enthalpy ΔH (negative) and favorable entropy ΔS (positive) were detected, which shows that those bindings were dominated by hydrophobic forces, but characterized by slightly electrostatic forces, suggesting that the inorganic particles also establish a number of bonds with the amphiphilic copolymers, as detected by the interactions of the amphiphilic copolymer bearing the acidic $-\text{P}(\text{O})(\text{OH})_2/-\text{OP}(\text{O})(\text{OH})_2$ group with the surfaces of the inorganic particles.

Generally, these results, to the best of our knowledge, no report have been published using the complete thermodynamic parameters (ΔH , ΔS , ΔG and K_B) to quantify and analyse the adsorption process of monomers/copolymers with inorganic particles surfaces.

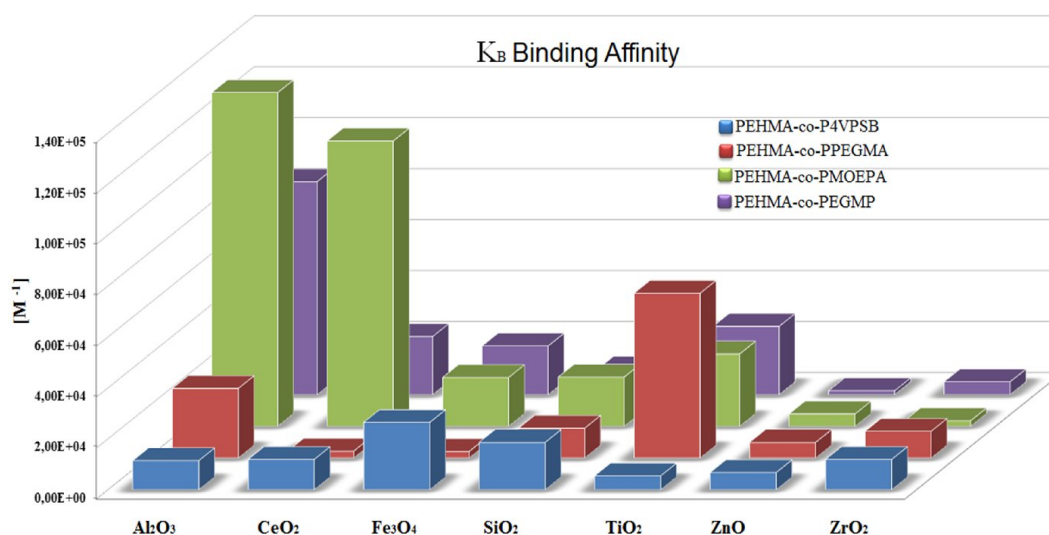


Figure 3.34: The binding affinity K_B for the interactions of amphiphilic copolymers (non-ionic, zwitter-ionic and acidic) with various inorganic particles.

Furthermore, the binding affinities (K_B) for the interactions of amphiphilic copolymers with inorganic nanoparticles were calculated (Figure 3.34). It showed that the use of the acidic anchor group such as $\text{P}(\text{O})(\text{OH})_2$ in case of PEHMA-co-PMOEPSA increased the binding affinity in most of the interactions with the

inorganic particles surfaces, e.g. the binding affinity of the interaction PEHMA-co-PMOEPA/ Al_2O_3 was two order of magnitude higher than that of PEHMA-co-P4VPB/ Al_2O_3 , and those of other inorganic particles.

Moreover, in order to investigate the influence of the temperature on the binding process of amphiphilic copolymers into the inorganic particles as well as the mechanisms of the interactions with each particle independently, the calorimetric titrations of the amphiphilic copolymers on the ZnO particle surface were performed over a range of temperature of 15-35 °C in 5 °C steps (*Chapter 3.5*). It was found that, an enthalpically as well as entropically driven binding interactions exist for PEHMA-co-PEGMP/ZnO and PEHMA-co-PMOEPA/ZnO containing an acidic anchor group by low temperature (15-20 °C).

On the other hand the interaction was improved by increasing the temperature of the system from 25 to 30 °C. In detail the interactions were driven by high favorable (negative) enthalpy contribution and low favorable (positive) entropy contributions, which suggest that the interactions take place through the formation of the P-O-M bonds or multiple hydrogen bonding with the particle surfaces (*Chapter 3.4.1*). The binding of PEHMA-co-P4VPSB containing zwitter-ionic anchor group at 15 °C were entropically driven with both positive enthalpy and entropy contributions, with increasing the titration temperature 20-30°C the interaction turn out to be less entropically driven by increasing the favorable (negative) enthalpy contributions.

On the other hand PEHMA-co-PEGMA/ZnO interaction was entropically driven in all temperatures, i. e. with unfavourable (positive) enthalpy contributions and favorable (positive) entropy contributions.

In the next part, with the purpose to prove the assumption of the mechanisms of the interactions for the used copolymers with each particle independently, the change in the specific heat capacity ΔC_p was implemented. Herein, the ΔC_p values for the interaction of the amphiphilic copolymers with the ZnO particle were measured at 15, 20, 25 and 30 °C. It was found that, the binding enthalpies ΔH at various temperatures are becoming more negative with increasing temperature (Figure 3.35).

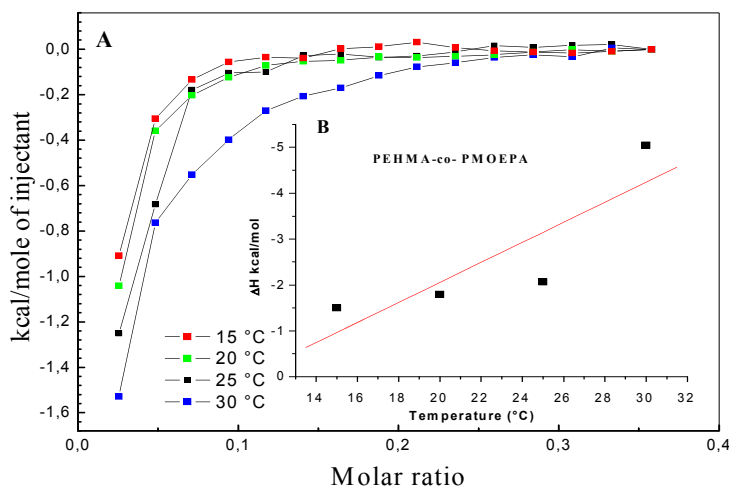


Figure 3.35: A) The binding isotherms of the interaction of ZnO nanocomposites with the amphiphilic copolymers PEHMA-co- PMOEP at 15, 20, 25 and 30°C., B) Plot of ΔH versus temperature for the calculation of ΔC_p .

The observed ΔC_p of the interaction PEHMA-co-PEGMA/ZnO was found to be small positive contribution which suggests that, this interaction is entropically dominated, in which the binding is attributed mainly to the extensive additional solvation, and partially to the burial of the polar groups of the interacting molecules. The ΔC_p values for the interactions of the copolymers, bearing the anchor groups P4VBP, PMOEP and PEGMA on the ZnO surface, were found to be small negative. The small contribution of ΔC_p suggests that electrostatic forces play a significant role in the heat capacity change, resulting from solvation upon binding compared with hydrophobic forces involved in the binding reactions.

As a final point, the ITC technique was presented here as a method to screen and improve the binding potency as well as the binding affinity in the polymer-inorganic-hybrids-systems. It shows that plotting the calculated thermodynamic parameters (ΔH) and ($-T\Delta S$) in a thermodynamic optimization plot (TOP) leads to classify the compounds into six regions relating to their enthalpic and entropic gain. In this plot, all points that fall above the optimization line (see *Chapter 3.6.1*) have a lower binding affinity (K_B) than the selected complex, and all points that fall below the optimization line have a higher binding affinity (K_B). Optimizing the binding affinity in the polymer-inorganic-hybrids-systems prove,

that the type of the polar group and its tendency to interact with the surfaces is much more important than the number of the polar groups (see *Chapter 3.6.3*). This approach is of general interest, since it provides a practical guideline aimed at screening and improving the binding potency in the organic-inorganic-hybrids-systems.

In conclusion, the above results proved firstly, the capability of multicomponent solvent systems as a versatile and powerful method to modify inorganic particles, starting from their commercially available aqueous dispersions. Various inorganic particles, such as Al_2O_3 , CeO_2 , TiO_2 , ZnO , ZrO_2 and Fe_3O_4 , were functionalized by amphiphilic copolymers. These amphiphiles carried different polar anchor groups such as PEG, sulfonates and phosphates/phosphonates guaranteeing a strong and irreversible adsorption of the polymers on the surface of the particles. Secondly, these studies represent the first detailed thermodynamic investigation of the adsorption of amphiphilic compounds (i.e. polymers) to a wide range of inorganic compounds (metal oxides) in complex solvent mixture by quantify and analyse their binding strength and binding affinity without need to a complex data evaluation or employing another supporting techniques. Our results strongly proved that isothermal titration calorimetry (ITC) can be used as a technique for the finding of the suitable anchor groups for specific particle, and for determination of the concentration of this anchor group in the polymer.

3.8 REFERENCES

- [1] Schmidtke, K., Stelzig, S., H., Geidel, C., Klapper, M., Müllen K., *Macromol. Symp.*, **2010**, 296, 28.
- [2] Stelzig, S. H., Klapper, M., Müllen, K., *Adv. Mater.*, **2008**, 20, 929.
- [3] Khrenov, V., Klapper, M., Koch, M., Müllen, K., *Macromol. Chem. Phys.*, **2005**, 206, 95.
- [4] Khrenov, V., Schwager, F., Klapper, M., Koch, M., Müllen, K., *Colloid Polym. Sci.*, **2006**, 284, 927.
- [5] Khrenov, V., Klapper, M., Koch, M., Müllen, K., *Polymer Bulletin*, **2007**, 58, 799.
- [6] S. Stelzig, J. Pahnke, G. Jonschker, M. Koch, M. Klapper, German Patent Application DE 10 2006058 201.2.
- [7] Schwager, F., Ph.D thesis, Max-Planck-Institut für Polymerforschung, **2009**.
- [8] Stelzig, S., Ph.D thesis, Max-Planck-Institut für Polymerforschung, **2010**.
- [9] Chellani, M., *Application Note*, **1999**, 10, 14.
- [10] Mizoue, L. S., Tellinghuisen, J., *Anal. Biochem.*, **2004**, 326, 125.
- [11] Ajayan, P. M. S.; L. S.; Braun P. V., *Nanocomposite Science and Technology*. Wiley-VCH Verlag GmbH & Co. KGaA: **2003**.
- [12] Jelesarov, I., Bosshard, H. R., *J. Mol. Recognit.*, **1999**, 12, 3.
- [13] Indyk L., Fisher, H. F. *Methods Enzymol.*, **1998**, 295, 350.
- [15] Haq, I., Ladbury, J. E., Chowdhry, B. Z., Jenkins, T. C., Chaires, J. B., *J. Mol. Biol.*, **1997**, 271, 244.
- [15] Privalov, P. L., Gill, S. J., *Pure Appl. Chem.*, **1989**, 61, 1097.
- [16] Silverstein, K. A. T., Haymet, A. D. J., Dill, K. A., *J. Am. Chem. Soc.*, **1998**, 120, 3166.
- [17] Frank, H. S., Evans, M. W., *J. Chem. Phys.*, **1945**, 13, 507.
- [18] Leavitt, S., Freire, E., *Curr. Opin. Struct. Biol.*, **2001**, 11, 560.
- [19] Nemethy, G., Scheraga, H. A., *J. Chem. Phys.*, **1962**, 36, 3382.
- [20] Sun, D. Z., Wang, S. B., Wei, X. L., Yin, B. L., *J. Chem. Thermodyn.*, **2005**, 37, 431.
- [21] Zajac, J., Trompette, J. L., Partyka, S., *J. Therm. Anal.*, **1994**, 41, 1277.
- [22] Denoyel, R., Rouquerol, J., *J. Colloid Interface Sci.*, **1991**, 143, 555.
- [23] Hergeth, W. D., Zimmermann, R., Bloss, P., Schmutzler, K., Wartewig, S., *Colloid Surf.*, **1991**, 56, 177.
- [24] Siffert, B., Li, J. F., *Colloids Surf.*, **1989**, 40, 207.
- [25] Holdgate, G. A., Tunnicliffe, A., Ward, W. H. J., Weston, S. A., Rosenbrock, G., Barth, P. T., Taylor, I. W. F., Pauptit, R. A., Timms, D. *Biochemistry*, **1997**, 36, 9663.
- [26] Vartapetian, R. S., Khozina, E. V., Karger, J., Geschke, D., Rittig, F., Feldstein, M. M., Chalykh, A. E., *Macromol. Chem. Phys.*, **2001**, 202, 2648.
- [27] Trens, P. Denoyel, R., *Langmuir*, **1993**, 9, 519.
- [28] Li, Y., Xu, R., Couderc, S., Holzwarth, J. F., Ghoreishi, S. M., Warr, J., Wyn-Jones, E., Bloor, D. M., *Langmuir* **2003**, 19, 2026.
- [29] Muller, D.; Carlsson, F.; Malmsten, M., *J. Colloid Interface Sci.*, **2001**, 236, 116.

- [30] Kenausis, G.L., Volrofs, J., Elbert, D. L., Huang, N., Hofer, R., Taylor, L.R., Textor, M., Hubbell, J. A., Spencer, N. D., *J. Phys. Chem. B*, **2000**, 104, 3298.
- [31] Kamal, M., Battisha, I. K., Salem, M. A., El Nahrawy, A. M. S., *J. Sol-Gel Sci. Technol.*, **2011**, 58, 507.
- [32] Kosmulski, M., Prochniak, P., Rosenholm, J. B. *Langmuir*, 2009, 113, 12806.
- [33] Pazik, R., Tekoriute, R., Hakanson, S., Seisenbaeva, G. A., Wiglusz, R., Streck, W., Gun'ko, Y. K., Kessler, V. G., *Chem., Eur. J.*, **2009**, 15, 6820.
- [34] Kreller, D. I., Gibson, G., van Loon, G. W., Horton, J. H., *J. Colloid Interface Sci.*, **2002**, 254, 205.
- [35] Kreller, D. I., Gibson, G., Novak, W., Gary W. Van Loon, Horton, J. H., *Coll. Surf. A: Physicochem. Eng. Aspects*, **2003**, 212, 249.
- [36] Corkill, J. M., Goodman, J. F., Tate, J. R., *Trans. Faraday Soc.*, **1966**, 62, 979.
- [37] Killmann, E., Winter, K., *Angew. Makromol. Chem.*, **1975**, 43, 53.
- [38] Morimoto, T., Naono, H. *Bull., Chem. Soc. Jpn.*, **1972**, 45, 700.
- [39] Adamson, A. W., *J. Am. Chem. Soc.*, **1954**, 76, 1578.
- [40] Breslow, R., Belvedere, S., Gershell, L., Leung, D., *Pure Appl. Chem.*, **2000**, 72, 333.
- [41] Schwager, F. Ph.D. thesis, Max-Planck-Institut für Polymerforschung, **2009**.
- [42] Stelzig, S. Ph.D. thesis, Max-Planck-Institut für Polymerforschung, **2010**.
- [43] Shekhawat G. S., Vedpriya A. *Nano Trends*, **2008**, 5, 1.
- [44] Huang Z. M., Zhang Y.-Z., Kotaki M., Ramakrishna S., *Composites Science and Technology*, **2003**, 63, 2223.
- [45] Albertsson, P. A. (1986) *Partition of Cell Particles and Macromolecules* (Wiley, New York).
- [46] Abbott, N. L., Blankschtein, D. & Hatton, T. A. *Macromolecules*, **1991**, 24, 4334–4348.
- [47] McPherson, A. (1999) *Crystallization of Biological Macromolecules* (Cold Spring Harbor Lab. Press, Plainview, NY).
- [48] Shalaby, M.N., *J. Disp. Sci. Tech.*, **2000**, 21, 839.
- [49] Moudgil, B. M., *Prog. Collo. Poly. Sci.*, **1990**, 82, 3.
- [50] a) Yurii, I., Matatov, M., Sheintuch M., *Ind. Eng. Chem. Res.*, **1998**, 37, 309.; b) Xu, Z., Yu, L., Han, L., *Front. Chem. Eng. China*, **2009**, 3, 318.
- [51] Basheva, E.S., Ganchev, D., Denkov, N.D., et al., *Langmuir*, **2000**, 16, 1000.
- [52] Acosta, E.J., Nguyen, T., Witthayapanyanon, A. et al., *Environ. Sci. Technol.*, **2005**, 39, 1275.
- [53] Christov, N.C., Denkov, N.D., Kralchevsky, P.A., et al., *Langmuir*, **2004**, 20, 565.
- [54] Bourgeat-Lami, E., Carlos, L. A. D., Caseri, W., Curie, H. A., de Zea Bermudez, V., Hayakawa, S., Hüsing, N., Kickelbick, G. *Hybrid Materials*, Wiley-VCH: Weinheim, Germany, **2007**.
- [55] Tsuruta, T., Hayashi, T., Kataoka, K., Kimura, Y., Ishihara, K., Eds.; CRC Press: Boca Raton, FL, **1993**.
- [56] Alexandratos, S. D., Smith, S. D., *J. Appl. Polym. Sci.*, **2004**, 91, 463.
- [57] Yu, S. H., Coelfen, H., Antonietti, M., *Chem. Eur. J.*, **2002**, 8, 2937.

- [58] Schuster, M., Rager, T., Noda, A., Kreuer, K. Maier, D., J., *Fuel Cells*, **2005**, 5, 355.
- [59] Mutin, H. P., Guerrero, G., Vioux, A. *J. Mater. Chem.*, **2005**, 15, 3761.
- [60] Forget, L., Wilwersa, F., Delhalle, J., Mekhalif, Z. *Appl. Surf. Sci.*, **2003**, 205.
- [61] Nowack, B., Stone, A. T., *Environ. Sci. Technol.*, **1999**, 33, 3627.
- [62] Meng, Q, Doetschman, DC, Rizos, AK, Lee, MH, Schulte, JT, Spyros A, Kanyi CW., *Environ. Sci. Technol.*, **2011**, 45, 3000.
- [63] Kreller, D. I., Gibson, G., vanLoon, G. W., Horton, J. H., *J. Colloid Interface Sci.*, **2002**, 254, 205.
- [64] Paciorek, K. J. L., Lin, W.-H., Masudaa, S. R. J., *Fluorine Chem.*, **1998**, 88, 55.
- [65] Guerrero, G., Mutin, P. H., Vioux, A., *Chem. Mater.*, **2001**, 13, 4367.
- [66] Lee, W. J., Kim, Y., Case, E. D., *J. Mater. Sci.*, **1993**, 28, 2079.
- [67] Welfle, K., Misselwitz, R., Hohneand, W., Welfle, H., *J. Mol. Recognit.*, **2003**, 16, 54.
- [68] Niedzwiecka, A., Stepinski, J., Darzynkiewicz, E., Sonenberg, N., Stolarski, R. *Biochemistry*, **2002**, 41, 12140.
- [69] a) Kauzmann, W., *Adv. Protein Chem.*, **1959**, 14, 1; b) Sturtevant, J. M., *Proc. Natl. Acad. Sci. USA* **1977**, 74, 2236; c) Privalov., P., Makhatadze. G., *J. Mol. Biol.*, **1993**, 232, 660.
- [70] Baldwin, R. L., *Proc. Natl. Acad. Sci. USA* **1986**, **83**, 8069.
- [71] Chunyan, H.; Junfeng, M.; Dingyin, T.; Yichu, S. ; Zhen, L.; Lihua, Z.; Yukui, Z., *J. Prot. Res.*, **2010**, 9, 4093–4101.
- [72] Cyrille, B.; Michael, W.; Volga B., Jingquan, L.; Thomas, D., *NPG Asia Mater.*, **2010**, 2, 23.
- [73] DeMaria, C. T.; Brewer G., *J. Bio. Chem.*, **1996**, 271, 12179.
- [74] Velazquez-Campoy, A.; Kiso Y.; Freire E. *Arch Biochem Biophys*, **2001**, 390, 169.
- [75] Lipinski, C.A.; Lombardo F.; Dominy, W., Feeney P.J., *Adv. Drug. Delivery Rev.*, **1997**, 23, 3.
- [76] Lipinski, C.A., *J. Pharmacol and Toxicol Methods*, **2000**, 44, 235.
- [77] Cabani, S., Gianni, P., Mollica, V., Lepori, L. *J. Solution Chem.* **1981**, 10, 563.
- [78] Ohtaka, H.; Muzammil, S.; Schon, A.; Velazquez-Campoy, A.; Vega, S., Freire, E.; *Int. J. Bioßchem Cell Biol.*, **2004**, 36, 1787.
- [79] Ohtaka, H.; Freire, E., *Progr. Biophys. Mol. Biol.*, **2005**, 88, 193.
- [80] Li L., Dantzer, J.J.; Nowacki, J.; O'Callaghan, B.J. ; Meroueh, S.O. ,*Chem Biol Drug Des.* **2008**, 71, 529.
- [81] Olsson, T.S.; Williams M.A.; Pitt W.R.; Ladbury J.E., *J Mol Biol.* **2008**, 384, 1002.
- [82] a) Niedzwiecka, A.; Stepinski, J.; Darzynkiewicz, E.; Sonenberg, N.; Stolarski. R. *Biochemistry*, **2002**, 41, 12140.
- [83] Kauzmann, W., *Adv. Protein Chem.* **1959**, 14, 1.
- [84] Freire, E., *Chem. Biol. Drug. Des.*, **2009**, 74, 468.
- [85] Trens, P.; Denoyel, R., Langmuir, **1993**, 9, 519.

CHAPTER 4

THERMODYNAMIC OF THE HOST-GUEST CHEMISTRY OF POLYPHENYLENE DENDRIMERS USING ITC

Abstract:

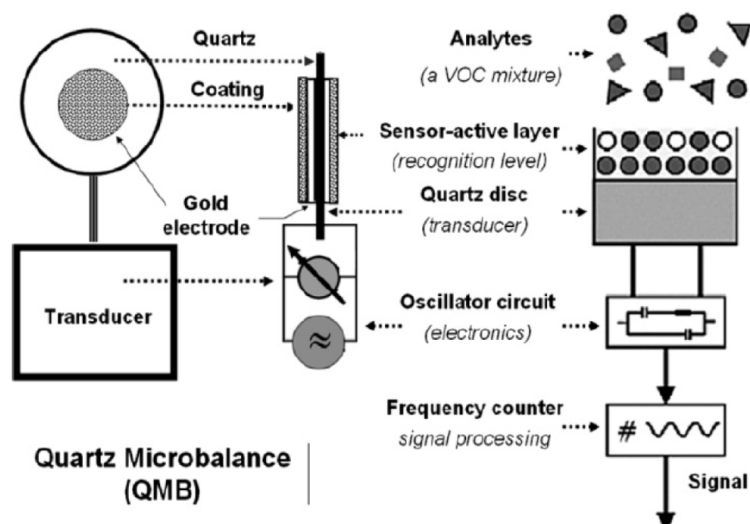
In this chapter, the interactions between various classes of volatile organic compounds (VOCs) with non-functionalized as well as functionalized polyphenylene dendrimers (PPDs) were quantified and analyzed using the ITC technique. Therefore, the influence of adding different functional groups in the interior layers (scaffold) of the polyphenylene dendrimer (Td-G2) on the sensitivity and also the selectivity to detect/uptake VOCs at very low concentrations (micromolar level) was studied. Likewise, the ability and sensitivity of PPDs for detection of highly explosive materials such as triacetone triperoxide (TATP) at very low concentrations (ppm level) has been investigated. In addition to the above, this ITC technique was proved as an analytical tool that can be applied to quantify and analysis of the adsorption behavior, reaction mechanisms and binding efficiencies of dendrimer-guest interactions or any other host-guest-systems by direct measurement of the heat of binding.

4.1 INTRODUCTION

Volatile organic compounds (VOCs) are potential environmental threats because of their increasing aerial concentration, toxicity and carcinogenic nature. They are primarily responsible for sick house syndrome ¹ and can cause and aggravate allergies, asthma, cancer, and emphysema. ² Recently, due to strict environmental regulations, it has become mandatory for food and chemical industries to monitor concentration of VOCs in the work environment at very low level. ³ This has led to an upsurge of research interest for novel VOC sensors.

Till date, metal oxide, ⁴ conjugated polymers, ⁵ and particle-polymer hybrids⁶ have been reported as promising materials for VOC-sensing. Though these materials are responsive to various VOCs, selectivity in terms of discriminating between polar and nonpolar VOCs still remains a challenging issue for sensor operations.

Polyphenylene dendrimers (PPDs) ⁷ and their derivatives have been regarded as interesting candidates for host-guest chemistry and also sensors because of their rigid framework containing stable internal cavities, and the tendency to fill these voids with small guest molecules. ⁸ A recent report by Schlupp *et al.* showed that they may be used as an active layer on quartz microbalance (QMB) for VOC sensing ⁹ (Scheme 4.1).



Scheme 4.1: A quartz microbalance (QMB) as a detector for volatile organic compounds (VOCs) (Adapted from Ref. 10).

In the quartz microbalance technique, the dendrimer is dissolved in THF, accelerated by a high voltage through a thin capillary and sprayed onto the top electrode of the QMB. This leads to the formation of a homogeneous, rigid layer. The thickness of the layer is controlled *in situ* by simultaneously monitoring the frequency of the QMBs to be coated. The resulting thickness is standardized corresponding to a frequency reduction of 10 kHz, at which point the coating is stopped. A standardized thickness (or mass) of the host compound on the sensor is a prerequisite for comparing the sensitivity and selectivity of the coatings and to assure reproducible results. In QMB studies coated sensors have been sequentially exposed to different VOCs in a gas mixing chamber with N₂ at 30-50 °C and at the highest possible concentration (400-1000 ppm).¹⁰

Although the molecules (i.e. PPDs) proved to be highly promising, the lone study left a few questions that deem to be answered.⁹ For example, (a) it has been claimed that the interaction of VOCs with PPDs is solely due to π - π electron donor acceptor (D-A) complexation that restricts inclusion of aliphatic hydrocarbons, alcohols, amines, aldehydes or carbonyl compounds into their voids and hence their detection using non-functionalized PPDs. The hypothesis needs to be reconfirmed since it imposes a constraint to the choice of molecules that can be detected using PPDs as sensors. (b) Based on gravimetric technique, an indirect attempt to estimate host-guest interaction energy (from Langmuir-like approximation of isotherms) and hence to predict the number of included guest molecules has been ventured. Such estimations are better accomplished through apply techniques like ITC as has been used in the present study. (c) Selectivity in terms of detection of polar solvents like benzaldehyde, acetophenone etc. In addition, it has also been emphasized by Schlupp *et al.* that PPD-VOC interaction takes place only via inclusion of VOCs within the voids and the role of dendrimer-surface is insignificant, which still remains to be verified. (d) Besides, all measurements in ref. 9 were reported at 50°C. Therefore, it remained an open question whether similar studies could be carried out at room temperature.

The isothermal titration calorimetry (ITC) technique is presented here as a new method to quantify and analyse the intermolecular forces in a dendrimer-based host-guest system, by direct measurement of the heat of binding, from which K_B ,

ΔG , ΔH , and ΔS values can be accurately determined. This understanding of the intermolecular interactions between host and guest are used to predict sensors performance.

4.2 EXPERIMENTAL SECTION

4.2.1 Materials

The unsubstituted polyphenylene dendrimer (Td-G2) was synthesized as reported earlier in ref.32. The substituted polyphenylene dendrimers with the internal functions groups (-COOMe and -COOH) were synthesized following the recipe developed by Dr. *Roland Bauer*.¹¹ The -NO₂, -CN and Pyridyl- functionalized dendrimers were synthesized by Mathias Grill in the dendritic materials subgroup.¹² All volatile organic compounds (VOCs) used in this study were obtained as pure liquids from Sigma-Aldrich Chemical GmbH (Germany). All VOCs were used without further purification.

4.2.2 ITC measurement

ITC measurements were performed using a Microcal VP-ITC titration microcalorimeter (MicroCal, Inc., Northhampton, MA, USA) at 25°C. To study the interactions of the dendrimers, 0.145 mM solution of polyphenylene dendrimer (PPD) in THF was placed in a calorimeter cell and aliquots containing 10 μ L of 50 mM VOCs (this corresponds to an amount of 50 μ mol ($5 \cdot 10^{-5}$ mol) VOC added in each injection) were added sequentially at intervals of 5 min from a syringe rotating at 320 rpm..

Control experiments heat of dilution of VOCs and polyphenylene dendrimers (PPD) in THF were also measured as control experiments. The heat curves were finally analyzed using Origin software[®] for estimation of thermodynamic parameters. To study the interaction of the polyphenylene dendrimers with the explosive material triacetone triperoxide (TATP), the following experimental parameters were set:

Number of injections:	16
Run temperature:	25°C
Reference power:	10 μ cal/s
Initial delay:	200 s
Syringe concentration:	0.001 mM (<i>Dendrimer</i>)
Cell concentration:	0.005mM (<i>TATP</i>)
Stirring speed:	307 rpm
Spacing:	300 s
Filter period:	1 s

For the investigation of the rebinding efficiency of the particles resulting from the molecularly imprinted polymers (MIPs) technique, a suspension of polymer nanoparticles (containing a total amount of 0.055 mM carboxylic acid groups) in toluene + 0.5% v/v acetic acid was placed in the sample cell, whereas the reference cell was filled with the pure solvent mixture. A 0.55 mM solution of (\pm)-propranolol (in syringe) in the same solvent mixture was titrated to the sample cell. The influence of the enthalpy caused by the titrant dilution was determined by repeating the titration with the reference cell filled with the pure solvent mixture. The released/absorbed heat caused by the dilution enthalpy was subtracted from the data obtained from the titration of the polymer nanoparticles with (\pm)-propranolol.

4.2.3 Fluorescence spectroscopy

0.145 mM solution of Td-G2 was prepared by dissolving an appropriate amount of Td-G2 in tetrahydrofuran (THF). 0.05 mM solution of the VOCs was prepared by dilution. Sample solutions were then prepared by mixing appropriate volume of the two stock solutions as given in Table IS (see support). Steady state fluorescence measurements were carried out at room temperature on a (SPEX Fluor log II (212)) spectrometer with a xenon lamp as the source for excitation. Excitation was done at 310nm for toluene/Td-G2 samples, while at 300 nm for the other VOCs.

RESULTS AND DISCUSSION

In the first part of this chapter the binding of a widely used class of volatile organic compounds (VOCs) as *guest* molecules to an unsubstituted polyphenylene dendrimer (Td-G2) as *host* was studied using the ITC technique. The results are supported by fluorescence studies. This includes studies on heat capacity changes, effect of solvents and estimation of the stoichiometry.

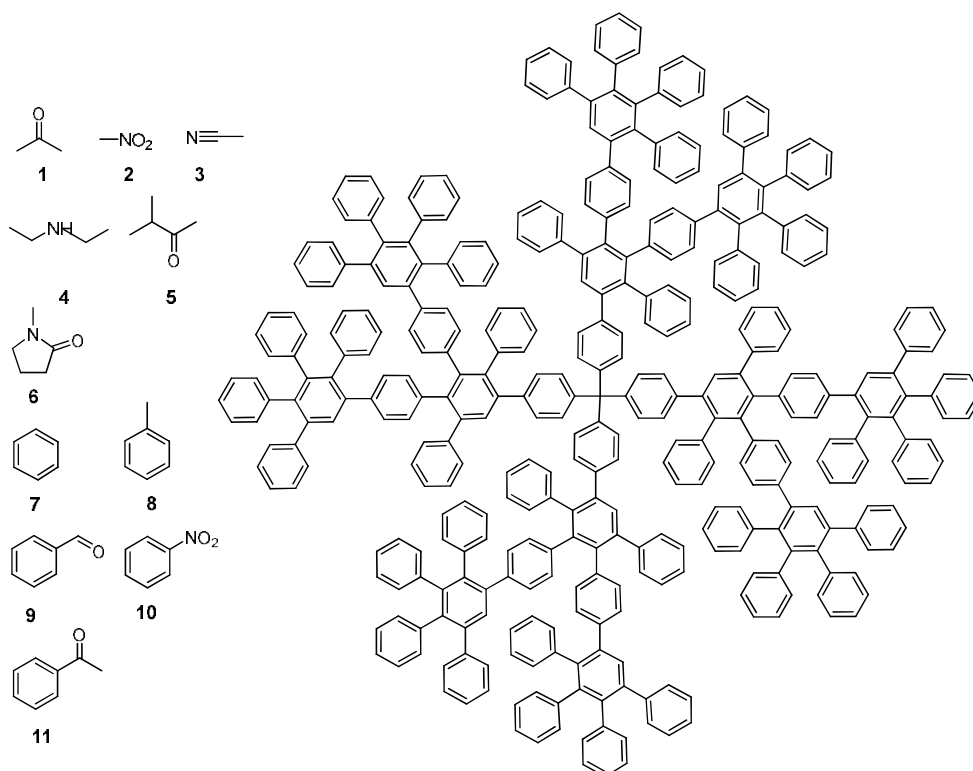
Subsequently, fluorescence spectroscopic studies VOC/Td-G2 host-guest interactions are reported. Furthermore, the interior functionalized polyphenylene dendrimers were utilized in an analogous manner to detect the impact of different classes of functional groups (neutral versus acidic or basic) on their adsorption behavior.

In the next part, the interactions of the highly explosive material triacetone triperoxide (TATP) with functionalized as well as non-functionalized polyphenylene dendrimers were performed. This includes studies on the influence of temperature on the binding process of dendrimers with TATP molecules as well as the mechanisms of the interactions

In the last part of this chapter, thermodynamic profiles as well as rebinding efficiency of nanosized molecularly imprinted polymer particles were studied using ITC technique. These particles were prepared by nonaqueous emulsion polymerization using a standard monomer mixture of methacrylic acid and ethylene dimethacrylate, containing (\pm)-propranolol as a template.

4.3 VOCS SENSOR STUDY

4.3.1 The interaction of the non-functionalized polyphenylene dendrimers and VOCs



Scheme 4.2: Non-functionalized polyphenylene dendrimer (Td-G2) and the VOCs used in this study: **1)** acetone, **2)** nitro methane, **3)** acetonitrile, **4)** diethyl amine, **5)** methyl isopropyl ketone (MIPK), **6)** 1-methyl-2-pyrrolidine (NMP), **7)** benzene, **8)** toluene, **9)** benzaldehyde, **10)** nitro benzene and **11)** acetophenone.

Figure 4.1 illustrates the raw data of ITC experiments for the interaction of VOCs as guest molecules to the non-functionalized polyphenylene dendrimer (Td-G2) with 64 phenyl rings (Scheme 4.2) as host. Each peak corresponds to the heat released on addition of an aliquot of the VOCs to a solution of polyphenylene dendrimer (Td-G2) in THF at 25 °C. From the Table 4.1 the enthalpic and entropic contributions to Gibb's free energy of binding were found to be different for the polar, nonpolar and the aliphatic VOCs. Most of the cases yielded low negative i.e. favorable heat changes (ΔH) and high positive i.e. favorable entropy changes (ΔS).

This implies that the interactions are predominantly entropic, most probably driven by hydrophobicity but at the same time characterized by slightly favorable enthalpy change that entails VOCs to establish different types of bonding with Td-G2 molecules. Here, the binding enthalpy or negative ΔH reflects the strength of complexation via non-covalent interactions e.g. van der Waals, π - π -stacking, CH- π , etc. relative to those existing with the solvent.¹³

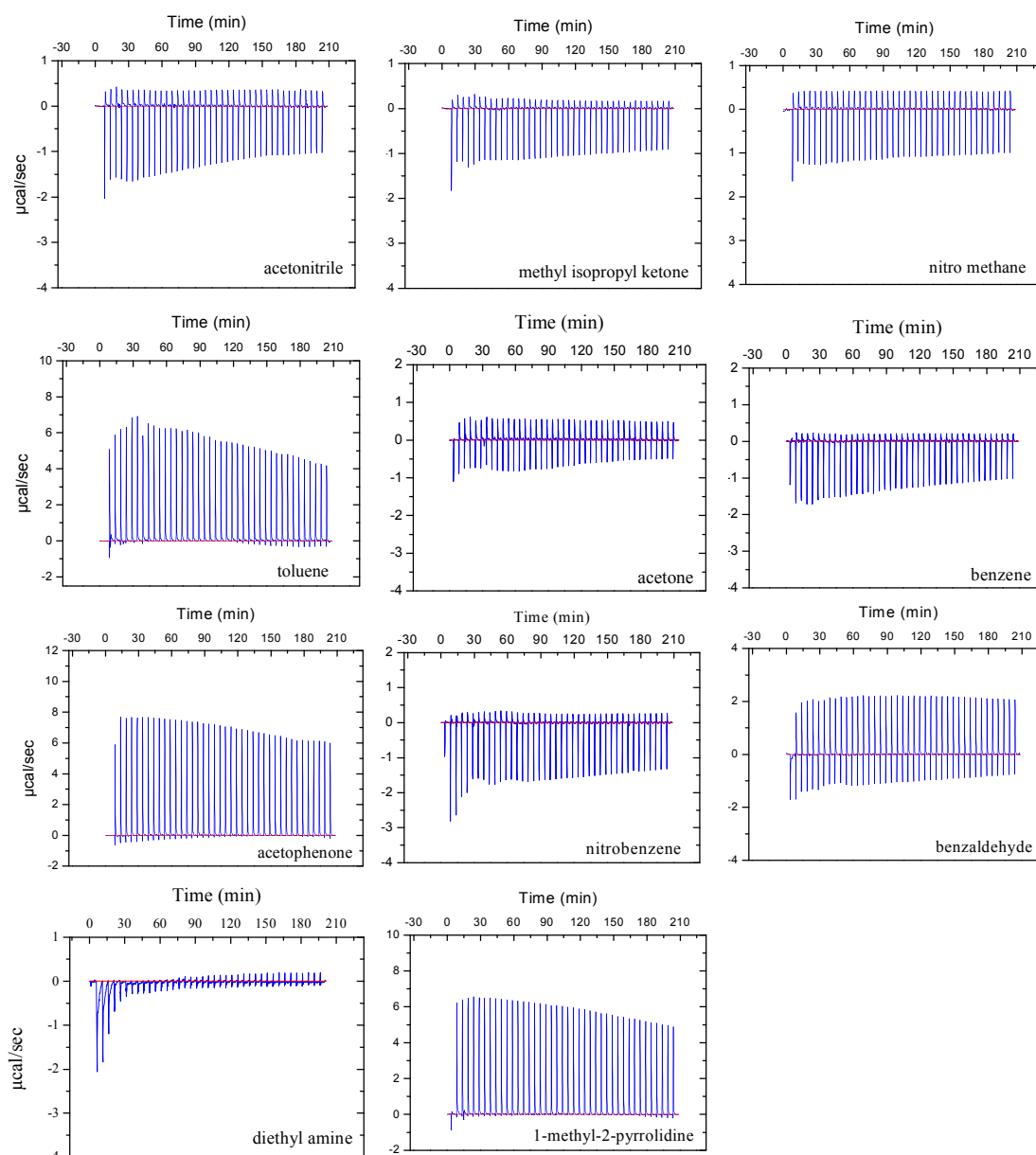


Figure 4.1: Binding isotherms for the interactions of volatile organic compounds (VOCs) with non-functionalized polyphenylene dendrimer (Td-G2) in THF at 25 °C.

Table 4.1: Thermodynamic parameters for interaction between Td-G2 and VOCs in THF at 25 °C.

VOCs	N	K M ⁻¹	ΔH kcal/mol	T ΔS kcal/mol	ΔG kcal/mol
acetone	7 ± 1.24	(5.89 ± 0.02) x10 ³	-0.034± 0.005	5.098	-5.132
benzene	11 ± 0.02	(6.10 ± 1.10) x10 ³	-0.038± 0.001	5.128	-5.166
nitro methane	2 ± 1.38	(8.90 ± 1.03) x10 ³	-0.055± 0.012	5.336	-5.391
toluene	5 ± 0.79	(1.03 ± 0.68) x10 ⁴	-0.061± 0.022	5.426	-5.487
acetonitrile	5 ± 0.56	(7.77 ± 1.44) x10 ³	-0.072± 0.007	5.247	-5.319
diethyl amine	7 ± 1.05	(6.48 ± 0.87) x10 ³	-0.075± 0.010	5.128	-5.200
MIPK ^[a]	4 ± 0.72	(6.49 ± 0.49) x10 ³	-0.093± 0.020	5.098	-5.191
NMP ^[b]	6 ± 0.38	(1.13 ± 0.71) x10 ⁴	-0.105± 0.018	5.336	-5.441
benzaldehyde	4 ± 0.44	(9.16 ± 0.79) x10 ³	-0.113± 0.014	5.277	-5.390
acetophenone	3 ± 0.25	(1.00 ± 0.25) x10 ⁴	-0.130± 0.042	5.336	-5.466
nitro benzene	2 ± 0.04	(1.15 ± 0.23) x10 ⁴	-0.135± 0.008	5.396	-5.531

Figure 4.3 shows a bar chart of ΔH values for different VOCs. It was observed that interaction of Td-G2 with polar aromatic compounds like nitro benzene ($\Delta H = -0.135$ kcal/mol), benzaldehyde ($\Delta H = -0.113$ kcal/mol) and acetophenone ($\Delta H = -0.130$ kcal mol⁻¹) yields higher negative ΔH values than those with nonpolar aromatic compounds e.g. benzene ($\Delta H = -0.038$ kcal mol⁻¹) and toluene ($\Delta H = -0.61$ kcal/mol) or aliphatic compounds like acetone ($\Delta H = -0.034$ kcal/mol), acetonitrile ($\Delta H = -0.072$ kcal/mol), methyl isopropyl ketone (MIPK) $\Delta H = -0.093$ kcal/mol and 1-methyl-2-pyrrolidine ((NMP) $\Delta H = -0.105$ kcal/mol). The explanation for this ΔH values differences can be attributed to the exclusively aromatic skeleton of Td-G2 dendrimer, which may form π π -electron donor-acceptor complexes.⁹ Therefore, this type of dendrimer shows a relatively weak affinity for benzene and toluene (see Scheme 4.2), and since the π -electron densities of these guests are virtually identical to that of the host (Td-G2) molecule. Those ITC results proves that the binding interaction of Td-G2 with polar aromatic compounds is much stronger than that with nonpolar aromatic and aliphatic compounds, which is in agreement with the result from QMB.⁴³ Obviously, it renders selectivity to the technique in terms of discriminating different classes of VOCs.

However, in contrast to QMB, ITC could successfully quantify the interaction between non-functionalized polyphenylene dendrimer (Td-G2) and nonpolar aromatic compounds like benzene or toluene and aliphatic compounds like acetone, which has never been reported earlier by any analytical technique.

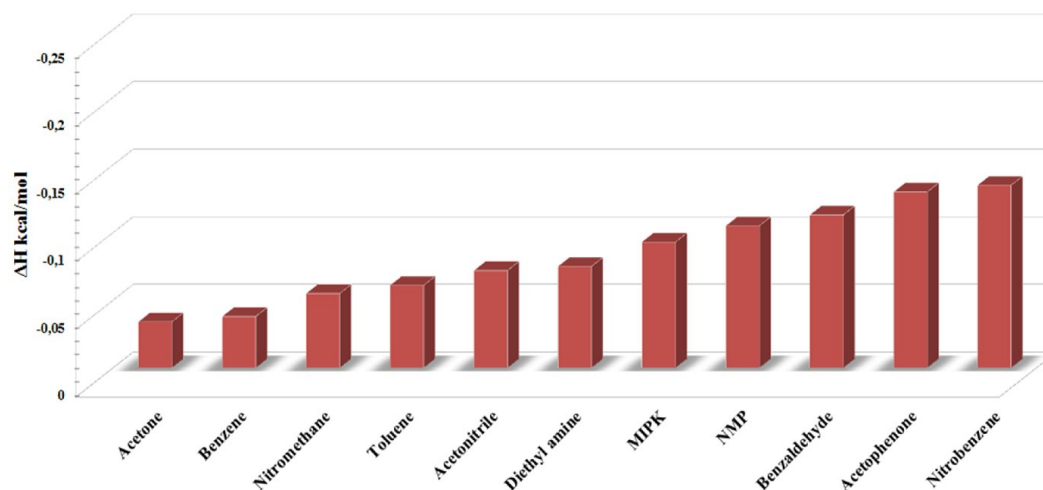


Figure 4.2: Enthalpic contributions ΔH as determined by ITC measurement for the interaction of VOCs with the (Td-G2) in THF at 25°C.

In a typical host guest interaction, change in entropy ΔS results from two opposing contributions i.e. a positive (favorable) change in solvation entropy and a negative (unfavorable) change in conformational entropy.¹⁴⁻¹⁶ In all cases the dominant driving force for binding is a large positive entropy change (see Table 4.1) that originates primarily from the release of solvent from the host and the guest upon binding, and a small loss of conformational entropy due to the little flexibility of the host (Td-G2-phenyl) reshaped to the geometry of the binding site. As long as both the host and the guest are dissolved with same solvent molecules, and upon binding through the non-covalent interactions, solvent molecules released into bulk solution, thereby increasing the entropy of the overall system.¹⁷ On the contrary, entropy is almost always unfavourable (negative), as the binding process involves the loss of conformational degrees of freedom for both the VOCs and the dendrimer molecule.¹⁸

4.3.1.1 Stoichiometry of the host-guest interaction

The study of the stoichiometry of the host-guest interaction (n), which can be determined from the fits of the titration curves (Figure 4.1), shows a widely difference for the used VOCs starting from 2 in case of nitromethane to 11 in case of benzene (Table 4.1). Previously, Schlupp *et al.*⁹ suggested that PPD/VOC interaction takes place only via inclusion of VOCs within the voids. In support of the hypothesis they even presented a correlation between energy of such interaction and the number of phenyl rings present in the host molecules. However, if this hypothesis were true, then for a given host there should also exist an inverse relationship between the n value and size of the VOCs since cavity size is fixed for a given PPD (Figure 4.3). The observed n values proved, that no such correlation could be obtained for the interaction of a large number of VOCs with Td-G2 (see Table 4.1).

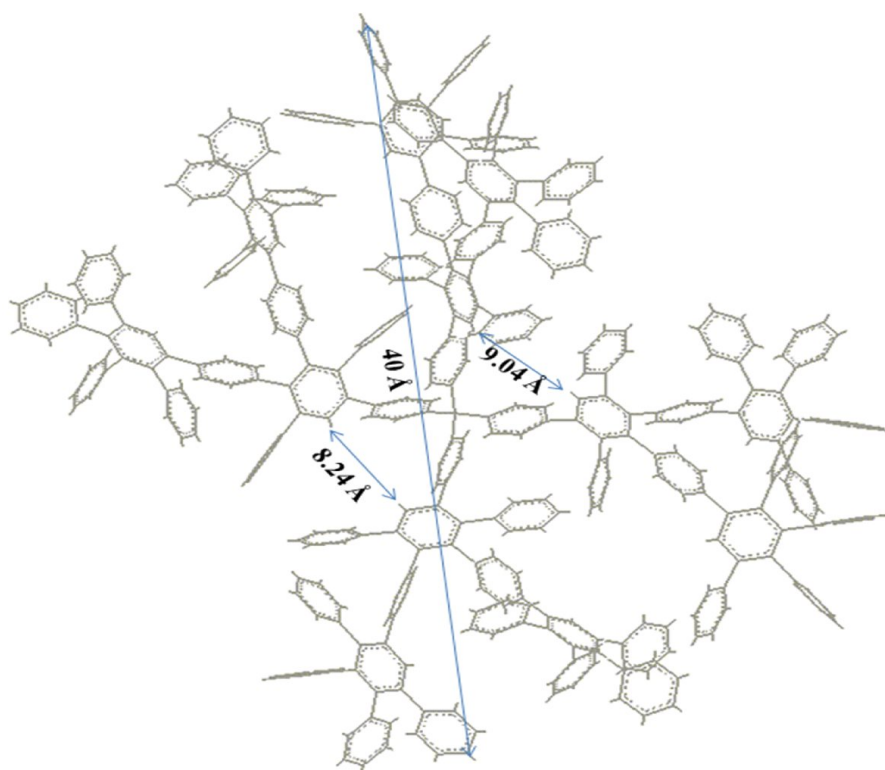


Figure 4.3: 3D molecular models of the unsubstituted polyphenylene dendrimer (Td-G2) with 64 phenyl rings.

In fact, a reverse trend was observed for nitromethane and benzene or diethyl amine (see Figure 4.4). Both benzene and diethyl amine are larger in size than nitromethane, but interestingly n values for benzene ($n= 11$) and diethyl amine ($n= 7$) are much higher than that for nitromethane ($n= 2$). Moreover, considering the cavity size of Td-G2 (Figure 4.3), it is highly improbable to assume that 11 molecules of benzene or 7 molecules of diethyl amine could be accommodated into the cavity alone. Thus it is inferred that interaction between the PPD and VOCs not only takes place inside the core of the cavity as found by the QMB study,⁹ but also take place on the PPD surface (outside the core).

Furthermore, sensitivity of detection by PPDs depends on the strength of interaction (the heat released i.e. $-\Delta H$) and not merely on the number of VOCs adsorbed inside core. Additionally, the binding affinity K_B showed that polar aromatic VOCs had the highest binding affinity, such as in the case of nitrobenzene and acetophenone ($K_B= 1.10 \times 10^4$ to $1.15 \times 10^4 \text{ M}^{-1}$). These values are about one order of magnitude higher than those found for the nonpolar aromatic and aliphatic VOCs (see Table 4.1 and Figure 4.4).

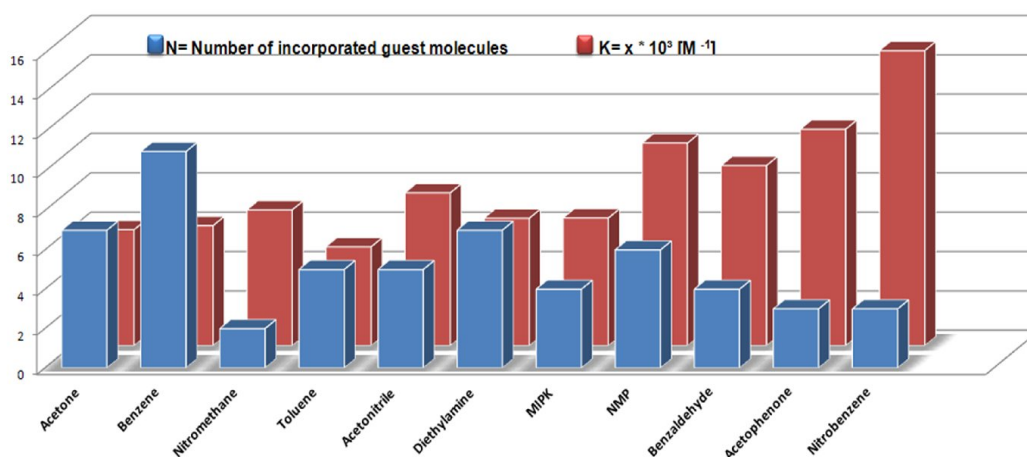


Figure 4.4: Number of incorporated guest molecules N and Binding affinity K_B for the interaction of VOCs with the (Td-G2-phenyl) in THF, at 25°C.

4.3.1.2 Heat capacity change (ΔC_p) in Td-G2/VOCs interaction

In order to probe deep into the mechanism of the interaction of VOCs with Td-G2, the change in heat capacity (ΔC_p) of interaction between Td-G2 and nonpolar-aromatic benzene, polar-aromatic benzaldehyde, and the aliphatic diethyl amine were measured (in THF) at 15, 25, 35 and 45 °C.

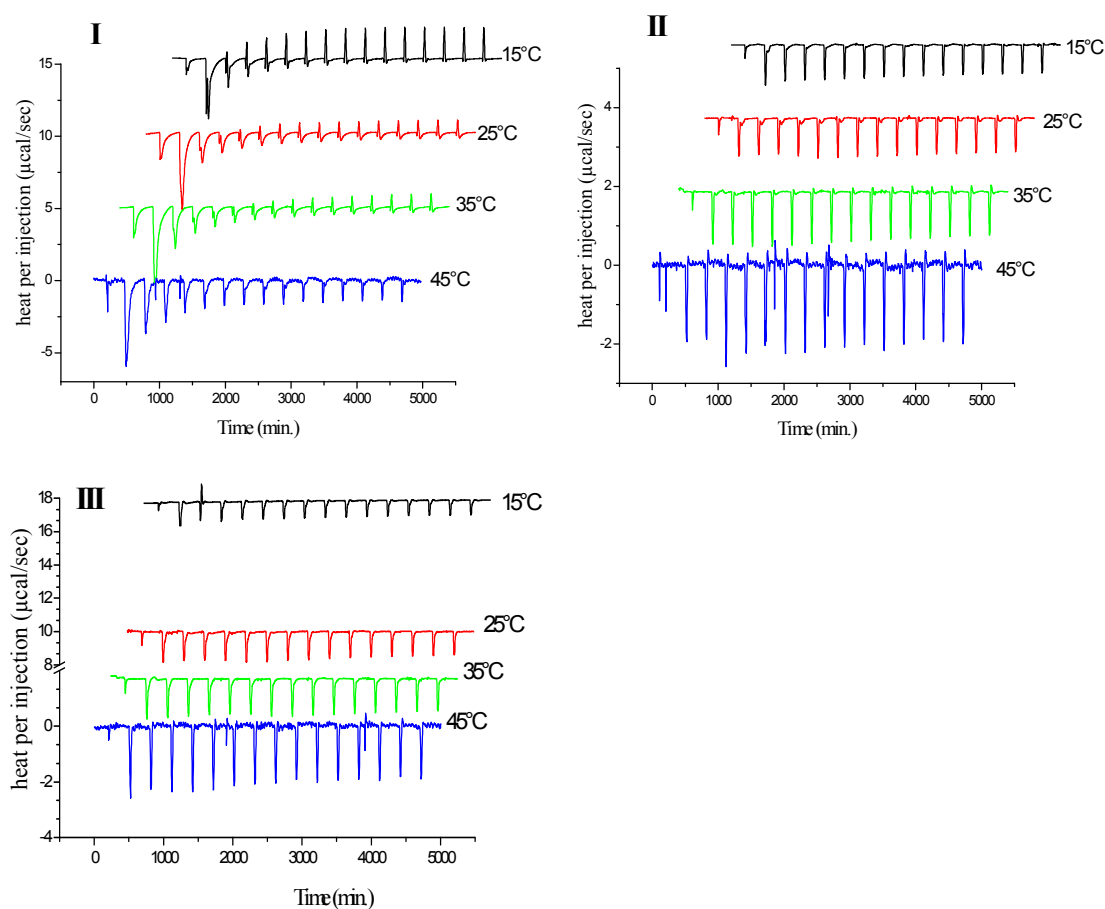


Figure 4.5: Binding isotherm for a titration of I) diethyl amine, II) benzaldehyde and III) benzene with Td-G2 at different temperatures.

The binding isotherm of the interaction of Td-G2 with benzene, diethyl amine and benzaldehyde at 15, 25, 35 and 45 °C were displayed in Figure 4.5. The results indicate that all binding reactions with Td-G2 are exothermic. The integration of binding isotherms shows that the binding enthalpies are strongly temperature dependent (Figure 4.6), becoming more negative with increasing temperature (see Table 4.2).

Practically, the interaction with benzene at 15 °C is entropically driven with both positive enthalpy and entropy contributions. Alternatively with increasing the titration temperature 25-45 °C the interaction turns out to be less entropically driven by increasing the favorable (negative) enthalpy contributions (Table 4.2). On the other hand the interactions of diethyl amine and benzaldehyde with Td-G2 showed at low temperature (15°C) a small favorable (negative) enthalpy and highly favorable (positive) entropy contributions, suggesting that the interactions are mainly controlled by hydrophobic forces compared with only small contributions of weak electrostatic forces. Furthermore, with increasing temperature from (25 to 45 °C), the interactions remain practically invariant with small favorable (negative) enthalpy and highly favorable (positive) entropy contributions.

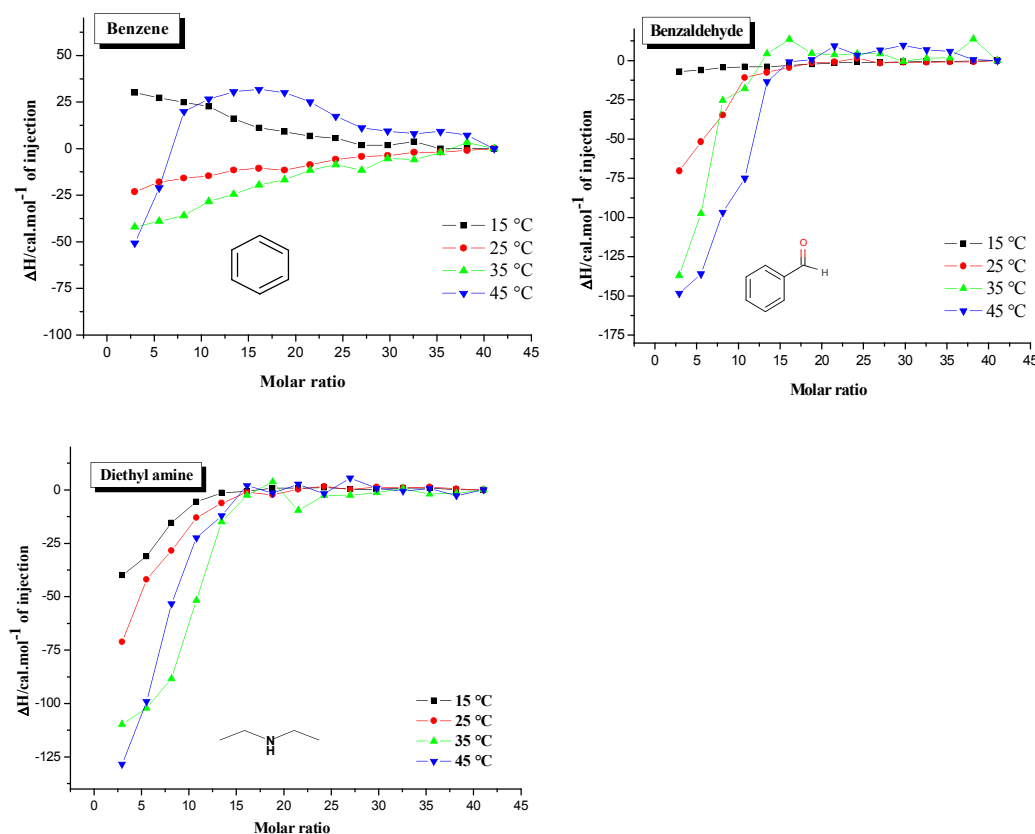


Figure 4.6: The integration of the binding isotherms of benzene, benzaldehyde and diethyl amine in THF to Td-G2 polyphenylene dendrimer determined at different temperatures.

Table 4.2: Thermodynamic parameters for interaction Td-G2/benzene, diethyl amine and benzaldehyde in THF detergent at different Temperatures.

VOC-guest	T °C	K_B M ⁻¹	ΔH kcal/mol	T ΔS kcal/mol	ΔG kcal/mol
Benzene	15	$(7.61 \pm 1.83) \times 10^3$	0.03 ± 0.002	5.33	-5.30
	25	$(6.10 \pm 0.32) \times 10^3$	-0.04 ± 0.003	5.12	-5.16
	35	$(2.11 \pm 0.49) \times 10^3$	-0.06 ± 0.004	5.47	-5.53
	45	$(2.05 \pm 0.01) \times 10^3$	-0.08 ± 0.002	4.81	-4.89
Diethyl-amine	15	$(3.06 \pm 0.65) \times 10^3$	-0.04 ± 0.001	5.08	-5.12
	25	$(6.48 \pm 1.08) \times 10^3$	-0.07 ± 0.001	5.13	-5.20
	35	$(3.14 \pm 0.69) \times 10^4$	-0.13 ± 0.003	5.79	-5.92
	45	$(2.09 \pm 0.18) \times 10^4$	-0.14 ± 0.006	5.95	-6.09
Benzaldehyde	15	$(2.09 \pm 0.66) \times 10^3$	-0.04 ± 0.002	4.53	-4.54
	25	$(9.86 \pm 0.11) \times 10^3$	-0.11 ± 0.004	5.27	-5.39
	35	$(7.10 \pm 1.91) \times 10^4$	-0.13 ± 0.009	5.49	-5.62
	45	$(1.11 \pm 0.57) \times 10^4$	-0.18 ± 0.002	5.83	-6.01

The change in heat capacity ΔC_p was estimated from the slope of ΔH versus temperature curves (see Figure 4.7) assuming a temperature independent ΔC_p in that range. ΔC_p values as well as the correlation coefficients of fitting the data points are listed in Table 4.3.

Table 4.3: Calculated ΔC_p values and correlation coefficients assuming a linear relation between ΔH and temperature.

VOC	ΔC_p k cal.mol ⁻¹ .K ⁻¹	Correlation coefficient (R ²)
Benzene	-3.82 ± 0.89	0.9026
Diethyl amine	-3.41 ± 0.05	0.9995
Benzaldehyde	-4.07 ± 0.49	0.9718

It was observed that in all the cases, ΔC_p values were large negative, i.e., the complexes had lower heat capacities than the components.¹⁹ The ΔC_p values for the binding of benzene, diethyl amine and benzaldehyde to Td-G2 were similar. This indicated a basic similarity in the binding processes and thermodynamic properties.

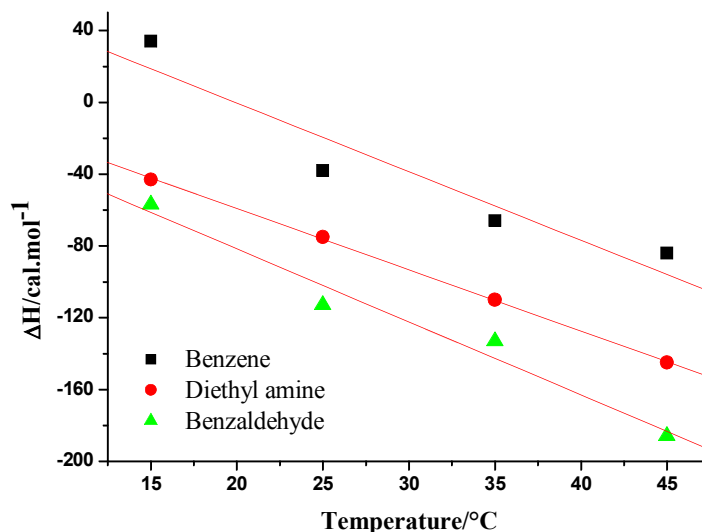


Figure 4.7: The binding isotherms of benzene, diethyl amine and benzaldehyde in THF to Td-G2 polyphenylene dendrimer determined at different temperatures.

The large negative ΔC_p values can be correlated with the burial of hydrophobic surface areas of the VOC- molecules from exposure to solvent upon complex formation.^{20, 21} These ΔC_p values prove that hydrophobic interactions are the driving forces in the binding of VOCs to the Td-G2 dendrimer. Moreover, another confirmed signature of the dominated hydrophobic interaction between Td-G2 and VOCs is the observed large positive entropy change ΔS (see Table 4.2).²² In case of benzaldehyde binding, ΔC_p was about 10 % higher than in the case of benzene and diethyl amine. This can be explained by regarding to the size of the benzaldehyde molecule, which is bulkier than benzene and diethyl amine, as a result, larger amount of THF to be released upon complex formation of benzaldehyde with the dendrimer.

However, small negative ΔH contributions obtained from (Td-G2)-VOCs titration in most of the cases (Table 4.2), implies that apart from hydrophilic interactions, there is a minor contribution from either *van der Waals* or electrostatic forces (including π - π electron donor-acceptor charge transfer complexation) or both to the mechanism of (Td-G2)-VOC interaction. However, spectroscopic studies (to be discussed subsequently) ruled out the possibility of donor-acceptor complexation.

4.3.1.3 Effect of solvent on the VOCs/Td-G2 complexation

Solvent molecules greatly outnumber the amounts of the host and guest present and therefore can have a remarkable effect upon the dynamics and energetics of interaction. When in solution, host and guest species are surrounded by solvent molecules, which interact with them. In order for binding to occur, many of these interactions must be broken, with both enthalpic and entropic consequences. This process is shown in a simplified way in Figure 4.8. Enthalpically, energy must be expended to break the solvent–host and solvent–guest bonds. The removal of solvent molecules from the host and the guest leads to the solvent molecules having more freedom in the solution, which increases the entropy and also leads to the formation of solvent–solvent bonds. The choice of solvent can have significant consequences on the binding of a guest.

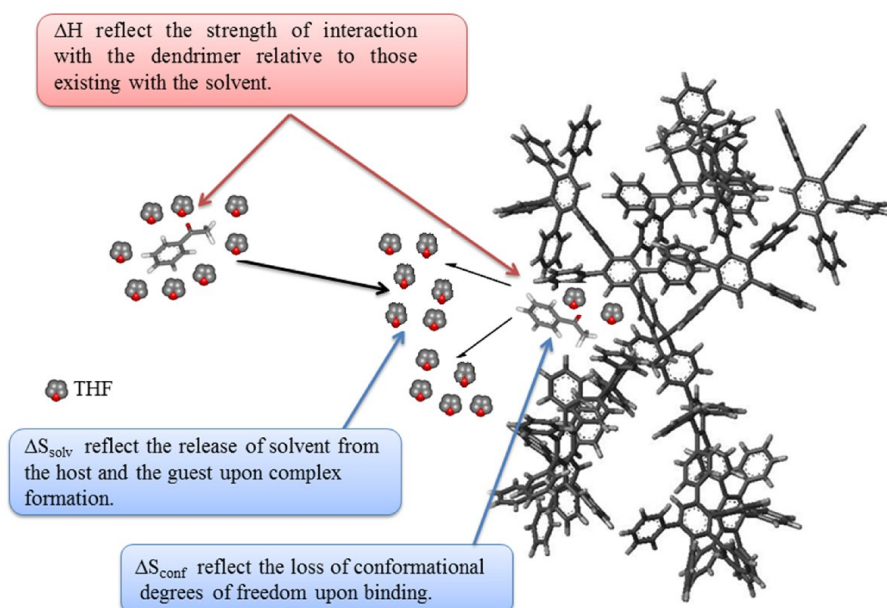


Figure 4.8: Host–guest binding equilibrium showing the desolvation of both species required prior to the binding occurring. The final complex is still solvated but overall there are more free solvent molecules present, hence increasing the entropy of the system.

To study the thermodynamic characteristics for the complexation VOCs/Td-G2 in different solvents, (Td-G2)-VOCs titrations were carried out in dichloromethane and chloroform, which have dielectric constants (ϵ) different from that of THF.

The results (Table 4.4) show that binding in dichloromethane and chloroform were enthalpically favorable (negative ΔH) (in all cases) and were predominantly entropy-driven (large positive $T\Delta S$) similar to that obtained in THF (see *Chapter 5.3.1*) which again indicates that electrostatic forces may not be playing a dominant role in such interaction. Had it been otherwise, thermodynamic parameters of interaction obtained in presence of different solvents would have been strikingly different. Thus, it may be concluded that the interaction between Td-G2 and VOCs is mediated by a combination of hydrophobic interactions and electrostatic forces.

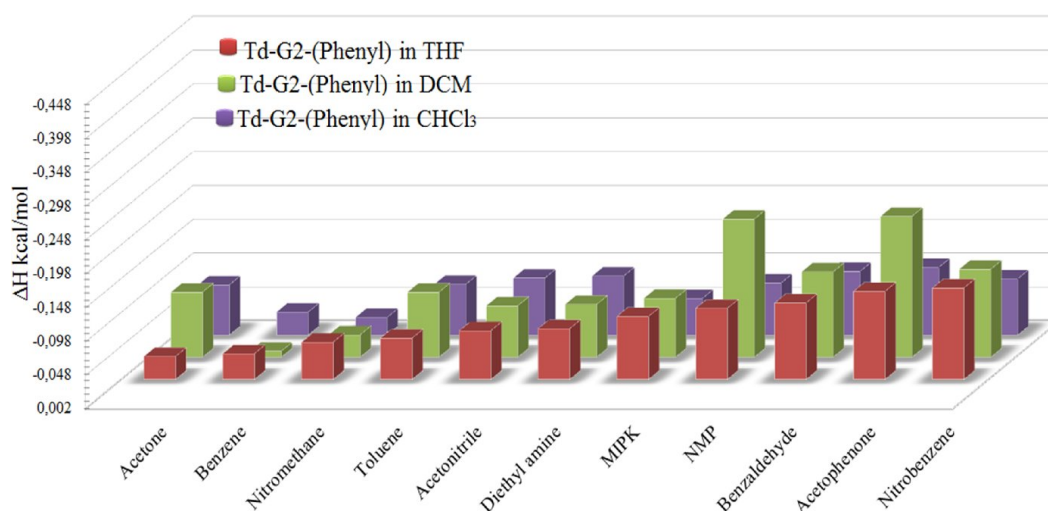


Figure 4.9: Enthalpic contributions ΔH as determined by ITC measurement for the interaction of VOCs with the (Td-G2) in THF, DCM and CHCl_3 at 25°C.

However, the slight difference in enthalpic contributions for VOCs/Td-G2 complexation in THF, DCM and CHCl_3 (see Figure 4.9) can be understood by the way in which the individual solvent molecules can interact with the host and the guest. Polar solvents are able to interact with host molecules *via* electrostatic interactions.²³ Such solvents are particularly able to inhibit binding of charged species, as the solvent dipole can interact strongly with a charged center, thus making the solvent–host or solvent– guest interactions harder to break.

Other solvents are able to disrupt the binding by means of electron-pair or hydrogen bond donation and acceptance. The vast majority of supramolecular interactions are electrostatic in nature,²⁴ meaning that polar solvents often act to

reduce the observed binding. For this reason, these studies were carried out in the least polar solvent possible to reduce the competition for the host.

Table 4.4: Thermodynamic parameters for interaction between Td-G2 and VOCs in dichloromethane and chloroform at 25 °C.

VOCs	N	K_B M ⁻¹	ΔH kcal/mol	T ΔS kcal/mol	ΔG kcal/mol
Dichloromethane					
acetone	6	1.03x10 ³	-0.096	4.025	-4.121
benzene	4	1.16x10 ³	-0.008	5.546	-5.554
nitro methane	2	2.03x10 ³	-0.033	4.472	-4.505
toluene	5	1.25x10 ⁴	-0.096	5.485	-5.581
acetonitrile	5	5.13x10 ³	-0.076	4.979	-5.055
diethyl amine	10	1.71x10 ⁴	-0.078	5.694	-5.772
MIPK	3	1.15x10 ⁴	-0.087	5.456	-5.543
NMP	9	8.65x10 ³	-0.248	5.128	-5.376
benzaldehyde	8	7.08x10 ³	-0.126	5.118	-5.244
acetophenone	4	2.78x10 ⁴	-0.218	5.843	-6.061
nitrobenzene	5	1.03x10 ⁴	-0.129	5.336	-5.465
Chloroform					
acetone	7	7.31x10 ³	-0.074	5.187	-5.261
benzene	14	1.81x10 ³	-0.034	5.578	-5.612
nitro methane	2	1.14x10 ³	-0.025	4.144	-4.169
toluene	9	9.38x10 ³	-0.074	5.336	-5.410
acetonitrile	5	6.13x10 ³	-0.084	5.694	-5.778
diethyl amine	7	3.48x10 ³	-0.087	4.740	-4.827
MIPK	4	3.54x10 ³	-0.054	4.800	-4.854
NMP	8	4.07x10 ⁴	-0.077	6.201	-6.278
benzaldehyde	4	1.00x10 ⁴	-0.094	5.366	-5.460
acetophenone	3	6.00x10 ³	-0.100	5.068	-5.168
nitrobenzene	8	1.13x10 ⁴	-0.083	5.456	-5.539

4.3.2 VOCs/Td-G2 complexation a spectroscopic study

The observations from ITC regarding the aptitude of the non-functionalized polyphenylene dendrimer (Td-G2) to interact with different VOCs is well supported by fluorescence spectroscopic studies in cooperation with Dr. Mainak Roy described in the following section.

Sample preparation was done in the same way as for ITC using THF as the solvent for both VOCs and Td-G2. The fluorescence spectrum of Td-G2 in THF shows an intense peak at ~ 378.5 nm when excited at ~ 310 nm which has been attributed primarily to absorption by the polyphenylene dendritic arms of Td-G2 (Figure 4.10).²⁵

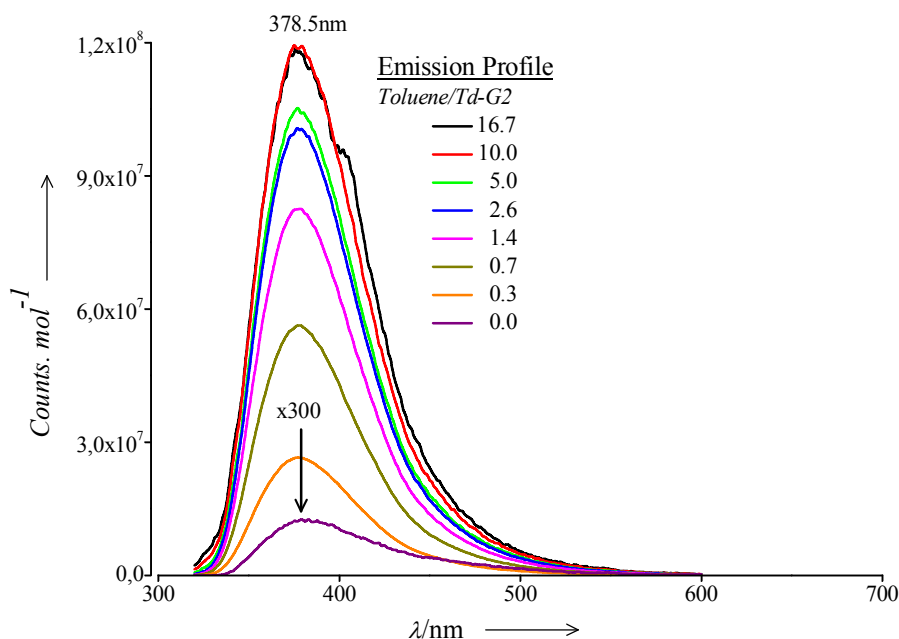


Figure 4.10: Fluorescence spectra (in THF) showing drastic increase in normalized fluorescence intensity due to toluene/Td-G2 interaction.

Additionally, control experiments have been carried out with only Td-G2 (see bottom most curve in Figure 4.10) that corroborates the observation that the emission at 378.5 nm arises from Td-G2. There are reports on absorption and fluorescence studies on different generations of dendrimers.^{25, 26} But the emission property of dendrimers was not used in those studies to probe their interaction with VOCs.

Hence the feasibility of using them also as an optical VOC sensor was not explored. When VOCs are added to the solution of Td-G2 in THF (Table 4.5), no significant shift in the emission peak position is observed.

Table 4.5: Composition of samples used for fluorescence measurements.

Sl. No.	Td-G2(mM)	VOCs(mM)	VOC/Td-G2
S ₀	0.145 (145 ppm)	0	0
S ₁	0.0145 (14.5 ppm)	0.005 (5ppm)	0.3
S ₂	0.0073 (7.3 ppm)	0.005 (5ppm)	0.7
S ₃	0.0037 (3.7 ppm)	0.005 (5ppm)	1.4
S ₄	0.0019 (1.9 ppm)	0.005 (5ppm)	2.6
S ₅	0.0010 (1 ppm)	0.005 (5ppm)	5.0
S ₆	0.0005 (0.5 ppm)	0.005 (5ppm)	10.0
S ₇	0.0003 (0.3 ppm)	0.005 (5ppm)	16.7

Stock solution for Td-G2= 0.145 mM, Stock solution for VOCs = 0.05 mM. Sample volume =10ml.

However, fluorescence intensity of Td-G2 normalized to its molar concentration increase drastically. Exemplarily, a series of fluorescence spectra (excited at 310 nm) for different toluene/Td-G2 ratios is shown in Figure 4.10. Initially the intensity grows sharply with the VOC/Td-G2 ratio which then tends to saturate or even decrease at higher values. For all the VOCs studied, polar or non-polar, aromatic or aliphatic, a similar trend was observed even at VOC concentration of 5 ppm (Table 4.5). Fluorescence spectra of Td-G2 with different polar and non-polar VOCs, all excited at 300 nm, are given in Figure 4.11. Similar increase in fluorescence quantum yield of fluorophores due to host-guest interaction has been reported previously.^{27, 28} Td-G2 consists of several tens of phenyl groups and thus has high absorption in the UV region.²⁷ The VOCs, studied in the present work, mostly do not absorb at ~300 nm or have very small absorbance at 5 ppm concentration (Table 4.5) compared to the high extinction coefficient ($\sim 3 \times 10^5 \text{ cm}^{-1} \text{ M}^{-1}$ in CH_2Cl_2) of Td-G2 at ~300 nm.²⁶

Therefore, partitioning of incident light, due to absorption by the VOCs, has not affected the fluorescence intensity of Td-G2. Even if the VOCs had absorbed in the studied spectral range, there should have been a decrease in the normalized fluorescence intensity of Td-G2 upon addition of VOCs which is contrary to our observation. Thus, the increase in normalized fluorescence intensity of Td-G2 upon addition of VOCs has been conclusively attributed to the host-guest interaction between Td-G2 and the VOCs and the extent of increase to the magnitude of such interaction.

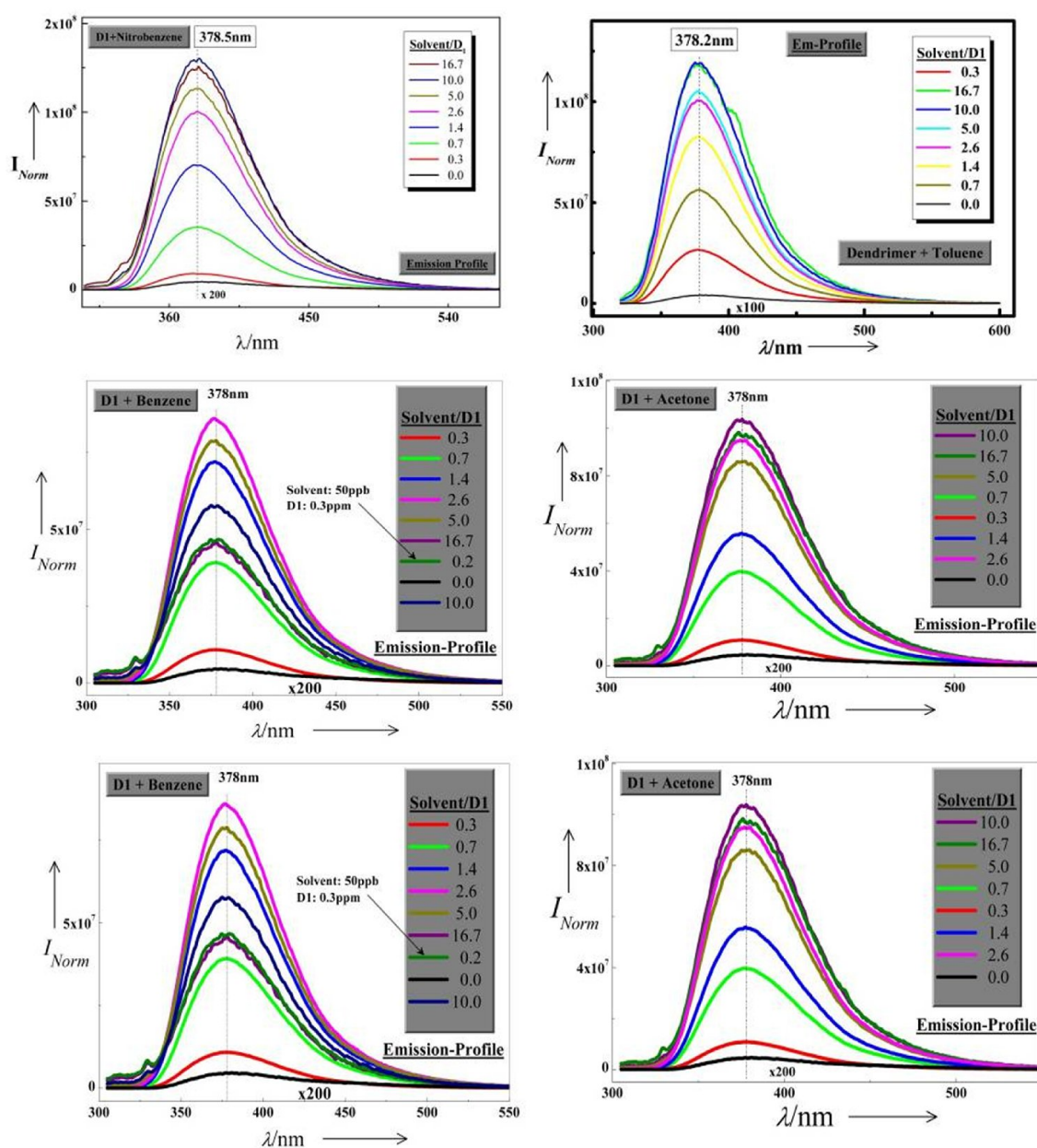


Figure 4.11: Fluorescence spectra of Td-G2 with different polar and nonpolar VOCs

Moreover, it is known from the literature that inter-phenyl interactions within the branches of the dendrimers (and not the core) are mainly responsible for their spectroscopic properties.²⁵ Therefore; the observed spectral change in the normalized fluorescence intensity of Td-G2 indicates that Td-G2/VOC interaction takes place primarily outside its core. Similar deduction has been made from stoichiometry study (i.e. estimation of N values) by ITC.

The ratio of the fluorescence peak intensity of a VOC loaded Td-G2 (I_{\max}) to that of the pure dendrimer (I_0), both excited at the same wavelength, 310 nm for toluene, gives a measure of the increased fluorescence intensity due to VOC-Td-G2 interaction. Already at 5 ppm of VOC concentration, this effect is pronounced and indicates the sensitivity of fluorescence spectroscopy towards detection of that VOC by Td-G2.

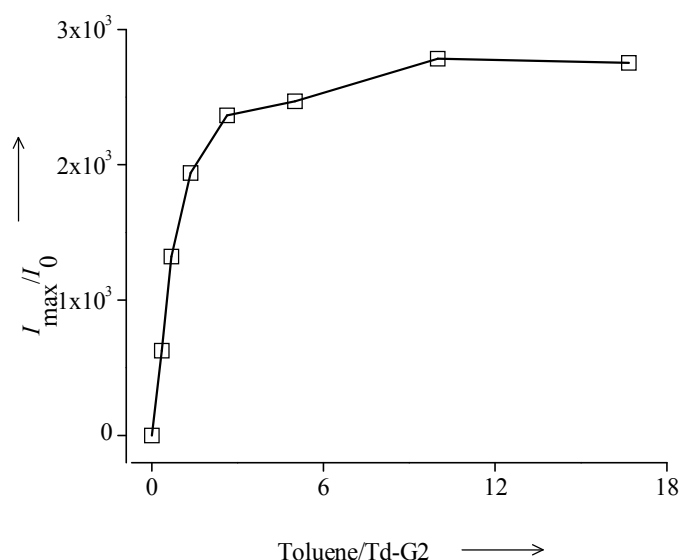


Figure 4.12: Plot of I_{\max}/I_0 vs. toluene/Td-G2 showing saturation of fluorescence intensity above toluene/Td-G2 ratio= 5.

Figure 4.12 shows a plot of I_{\max}/I_0 vs. VOC/Td-G2 for toluene. The plot serves as a rough calibration curve for toluene concentration probed using Td-G2 fluorescence. It is observed that the rising curve saturates at a ratio of VOC/Td-G2=5 for toluene, which suggests that a Td-G2 molecule can interact with maximum of 5 molecules of toluene. The number is in agreement with the stoichiometry (N) value calculated for toluene from ITC. At still higher values of VOC/Td-G2 ratio (beyond saturation limit), fluorescence intensity often

decreases. This may be due to overcrowding of VOCs around the fluorophore that tend to waken VOC-Td-G2 interaction due to steric repulsion.

Throughout the entire range of VOCs studied, no new emission peak (in the spectral range studied) and no shift in the fluorescence peak position is observed. Moreover, there is no apparent quenching of normalized fluorescence for any of the VOCs studied. These results together imply that no new electronic states, either emissive or non-emissive, have been formed due to interaction of Td-G2 with the VOCs. While emissive states would have induced a shift in fluorescence peak position, non-emissive states would have reduced fluorescence quantum yield due to non-radiative transition.

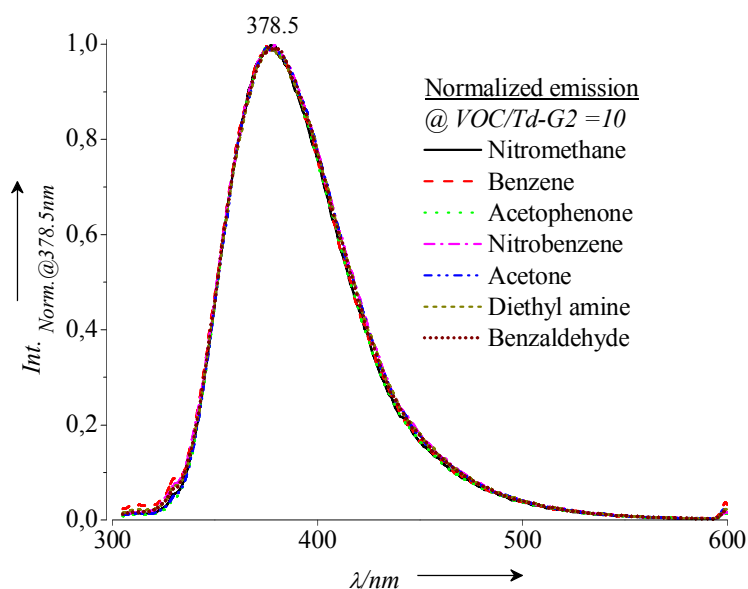


Figure 4.13: Normalized emission spectra (excited at 300 nm) of different Td-G2/VOC complex at VOC/Td-G2 ratio= 10.

Figure 4.13 shows a series of fluorescence spectra of Td-G2 loaded with VOCs with different dielectric constants at VOC/Td-G2=10. This allows comparison of the emission profiles of different VOC-Td-G2 complex at a fixed VOC/Td-G2 ratio. All the samples were excited at 300 nm and the emission spectra were normalized at ~378.5 nm.

For all VOCs studied, whether they polar or nonpolar, no shift in the fluorescence peak position was observed. The samples have almost overlapping normalized emission spectra implying that the systems differ only in fluorescence quantum

yield. Earlier significant peak-shift was reported²⁷ for electrostatic interaction between ion-pair complex of Td-G2 (decorated with carboxylic acid group at its outer rim) and a cationic dye pinacyanol. Binding of quadruplex with berberine also resulted in the shift of its fluorescence λ_{\max} ²⁸ due to π - π stacking of berberine on quadruplex and stabilization of negative charge density of guanines by positively charged berberine. Therefore, it may be inferred that π - π electron donor-acceptor complexation is not the dominant mode of interaction between the neutral Td-G2 (see Scheme 4.2) and the VOCs studied in the present work. Had it been so, the emission profile at a fixed VOC/ Td-G2 ratio would have differed for VOCs with widely differing dielectric constants and also for the same VOC at different Td-G2/VOC ratio, which is not the case here.

A small residual fluorescence (*asymmetric tail*) at higher wavelengths is observed for pure Td-G2, which is absent for the VOC-loaded samples. This indicates that the electronic levels of Td-G2 have got modified due to interaction with the VOCs. But the extent of electronic modification is the same for different VOCs at a fixed VOC/Td-G2 ratio (see overlapping emission profiles in the Figure 4.13).

Excitation profile of pure Td-G2 exhibits a single maximum at ~ 332 nm and negligibly weak contribution at ~ 310 nm (see bottom most curve of Figure 4.14).

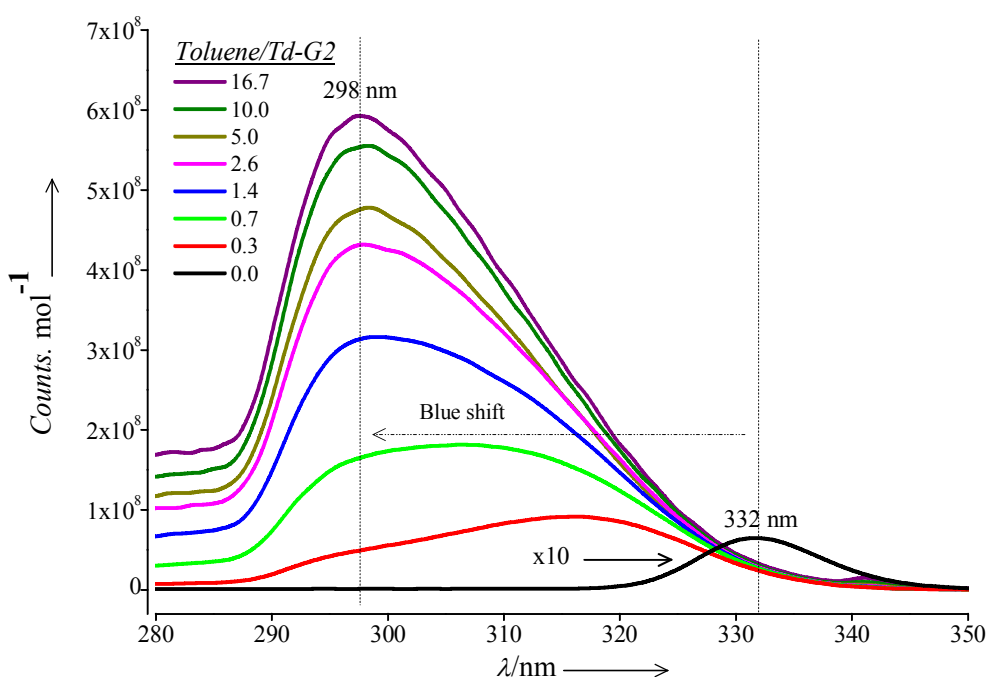


Figure 4.14: Excitation profiles exhibiting blue shift of maximum due to toluene-Td-G2 interaction.

Since, pure Td-G2 was excited far away from its excitation maximum, its fluorescence yield was very low. On adding VOCs the excitation spectrum, exemplarily shown in Figure 4.14 for toluene, becomes broader, asymmetric and the excitation peak maximum blue-shifts gradually from 332nm to 298 nm. The spectra in Figure 4.14 are normalized to the molar concentration of Td-G2 for comparison of their intensities. For toluene/Td-G2 ratio = 0.3, 0.7 and 1.4, two excitation maximum at ~298 and 316 nm are clearly evident.

With increasing toluene/Td-G2 ratio, intensity of the peak at ~298 nm becomes more and more dominant at the expense of the latter. However, the asymmetric nature of the excitation profile clearly indicates remnant contribution of the other excited state(s). Since the excitation wavelength (310 nm for toluene) now nearly coincides with the excitation peak maximum, fluorescence intensity of the samples increases remarkably.

The VOC molecules upon interaction with Td-G2 get adsorbed on its dendritic arms and also get incorporated into its core that changes the local symmetry around the fluorophore (conjugated phenyl and triphenylene rings) and hence modifies the selection rules governing emission. Furthermore, due to increased crowding and rigidity of the system, torsional, rotational and vibrational motions of Td-G2 get restricted. Supporting evidence to the changed symmetry and restricted vibration of Td-G2 due to interaction with the VOCs comes from Raman spectroscopic studies of the samples.

The Raman spectrum (Figure 4.15) show partial quenching of Raman bands of Td-G2 due to the pre-mentioned interactions. As a result, non-radiative processes from the excited state corresponding to the 298 nm peak, that was earlier the predominant mode of decay, decreases that in turn increases the fluorescence yield (at λ_{ex} = 310 nm for toluene and 300 nm for other VOCs) and induces a blue shift in the excitation peak maximum. Vanishing of the excitation peak at ~332 nm for pure Td-G2 indicates that attachment of the VOCs creates extra non-radiative pathways for the relaxation of the particular excited state.

As a result; based on temperature dependent ITC studies and fluorescence measurements, it has been possible to prove that interaction between the polyphenylene dendrimer and VOCs not only takes place inside the core of the

cavity but also on the dendrimer surface outside the core, as well as the π - π electron donor-acceptor complexation is not the dominant mode of interaction between the neutral Td-G2 and the VOCs studied in the present work.

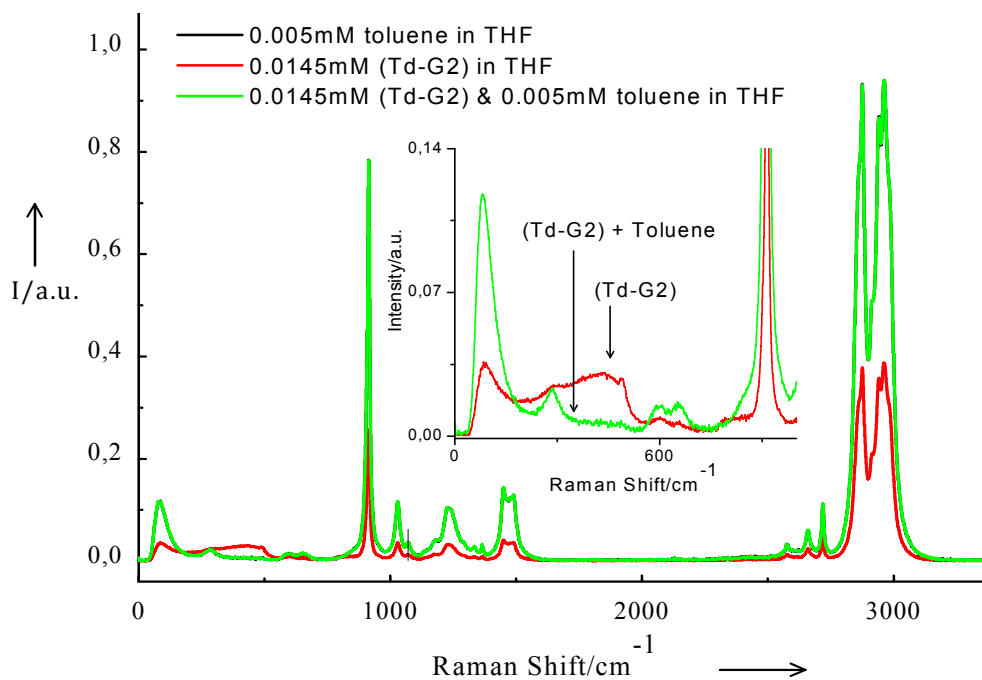


Figure 4.15: Raman spectrum of Td-G2 with Toluene in THF at 25°C.

In summary, the thermodynamic and spectroscopic data obtained along with the analysis of the mechanism of interaction provide detailed information that will help in designing new dendrimer molecules which would improve the host-guest interaction, thus can increase the sensitivity, selectivity as well as adaptability for uptake of a specific molecule.

4.3.3 Study of the in scaffold functionalized polyphenylene dendrimers

Polyphenylene-based dendrimers are identifiable in the literature as inherently rigid “shape-persistent” dendrimers due to the nature of the phenyl-phenyl bonds and the large number of twisted interlocked phenyl rings with reduced mobility.²⁹ Their rigidity and shape-persistence have been demonstrated by a number of techniques such as atomic force microscopy (AFM),^{30, 31} and solid-state NMR, which showed that the phenyl rings in the dendrimers (display very limited dynamics with heavily restricted movements) especially those in the core and scaffold.^{32, 33} This rigidity means that the dendrimers have a well-defined nanoporosity, and that functional groups in the core, interior layers (scaffold) and/or on the surface of the dendrimer are essentially fixed in well-defined and predictable spatial relationships with each other, which affects their interactions and so offers the possibility of controlling the chemical or physical properties of the dendrimers.

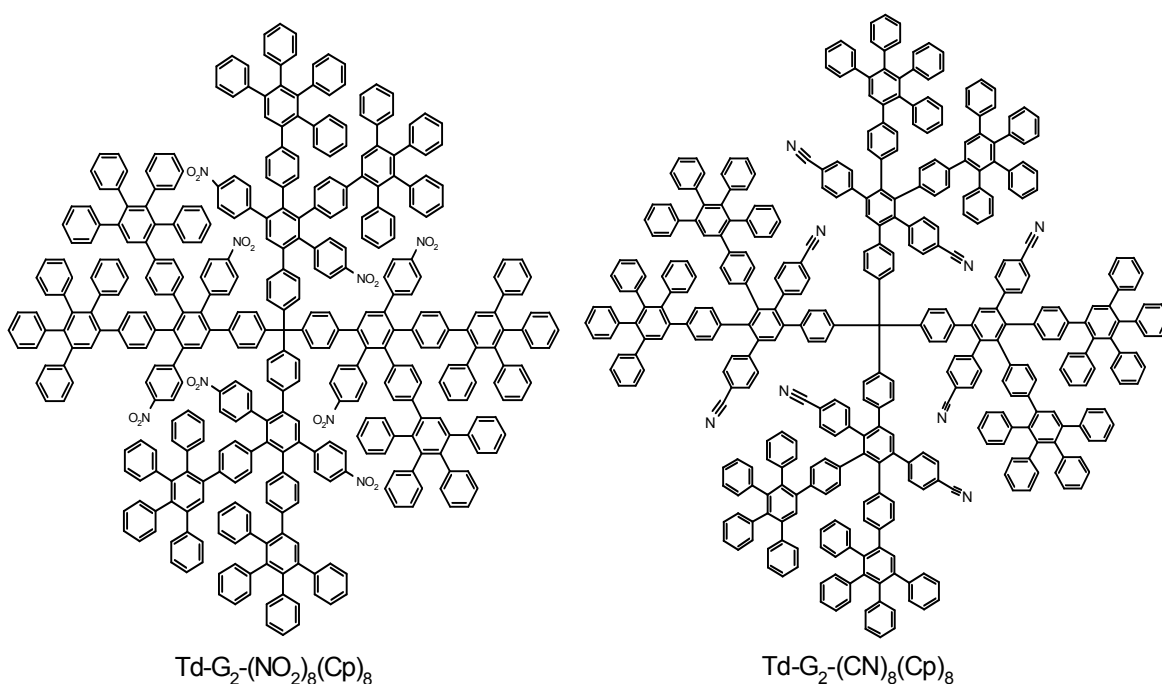
In the following section, the adsorption behaviors of five different functionalized polyphenylene dendrimer bearing methyl ester-, carboxyl-, cyano-, nitro- and pyridyl groups at the interior of the dendrimer (see Scheme 4.3, 4.4, 4.5 and 4.6) with various common VOCs were studied. All these dendrimers (designed and synthesized by Mathias Grill in Prof. Klaus Müllen’s group) were studied in the same way as was described for the unsubstituted polyphenylene dendrimer Td-G2 (*Chapter 5.3*).

4.3.3.1 Polyphenylene dendrimers bearing neutral functional groups

The influence of neutral functional groups in the interior of the polyphenylene dendrimers on sensoric activity has been studied. For this purpose, dendrimers of the second generation (G2) carrying electron withdrawing (-NO₂ and -CN) substituents have been synthesized (see Scheme 4.3).¹²

From the titration curves and the thermodynamic parameters it was found that enthalpic and entropic contributions to the free energy of binding are clearly different for the aliphatic and aromatic VOCs, all the bindings yielded low

favorable (negative) heat of interaction ΔH and high favorable (positive) entropic changes ΔS (Table 4.6). This thermodynamic signature indicates that these interactions are predominantly entropic, most probably driven by hydrophobicity,³⁴ but characterized by a slightly favorable enthalpy, suggesting that the VOCs also establish a number of bonds (such as: hydrogen bonds, van der Waals, π - π , C-H- π , etc.) with the dendrimers molecules.



Scheme 4.3: Nitro- and cyano- substituted polyphenylene dendrimers (Td-G2) used in this study.

In details, the thermodynamic parameters observation of the $\text{Td-G}_2\text{-(NO}_2\text{)}_8\text{(Cp)}_8$ interaction with the polar aromatic guests like benzaldehyde ($\Delta H = -0.181$ kcal/mol), acetophenone ($\Delta H = -0.136$ kcal/mol) and nitro-benzene ($\Delta H = -0.079$ kcal/mol) yields higher negative ΔH values than those with nonpolar aromatic compounds like benzene ($\Delta H = -0.058$ kcal/mol) and toluene ($\Delta H = -0.63$ kcal/mol), which reflect stronger interaction. As well the interaction with non-aromatic guests like diethyl amine ($\Delta H = -0.120$ kcal/mol) and acetonitrile ($\Delta H = -0.096$ kcal/mol) demonstrate higher negative ΔH contributions than the MIPK ($\Delta H = -0.044$ kcal/mol) and NMP ($\Delta H = -0.018$ kcal/mol) (Figure 4.16).

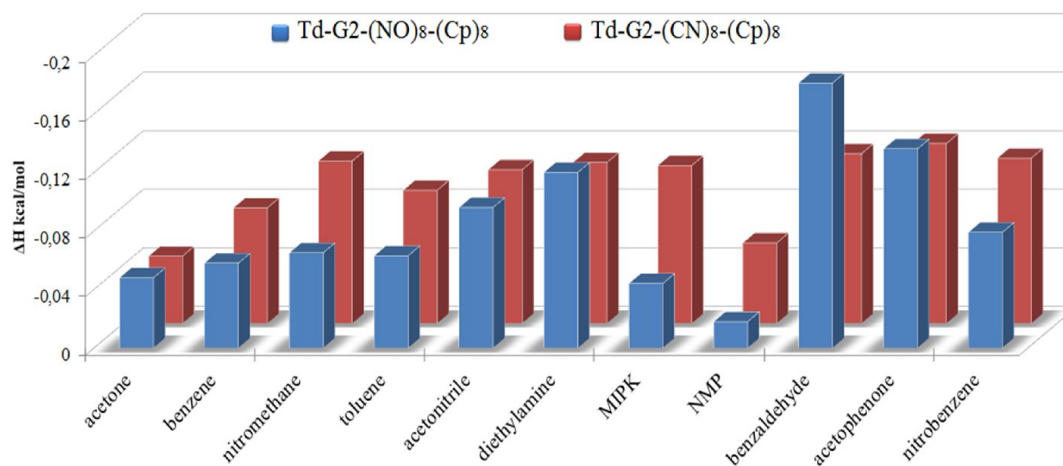


Figure 4.16: Enthalpic contributions ΔH as determined by ITC measurement for the interaction of VOCs with the Td-G2-(NO)₂₈-(Cp)₈ and Td-G2-(CN)₈-(Cp)₈ in THF at 25°C.

This observation renders the selectivity and capability of Td-G2-(NO)₂₈-(Cp)₈ to uptake/detect different classes of VOCs, such as nonpolar, aromatic solvents like benzene or toluene as well as non-aromatic acetone, diethyl amine, acetonitrile and nitro methane. Generally, the driving forces for the VOCs/Td-G2-(NO)₂₈-(Cp)₈ interactions can be based on various types of weaker forces (van der Waals, hydrogen bonding, the hydrophobic force, etc.).

Alternatively, the interaction of VOC guests with the polyphenylene dendrimer bearing the *cyano* group in the interior (Td-G2-(CN)₈-(Cp)₈) (Figure 4.16) leads to almost more (negative) enthalpy contributions than those observed with the *nitro* substituted polyphenylene dendrimer. This observation reflects the ability of the interior cyano functionalized PPD to uptake the non-aromatic solvents like MIPK ($\Delta H = -0.108$ kcal/mol), NMP ($\Delta H = -0.055$ kcal/mol), nitro methane ($\Delta H = -0.111$ kcal/mol), acetonitrile ($\Delta H = -0.105$ kcal/mol), and acetone ($\Delta H = -0.046$ kcal/mol) as well as aromatic solvents such as benzaldehyde ($\Delta H = -0.116$ kcal/mol), acetophenone ($\Delta H = -0.123$ kcal/mol) and nitrobenzene ($\Delta H = -0.113$ kcal/mol). Moreover, Td-G2-(CN)₈-(Cp)₈ shows the tendency to interact vastly with nonpolar aromatic solvents such as benzene ($\Delta H = -0.079$ kcal/mol) and toluene ($\Delta H = -0.091$ kcal/mol).

In comparison to the periphery substituted polyphenylene dendrimer (Td-G2-(CN)₁₆),⁹ these results demonstrate that the access of the *cyano* group in the interior part of the polyphenylene dendrimer increased the selectivity as well as the sensitivity of the polyphenylene dendrimer to uptake even the non-aromatic solvents.

Table 4.6: Thermodynamic parameters for interaction of VOCs with the Td-G2-(NO₂)₈-(Cp)₈ and Td-G2-(CN)₈-(Cp)₈ in THF at 25°C.

VOCs	N	K _B M ⁻¹	ΔH kcal/mol	TΔS kcal/mol	ΔG kcal/mol
Td-G2-(NO₂)₈-(Cp)₈					
acetone	10	1.13x10 ⁴	-0.048	5.486	-5.534
benzene	7	1.85x10 ³	-0.058	4.382	-4.460
nitro methane	3	1.50x10 ⁴	-0.065	5.694	-5.759
toluene	5	1.96x10 ³	-0.063	4.442	-4.505
acetonitrile	5	1.18x10 ³	-0.096	4.084	-4.180
diethyl amine	6	1.85x10 ⁴	-0.120	5.694	-5.814
MIPK	4	2.30x10 ³	-0.044	5.903	-5.947
NMP	3	2.56x10 ³	-0.018	4.992	-5.010
benzaldehyde	3	5.48x10 ³	-0.181	3.547	-3.728
acetophenone	2	9.03x10 ⁴	-0.136	6.618	-6.754
nitrobenzene	3	1.54x10 ³	-0.079	4.323	-4.402
Td-G2-(CN)₈-(Cp)₈					
acetone	5	1.74x10 ⁴	-0.046	5.724	-5.770
benzene	6	3.56x10 ³	-0.079	4.770	-4.849
nitro methane	4	3.99x10 ⁴	-0.111	6.171	-6.282
toluene	4	3.29x10 ⁴	-0.091	5.336	-5.427
acetonitrile	5	1.31x10 ⁴	-0.105	5.694	-5.799
diethyl amine	4	1.94x10 ⁴	-0.110	5.014	-5.124
MIPK	8	8.93x10 ³	-0.108	4.800	-4.908
NMP	3	7.46x10 ³	-0.055	4.187	-4.242
benzaldehyde	6	3.14x10 ³	-0.116	4.651	-4.767
acetophenone	3	8.53x10 ³	-0.123	5.247	-5.370
nitrobenzene	3	8.11x10 ³	-0.113	5.217	-5.33

The related binding affinity observation (see Figure 4.17), prove that utilization of a polyphenylene dendrimer (Td-G2-(CN)₈-(Cp)₈ bearing *cyano* groups in the interior leads to increased binding affinity in most of the interactions with VOCs. The binding affinity of toluene or acetonitrile with Td-G2-(CN)₈-(Cp)₈ was one order of magnitude higher than the interaction found for Td-G2-(NO₂)₈-(Cp)₈.

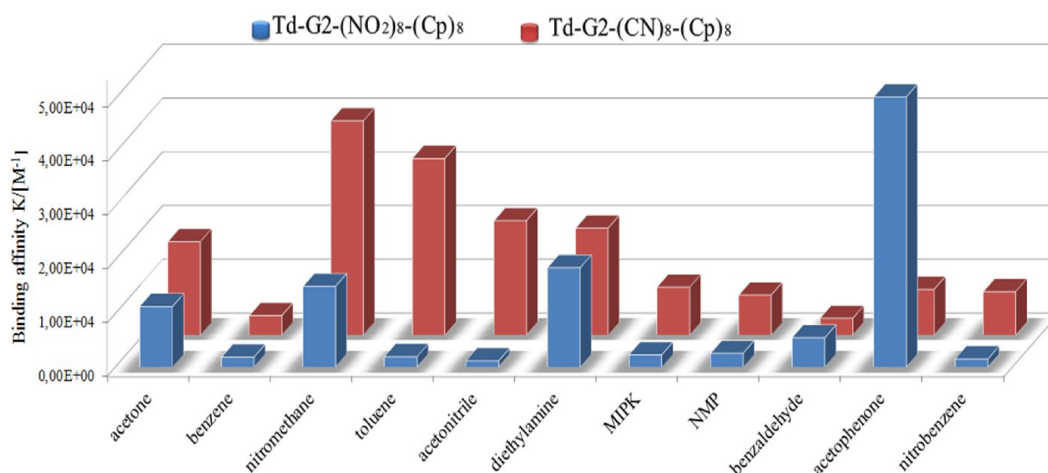
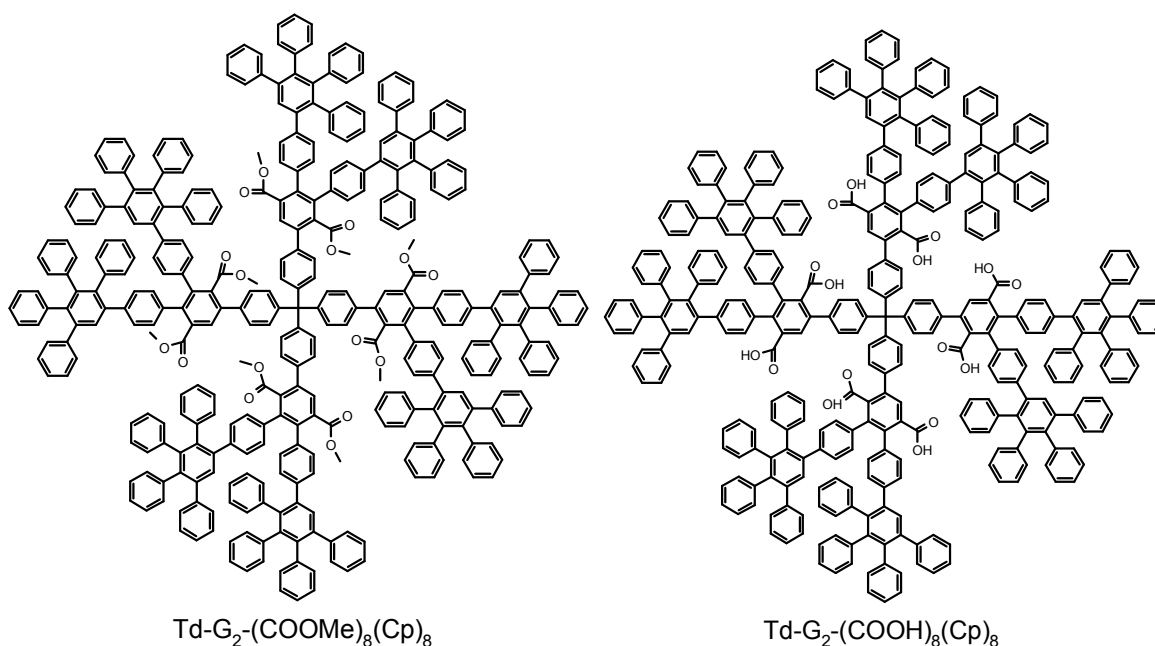


Figure 4.17: The binding affinity K_B for the interactions of VOCs with the Td-G2-(NO₂)₈-(Cp)₈ and Td-G2-(CN)₈-(Cp)₈ in THF at 25°C (see Table 5.6).

4.3.3.2 Polyphenylene dendrimers bearing acidic functional groups

In the present part, the adsorption behavior of polyphenylene dendrimers bearing acidic functional groups to various VOCs was studied. For this purpose, dendrimers of the second generation (G2) have been synthesized by Dr. *Roland Bauer* and *Matthias Grill* (dendritic materials sub group)^{11, 12} carrying electron withdrawing (COOMe and COOH) substituents (Scheme 4.4).



Scheme 4.4: Methyl ester- and carboxyl- substituted polyphenylene dendrimers (Td-G2) used in this study.

The calculated thermodynamic parameters proved clearly a higher interaction of Td-G2-(COOH)₈-(Cp)₈ with all investigated VOCs in comparison to the Td-G2-(COOMe)₈-(Cp)₈ with the same VOCs. This observation reflected in the ΔH contributions of the interactions (see Table 4.7).

In detail, the enthalpy ΔH observation for the interaction of Td-G2-(COOH)₈-(Cp)₈ with non-aromatic guests like acetone, acetonitrile, diethyl amine, MIPK and NMP yields about 3 times greater ΔH values than that with Td-G2-(COOMe)₈-(Cp)₈. Additionally, the interaction with nonpolar aromatic guest like benzene and toluene yielded also more negative ΔH values than that with Td-G2-(COOMe)₈-(Cp)₈, as well the interaction with the polar aromatic guests like benzaldehyde, acetophenone and nitro-benzene (Figure 4.18).

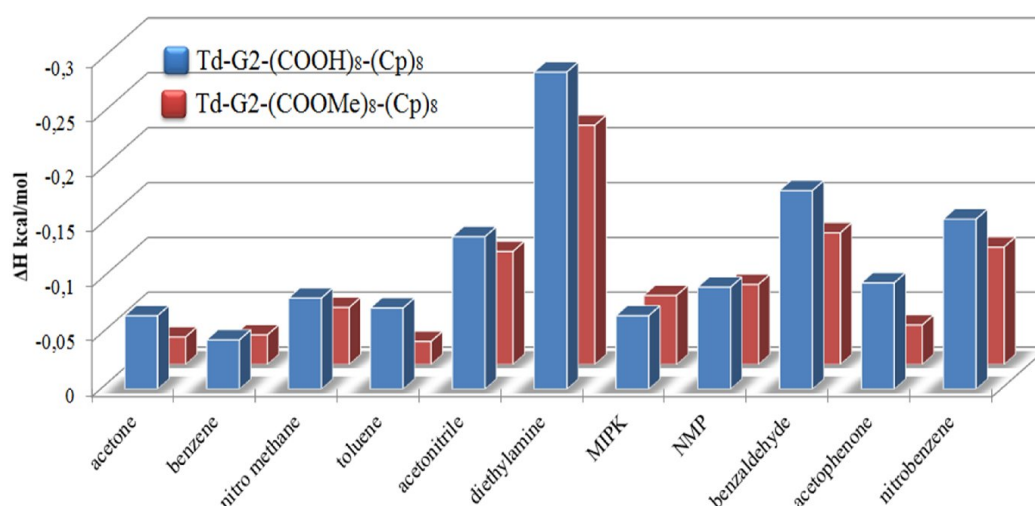


Figure 4.18: Enthalpic contributions ΔH as determined by ITC measurement for the interaction of VOCs with the Td-G2-(COOH)₈-(Cp)₈ and Td-G2-(COOMe)₈-(Cp)₈ in THF at 25°C.

These results can be correlated to the presence of COOH groups in the cavities of the Td-G2-(COOH)₈-(Cp)₈ dendrimer, which increased the ability of the dendrimer to build hydrogen bonds (besides the possible van der Waals, π - π and C-H---- π interactions) with the guest molecules. Consequently, a larger number of guest molecules can interact with the Td-G2-(COOH)₈-(Cp)₈ dendrimer and hence the interaction energy ΔH is higher than that for the presence of COOMe groups (see Table 4.7).

Table 4.7: Thermodynamic parameters for interaction of VOCs with the Td-G2-(COOH)₈-(Cp)₈ and Td-G2-(COOMe)₈-(Cp)₈ in THF at 25°C.

VOCs	N	K _B M ⁻¹	ΔH kcal/mol	TΔS kcal/mol	ΔG kcal/mol
Td-G2-(COOH)₈-(Cp)₈					
acetone	12	2.12x10 ³	-0.067	4.472	-4.539
benzene	7	2.21x10 ³	-0.045	5.012	-5.057
nitro methane	5	3.84x10 ²	-0.083	3.428	-4.258
toluene	4	4.64x10 ³	-0.074	5.426	-5.500
acetonitrile	9	1.48x10 ³	-0.139	4.203	-4.342
diethyl amine	6	5.42x10 ³	-0.289	3.309	-3.598
MIPK	5	1.04x10 ³	-0.067	4.114	-4.181
NMP	7	1.03x10 ³	-0.093	4.025	-4.118
benzaldehyde	4	5.48x10 ³	-0.181	3.547	-3.728
acetophenone	4	8.39x10 ³	-0.097	3.888	-3.985
nitrobenzene	5	6.40x10 ³	-0.155	5.038	-5.193
Td-G2-(COOMe)₈-(Cp)₈					
acetone	8	3.07x10 ⁴	-0.025	6.082	-6.107
benzene	5	1.68x10 ³	-0.027	5.754	-5.781
nitro methane	3	9.84x10 ³	-0.052	5.396	-5.448
toluene	5	2.22x10 ⁴	-0.021	5.903	-5.924
acetonitrile	4	6.33x10 ³	-0.103	4.830	-4.933
diethyl amine	5	1.57x10 ⁴	-0.218	5.014	-5.674
MIPK	5	1.00x10 ⁴	-0.063	5.098	-5.161
NMP	5	1.03x10 ³	-0.073	5.366	-5.439
benzaldehyde	4	1.30x10 ⁴	-0.119	5.336	-5.455
acetophenone	3	3.12x10 ³	-0.036	5.040	-5.076
nitrobenzene	3	3.29x10 ³	-0.107	5.008	-5.124

Furthermore, the binding affinity for the interactions shows that utilization of the polyphenylene dendrimer (Td-G2-(COOMe)₈-(Cp)₈ bearing the methyl ester (*COOMe*) group in interior increased the binding affinity for most of the interactions with VOCs. Comprehensively, the binding affinity of the interaction of nitromethane with Td-G2-(COOMe)₈-(Cp)₈ was one order of magnitude higher than that found of Td-G2-(COOH)₈-(Cp)₈, as well as in the cases of other VOCs (Figure 4.19).

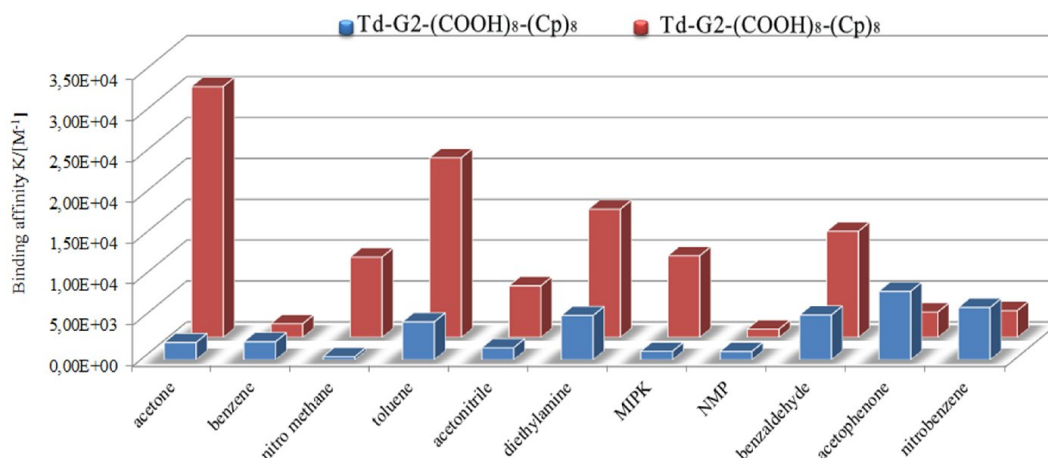
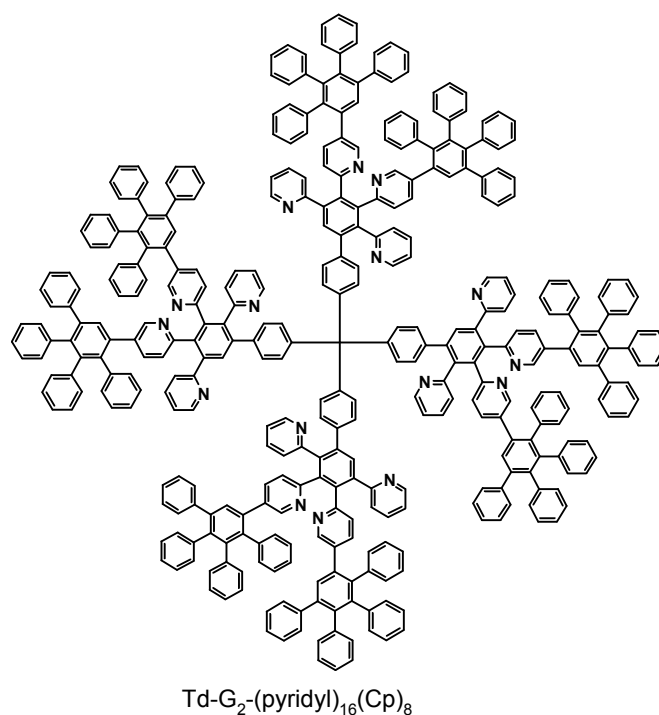


Figure 4.19: The binding affinity K_B for the interactions of VOCs with the Td-G2-(COOH)₈-(Cp)₈ and Td-G2-(COOMe)₈-(Cp)₈ in THF at 25°C.

4.3.3.3 Polyphenylene dendrimers bearing basic functional groups



Scheme 4.5: Pyridyl functionalized PPD (Td-G₂-(pyridyl)₁₆-(Cp)₈) used in this study.

In this part, a polyphenylene dendrimer bearing a basic functional group was studied, in practical a polyphenylene dendrimer of the second generation (G2) with *pyridyl* groups has been synthesized by *Mathias Grill* (dendritic materials sub group)¹² (Scheme 4.5) and exactly in the same manner as with neutral and

acidic substituted polyphenylene dendrimer the microcalorimetric titration with the VOCs were carried out. Figure 4.20 shows the enthalpic contributions of the interactions between the Td-G2-(pyridine)₁₆-(Cp) dendrimer and the VOCs guests. The observed reaction enthalpy proved, that the interaction of pyridyl functionalized PPD in scaffold with polar aromatic guests like benzaldehyde ($\Delta H = -0.131$ kcal/mol), acetophenone ($\Delta H = -0.097$ kcal/mol) and nitro-benzene ($\Delta H = -0.089$ kcal/mol) yielded higher negative ΔH values than that with non-polar aromatic compounds like benzene ($\Delta H = -0.03$ kcal/mol) and toluene ($\Delta H = -0.04$ kcal/mol). These outcomes reflected a stronger interaction of the pyridyl substituted dendrimer with the polar aromatic VOCs.

On the other hand the interaction with the non-aromatic guests like diethyl amine ($\Delta H = -0.089$ kcal/mol), acetonitrile ($\Delta H = -0.086$ kcal/mol), and acetone ($\Delta H = -0.058$ kcal/mol) demonstrated more negative ΔH contributions than the NMP ($\Delta H = -0.048$ kcal/mol) and MIPK ($\Delta H = -0.040$ kcal/mol) (see Table 4.8). This observation proves the selectivity of the Td-G2-(pyridyl)₁₆-(Cp)₈ to uptake different classes of VOCs, such as non-aromatic solvents (acetone, diethyl amine, acetonitrile and nitro methane) as well as the polar aromatics.

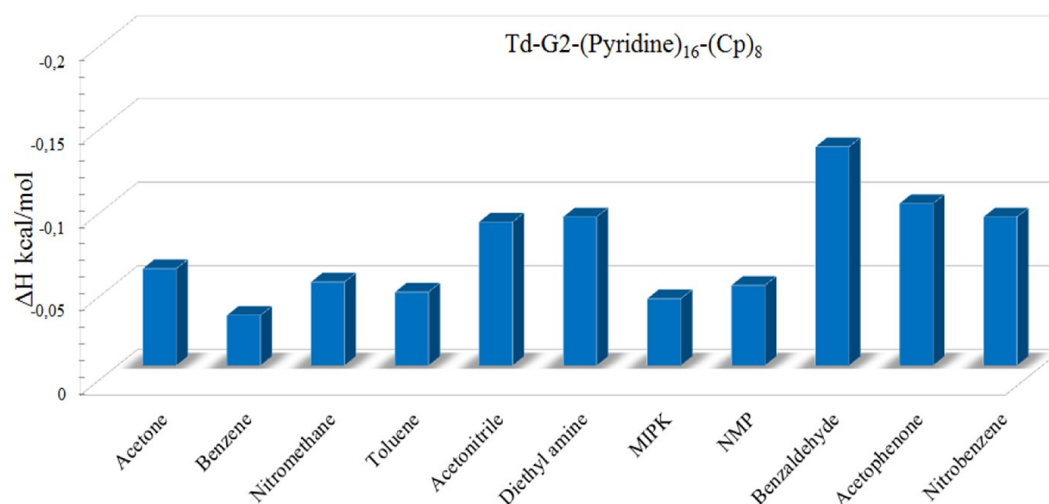
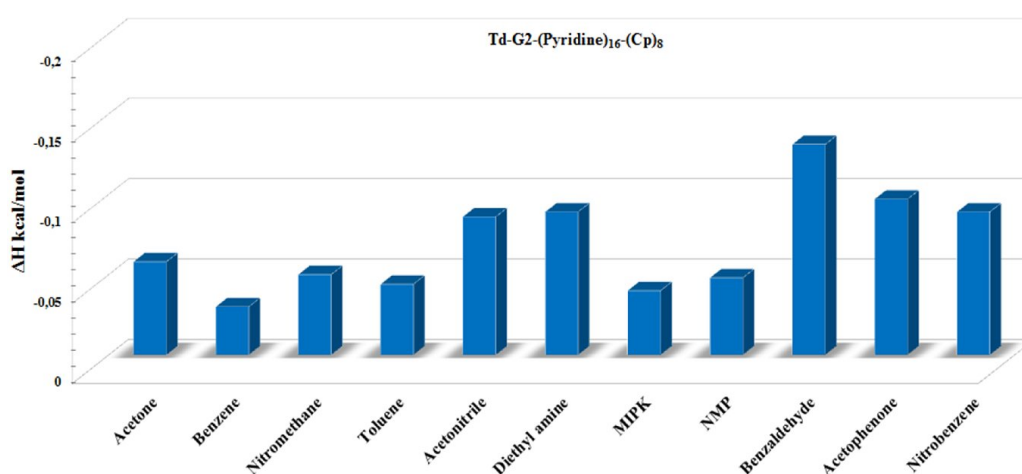


Figure 4.20: Enthalpic contributions ΔH as determined by ITC measurement for the interaction of VOCs with the in THF at 25°C.

Table 4.8: Thermodynamic Parameters for interaction of VOCs with the Td-G2-(pyridine)₁₆-(Cp)₈ in THF at 25°C.

VOCs	N	K _B M ⁻¹	ΔH kcal/mol	TΔS kcal/mol	ΔG kcal/mol
Td-G2-(pyridine)₁₆-(Cp)₈					
acetone	5	4.06x10 ⁴	-0.058	5.545	-5.603
benzene	7	1.13x10 ³	-0.030	4.144	-4.174
nitro methane	6	6.27x10 ⁴	-0.050	6.469	-6.528
toluene	6	5.13x10 ³	-0.044	4.426	-4.470
acetonitrile	3	1.54x10 ⁴	-0.086	4.203	-4.318
diethyl amine	6	8.27x10 ³	-0.089	5.309	-5.398
MIPK	3	5.99x10 ³	-0.040	5.098	-5.138
NMP	4	1.03x10 ⁴	-0.048	6.261	-6.380
benzaldehyde	5	1.56x10 ³	-0.131	4.233	-4.364
acetophenone	3	9.82x10 ³	-0.097	5.187	-5.284
nitrobenzene	3	4.31x10 ³	-0.089	4.949	-5.001

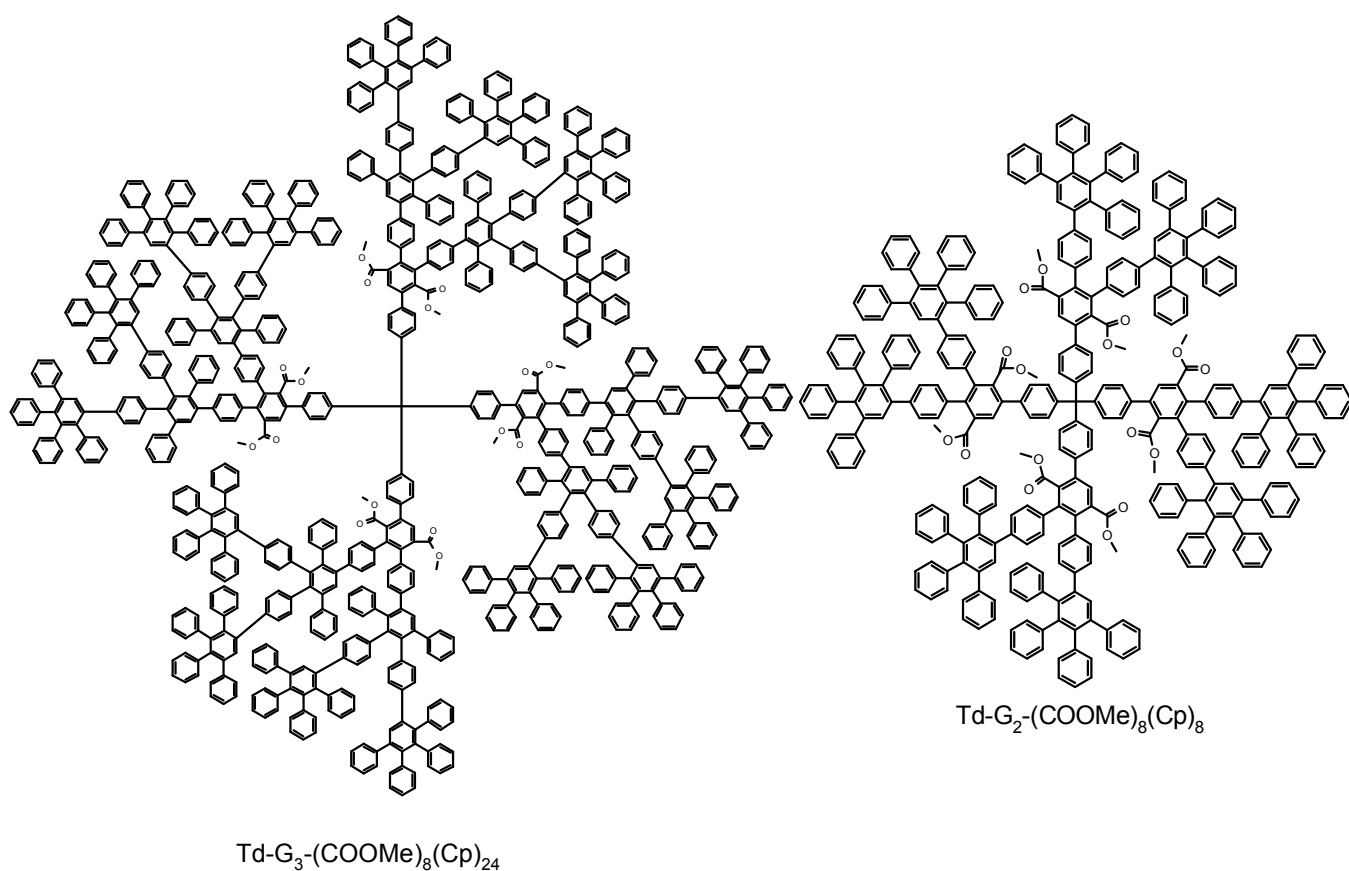
The calculated binding affinity K_B for the Td-G2-(pyridine)₁₆-(Cp)₈ /VOCs interactions, showed that Td-G2-(Pyridyne)₁₆-(Cp)₈ had the highest binding affinity to nitromethane (K_B = 6.27x10⁴ M⁻¹) and the lowest to benzene (K_B= 1.13x10³ M⁻¹). These values reflect the high selectivity (*Thermodynamic selectivity*: the ratio of the binding constants for a host binding two different guests)^{24c} of the Td-G2-(Pyridyne)₁₆-(Cp)₈ dendrimer to uptake nitro methane guest molecules than the other VOCs guests used in this study (Figure 4.21).

**Figure 4.21:** The binding affinity K_B for the interactions of VOCs with the Td-G2-(pyridyne)₁₆-(Cp)₈ in THF at 25°C.

These observations (*Chapter 4.3.3.1 to 4.3.3.3*) reflect noticeably the influences of the nature of the functional groups that were incorporated in the interior (scaffold) of the dendrimer on the capability, sensitivity and the selectivity of the dendrimers to detect/uptake different classes of VOCs. In practical, using the electron withdrawing ($-\text{NO}_2$ and $-\text{CN}$) substituents increase the capability and the selectivity of the dendrimer to uptake the polar aromatic (e.g. benzaldehyde and acetophenone), nonpolar aromatic (benzene and toluene) as well as the aliphatic VOCs (such as acetone, MIPK and nitromethane). On the other hand, adding an acidic substitution group such as (COOH) leads to increasing the sensitivity to uptake all aliphatic and polar aromatic VOCs used in this study. Finally, adding the basic functional group pyridine in the interior layers led to increase the ability and the sensitivity of the polyphenylene dendrimer to uptake the aliphatic VOCs such as nitromethane, acetone and acetonitrile.

4.3.4 The influence of the dendrimer generation on the VOCs/polyphenylene complexation

In order to declare the influence of the dendrimer generation or else the number of the phenyl groups on the VOCs/polyphenylene complexation, a third generation of methyl ester substituted polyphenylene dendrimer Td-G₃-(COOMe)₈-(Cp)₂₄ (Scheme 4.6) with 124 phenyl rings were studied in a similar way as it was described for the second generation Td-G₂-(COOMe)₈-(Cp)₈ (see Chapter 5.3.3.2).



Scheme 4.6: G3 and G2 of the methyl ester-substituted polyphenylene dendrimers used in this study.

The calculated thermodynamic parameters for the interactions of the Td-G₃-(COOMe)₈-(Cp)₂₄ with the given solvent molecules (VOCs) led to an entropically driven process with low negative ΔH contribution accompanied by high positive ΔS contribution, which was the same observation made for Td-G₂-(COOMe)₈-(Cp)₈.

In detail, the interaction of the Td-G3-(COOMe)₈-(Cp)₂₄ with non-polar aromatic compounds like benzene ($\Delta H = -0.062$ kcal/mol) and toluene ($\Delta H = -0.053$ kcal mol⁻¹) reflects a stronger interaction than that of Td-G2-(COOMe)₈-(Cp)₈ (Figure 4. 22).

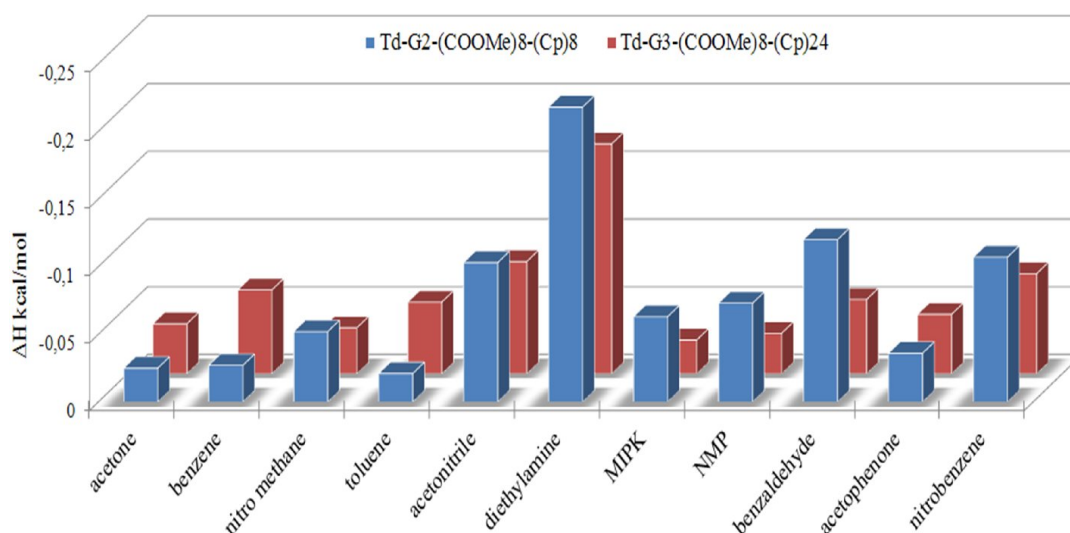
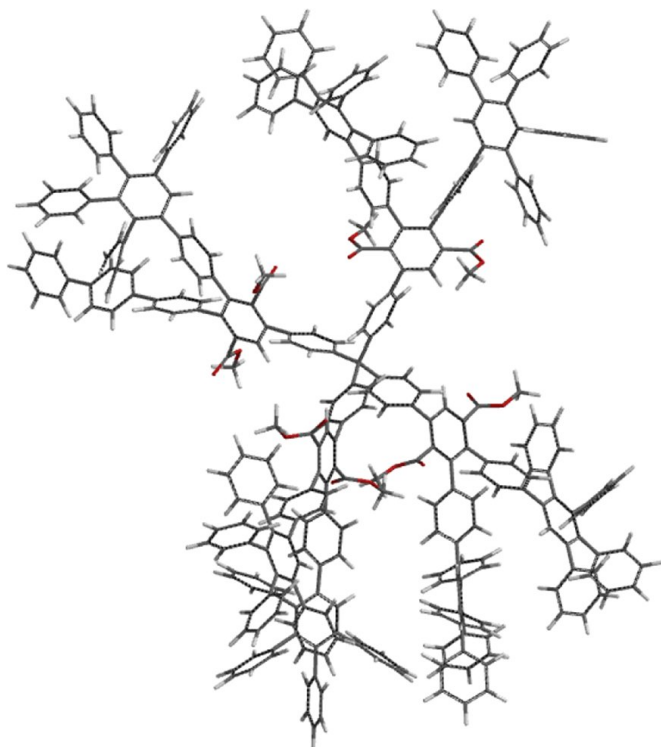


Figure 4.22: Enthalpic contributions ΔH as determined by ITC measurement for the interaction of VOCs with the Td-G3-(COOMe)₈-(Cp)₂₄ and Td-G2-(COOMe)₈-(Cp)₈ in THF at 25°C.

Reason for that might be, that increasing the number of phenyl rings from 64 to 124 led to raise the possibility of the π - π -interactions (see *Chapter 1.4*) between solvents and the phenyl moieties of the Td-G3-(COOMe)₈-(Cp)₂₄ dendrimer. On the other hand, the increase of phenyl rings to 124 as in the Td-G3-(COOMe)₈-(Cp)₂₄ led to a decrease in the binding enthalpy with a decrease in the entropy contribution of all other VOCs (see Table 4.9). In the case of G3 dendrimer, excess phenylene groups at the periphery create an additional hindrance to the incoming solvent molecules. Moreover, due to free rotation of these rings, it is possible that the end rings may dive back into the interior and hence block the incoming solvent molecules (see Figure 4.23), thereby reducing the effective number of interacting solvent molecules and hence ΔH when compared to Td-G2-(COOMe)₈-(Cp)₈.

Td-G2-(COOMe)₈-(Cp)₈



Td-G3-(COOMe)₈-(Cp)₂₄

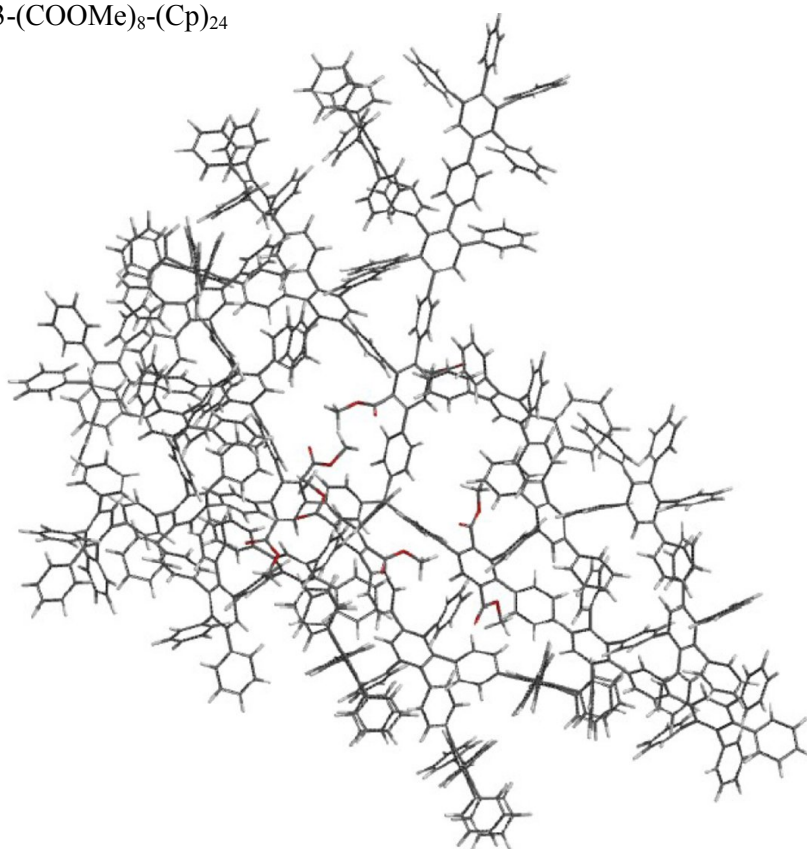


Figure 4.23: 3D structures of the Td-G2-(COOMe)₈-(Cp)₈ and Td-G3-(COOMe)₈-(Cp)₂₄ used in this study.

Table 4.9: Thermodynamic parameters for interaction of VOCs with the Td-G3-(COOMe)₈-(Cp)₂₄ and Td-G2-(COOMe)₈-(Cp)₈ in THF at 25°C.

VOCs	N	K _B M ⁻¹	ΔH kcal/mol	TΔS kcal/mol	ΔG kcal/mol
Td-G3-(COOMe)₈-(Cp)₂₄					
acetone	12	8.77x10 ³	-0.037	5.277	-5.314
benzene	16	4.10x10 ⁴	-0.062	4.889	-4.951
nitro methane	5	6.13x10 ³	-0.034	5.038	-5.072
toluene	6	7.66x10 ³	-0.053	5.24	-5.293
acetonitrile	9	1.08x10 ³	-0.083	3.875	-3.958
diethyl amine	4	3.12x10 ³	-0.170	4.114	-4.284
MIPK	5	8.56x10 ³	-0.025	6.02	-6.045
NMP	3	4.50x10 ³	-0.030	4.949	-4.979
benzaldehyde	9	8.83x10 ³	-0.055	5.336	-5.391
acetophenone	4	5.12x10 ³	-0.044	5.217	-5.261
nitrobenzene	5	1.61x10 ³	-0.074	4.14	-4.214
Td-G2-(COOMe)₈-(Cp)₈					
acetone	8	3.07x10 ⁴	-0.025	6.082	-6.107
benzene	5	1.68x10 ³	-0.027	5.754	-5.781
nitro methane	3	9.84x10 ³	-0.052	5.396	-5.448
toluene	5	2.22x10 ⁴	-0.021	5.903	-5.924
acetonitrile	4	6.33x10 ³	-0.103	4.830	-4.933
diethyl amine	5	1.57x10 ⁴	-0.218	5.014	-5.674
MIPK	5	1.00x10 ⁴	-0.063	5.098	-5.161
NMP	5	1.03x10 ³	-0.073	5.366	-5.439
benzaldehyde	4	1.30x10 ⁴	-0.119	5.336	-5.455
acetophenone	3	3.12x10 ³	-0.036	5.040	-5.076
nitrobenzene	3	3.29x10 ³	-0.107	5.008	-5.124

The measured binding affinity K_B indicated that the interactions with the Td-G3-(COOMe)₈-(Cp)₂₄ leads in the most used VOCs to reduce the binding affinity at least one order of magnitude than those found for the interactions with the Td-G2-(COOMe)₈-(Cp)₈ (see Figure 4.24). These observations demonstrated the influence of the generation as well as the number of the phenyl group on the capability, sensitivity and the selectivity of the dendrimer to interact with different classes of VOCs. In particular, Td-G3-(COOMe)₈-(Cp)₂₄ shows a high sensitivity and selectivity to detect acetone, acetophenone as well as the nonpolar aromatic benzene and toluene.

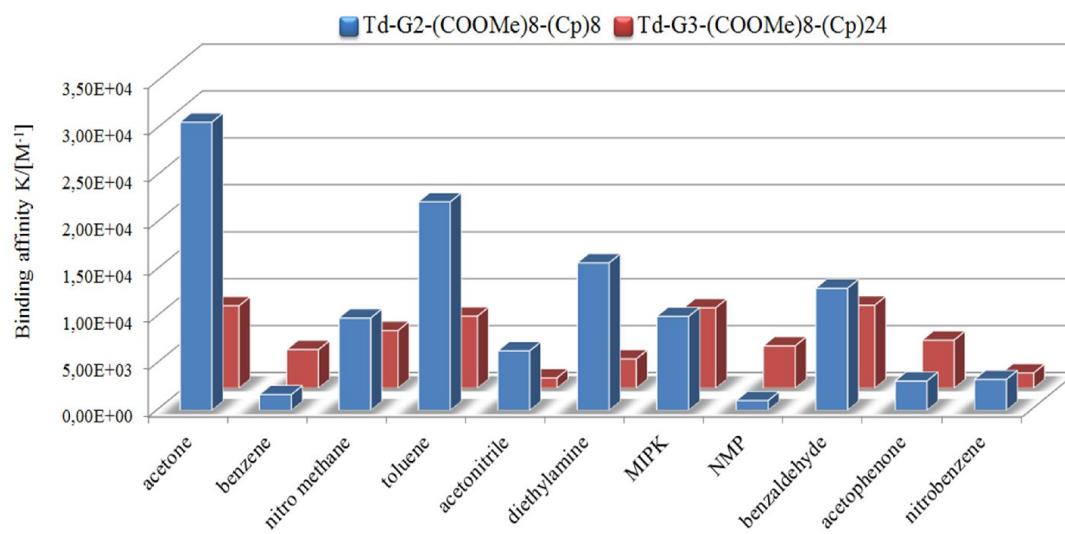


Figure 4.24: The binding affinity K_B for the interactions of VOCs with the Td-G3-(COOMe)₈-(Cp)₂₄ and Td-G2-(COOMe)₈-(Cp)₈ in THF at 25°C.

4.4 TRIACETONE TRIPEROXIDE (TATP) SENSOR STUDY

Detection and analysis of explosive materials has become an integral part of national and global security.³⁵ A number of different methods have been developed in the past for the detection of explosives.³⁶ Sensors are one of those methods of detection which have the capability to mimic the canine system which are known to be the most reliable method of detection. The most common explosive material is triacetone triperoxide (TATP) (Figure 4.25).

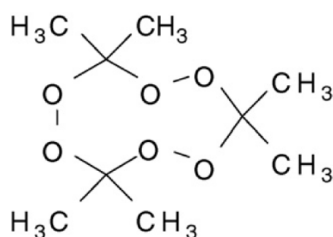
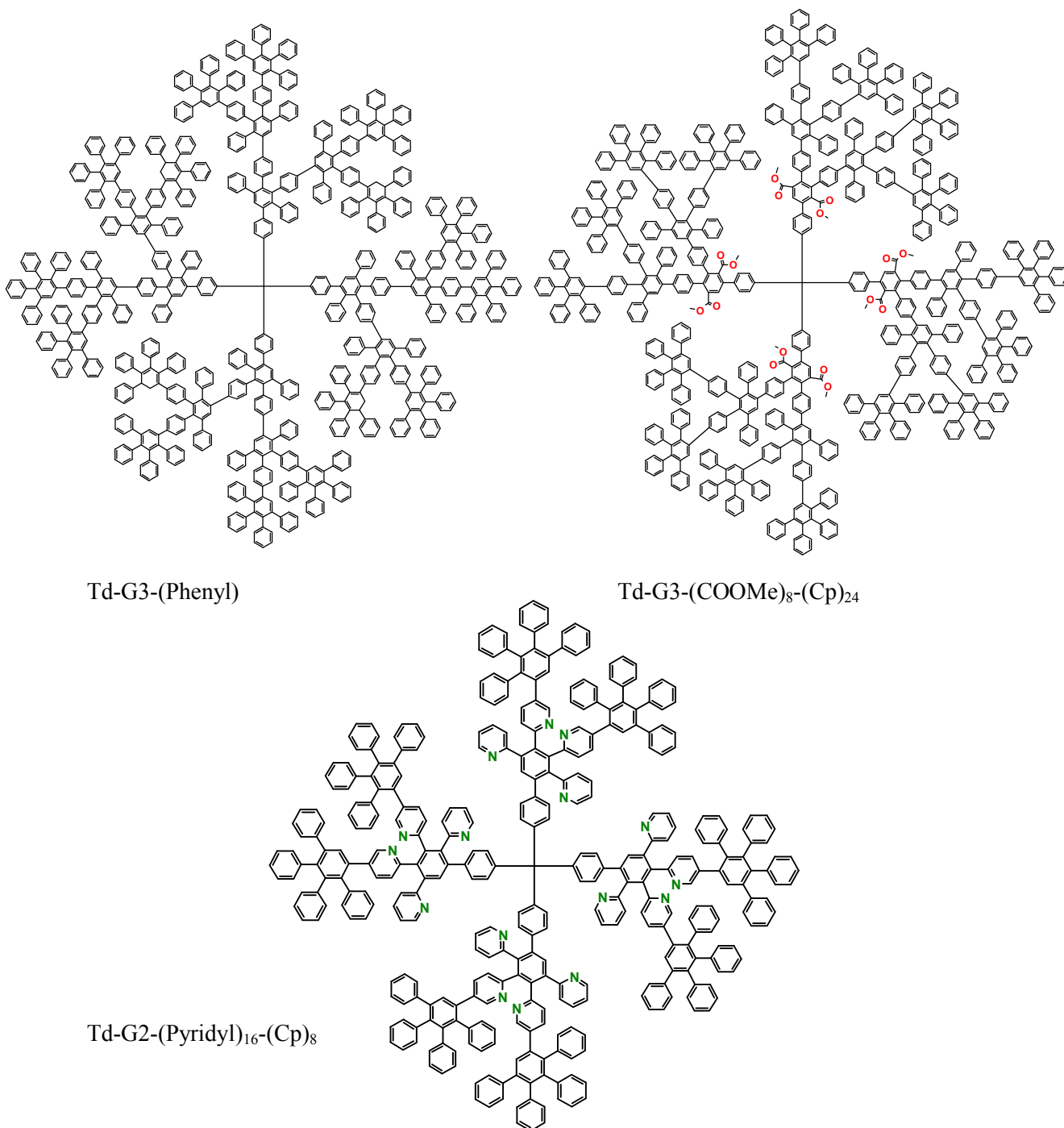


Figure 4.25: Chemical structure of the explosive triacetone triperoxide (TATP).

This compound does not contain nitro or aromatic functionalities but incorporate cyclic peroxides that are stable enough to be transported, but are moderately shock sensitive.³⁷ To ensure accurate, fast and economical monitoring or detection of explosives/explosive related material, there is a need to develop portable, easy to operate and low cost sensors. Based on the origin of obtainable signals, most commonly used sensors for the detection of explosives can broadly be classified as: (i) electrochemical sensors, (ii) mass sensors, (iii) optical sensors and (iv) biosensors.³⁸

The categorization of these sensors is based primarily on the principal physics and operating mechanisms. Consequently, there is a novel chemical sensor device based on QMBs which has been developed to trace TATP.³⁹ Sensing with QMBs is a surface process (see *Chapter 4.1*). Since there are no direct methods to investigate the supramolecular interaction of deposited material on a quartz surface on a molecular level, an intense screening is the only way to obtain more information on the interplay between airborne TATP and the individual affinity layer.

After employing the ITC technique to detect and quantify the VOCs/polyphenylene complexation, further investigations were done for quantifying and for screening the interactions between the TATP and the polyphenylene dendrimers by using a similar technique.



Scheme 4.7: Polyphenylene dendrimers used to study triacetone triperoxide TATP sensoric.

In practice, a second generation polyphenylene dendrimer with *pyridyl* functional groups $Td-G2-(Pyridyl)_{16}-(Cp)_8$, a third generation *methyl ester* functionalized polyphenylene dendrimer $Td-G3-(COOMe)_8-(Cp)_{24}$ and a third generation non-functionalized polyphenylene dendrimer $Td-G3-(Phenyl)$ were studied (see Scheme 4.7).

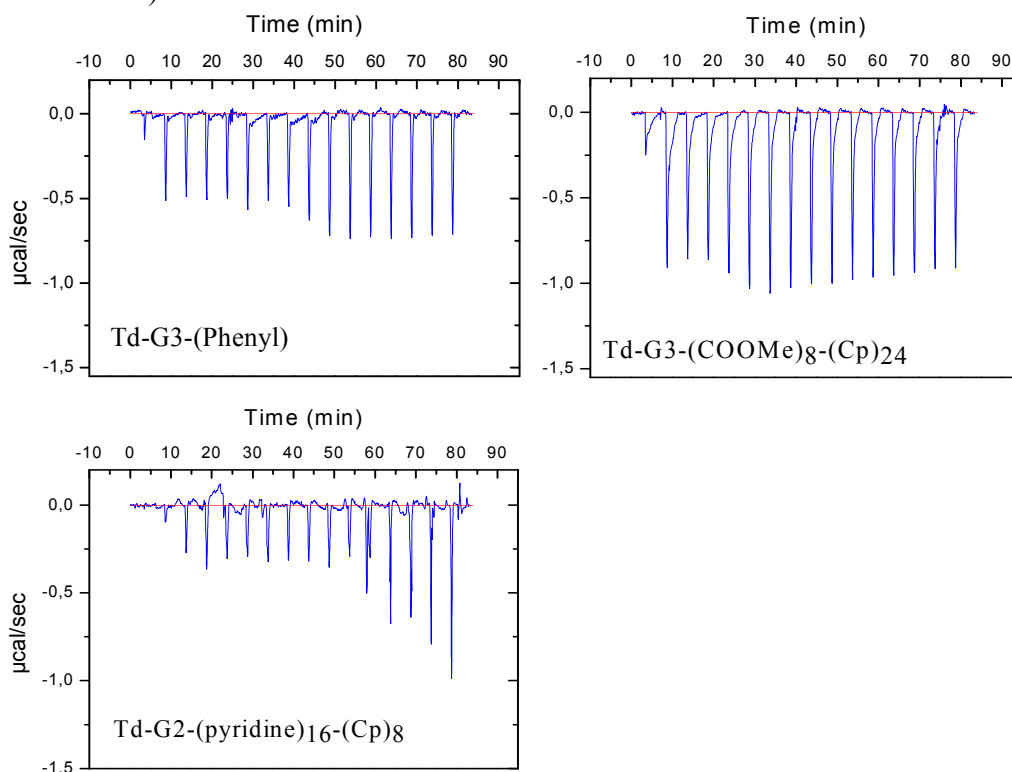


Figure 4.26: Binding isotherms for the titration of 0.001 mM solution of Td-G3-(phenyl), Td-G3-(COOMe)₈-(Cp)₂₄ and Td-G2-(pyridyl)₁₆-(Cp)₈ in CHCl₃ into a solution of TATP (0.0054mM) in the same solvent at 25°C.

Table 4.10: Thermodynamic parameters for the interaction of 0.001 mM solution of Td-G3-(phenyl), Td-G3-(COOMe)₈-(Cp)₂₄ and Td-G2-(pyridyl)₁₆-(Cp)₈ in CHCl₃ into a solution of TATP (0.0054 mM) in the same solvent at 25°C.

VOCs	K_B M ⁻¹	ΔH kcal/mol	T ΔS kcal/mol	ΔG kcal/mol
Td-G3-(phenyl)	$(5.80 \pm 0.431) \times 10^7$	9.24	16.54	-7.30
Td-G2-(pyridyl) ₁₆ -(Cp) ₈	$(1.23 \pm 0.480) \times 10^9$	35.14	45.02	-9.88
Td-G3-(COOMe) ₈ -(Cp) ₂₄	$(9.01 \pm 0.008) \times 10^8$	-42.09	-33.39	-8.70

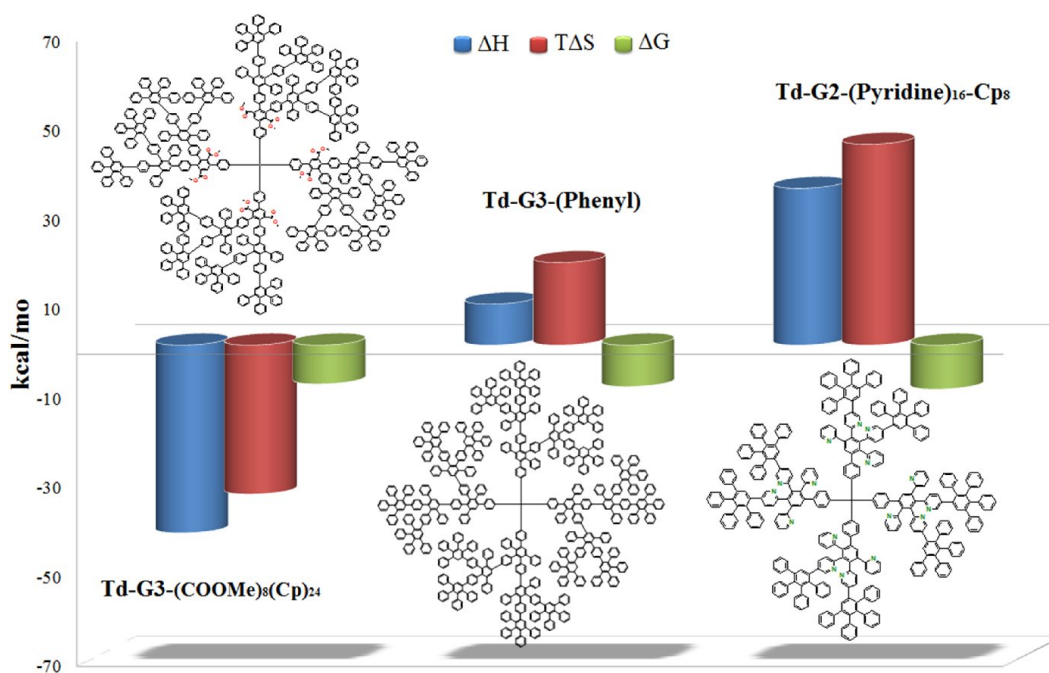


Figure 4.27: Schematic diagram presenting the thermodynamic profiles observed for the interaction of TATP (0.00054 mM) with (0.001 mM) polyphenylene-dendrimers in CHCl_3 at 25°C .

The observed titration curves and the thermodynamic parameters (Figure 4.26, Figure 4.27 and Table 4.10) shows that the enthalpic and entropic contributions are noticeably different between the Td-G3-(COOMe)₈(Cp)₂₄ on one hand and the Td-G2-(Pyridyl)₁₆(Cp)₈ as well as the Td-G3-(Phenyl) on the other hand. The interaction with Td-G3-(COOMe)₈(Cp)₂₄ yielded highly favorable (negative) heat of interaction ΔH and highly unfavorable (negative) entropic changes ΔS , signifying that the interaction is mainly controlled by hydrophilic forces.⁴⁰ The high binding enthalpy ΔH reflects the strength of the interactions between the TATP guest and the dendrimer host, suggesting that there are a large number of hydrogen bond contacts between the dendrimer and the TATP molecules.^{41, 42} On the contrary, the interaction of TATP with the G3- non-functionalized polyphenylene dendrimer as well as the Td-G2-(pyridyl)₁₆(Cp)₈ yielded high unfavorable (positive) heat of interaction ΔH and high favorable (positive) entropic changes ΔS .

This thermodynamic signature indicates that these bindings are predominantly controlled by hydrophobic forces,⁴³ suggests a hydrophobic transfer of TATP

molecules from bulk solvent to the dendrimer binding sites and release.^{44, 45} This unlike forces, recommends that the TATP/ polyphenylene dendrimer interactions occurred in two different mechanisms of binding, depending on the dendrimer generation and the nature of the functional groups that were incorporated in the interior (scaffold) of the dendrimer (see *Chapter 4.3.3* and *Chapter 1.5*).

Moreover, on the basis of binding constant K_B (see Table 4.10), which reflected the affinity of the dendrimers to the TATP molecules. Using of polyphenylene based dendrimers proves a very strong binding affinity toward TATP molecules. Also adding of functional groups like *COOMe* or *pyridine* in the interior (scaffold) of the dendrimers leads to variation of the binding affinity (Table 4.8 and Figure 4.28).

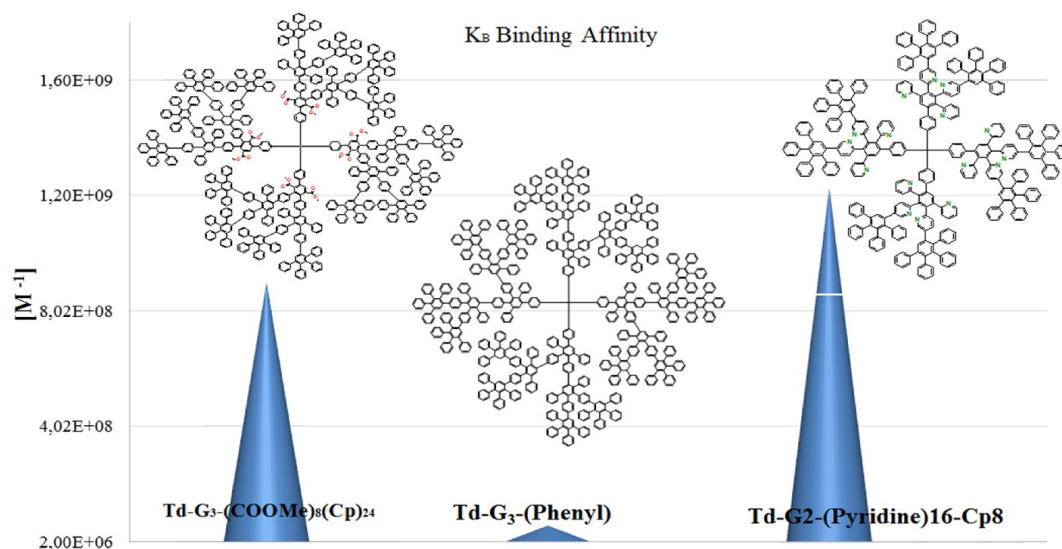


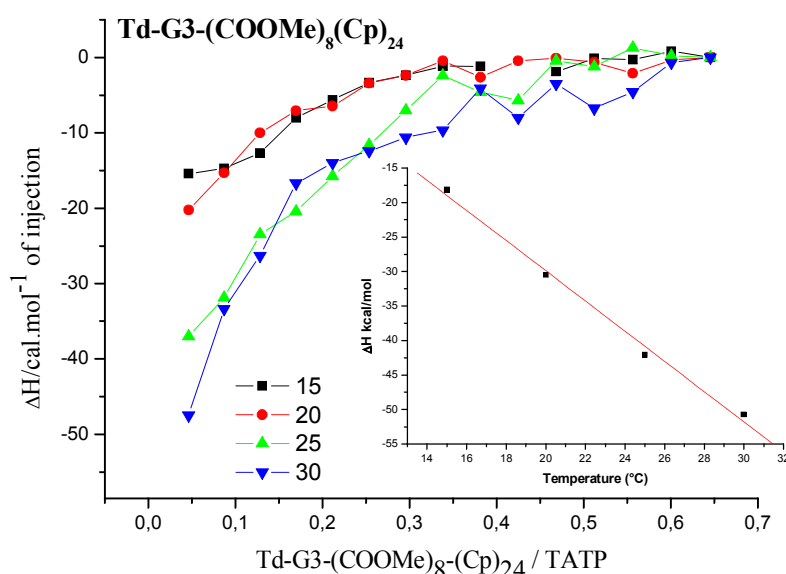
Figure 4.28: The binding affinity K_B as determined by ITC measurement for the interaction of TATP (0.00054 mM) with (0.001 mM) polyphenylene-dendrimers in $CHCl_3$ at 25°C.

Additionally, in order to investigate the influence of temperature on the binding process of the dendrimers with TATP molecules as well as the mechanisms of interactions, the change in heat of capacity (ΔC_p) were calculated.

Practically, heat of capacity (ΔC_p) for the interaction of Td-G3-(COOMe)₈(Cp)₂₄ with TATP in $CHCl_3$ were measured at 15, 20, 25 and 30 °C (see Figure 4.29). The values of the binding affinity at different temperature as well as the other thermodynamic parameters are summarized in Table 4.11.

Table 4. 11: Thermodynamic parameters of binding of G3-(COOMe)₈(Cp)₂₄ with TATP in CHCl₃ at different temperatures.

	T °C	K _B M ⁻¹	ΔH kcal/mol	TΔS kcal/mol	ΔG kcal/mol
Td-G3-(COOMe) ₈ (Cp) ₂₄	15	5.95 x10 ⁷	-18.14	-8.46	-9.67
	20	2.07 x10 ⁷	-30.46	-22.18	-8.28
	25	9.01 x10 ⁸	-42.09	-33.39	-8.70
	30	6.42 x10 ⁷	-50.72	-40.98	-9.74

**Figure 4.29:** Plot of ΔH versus temperature for the calculation of ΔC_p for the binding of TATP to Td-G3-(COOMe)₈(Cp)₂₄.

The interaction of Td-G3-(COOMe)₈(Cp)₂₄ with TATP were found to be slightly negative ($\Delta C_p = -2.18 \text{ kcal}\cdot\text{mol}^{-1}\cdot\text{K}^{-1}$). This small value of ΔC_p suggests that hydrophilic forces play a significant role in the heat capacity change upon binding, in instances where the overall heat capacity change is large (see *Chapter 3.5*).⁴⁶⁻⁴⁹

Furthermore, if small negative changes in the heat capacity are associated with an unfavorable (negative) entropic change (Table 4.11); this contribution means that hydrophobic interactions are not involved in the binding reaction of Td-G3-(COOMe)₈(Cp)₂₄ with TATP. Consequently, these interactions are dominated by hydrophilic interactions.

In conclusion, these results identify two different kinds of interaction mechanisms can be found in the polyphenylene dendrimer and its derivative to interact with the TATP molecules. A correlation with the QMB results (see Ref. 39 and Mathias Grill Dissertation) here cannot be created. The reason of this is the different principle of measurements between QMB and ITC (see *Chapter 5.1* and *Chapter 1.5*). The only possibility to compare between TATP/dendrimers interactions can be occurred when the dendrimers have the same interacting mechanisms (hydrophobic or hydrophilic). Moreover, a general common observation with the quartz microbalance (QMB) technique study³⁹ can be found, that the functionalized polyphenylene dendrimers interacting with the TATP stronger than the non-functionalized polyphenylene dendrimers.

4.5 ITC OF MOLECULARLY IMPRINTED POLYMER NANOSPHERES

The ‘molecular imprinting’ technique is a synthetic method uniquely suited for the preparation of artificial systems capable of molecular recognition and catalysis.⁵⁰ Molecular imprinting is based on the polymerization of mixtures containing a template molecule as well as interacting and cross-linking monomers. After template removal, binding sites complementary to the template are left in the resulting polymer. They are held in place by the cross-linked structure and, like the binding sites of biological receptors, are capable of selectively rebinding the template.⁵¹

In this part (*in cooperation with Gita Dvorakova and Dr. Andrea Biffis from university of Padova, Italy*) the ITC technique was applied in order to understand the imprinting effect and the rebinding efficiency of nanosized molecularly imprinted polymer particles. These particles were synthesized by means of a recently developed nonaqueous emulsion polymerization (by Robert Haschick/polymerization procedures subgroup)⁵² using a standard monomer mixture of methacrylic acid and ethylene dimethacrylate, containing (\pm)-propranolol as a template (Figure 4.30).

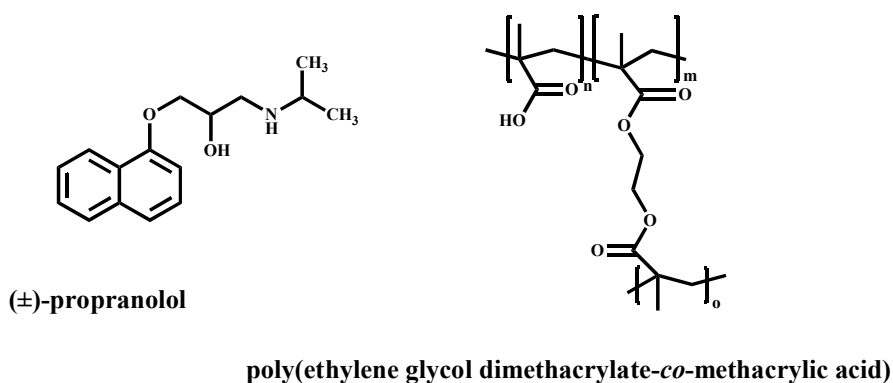


Figure 4.30: Propranolol template and monomer mixture of methacrylic acid and ethylene dimethacrylate used in this study.

The interaction of (\pm)-propranolol with polymer particles sample **1** (non-imprinted) and sample **2** (imprinted) in toluene +0.5% v/v acetic acid at 25 °C was investigated (Figure 4.31). In the present case, ITC allowed to determine that there are noticeably different enthalpic and entropic contributions to the free

energy of binding to polymer **1** (ΔH -1.28 kcal/mol and $T\Delta S$ 5.13 kcal/mol) and **2** (ΔH -0.36 kcal/mol and $T\Delta S$ 8.14 kcal/mol) (see Table 4.12)

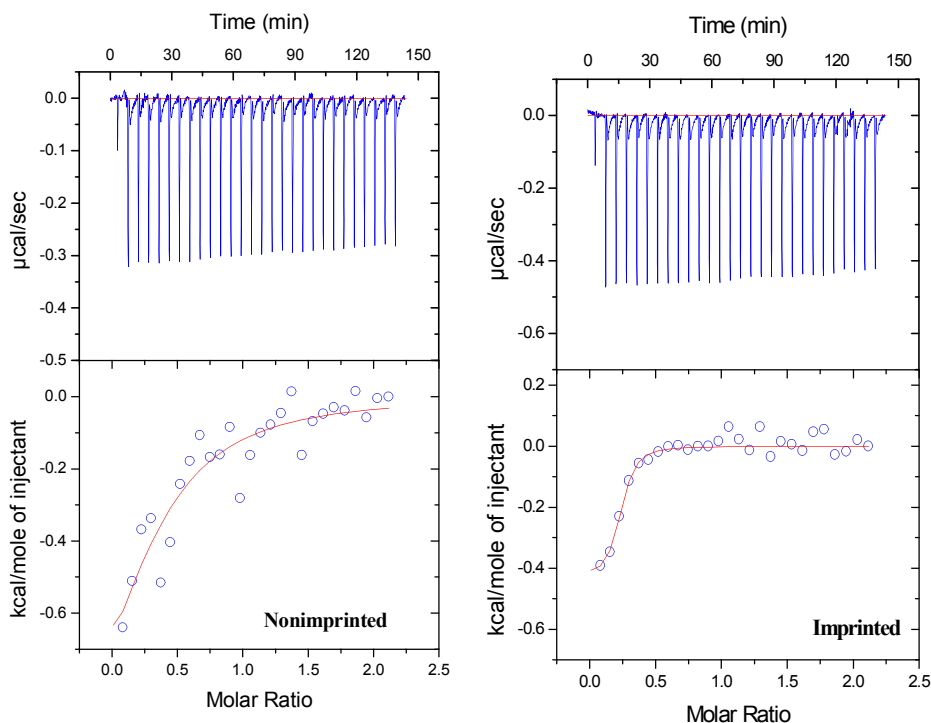


Figure 4.31: Experimental curve for the titration of a 0.55 mM solution of *rac*-propranolol in (95.5%/toluene/0.5% acetic acid (v/v)) solvent into 0.055 mM of poly(ethylene glycol dimethacrylate-co-methacrylic acid) in the same solvent at 25°C.

Table 4.12: Thermodynamic parameters obtained by the ITC measurements.

	K_B M^{-1}	ΔH kcal/mol	$T\Delta S$ kcal/mol	ΔG kcal/mol
non-imprinted 1	$(5.10 \pm 0.31) \times 10^4$	-1.28 ± 0.25	5.13	-6.41
imprinted 2	$(1.68 \pm 0.28) \times 10^6$	-0.36 ± 0.04	8.14	-7.14

The thermodynamic signature indicates that the binding is predominantly entropic, most probably driven by hydrophobicity.⁵³ This is not surprising, since the enthalpic contribution, which should stem mainly from the direct interaction between template and polymer-bound carboxylic acid groups, is offset by the presence of acetic acid in the rebinding solvent.

The entropy changes arise from the release of solvent molecules upon binding and are more favorable for the imprinted polymer, as also previously reported by other groups.^{54, 55} Since the template is expected to fit better in the imprinted cavities,

consequently releasing a greater number of solvent molecules. The determined binding constant K_B , which reflects the interaction affinity of (\pm)-propranolol to the polymer particles, was about two orders of magnitude higher for the imprinted ($1.68 \times 10^6 \text{ M}^{-1}$), than for the non-imprinted ($5.10 \times 10^4 \text{ M}^{-1}$), and unequivocally demonstrates the existence of a marked imprinting effect in the nanoparticles.

ITC was proven to be a suitable method to investigate the thermodynamics of non-covalently imprinted polymers and to be an excellent tool to assess the efficiency of the initial molecular imprinting process, in particular the enthalpies of the reactions of non-imprinted (\pm)-propranolol to the polymer particles studied are higher in comparison to those of imprinted, which shows a significant heat during titration. Additionally, the binding affinity for the imprinted polymer was significantly higher than for the non-imprinted polymer. Thus, a mechanism of non-covalently imprinted polymers was proven by a direct thermodynamic characterization method.

4.6 CONCLUSION

The interactions between non-functionalized as well functionalized polyphenylene dendrimers (in scaffold) and several kinds of VOCs were applied by using the ITC technique at very low concentrations (micromolar level). For all the VOCs (polar aromatic, non-polar aromatic, ketones, nitro compound, nitrile compound as well as cyclic amide) studied, the interaction was found to be strongly thermodynamically driven by both negative change in enthalpy and positive change in entropy. Compared to existing techniques, ITC enables monitoring of not only the nature of molecular interactions, but also the sensitivity and the selectivity of polyphenylene dendrimers (PPDs) towards VOC-molecules.

In the first series of experiments, the interactions between non-functionalized polyphenylene dendrimer (Td-G2) and different classes of volatile organic compounds VOCs were investigated. Depending on the polarity of molecules, the extent of interaction varies widely from one VOC to the other, thereby rendering high degree of selectivity and sensitivity of polyphenylene dendrimer towards VOCs (see *Chapter 5.3.1*). Furthermore, the range of investigated VOC-molecules could be extended to aliphatic solvent systems at extremely low detection levels (micromolar level). For all the VOCs studied, the interactions were found to be strongly thermodynamically driven by both negative change in enthalpy and positive change in entropy. Moreover; based on ITC studies and fluorescence measurements, it has been possible to prove that interaction between the PPDs and VOCs not only takes place inside the core of the cavity but also on the polyphenylene dendrimer surface outside the core, besides the π - π electron donor-acceptor complexation is not the dominant mode of interaction between the neutral polyphenylene dendrimer and the VOCs studied in the present work.

As an extension of the study of non-functionalized polyphenylene dendrimer (Td-G2)/VOCs, different functionalized dendrimers bearing methyl ester-, carboxyl-, cyano-, nitro- and pyridyl groups at the interior (scaffold) (see Scheme 4.4, 4.5 and 4.6) were studied. The study of these functionalized dendrimers shows noticeably the influences of the nature of the functional groups on the capability, sensitivity and the selectivity of the dendrimers to uptake different classes of

VOCs. It proved that incorporation of the electron withdrawing ($-\text{NO}_2$ and $-\text{CN}$) substituents in the dendrimers scaffold leads to an increase of the capability and selectivity of the PPDs to detect polar aromatic (e.g. benzaldehyde and acetophenone), nonpolar aromatic (benzene and toluene) as well as aliphatic VOCs (i.e. acetone, MIPK and nitro methane). On the other hand, employing an acidic substitution group such as (COOH) leads to increasing the sensitivity to detect/uptake aliphatic and polar aromatic VOCs. On the other side using of (COOMe) groups leads to slightly increased sensitivity of the dendrimer to detect/uptake aliphatic VOCs (such as acetonitrile and diethyl amine). This observation can be related to the presence of COOH groups in the cavities of the dendrimer, which increases the ability of the dendrimer to build hydrogen bonds with the guest molecules. Furthermore, adding the basic *pyridyl* group in the interior scaffold leads to an increase of the sensitivity of the PPDs to uptake/detect aliphatic VOCs such as acetone and acetonitrile (Figure 4.32).

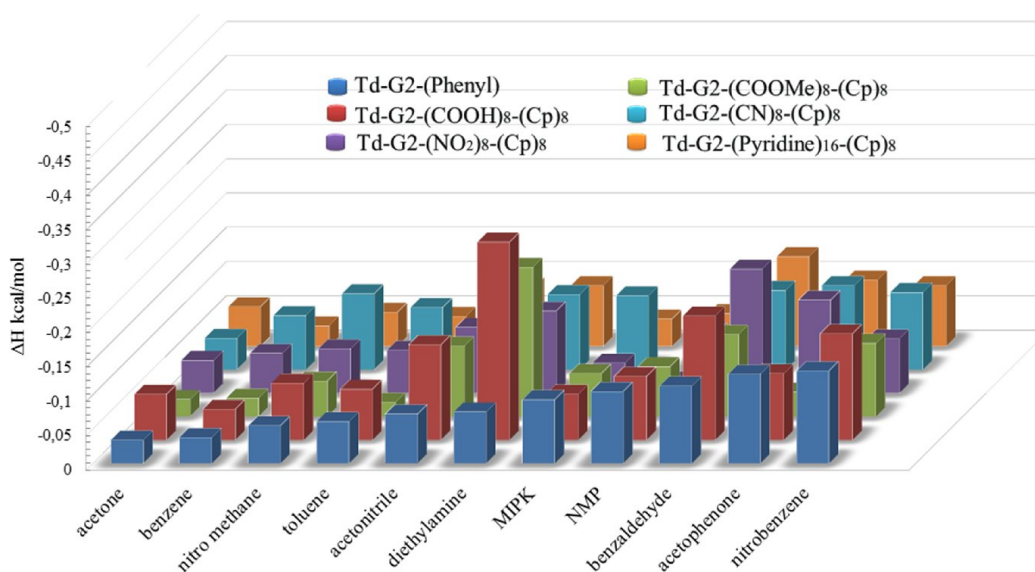


Figure 4.32: The enthalpy change ΔH signatures for the interactions of different functionalized dendrimers bearing (*methyl ester-, carboxyl-, cyano-, nitro- and pyridyl*) groups at the interior layers (scaffold) with various VOCs in THF at 25°C.

Considering the binding affinity K_B for the interactions, the employing of the functional groups at the interior (scaffold) of the polyphenylene dendrimer leading to a noticeably variation of the binding affinity toward the VOCs (Figure 4.33). In practical, polyphenylene dendrimer bearing *cyano* or the *pyridyl* groups leads to a

raise of the binding affinity one to two orders of magnitude in most of the interactions with VOCs used, e.g. nitro methane, toluene, acetonitrile, diethyl amine and acetone. A use of the *carboxyl* group as a functional group in the interior of the dendrimer leads to decrease of the binding affinity in most of the interactions with VOCs. Additionally, using of the *methyl ester (COOMe)* group leads to a slightly increase of the binding affinity with acetone, toluene as well as benzaldehyde. Likewise, using of the *nitro* group leads to an increase the binding affinity with polar aromatic acetophenone (*Chapter 4.3.3*).

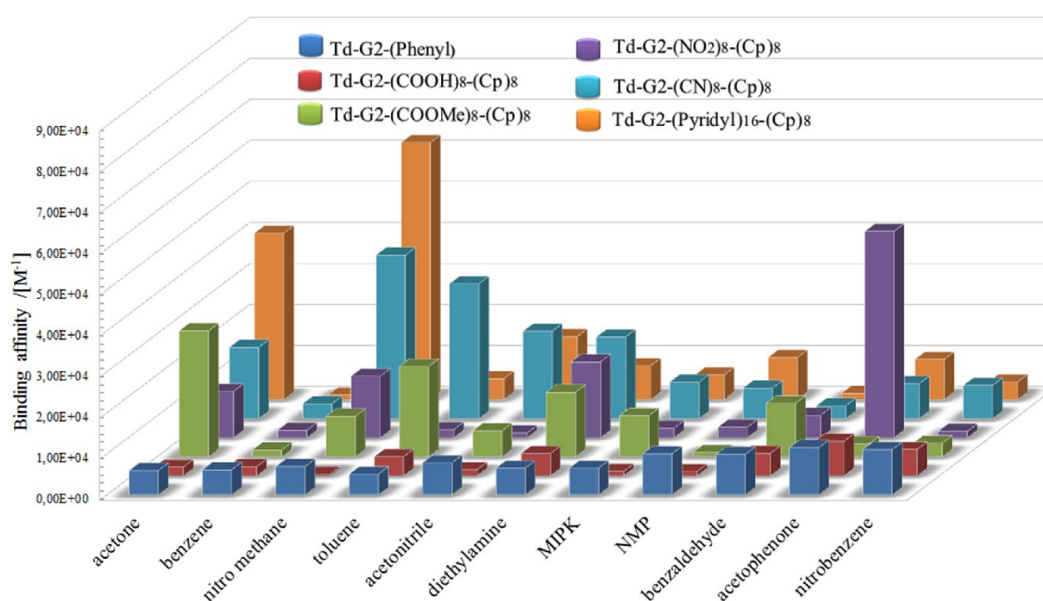


Figure 4.33: The binding affinity K_B for the interactions of different functionalized dendrimers bearing (*methyl ester*-, *carboxyl*-, *ciano*-, *nitro*- and *pyridyl*) groups at the interior layers (scaffold) with various VOCs in THF at 25°C

Furthermore, after applying the ITC technique to analysis and quantify the VOCs/polyphenylene complexation, further investigations have been done for quantifying and for screening the interactions between the explosive material *triacetone triperoxide (TATP)* and PPDs using the ITC technique. In practical, a second generation of polyphenylene dendrimer with *pyridyl* functional groups *Td-G2-(Pyridyl)₁₆-(Cp)₈*, a third generation of *methyl ester* substituted polyphenylene dendrimer *Td-G3-(COOMe)₈-(Cp)₂₄* and a third generation of unsubstituted polyphenylene dendrimer *Td-G3-(Phenyl)* were studied. The observed thermodynamics parameters proved that non-functionalized polyphenylene dendrimers and the functionalized one interacting strongly with the

explosive materials TATP. In agreement with the result of QMB technique the ITC technique demonstrated, that polyphenylene dendrimer and its derivatives can be used as sensor-active substances to detect the explosive material TATP (*Chapter 4.4*).

As a final point, the ITC technique was applied with the purpose of understanding the imprinting effect and rebinding efficiency of nanosized molecularly imprinted polymer particles. These particles were synthesized by means of non-aqueous emulsion polymerization using a standard monomer mixture of methacrylic acid and ethylene dimethacrylate, containing (\pm)-propranolol as a template. The observed results, demonstrated that the reaction enthalpies of the non-imprinted (\pm)-propranolol to the polymer particles are higher in comparison to those of imprinted polymers. On the other hand, the binding affinity for the imprinted polymer shows significantly higher affinity than for the non-imprinted polymer (*Chapter 4.5*). These results proved that ITC techniques can be used as techniques to quantify and study the molecular imprinting method. Systematic calorimetric investigations are promising measurements to gain further insight in the mechanism involved in the molecular imprinting of synthetic polymers.

In summary, the type and number of binding sites must be selected in a fashion that is most complementary to the characteristics of the binding sites of the guest, and these binding sites should be spaced somewhat apart from one another to minimise repulsions between them, but arranged so that they can all interact simultaneously with the guest. The more favourable interactions there are the better. The most stable complexes are generally obtained with hosts that are preorganised for guest binding, thus where there is no entropically and enthalpically unfavourable rearrangement on binding that reduces the overall free energy of complexation.

4.7 REFERENCES

- [1] Dorsey, A., McClure, P.R., McDonald A.R., Singh, M., U.S. Dep. of Health and Human Services–Agency for Toxic Substances and Disease Registry, Atlanta **2000**.
- [2] Neumann, H. G., Thielmann, H. W., Filser, J. G., Gelbke, Greim, H. P. H. H. Kappus, Norpoth, K. H., Reuter, U., Vamvakas, S., Wardenbach P., Wichmann, H. E., *J.Cancer Research and Clinical Oncology* **1998**, 124, 661.
- [3] Hodgson, M. J., Frohlinger, J., Permar, E., Tidwell, C., Traven, N. D., *S. J. Occ. Env. Med.* **1991**, 33, 527.
- [4] Srivastava, A. K., *Sensors and Actuators B-Chemical*, **2003**, 96, 24.
- [5] Hamilton, S., Hephher, M., *Sensors and Actuators B-Chemical*, **2005**, 107, 424.
- [6] Hamilton, S., Hephher M., Sommerville J., *Sensors and Actuators B-Chemical*, **2005**, 107, 424.
- [7] Wiesler, U.-M., Berresheim, A.J., Morgenroth, F., Lieser G., Müllen K., *Macromolecules.*, **2001**, 34, 187.
- [8] a) Hasheimi, A. B., Hart, H., Ward, D.L., *J. Am. Chem. Soc.* **1986**, 108, 6675; b) Venugopalan, P., Bürgi, H.-B., Frank, N.L., Baldridge, K.K., Siegel, J.S., *Tetrahedron Letter.* **1995**, 36, 2419.
- [9] Schlupp, M., Weil, T., Berresheim, A.J., Wiesler, U.-M., Bargon, J., Müllen, K., *Angew. Chem., Int. Ed. Engl.*, **2001**, 40, 4011.
- [10] Andreitchenko, E.V. PhD Thesis, Max-Planck-Institute for Polymer Research, **2006**.
- [11] Grill, M. PhD thesis, Max-Planck-Institute for Polymer Research, **2011**.
- [12] Bauer R. E., Clark C. G., Müllen K., *New J. Chem.*, **2007**, 31, 1275.
- [13] a) Frank, H. S., Evans, M. W., *J. Chem. Phys.* **1945**, 13, 507 ; b) Leavitt, S., Freire, E., *Curr. Opin. Struct. Biol.*, **2001**, 11, 560.
- [14] Holdgate, G. A., Tunnicliffe, A., Ward, W. H. J., Weston, S. A., Rosenbrock, G., Barth, P. T., I. Taylor, W. F. , Paupit, R. A., Timms, D., *Biochemistry*, **1997**, 36, 9663.
- [15] Tobey, S. L. , Anslyn, E. V, *J. Am. Chem. Soc.*, **2003**, 125, 14807.
- [16] Blokzijl, W., *Angew. Chem. Int. Ed. Engl.* **1993**, 32, 1545.
- [17] a) Tobey, S. L., Anslyn, E. V. , *J. Am. Chem. Soc.* **2003**, 125, 14807. ; b) Zajac, J., Trompette, J. L., Partyka, S., *J. Therm. Anal.* **1994**, 41, 1277. ; c) Denoyel, R., Rouquerol, J., *J. Colloid Interface Sci.* **1991**, 143, 555.
- [18] Blokzijl, W., *Angew. Chem. Int. Ed. Engl.* **1993**, 32, 1545.
- [19] Arouri, A., Garidel, P., Kliche, W., Blume, A., *Eur Biophys J.*, **2007**, 36, 647.
- [20] Gribenko, A., Guzman-Casado, M. , Lopez, M., Makhatadze, G., *Protein Sci.*, **2002**, 11, 1367.
- [21] Dominguez-Pérez, I., Teñlez-Sanz, R., Leal, I., Ruíz-Pérez, L., González-Pacanoska, D., García-Fuentes, L., *Biochim Biophys Acta* , **2004**, 1702, 33.
- [22] Lee, W. J.; Kim, Y.; Case, E. D., *J. Mater. Sci.* , **1993**, 28, 2079.
- [23] a) Smithrud, D. B., Sanford, E. M., Chao, I., Ferguson, S. B., Carcanague, D. R., Evanseck, J. D. K., Houk, N., Diederich, F., *Pure & Appl. Chem.*, **1990**, 62, 2227. ; b) Fuchs, R., Peacock, L. A., Stephenson, W. K., *Can. J. Chem.*, **1982**, 60, 1953.

- [24] a) Ma, J. C., and Dougherty, D., *Chem. Rev.*, 1997, **97**, 1303. ; b) Berryman, O. B., Bryantsev, V. S., Stay, D. P., Johnson, D. W., Hay, B. P., *J. Am. Chem. Soc.*, **2007**, 129,48. ; c) Steed, J. W., Turner, D. R., Wallace, K.J., (*Core Concepts in Supramolecular Chemistry and Nano-chemistry*), John Wiley, Chichester, NY, **2007**, 15.
- [25] Liu D., De Feyter S., Cotlet M., Stefan A., Wiesler U.-M., Herrmann A, Koehler D., Qu J., Muellen K. and De Schryver F.C., *Macromolecules*, **2003**, 36, 5918.
- [26] Qin T., Zhou G., Scheiber H., Bauer R. E., Baumgarten M., Anson C. E., List E. J. W., Mullen K., *Angew. Chem., Int. Ed. Engl.*, **2008**, 47, 8292.
- [27] Kohn F., Hofkens J., Wiesler U.-M, Cotlet M., Auweraer M., Muellen K., and De Schryver F. C., *Chem. Eur. J.* , **2001**, 7, 4126., 47, 8292.
- [28] Arora A., Balasubramanian C., Kumar N., Agrawal S., Ojha R. P. and Maiti S., *FEBS Journal* , **2008**, 275, 3971.
- [29] a) Xu, ZF., Kahr, M., Walker, KL., Wilkins, CL., Moore, JS., *J. Am Chem. Soc.*, **1994**, 116, 4537. ; b) Hart H, *Pure Appl Chem.*, **1993**, 65, 27.
- [30] Zhang, H., Grim, PCM., Foubert, P., Vosch, T., Vanoppen, P., Wiesler, UM., Berresheim, AJ. , Müllen, K., De Schryver, FC., *Langmuir*, **2000**, 16, 9009.
- [31] Zhang, H., Grim, PCM., Vosch, T., Wiesler, UM., Berresheim, AJ., Müllen, K., De Schryver, FC., *Langmuir*, **2000**, 16, 9294.
- [32] Wind, M., Saalwachter, K., Wiesler, UM., Müllen, K., Spiess, HW., *Macromolecules*, **2002**, 35, 10071.
- [33] Wind, M., Wiesler, UM., Saalwachter, K., Müllen, K., Spiess, HW., *Adv. Mater.*, **2001**, 13, 752.
- [34] Baars, M. W. P. L.; Meijer, E. W. *Top Curr Chem* **2000**, 210, 131.
- [35] a) Moore, D. S., *Rev. Sci. Instrum.*, **2004**, 75, 2499. ; b) Steinfeld, J. I., Wormhoudt, J. *Annu. Rev. Phys. Chem.*, **1998**, 49, 203.
- [36] Singh, S., *J. Hazard. Mater.*, **2007**, 144, 15.
- [37] a) Federoff, B. T., (*in Encyclopedia of Explosives and Related Items*), ed. Federoff, B. T., Aaronson, H. A., Reese, E. F., Sheffield, O. E., Clift, G. D. Picatinny Arsenal, Dover, NJ, **1960**, vol. 1, pp. A42. ; b) Yinon, J., (*Forensic and Environmental Detection of Explosives*), John Wiley, Chichester, NY, **1999**, 10. ; (c) Meyer, R., Köhler J., Homburg, A. *Explosives*, John Wiley- VCH, Weinheim, 5th ed., **2002**, p. 346.
- [38] a) Wang, J., Pumera, M., Chatrathi, M.P., Escarpa, A., Musameh, M., *Anal. Chem.* **2002**, 74, 1187. ; b) McGill, R.A., Isna, T.E.M., Chung, R., Nguyen, V.K., Stepnowski, J., *Sens. Actuators B*, **2000**, 65, 5.; c) Lopez-Avila, V., Hill, H.H., *Anal. Chem.*, **1997**, 69, 289.; d) Naal, Z., Park, Bernhard, J.H., Shapleigh, S. J.P., Batt, C.A., Abrun, H.D., *Anal. Chem.*, **2002**, 74, 140.
- [39] Lubczyka, D., Sieringa, C., Lörgena, J., Shifrina, Z. B., Müllen, K., Waldvogel, S. R., *Sens. Actuators B*, **2010**, 143, 561.
- [40] a) Haq, I., Ladbury, J. E., Chowdhry, B. Z., Jenkins, T. C., Chaires, J. B., *J. Mol. Biol.* **1997**, 271, 244. ; b) Privalov, P. L., Gill, S. J., *Pure Appl. Chem.* **1989**, 61, 1097, ; c) Silverstein, K. A., Haymet, T. A. D., Dill, J. K. A., *J. Am. Chem. Soc.*, **1998**, 120, 3166.

- [41] a) Frank, H. S., Evans, M. W., *J. Chem. Phys.* **1945**, 13, 507. ; b) Leavitt, S., Freire, E., *Curr. Opin. Struct. Biol.* **2001**, 11, 560.
- [42] a) Campoy, A. V., Todd, M.J., Freire, E., *Biochemistry* **2000**, 39, 2201. ; b) Todd, M.J., Luque, I., A. Campoy, V., Freire, E., *Biochemistry* **2000**, 39, 11876. ; c) Campoy, A. V., Luque, I., Todd, M.J., Milutinovich, M., Kiso, Y., Freire, E., *Protein Sci.* **2000**, 9, 1801. ; d) Velazquez-Campoy, A., Kiso, Y., Freire, E., *Arch. Biochem. Biophys.* **2001**, 390, 169. ; e) Freire, E., *Nat. Biotechnol.* **2002**, 20, 15–16; f) Ohtaka, H., Velazquez-Campoy, A., Xie, D., Freire, E., *Protein Sci.* **2002**, 11, 1908.
- [43] a) Holdgate, G. A., Tunnicliffe, A., Ward, W. H. J., Weston, S. A., Rosenbrock, G. P., Barth, T., Taylor, I. W. F., Pauptit, R. A., Timms, D., *Biochemistry* **1997**, 36, 9663. ;
- [44] a) Tobey, S. L., Anslyn, E. V., *J. Am. Chem. Soc.* **2003**, 125, 14807. ; b) Zajac, J., Trompette, J., Partyka, L. S., *J. Therm. Anal.* **1994**, 41, 1277. ; c) Denoyel, R., Rouquerol, J., *J. Colloid Interface Sci.* **1991**, 143, 555.
- [45] Blokzijl, W., *Angew. Chem. Int. Ed. Engl.*, **1993**, 32, 1545.
- [46] Kauzmann, W., *Adv. Protein Chem.*, **1959**, 14, 1.
- [47] Tanford, C., *The hydrophobic Effect: Formation of Micelles and Biological Membranes*, Wiley, New York, **1980**.
- [48] Sturtevant, J. M., *Proc. Natl. Acad. Sci. USA* **1977**, 74, 2236.
- [49] Baldwin, R. L., *Proc. Natl. Acad. Sci. USA* **1986**, 83, 8069.
- [50] a) Sellergren, B., *Molecularly Imprinted Polymers*, 2nd Ed., Elsevier, Amsterdam **2001**; b) Komiyama, M., Takeuchi, T., Mukawa, T., Asanuma, H., *Molecular Imprinting from Fundamentals to Applications*, Wiley-VCH, Weinheim **2003**.
- [51] a) Piletsky, S., Turner, A., *Molecular Imprinting of Polymers*, Eds., Landes Bioscience, Austin **2004**; b) Yan, M., Ramström, O., *Molecularly Imprinted Materials. Science and Technology*, Eds., Marcel Dekker, New York **2005**.
- [52] a) Müller, K., Klapper, M., Müllen, K., *Macromol. Rapid Commun.* **2006**, 27, 586. ; b) Müller, K., Klapper, M., Müllen, K., *J. Polym. Sci., Part A: Polym. Chem.* **2007**, 45, 1101. ; c) Klapper, M., Nenov, S., Haschick, R., Müller, K., Müllen, K., *Acc. Chem. Res.* **2008**, 41, 1190.
- [53] Baars, M. W. P. L.; Meijer, E. W. *Top Curr. Chem.*, **2000**, 210, 131.
- [54] Chen, W.-Y., Chen, C.-S., Lin, F.-Y., *J. Chromatogr., A*, **2001**, 923, 1.
- [55] a) Tobey, S. L., Anslyn, E. V., *J. Am. Chem. Soc.*, **2003**, 125, 14807. ; b) Zajac, J., Trompette, J. L., Partyka, S., *J. Therm. Anal.*, **1994**, 41, 1277.

CHAPTER 5

CONCLUSION AND OUTLOOK

CONCLUSION AND OUTLOOK

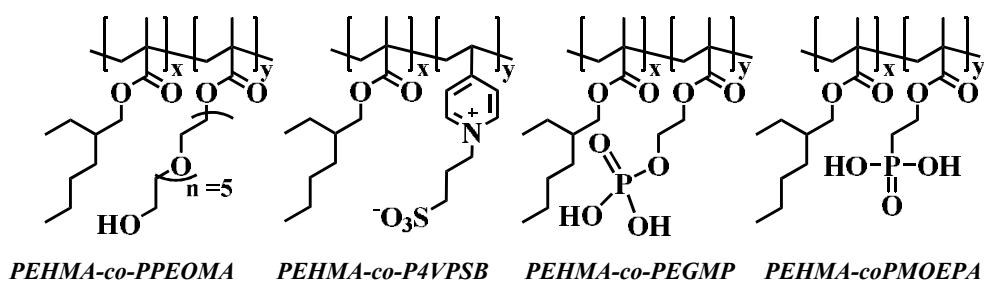
For many years, the underlying thermodynamic variables (ΔH , ΔS and ΔG) of chemical reactions have not been utilized as guiding tools in design and development of compounds, partly because of a lack of adequate microcalorimetric instrumentation and appropriate formalisms for data interpretation and analysis. This situation is rapidly changing, as better instruments with the required sensitivity, throughput and data processing capabilities have become available.

A rigorous understanding of any chemical system that undergoes some change requires quantification of its thermodynamic and kinetic properties. Combined with structural details, these thermodynamic data can be assimilated to enable a picture of mechanism and strength of the interactions. Isothermal Titration Calorimetry (ITC) technique provides the thermodynamic data required for developing this understanding with a simple sample preparation without the need to a complex data evaluation. These considerations have led to ITC being a tool for the synthetic chemist to find more suitable approaches to design and improve new compounds for future applications.

CHAPTER 1 illustrates the essential theoretical background necessary to interpret and analyse physicochemical reactions studied in this work. The experimental approaches applied for functionalization/stabilization of inorganic particles, practically, in polymer-inorganic-hybrid systems were presented and discussed. The next part, demonstrate the development in the host-guest chemistry in the last decades, predominantly, in the systems that dendrimers act as a host molecules. The following part deals with the principles of thermodynamic calculations on macromolecular-ligand binding models, which is based on the first and second thermodynamic laws, as well the ITC technique was presented as a method used to analysis and quantify the intermolecular interactions in the systems studded in this work. The last part of this chapter is dealing with the thermodynamic signatures for each non-covalent binding depending on their enthalpy as well as entropy observation during the reaction.

CHAPTER 2 presents the preparation of an ITC experiment for analysis and quantify the adsorption behavior in the systems studied in this work, different steps should be take on like: sample preparation, sample and reference cell loading, injection syringe loading, experimental parameters, control experiments, and data analysis. A typical ITC experiment requires only about 1-2 hours, with only a few minutes of “hand-on time”. ITC experiments are non-invasive and can be applied on a broad range of solution conditions, including turbid solution. The last part of this chapter dealing with the problems that occurred during the ITC experiments and the suitable guidelines and action plans are provided that can be used to fix it.

CHAPTER 3 demonstrates the quantification and analyse of the adsorption process and binding efficiencies in the polymer-inorganic–hybrid-systems using the ITC technique. Therefore the interaction of amphiphilic copolymers PEHMA-co-PPEOMA^{n≈5}, PEHMA-co-P4VPSB, PEHMA-co-PEGMP and PEHMA-co-PMOEPSA on the surface of inorganic nanoparticles (SiO₂, Al₂O₃, CeO₂, TiO₂, ZnO, ZrO₂ and Fe₃O₄) in a multicomponent solvent system was investigated.



In the first part of this chapter, the interactions of low molecular weight model compounds were applied, i.e. EHMA as a model compound to monitor the influence of the hydrophobic part of the copolymers on the adsorption process with inorganic particles, and the monomers PEOMA, EGMP and 4VPSB in a similar manner to EHMA, as a model compound to monitor the influence of the hydrophilic segment of the copolymers on the adsorption process. It was found the interaction of the hydrophobic monomer EHMA on inorganic particle surfaces lead to an entropically driven process with a positive ΔH and ΔS contributions,

which was characteristic for hydrophobic interactions. That means that the hydrophobic monomer (EHMA) does not react on the particles surface at all, therefore this monomer can as expected only act as a compatibilizer of the hybrid particles in the polymer matrix. Conversely the titration of the hydrophilic monomers PEGMA, EGMP and 4VPSB showed a clearly enthalpically driven process with a higher (negative) binding enthalpy ΔH compensated by a negative ΔS value. The dominant negative enthalpy suggested the presence of a large number of van der Waals interactions or hydrogen bonds between the monomers PEOMA, EGMP and 4VPSB and the inorganic particles (see *Chapter 3.3*). These observations identify the used of the hydrophilic monomers as a surfactant in a multicomponent system for stabilization of the inorganic particles by providing interactions with their surfaces. Generally, these studies offer for the first time, a complete and comprehensive thermodynamic study of monomer/inorganic particles adsorption process in solution.

In the next part of this chapter, in order to compare the adsorption behavior between the different classes of anchor groups, *non-ionic*, *zwitter-ionic* and *acidic* with the inorganic particles, the interaction of PEHMA-co-PPEOMA^{n \approx 5}, PEHMA-co-P4VPSB, PEHMA-co-PMOEPA and PEHMA-co-PEGMP onto Al₂O₃, CeO₂, TiO₂, ZnO, ZrO₂ and Fe₃O₄ nanoparticles were applied (see *Chapter 3.4*). Three main interactions must be considered for the adsorption of amphiphilic copolymers molecules with inorganic particles, namely:

- i. The interaction of the solvent molecules displaced by the adsorbed copolymer segments with the particle surface;
- ii. The interaction between the copolymer segments and solvent molecules; and
- iii. The interaction between the copolymer and the particle surface.

Therefore understanding of these adsorption mechanisms and the energy changes during the adsorption process (polymer/inorganic particles) might lead to a more rational and optimized design of the binding components (concerning adsorption strength, amount of modification agent needed to fulfil a special purpose, surface coverage, irreversibility of the adsorption, etc.).

In the next part of this chapter, in order to probe deep into the mechanism of the interaction of amphiphilic copolymers with inorganic particles, the change in the specific heat capacity (ΔC_p) was applied. Herein, the ΔC_p values for the interaction of the amphiphilic copolymers with the ZnO particle surface were measured at 15, 20, 25 and 30 °C. The experimental results show that the binding enthalpies ΔH at various temperatures are becoming more negative with increasing temperature. The observed ΔC_p of the interaction PEHMA-co-PEOMA/ZnO was found small and positive which suggests, this interaction is entropically dominated, whereas the binding is attributed mainly to the extensive additional solvation, and partially to the burial of the polar groups of the interacting molecules. The ΔC_p values for the interactions of the copolymers, bearing the anchor groups P4VBP, PMOEPA and PEGMA on the ZnO surface, were found small negative. This small contribution of ΔC_p suggests that electrostatics forces play a significant role in the heat capacity change, resulting from solvation upon binding compared with hydrophobic interactions are involved in the binding reactions (see *Chapter 3.5*).

As a final point of this chapter, regarding to the thermodynamic profile observation (binding affinity, binding enthalpy and binding entropy) for the interactions of amphiphilic copolymers with the nanoparticles, the ITC technique was presented here as a method to screen and improve the binding potency as well as the binding affinity in the organic-inorganic-hybrids-systems. It shows that plotting the calculated thermodynamic parameters (ΔH) and ($-T\Delta S$) in a thermodynamic optimization plot (TOP) leads to classify the compounds into six regions relating to their enthalpic and entropic gain. Optimizing the binding affinity in the organic-inorganic-hybrids-systems prove, that the type of the polar group and its tendency to interact with the surfaces is much more important than the number of the polar groups (see *Chapter 3.6.3*). This study is of general interest, since it provides a practical guideline aimed at screening and improving the binding potency in the organic-inorganic-hybrids-systems as well as other systems.

This knowledge of the adsorption mechanisms and energy changes during the interactions leads to a more rational and optimized design of the binding components (concerning adsorption strength, amount of modification agent needed to fulfill a special purpose, surface coverage, irreversibility of the adsorption, etc.). Aside to the presented interactions between polymer and inorganic particles, ITC offers the potential to become also an important tool to analyze, for example, the aggregation behavior of polymers, which plays an important role in the formation of micelles, emulsions or in the self-assembly of amphiphilic block copolymers (e.g. polyelectrolytes).

The developments in polymer science, together with the latest achievements of inorganic chemistry, create a base from which to address the fundamental problem of increasing the sensitivity of nanoparticles to their environment, and to work out pathways for nanoparticle synthesis with controlled size, shape and other properties, and, as a result, to elaborate new advanced areas of application.

CHAPTER 4 illustrates the thermodynamic investigation of the reaction mechanisms and binding efficiencies in a polyphenylene dendrimers (PPDs)-based host-guest system. ITC technique was applied for the first time to quantify/analyse the interactions between PPDs and volatile organic compounds (VOCs) and explosive materials (such as: triacetone triperoxide (TATP)). The first part of this chapter demonstrated the capability of the ITC technique as a method can be used to study the adsorption behavior and the binding efficiency of dendrimers towards small guest molecules at very low concentrations (micromolar level). The interaction between non-functionalized polyphenylene dendrimer (Td-G2) and several kinds of VOCs was applied. For all the VOCs (polar aromatic, non-polar aromatic, ketones, nitro compound, nitrile compound as well as cyclic amide) studied, the interaction was found to be strongly thermodynamically driven by both negative change in enthalpy and positive change in entropy. Furthermore; based on temperature dependent ITC studies and fluorescence measurements (*Chapter 4.3.2*), it has been possible to prove that interaction between polyphenylene dendrimers and VOCs not only takes place inside the core of the cavity but also on the dendrimer surface outside the core, as

well as the π - π electron donor-acceptor complexation is not the dominant mode of interaction between the neutral Td-G2 and the VOCs studied in the present work (*Chapter 4.3.1*).

In the second part of this chapter, different functionalized dendrimers bearing *methyl ester*-, *carboxyl*-, *cyano*-, *nitro*- and *pyridyl* groups at the interior (scaffold) were studied. The study of these functionalized dendrimers showed noticeably the influences of the nature of the functional groups on the capability, sensitivity and the selectivity of the dendrimers to detect/uptake different classes of VOCs. The observed thermodynamic parameters proved, that the use of electron withdrawing ($-NO_2$ and $-CN$) substituents in the dendrimer scaffold leads to an increase of the capability and selectivity of the dendrimer to interacting with the polar aromatic (e.g. *benzaldehyde* and *acetophenone*), nonpolar aromatic (*benzene* and *toluene*) as well as the aliphatic VOCs (such as *acetone*, *MIPK* and *nitro methane*). On the other side, employing an acidic substitution group such as ($COOH$) leads to increasing the sensitivity of polyphenylene dendrimers to uptake all aliphatic and polar aromatic VOCs. In contrary using of the ($COOMe$) groups leads to slightly increased in the sensitivity of the dendrimer to interact with the aliphatic VOCs (such as *acetonitrile* and *diethyl amine*). This observation can be related to the presence of the $COOH$ groups in the cavity of the dendrimer, which increased the ability of the dendrimer to build hydrogen bonds with the guest molecules than that with $COOMe$. Furthermore, adding the basic functional group *pyridyl* in the interior layers leads to increase the selectivity and the sensitivity of the polyphenylene dendrimer to interact with the aliphatic VOCs such as acetone and acetonitrile (*Chapter 4.3.3*).

In the next part of this chapter, ITC technique was applied to study the capability, selectivity and sensitivity of polyphenylene dendrimer and its derivate for detecting high explosive material such as *triacetone triperoxide (TATP)*. Practically, a second generation of polyphenylene dendrimer with *pyridyl* functional groups *Td-G2-(Pyridyne)₁₆-(Cp)₈*, a third generation of *methyl ester* substituted polyphenylene dendrimer *Td-G3-(COOMe)₈-(Cp)₂₄* and a third generation of non-functionalized polyphenylene dendrimer *Td-G3-(Phenyl)* have been studied. The observed thermodynamic parameters (ΔH) and (ΔS) showed

that TATP is interacting strongly with non-functionalized polyphenylene dendrimers as well as the functionalized one. The interaction of TATP with Td-G₃-(COOMe)₈(Cp)₂₄ signifying that the interaction was mainly controlled by hydrophilic forces, suggesting, that there are a large number of hydrogen bond contacts between the dendrimer and the TATP molecules. On the contrary, the interaction of TATP with the Td-G₂-(pyridyl)₁₆(Cp)₈ as well as the G₃- non-functionalized polyphenylene dendrimer demonstrated interactions predominantly controlled by hydrophobic forces, suggesting a hydrophobic transfer of TATP molecules from bulk solvent to the dendrimer binding sites and release. These different forces suggesting that the TATP/ polyphenylene dendrimer interactions occurred in two different mechanisms of binding, depending on the dendrimer generation and the nature of the functional groups, that were incorporated in the interior (scaffold) of the dendrimer (see *Chapter 5.3.1.3* and *Chapter 1.5*). Using the ITC technique demonstrated, that the polyphenylene dendrimer and its derivate have the potential to be used as sensor-active substances to detect the explosive material TATP (*Chapter 4.4*).

In the last part of this chapter the ITC technique was applied with the purpose of understanding the imprinting effect and rebinding efficiency of nanosized molecularly imprinted polymer particles. Practically, these particles were synthesized by means of nonaqueous emulsion polymerization using a standard monomer mixture of *methacrylic acid* and *ethylene dimethacrylate*, containing (\pm)-*propranolol* as a template. The thermodynamic signature indicates, that the binding is predominantly entropic, most probably driven by hydrophobicity. The entropy changes arise from the release of solvent molecules upon binding and are more favorable for the imprinted polymer. Since the template is expected to fit better in the imprinted cavities, consequently releasing a greater number of solvent molecules. The determined binding constant K_B , which reflects the interaction affinity of (\pm)-*propranolol* to the polymer particles, is much higher for the imprinted polymers than for the non-imprinted polymer and unequivocally demonstrates the existence of a marked imprinting effect in the nanoparticles. ITC was proven to be a suitable method to investigate the thermodynamics of molecular recognition reactions of non-covalently imprinted polymers and to be

an excellent tool to assess the efficiency of the initial molecular imprinting process (*Chapter 4.5*).

In summary the current work presents a concept for the application of Isothermal titration calorimetry “*faraway from its original utilization in biological system*” as a technique that can directly quantify and analyse the adsorption process in complex chemical systems like organic-inorganic-hybrids-systems. These studies gave a first and deeper insight in the mechanism of the underlying adsorption process. By elucidating the mechanism and the thermodynamic profile of the adsorption processes, ITC offers a pathway towards a systematic design of hybrid materials, not only by supporting the optimization of these processes but also by creating a library, containing adsorption characteristics of surface active compounds with inorganic surfaces. Such a library will be a sophisticated tool to find and predict potential candidates for a specific modification of inorganic surfaces.

Furthermore, using the ITC as an analytical tool to quantify the intermolecular interactions in the dendrimer-guest systems by direct measurement of the heat of binding, from which K_B , ΔG , ΔH , and ΔS values can be easily observed in one single experiment leads to an additional understanding of the interaction mechanisms in host-guest systems. In this way ITC offers the potential to also become an important tool to help in designing new host molecules to trap a variety of chemical guests and will be the determining factor in the development of more efficient host-guest systems applications like gas storage and separation, drug delivery as well as sensing.

CHAPTER 6

APPENDIX

6.1 LIST OF ABBREVIATIONS**A**

a	distance
AUC	Analytical Ultracentrifugation
AJ	adiabatic jacket
AFM	Atomic force microscopy
ATRP	Atom transfer radical polymerization

D

DSC	Differential Scanning Calorimetry
DTA	Differential Thermal Analysis
DMA	Dynamic Mechanical Anal
D	dielectric constant, dilution factor
DNA	deoxyribonucleic acid
DCM	dichloromethane

F

F	electrical force
Fl	Fluorescence

H

ΔH	change in enthalpy
HDMA	10-Hydroxydecylmethacryl
HEMA	2-Hydroxyethylmethacryl

J

JFB	feedback mechanism
-----	--------------------

K

k_1, k_2	constants of the reactions
K_a	affinity constant
K_d	dissociation constant

L

L	guest molecule
[L]	concentration of the free Ligand
$[L_T]$	total concentration of the Ligand

N

n	stoichiometry
N_2	nitrogen
NMP	1-methyl-2-pyrrolidine

C

ΔC_p	heat capacity
CFB	cell feedback signal
$CHCl_3$	chloroform
CRP	controlled radical polymerization

E

EHMA	2-Ethylhexyl methacrylate
EGMP	(ethylene glycol) methacrylate phosphate
EHIB	2-Ethylhexyl isobutyrate
EO	ethylene oxide

G

ΔG	Gibbs free energy
ΔG_m	molar Gibbs energy
G	Generation

I

I	ion
I	dimensionless ionic strength
ITC	isothermal titration calorimetry
I_{max}	fluorescence-peak intensity
I_0	peak intensity of isolated Td-G2

M

M	host molecule
[M]	concentration of the Host
$[M_T]$	total concentration of th macromolecule
[ML]	concentration of the complex
MC	measure cell
MIPs	molecularly imprinted polymers
MPS	3-(trimethoxysilyl)propyl methacrylate
MIPK	methyl isopropyl ketone

P

PEG	poly (ethylene glycol)
PEGMA	poly (ethylene glycol)methacrylate
PEOIB	poly (ethylene oxide) isobutyrate
PS	polystyrene
PPDs	polyphenylene dendrimer
PMMA	poly(methyl methacrylate)
PEOMMA	Poly (ethylene oxide) methyl Methacrylate
PAMAM	poly(amidoamine)
PPI	poly (propylene imine)

R

r_{ij}	distance
R	gas universal constant
RC	reference cell Resonance
RO	reference output
RRC	electrical resistance
RAJ	electrical resistance
ROP	ring opening polymerization
ROMP	ring opening metathesis Polymerization

U

U	internal energy
---	-----------------

T

THF	Tetrahydrofuran
TOPO	tri- <i>n</i> -octylphosphine oxide
T	absolute temperature
Td-G2	unsubstituted-polyphenylene dendrimer
TATP	triacetone triperoxide.
TOP	thermodynamic optimization plot
TiO ₂	titanium dioxide

X

X	molar ratio
---	-------------

Q

q	Electric charge
q'	molar heat
Q	heat
QMB	quartz microbalance

S

ΔS	change in entropy
SPR	Surface Plasmon
ST	rotating syringe

V

v	number of moles
V _{inj}	injection volume
V _{cell}	volume of the calorimetric cell
4VP	4-vinylpyridine
VOCs	volatile organic compounds

6.2 LIST OF FIGURES AND SCHEMAS**CHAPTER 1**

1.1	Functional Supramolecular systems.	2
1.2	Grafting-to and grafting-from approaches.	5
1.3	Tri- <i>n</i> -octylphosphine oxide (TOPO)-covered CdSe.	5
1.4	Radical polymerization (ATRP) of methyl methacrylate.	7
1.5	Simplified representation of an emulsion polymerization system.	7
1.6	The principle of miniemulsion polymerization.	9
1.7	The host–guest complexation.	10
1.8	Commons host molecules used in host-guest-chemistry.	11
1.9	Basic architectural components of a dendrimer.	12
1.10	Dendritic growth via divergent approach.	13
1.11	Dendritic growth via convergent approach.	14
1.12	Building block (cyclopentadienone).	15
1.13	PPD at the, A) surface and B) in scaffold	16
1.14	Energy of binding.	18
1.15	Principal orientations of aromatic–aromatic interactions.	20
1.16	Schematic representation of the hydrophobic binding.	21
1.17	Simplified schema of VP-ITC calorimeter.	24
1.18	ITC experimental curve.	25
1.19	Binding isotherms for different values of <i>c</i> parameter.	29
1.20	Schematic diagram of molecular interaction often observed.	31
1.21	Structure and molar mass of the monomers used.	34
1.22	Structure and molar mass of the amphiphilic copolymers.	34

CHAPTER 2

2.1	Functional Supramolecular systems.	43
-----	------------------------------------	----

CHAPTER 3

3.1	ZnO particles, using an inverse emulsion technique.	52
3.2	Functionalization of the inorganic nanoparticles.	53
3.3	Structure and molar mass of the monomers and copolymers.	56
3.4	Binding isotherms of A) EHMA B) PEGMA ^{n≈5} .	58
3.5	Isotherms for the titration of 55 mM solution of EHMA.	60
3.6	Isotherms of A) PEGMA, B) EGMP and C) 4VPSB.	62
3.7	Isotherms for the titration of 55 mM solution of PPOMA ^{n≈5} .	64
3.8	Isotherms for the titration of 55 mM of A) EHIB, B) PEGIB.	65
3.9	Thermodynamic profiles low molecular weight monomers.	66
3.10	Isotherm for the titration of 55 mM of PEHMA-co-PPEGMA.	69
3.11	PEO side chain with the surface of the SiO ₂ .	70
3.12	A) HEMA, B) HDMA, C) PEOMMA and D) PEGMA ^{n≈5} .	71
3.13	Binding isotherms for the titration of PEHMA-co-PPEOMA.	74
3.14	Thermodynamic profiles of PEHMA-co-PPEGMA.	77
3.15	Isotherms of amphiphilic copolymer PEHMA-co-PPEGM.	77
3.16	Binding isotherms for the interactions of PEHMA-co-P4VPSB.	79
3.17	Thermodynamic profiles of PEHMA-co-P4VPSB.	80
3.18	Binding isotherms for the titration of PEHMA-co-P4VPSB.	82
3.19	Binding isotherms for the interactions of PEHMA-co-PEGMP.	85
3.20	Thermodynamic profiles of PEHMA-co-PEGMP.	86
3.21	Binding isotherms for the interactions of PEHMA-co-PMOEPA.	88
3.22	Thermodynamic profiles of PEHMA-co-PMOEPA.	89
3.23	Isotherms of PEHMA-co-PMOPPA and PEHMA-co-PMOEPA.	90
3.24	Binding isotherms of the amphiphilic copolymers.	92
3.25	Amphiphilic copolymers at different temperatures.	94
3.26	Temperature dependence of K _B for the amphiphilic copolymers.	95
3.27	Plot of ΔH versus temperature for calculation of ΔC _p .	96
3.28	The TOP of PEHMA-co-P4VPSB into the SiO ₂ .	100
3.29	The -TΔS, ΔH points (■) for all complexes.	100
3.30	TOP for all copolymer/nanoparticles complexes.	102
3.31	Affinity optimization of the amphiphilic copolymers.	105
3.32	The role of the monomers in PEHMA-co-PPEGMA ^{n≈5} .	108

3.33	ΔH signatures for the interactions of amphiphilic copolymers.	109
3.34	K_B for the interactions of amphiphilic copolymers.	110
3.35	A) ZnO/PEHMA-co- PMOEPA, B) Calculation of ΔC_p .	112

Scheme

3.1	The changes in (ΔH), (ΔS), and (ΔG).	61
3.2	Chemical structures of the amphiphilic copolymers.	68
3.3	PEHMA-co-P4VPSB bearing zwitterionic anchor group .	78
3.4	Amphiphilic copolymers bearing zwitterionic anchor group.	81
3.5	Amphiphilic copolymers bearing acidic anchor group.	83
3.6	The formation of hydrogen bond and bidentate Phosphonate.	83
3.7	Amphiphilic copolymers bearing acidic anchor group.	90
3.8	Amphiphilic copolymers bearing different anchor groups.	101

CHAPTER 4

4.1	Isotherms for the interactions of (VOCs) into (Td-G2).	124
4.2	ΔH for the interaction of VOCs with the (Td-G2).	126
4.3	3D molecular models of (Td-G2) with 64 phenyl rings.	127
4.4	N and K_B VOCs with the (Td-G2-Phenyl).	128
4.5	Titration of benzene, diethyl amine and benzaldehyde/ Td-G2.	129
4.6	Benzene, benzaldehyde and diethyl amine/Td-G2.	130
4.7	The integration of the isotherm in figure 4.5 THF to Td-G2.	132
4.8	Host-guest binding equilibrium.	133
4.9	ΔH for VOCs with the (Td-G2) in THF, DCM and $CHCl_3$.	134
4.10	Fluorescence spectra (in THF) for toluene/Td-G2 interaction.	136
4.11	Fluorescence spectra of Td-G2 with different VOCs.	138
4.12	I_{max}/I_0 vs. toluene/Td-G2 of fluorescence toluene/Td-G2.	139
4.13	Normalized emission spectra of different Td-G2/VOC.	140
4.14	Shift of maximum due to toluene-Td-G2 interaction.	141
4.15	Raman spectrum of Td-G2 with Toluene in THF at 25.	143
4.16	ΔH for VOCs/Td-G2-(NO_2) ₈ -(Cp) ₈ and Td-G2-(CN) ₈ -(Cp) ₈ .	146

4.17	K_B for VOCs/Td-G2-(NO ₂) ₈ -(Cp) ₈ and Td-G2-(CN) ₈ -(Cp) ₈ .	148
4.18	ΔH for VOCs/Td-G2-(COOH) ₈ - and Td-G2-(COOMe) ₈ .	149
4.19	K_B for VOCs/Td-G2-(COOH) ₈ and Td-G2-(COOMe) ₈ .	151
4.20	ΔH for VOCs/Td-G2-(pyridine) ₁₆ -(Cp) ₈ .	152
4.21	K_B for the interactions of VOCs/Td-G2-(pyridyne) ₁₆	153
4.22	ΔH for VOCs/Td-G3-(COOMe) ₈ and Td-G2-(COOMe) ₈ .	156
4.23	3D of the Td-G2-(COOMe) ₈ and Td-G3-(COOMe) ₈ .	157
4.24	K_B for VOCs/Td-G3-(COOMe) ₈ and Td-G2-(COOMe) ₈ .	159
4.25	Chemical structure of the explosive (TATP).	160
4.26	(Phenyl), Td-G3-(COOMe) ₈ and Td-G2-(pyridyl) ₁₆ /TATP.	162
4.27	TATP (0.00054 mM) with (0.001 mM) PPD in CHCl ₃ .	163
4.28	K_B for the interaction of TATP (0.00054 mM)/PPD.	164
4.29	ΔH versus temperature for ΔC_p for TATP/Td-G3-(COOMe) ₈ .	165
4.30	Propranolol template and mixture of methacrylic.	167
4.31	Rac-propranolol/poly(ethylene glycol acid).	168
4.32	ΔH signatures for functionalized dendrimers with VOCs.	171
4.33	K_B for different functionalized dendrimers with VOCs.	172

Scheme

4.1	A quartz microbalance (QMB) as a detector for (VOCs).	118
4.2	Non-functionalized PPD (Td-G2) and the VOCs used.	123
4.3	Nitro- and cyano- substituted PPD used in this study.	145
4.4	methyl ester-, carboxyl- PPD (Td-G2) used in this study.	148
4.5	Pyridyl substituted PPD used in this study.	151
4.6	G3 and G2 of the methyl ester- PPD used in this study.	155
4.7	PPDs used to study triacetone triperoxide TATP sensoric.	161

6.3 LIST OF TABLES**CHAPTER 1**

1.1	Standard techniques for the binding constants.	23
-----	--	----

CHAPTER 3

3.1	Surface active compounds/SiO ₂ .	66
3.2	Thermodynamic parameters PEGMA –mol- % with SiO ₂ .	74
3.3	PEHMA-co-PPEGMA/Al ₂ O ₃ , CeO ₂ , etc.	76
3.4	PEHMA-co- P4VPSB /Al ₂ O ₃ , CeO ₂ , etc.	80
3.5	PEHMA-co- PEGMP /Al ₂ O ₃ , CeO ₂ , etc.	86
3.6	PEHMA-co- PMOEPa /Al ₂ O ₃ , CeO ₂ , etc.	89
3.7	Copolymers/ZnO at different temperatures.	93
3.8	Calculated ΔC _p values and correlation coefficients.	96
3.9	Enthalpy of different chemical functionalities at 25 °C.	98
3.10	Amphiphilic copolymers /Al ₂ O ₃ , CeO ₂ , etc.	104

CHAPTER 4

4.1	Thermodynamic Parameters for Td-G2 and VOCs.	125
4.2	Td-G2/benzene, diethyl amine and benzaldehyde.	131
4.3	Calculated ΔC _p values and correlation coefficients.	131
4.4	Td-G2 and VOCs in dichloromethane and chloroform.	135
4.5	Composition of samples used for FI measurements.	137
4.6	VOCs/Td-G2-(NO ₂) ₈ and Td-G2-(CN) ₈ - in THF.	147
4.7	VOCs/Td-G2-(COOH) ₈ and Td-G2-(COOMe) ₈ in THF.	150
4.8	VOCs with the Td-G2-(Pyridine) ₁₆ -(Cp) ₈ in THF.	153
4.9	VOCs / Td-G3-(COOMe) ₈ and Td-G2-(COOMe) ₈ in THF.	158
4.10	Phenyl, Td-G3-(COOMe) ₈ -and Td-G2-(Pyridyl) ₁₆ /TATP.	162
4.11	G3-(COOMe) ₈ (Cp) ₂₄ with TATP.	165
4.12	Thermodynamic parameters obtained by the ITC measurements.	168

6.6 ACKNOWLEDGEMENTS

I would like to thank all the people who contributed to this work, especially my supervisor, my project leader and my collaboration partners. I would like to express many thanks to my colleagues, friends and family for the constant support during the last years.

